Development of an *Escherichia coli* Biofilm Platform for use in Biocatalysis

James Thomas Leech

A thesis submitted to the University of Birmingham

for the degree of

Doctor of Philosophy

Biochemical Engineering

School of Chemical Engineering

College of Engineering and Physical Sciences

September 2017

Abstract

Whole-cell biocatalysis is a common means of producing bulk and fine chemicals using the native abilities of microorganisms such as bacteria and fungi. In nature, many bacteria protect themselves from environmental stresses by forming a multicellular, multicomponent biofilm. In industrial and medical settings, biofilms are generally seen as detrimental factors which lead to biofouling, contamination and the exacerbation of human infections. However, biofilms have been proven in many cases to be superior to planktonic cultures in biocatalysis processes. This study outlines the development of a multipurpose biofilm biocatalyst in the well-studied bacterium *Escherichia coli.*

Using Crystal Violet Stain quantification and Confocal Laser Scanning Microscopy, a novel, inexpensive and reproducible biofilm generation method was developed and optimised in the K-12 lab-strain PHL644 and the industrially-relevant strain BL21 Star (DE3). Reporter Gene constructs and Flow Cytometry allowed the inference of heterogeneity in curli fimbriae gene expression in biofilm cells, and differences between planktonic and biofilm-phase populations.

Four biofilm-modulating plasmids, overexpressing CsgD, DgcM, DgcO and DgcC, were tested for their effects on biofilm formation and whether they might be used to improve biofilm formation. Significant effects on curli gene expression and biofilm architecture were noted. From this data, DgcC was suggested as a possible overexpression target for synthetic biology to increase biofilm abundance in BL21 Star (DE3).

Three biocatalysis reactions were tested in the biofilm model. Plasmid-expressed TrpBA tryptophan synthase was found to severely reduce both growth rate and biofilm formation in both PHL644 and BL21 Star (DE3). Plasmid-expressed PrnA halogenase and CV2025 transaminase were found to have little effect on biofilm formation but were unable to produce a detectable product in either planktonic or biofilm phase cultures. Although optimisation was not possible due to time constraints, several suggestions were made as to the biocatalytic potential of this novel biofilm protocol.

Acknowledgements

For support and guidance in all aspects of this project I would like to thank Tim Overton, Isaac Vizcaino-Caston and Mark Simmons.

For technical support, I would like to thank Ronnie Baglin, Elaine Mitchell and David French.

I would like to thank my colleagues from Biochemical Engineering and especially those in Tim Overton's research group.

I would also like to thank the BBSRC who funded this project.

I would like to thank my family for their support.

Lastly AKL and MF, for everything.

Contents

List of Figures

Chapter 4

Chapter 5

List of Tables

Chapter 1

Chapter 2

Chapter 3

List of Abbreviations

(S)-(-)-α-MBA	(S)-(-)-α-Methylbenzylamine
5' UTR	5' Untranslated Region
Ag43	Antigen 43
AHL	N-Acyl-L-Homoserine Lactone
AI-2	Autoinducer-2
bp	Base Pair
CA	Colanic Acid
c-di-GMP	Cyclic Diguanosine Monophosphate
CLSM	Confocal Laser Scanning Microscopy
CV	Crystal Violet
DGC	Diguanylate Cyclase
EAEC	Enteroaggregative *Escherichia coli*
ECM	Extracellular Matrix
eGFP	Enhanced Green Fluorescent Protein
EHEC	Enterohaemorrhagic *Escherichia coli*
EPS	Extracellular Polymeric Substances
FAD	Flavin Adenine Dinucleotide (oxidised)
$FADH_2$	Flavin Adenine Dinucleotide (reduced)
GFP	Green Fluorescent Protein
HPLC	High-Performance Liquid Chromatography
IPTG	Isopropyl β-D-1-thiogalactopyranoside
LB	Luria-Bertani Broth
Mg^{2+}	Magnesium Ion
MRSA	Methicillin-Resistant *Staphylococcus aureus*
NAD^+	Nicotinamide Adenine Dinucleotide (oxidised)
NADH	Nicotinamide Adenine Dinucleotide (reduced)
OD	Optical Density
ORF	Open Reading Frame
PBS	Phosphate Buffered Saline
PC	Polycarbonate
PCR	Polymerase Chain Reaction
PDE	Phosphodiesterase
PLP	Pyridoxal 5'-Phosphate
PNAG	Poly-N-Acetylglucosamine
PNPase	Polynucleotide Phosphorylase
PS	Polystyrene
PTFE	Polytetrafluoroethylene
RBS	Ribosome Binding Site
RCF	Relative Centrifugal Force
RNAP	RNA Polymerase
RPM	Revolutions Per Minute
RPP	Recombinant Protein Production
SCEB	Spin Coated Engineered Biofilm
SDS-PAGE	Sodium Dodecyl Sulphate Polyacrylamide Gel Electrophoresis
sRNA	Small RNA
SS	Stainless Steel
TMAO	Trimethylamine N-oxide
UTI	Urinary Tract Infection
UV	Ultraviolet
ω-TA	Omega-Transaminase

Chapter 1

Introduction and Literature Review

This chapter covers the relevant scientific knowledge surrounding both biocatalysis and biofilms, and how the two areas may be converged to provide industrially-relevant outputs. Furthermore, this chapter will outline the major research techniques used in this project and explain how they were used to fulfil the project aims.

1.1 Industrial Production of Chemicals

1.1.1 Biocatalysis

Biocatalysis is the production of useful substances utilising enzymes. Human use of biocatalysis can be traced back thousands of years to the processes of beer brewing and bread-making which arose in the Neolithic period (Dequin S, 2001). Brewing and baking harness the enzymes of the yeast *Saccharomyces cerevisiae* to convert sugars into ethanol and carbon dioxide respectively (Randez-Gil F *et al*., 2013). Traditionally, these processes were improved by selecting yeast cultures which produced desirable outcomes, such as better flavour and better tolerance to fermentation conditions. Artificial selection is slow and relies on natural variation and evolution within yeast populations (Gallone B *et al*., 2016). Advancements in genetic engineering in the past 30 years have enabled researchers to directly modify myriad organisms, creating novel processes with more desirable traits and higher yields (Adrio JL & Demain AL, 2005). These processes are constantly being refined and improved and thus novel, lucrative biocatalysis strategies are a major focus for both research and industry (Choi JM *et al*., 2015, Reetz MT, 2013).

1.1.2 Chemical Synthesis

The production of fine chemicals and pharmaceuticals has traditionally been the domain of chemical synthesis. In chemical synthesis, compounds are assembled through harsh high temperature or pressure conditions using chemical catalysts which are potentially harmful to the end user (Koeller KM & Wong CH, 2001). The products of these reactions are often impure, producing unwanted side reactions, and require a great deal of purification. In the production of compounds requiring enantiomeric specificity or regioselectivity, chemical synthesis can lead either to a reduction of overall productive yield or potentially dangerous side effects when used in pharmaceutical treatments. Perhaps the most well-known example of this problem is the drug Thalidomide. Chemical synthesis of Thalidomide created a racemic mixture of *R*- and *S*-form molecules. The *R*-form produced the desired effect of relieving morning sickness in pregnant women. However, the *S*-form was found to be teratogenic in humans, causing birth defects in the developing foetus (Smith SW, 2009). In biological cells, the synthesis of chemicals is driven by DNA-encoded enzymes, which represent a more specific and controllable means of synthesising chemicals in terms of stereo- and regioselectivity (Cooper GM & Hausman RE, 2007).

1.1.3 Enzymes

Enzymes are present in all living cells on Earth and catalyse thousands of different reactions within a cell (Cooper GM & Hausman RE, 2007). Enzymes consist of polypeptide chains capable of folding into highly-structured 3D catalytic platforms. Enzymes can be modified after translation to perform more specific tasks, and may bind other molecules or proteins to reduce or increase enzymatic activities. The binding of reactant chemicals is extremely precise and regulated, such that only chemicals with the correct structures may bind the site

of reaction (Cooper GM & Hausman RE, 2007). Enzymes are dynamic catalysts, and can alter their conformation to perform their reaction, preventing the escape of intermediates and decreasing the chance of side-reactions (Eisenmesser EZ *et al*., 2002). In some cases, enzymes may function together as a bound complex, performing multiple-step reactions in close proximity, further increasing reaction efficiency (Santacoloma PA *et al*., 2011). Due to the specificity of the reactions performed by enzymes, and their defined structure, enantiomeric specificity and regioselectivity can be promoted, if not guaranteed (Cooper GM & Hausman RE, 2007). In contrast to chemical synthesis, enzymes can perform reactions at physiological conditions such as temperature and pressure, reducing costs required to catalyse reactions (Choi JM *et al*., 2015).

1.1.4 Recombinant Enzymes

Due to advances in molecular biology, heterologous proteins and enzymes (i.e. from a different organism) can be artificially produced in another suitable living host (Overton TW, 2014). The process by which this is achieved is depicted in Figure 1.1. This is usually desired due to insufficient yield of enzyme from the native producer. The microorganisms most often used for the production of recombinant proteins are the previously mentioned yeast *S. cerevisiae* and the bacteria *Escherichia coli* and *Bacillus subtilis* (Westers L *et al*., 2004). Recombinant protein hosts are strains of a naturally-occurring species which have been cultivated or mutated to confer high growth rate, high levels of protein production and high functional yield of the produced proteins (Overton TW, 2014). Harvesting of enzymes from these organisms has also been consistently optimised, allowing rapid purification of recombinant enzymes for further application (Rosano GL & Ceccarelli EA, 2014).

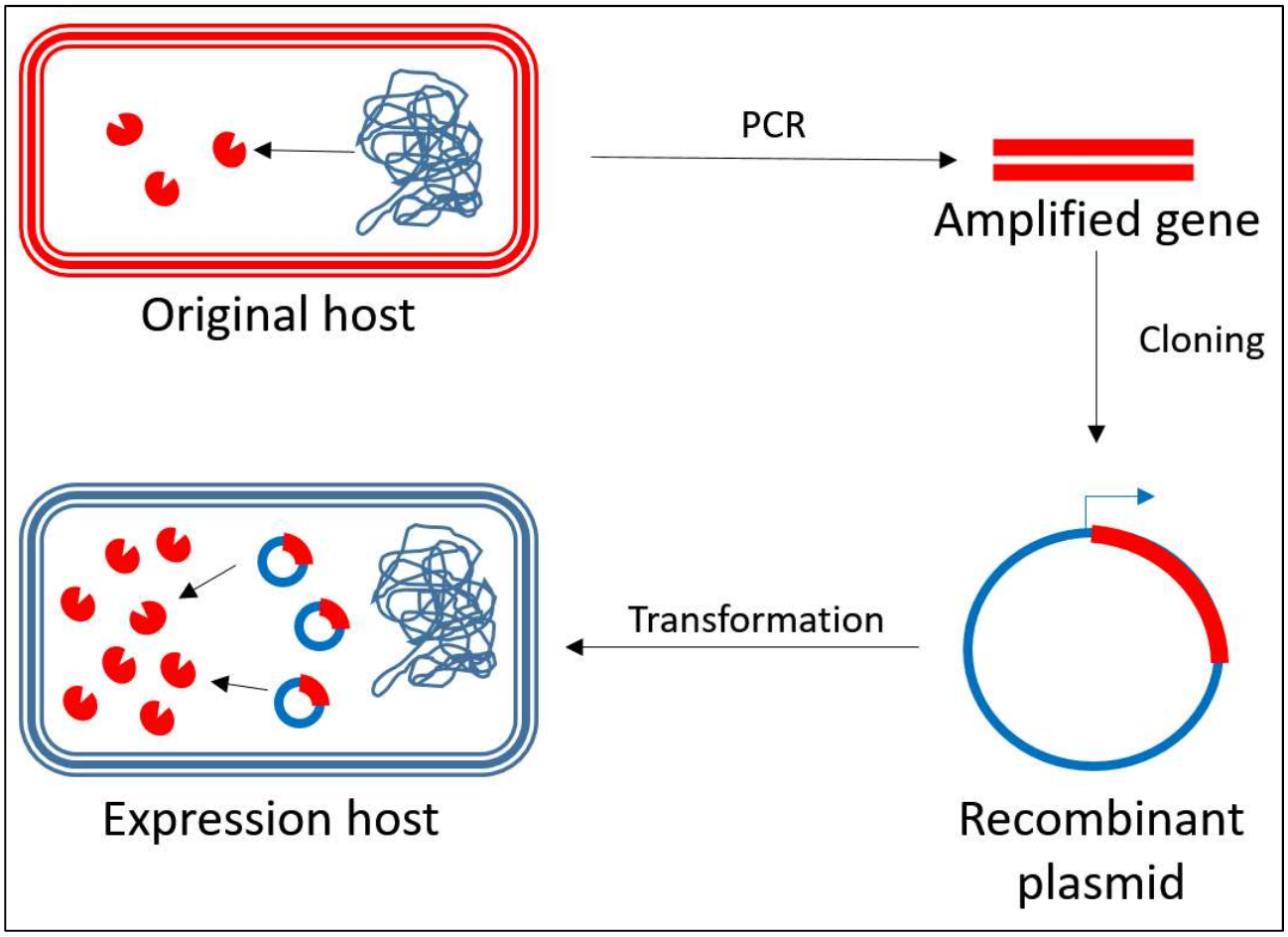

Figure 1.1: *Standard process for recombinant enzyme production. An enzyme of interest is detected in a native host, and its gene is amplified by PCR or synthesised artificially. The gene is cloned into a recombinant plasmid which can be transformed and expressed in a more amenable host. This permits higher expression of the enzyme and more simple growth conditions.*

Purified enzymes are able to efficiently perform their specific reactions *in vitro* given the appropriate conditions, reactants and cofactors. As the enzymes have evolved in their original host to work in biologically active conditions, relatively mild temperatures and pH levels can be implemented, reducing damage to product compounds and use of environmentally-damaging chemicals (de Regil R & Sandoval G, 2013). In cells, reacting

molecules must be transported across membrane barriers and may bind other enzymes, both of which may reduce the rate of the desired reaction. Enzyme purification eliminates this issue by removing these barriers as well as other, potentially interfering enzymes, allowing direct access to the reactants. (Choi JM *et al*., 2015).

Examples of successful industrial implementation of heterologous enzyme production include the enzyme chymosin. Chymosin (also known as rennin) cleaves milk caseins to produce insoluble protein known as curd. Curd is used to produce cheese. Traditionally, chymosin was obtained from the digestive system of young mammals such as cows. However, due to increased demand for cheese and curd-based products in the 20th and 21st centuries, chymosin is now predominantly produced in various species of the yeast *Aspergillus* and the bacterium *E. coli*. Indeed, it was reported that 80% of industrially-utilised chymosin in 2016 came from recombinant production (Wei ZY *et al.*, 2016).

Recombinant enzyme production has also been employed in the synthesis of pharmaceuticals. Sitagliptin (trade name Januvia; Merck) is a diabetes drug which is produced using *Arthrobacter* sp. *R*-selective transaminase (*R*-ATA). Due to the stereoselectivity of *R*-ATA, only one form of the drug is produced by the enzyme, eliminating potential side effects caused by an *S*-form. Furthermore, the reaction was found to have a greater yield than the traditional rhodium-catalysed reaction, as well as eliminating the use of a polluting heavy metal (Desai AA, 2011).

1.1.5 Immobilised Enzymes

Although purified enzymes have been shown to be effective in producing abundant and pure chemicals, the process can be improved in several ways. One common issue is that the enzymes are unstable in reaction buffers, which may be alleviated by enzyme

immobilisation. Enzymes can be attached to an amenable surface through various techniques. Immobilisation affords increased chemical and structural stability, and the ability to reuse the enzymes without re-purification, both of which improve the overall efficiency and productive yield of the reaction. Immobilisation strategies commonly employ an insoluble, easily manipulated, macroscopic platform such as a gel bead (Datta S *et al*., 2013). The most commonly employed gel platform is alginate, a polysaccharide from seaweed, which forms beads when dropped into a calcium chloride solution. Alginate is considered to be relatively unreactive and so has little effect on the reaction being employed (Guzik U *et al*., 2014). Enzymes can be adsorbed on the outer shell of these beads through various methods and can thus be inserted into and removed from reaction buffers easily. Additionally, enzymes may be encapsulated inside beads to prevent detachment of enzymes from the immobilisation matrix (known as leakage), but this method reduces mass transfer of reactants and products to the enzymes (Rother C & Nidetzky B, 2014). Other physical disadvantages of any immobilised protein technique include potential damage to the enzymes during immobilisation, detachment of enzymes from the immobilisation matrix (leakage) and blocking of active sites, all of which may reduce catalytic efficiency (DiCosimo R *et al*., 2013).

The primary disadvantage of purified enzyme biocatalysis is one of expense. Many enzymes require cofactors to perform their function. Common cofactors include electron donors such as NADH or $FADH_2$, vitamins such as pyridoxal 5'-phosphate (Vitamin B_6), or metal ions such as Mg^{2+} (Richter M, 2013). Some enzymes consume these cofactors in the reaction, which cannot be regenerated by the enzyme. Production or purchase of active forms of these cofactors is often expensive and their addition to reactions is therefore cost-inefficient. To counteract this, some reaction strategies include the addition of a cofactor regenerator,

for example an oxidoreductase to reduce NAD^+ back into NADH, allowing the reaction to continue (Uppada V *et al*., 2014). Performing a second enzyme purification for a cofactor regenerator may further increase the overall cost of the process. As purified enzymes are reused multiple times they inevitably denature, losing their specific 3D structure and reducing the reaction efficiency to a counter-productive degree. Denatured enzymes may lose their specificity, performing unwanted side-reactions, reversing the reaction or merely ceasing effective catalytic activity. This means that the enzymes must be continually replaced and repurified, further increasing costs. The advantages and disadvantages of purified enzyme biocatalysis are outlined in Figure 1.2 (Weber N *et al*., 2014).

1.1.6 Whole-Cell Biocatalysis

Living cells compartmentalise their enzymes in an envelope of membranes and polymer walls, affording protection from outside influences. Enzymes within cells are degraded and replaced, or refolded with chaperones, refreshing the biocatalytic potential. Essential cofactors are produced using primary or secondary metabolism, then regenerated, providing a constant and sustainable supply (Wachtmeister J & Rother D, 2016). All of these factors benefit native or recombinant enzymes, and may increase their overall efficiency. An efficient whole-cell biocatalyst is able to maintain itself with very little input from the user, except for basic nutrients for growth and survival. This means that costs are reduced due to the elimination of enzyme purification and maintenance steps (de Carvalho CCCR, 2016).

Development of a whole-cell biocatalyst most often begins with a wild-type organism which naturally produces a useful enzyme. However, isolation and growth of non-lab strain organisms can be problematic as different species require diverse, potentially expensive, growth requirements. Using RPP, enzymes can be produced in a more amenable host such

as *E. coli*, which has a rapid growth rate on simple media and is the best-studied microorganism in terms of industrial potential (Overton TW, 2014).

An example of the potential of *E. coli* in biocatalysis is in the production of L-carnosine, a dipeptide reported to have pharmaceutical benefits in diseases such as diabetes and Alzheimer's (Vistoli G *et al*., 2013). L-carnosine production from the amino acids L-alanine and L-histidine requires DmpA from *Ochrobactrum anthropi*, a rare human pathogen. When recombinantly expressed in *E. coli*, and with further optimisation of the reaction, a 71% conversion rate could be obtained with a yield of 3.7 g/L of *E. coli* culture (Heyland J *et al*., 2010).

Additional examples of bacterial whole-cell biocatalysis include the production of L-glutamate and L-lysine in *Corynebacterium glutamicum*. Annual production of these chemicals exceeds 2.9 and 1.9 million tons per year respectively (Burkovski A, 2015).

Whole cell biocatalysis, while promising, presents disadvantages in purification and separation as cells produce more chemicals than ones desired from a biocatalytic process. The most commonly cited example of this is the production of endotoxin by *E. coli* which elicits fever reactions in humans (Mamat U *et al*., 2015). Inefficient or blocked entry and exit of chemicals from the cell may reduce the reaction rate drastically, as only reactants and products capable of transport across the cell membrane can gain access to the recombinant enzymes. Reactants supplied to a microorganism may be sequestered by native enzymes instead of the desired synthesis pathway. In addition to these problems, there is no guarantee that the reactants will be exposed to the reacting enzyme within the cell. Lastly, planktonic (free-suspended) cells are difficult to handle and separate from reaction media, leading to contamination or poor purification of the product (de Carvalho CCCR, 2016). The

advantages and disadvantages of purified enzyme and whole cell biocatalysis are depicted in Figure 1.2.

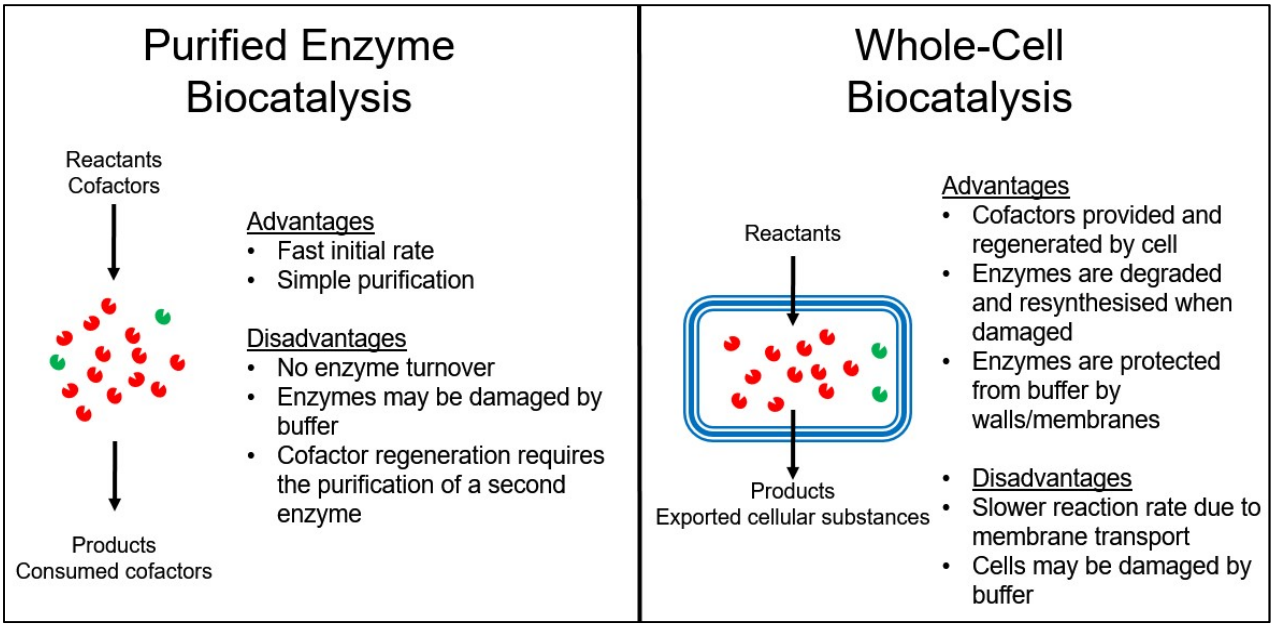

Figure 1.2: *Comparison of biocatalysis techniques. Purified enzymes (left) are open to both buffers and reactants, increasing initial reaction rate but leading to potential damage. Additionally, cofactors must be supplied to maintain the reaction rate as they are not regenerated. Whole-cells (right) protect and replenish their enzymes and provide mechanisms of cofactor regeneration. However, reactants and products must be able to move efficiently in or out of the cell across membranes, potentially reducing reaction and product recovery rates.*

1.2 Biofilms

1.2.1 Bacterial Biofilm

Chemical immobilisation of whole cells has been successful in certain processes, but harsh immobilisation conditions may damage the host cells, and poor mass transfer may reduce reaction rates (Le-Tien C *et al*., 2004). However, many bacteria, including *E. coli*, are capable of self-immobilising as a population on a surface. Self-immobilised bacterial populations are termed biofilms (Beloin C *et al*., 2008).

A biofilm is a structured conglomeration of microorganisms which group together to colonise environmental and host niches and protect themselves from mechanical, biological and chemical challenges. Cells in a biofilm produce and maintain an extracellular matrix which mediates this protection. This matrix provides protection against mechanical and chemical insults (Yang L *et al*., 2011a). Biofilms can consist of anything from one strain of microorganism to multiple diverse species (Yang L *et al*., 2011b). This multicellular existence affords many benefits over singular planktonic lifestyles, which will be explored in the subsequent sections. The predominance of references to biofilms in scientific literature are of their detrimental effects in industrial and medical settings; nevertheless the same detrimental properties may prove to be a boon in terms of potential catalytic outputs (Wu H *et al*., 2015).

1.2.2 Biofilms in Industrial Settings

In industrial settings, biofilms are generally considered to be detrimental to expensive processes, and lead to biofouling. Many industrial processes involve pipework to allow the transfer of water or other fluids. This pipework is usually made of glass, plastics or metals

which have been conditioned to allow smooth flow of fluids with as little resistance as possible. However, many studies have shown that these surfaces can be colonised by many species of bacteria, such as the disease-causing *Pseudomonas aeruginosa* and *Legionella pneumophila* (Liu X *et al*., 2014, Abdel-Nour M *et al*., 2013). Biofilms of these species will persist in the system and cannot be removed easily, as they are resistant to both shear forces and disinfectant agents. Bacteria can be sloughed off the biofilm by fluid flow, leading to contamination of the fluid being transferred, and potentially contaminating foodstuffs. In addition to the obvious food contamination problems, biofilms can form extensive meshes which can reduce or block flow. This can lead to reductions in flow rate and increased pressure in the system, and an overall reduction in efficiency of the process in question (Liu X *et al*., 2014).

1.2.3 Biofilms in Medical Settings

Biofilms are also seen as detrimental in medical settings. A common instance of this is the prevalence of fouling in urinary catheters. Urinary catheters consist of a tube inserted into the urethra of a patient to aid in draining urine (Lawrence EL & Turner IG, 2005). As the device has a consistent slow flow of urine passing through it, bacteria are able to colonise the tubes as biofilms (Trautner BW & Darouiche RO, 2004). These biofilms are resistant to the harsh conditions of the urinary tract, including changes in pH and shear forces applied by flow. As with industrial pipework, catheter biofilms can block the flow of urine and prevent efficient drainage, but can also lead to host infections. The urinary tract is the niche of a number of bacterial species, including uropathogenic *E. coli* (UPEC) and *Proteus mirabilis* (Jacobsen SM *et al*., 2008). In a normal urinary tract, these bacteria are prevented from attaching to the tract walls by the immune system which detects and eliminates infection.

When a catheter is utilised, the bacteria attach to the material of the tube and thus are not exposed to immune system mechanisms. This allows for unregulated growth of biofilms inside the catheter. As the catheter remains inside a host for extended periods of time, biofilm growth is almost an inevitability, and can be difficult to remove. Medical intervention for catheter biofilm removal includes broad-spectrum antibiotics, but due to the resistant nature of biofilms this may be ineffective (Soto SM, 2014). As such, primary treatment for infected catheters is simply to replace the device, reducing the cost-effectiveness of this intervention (Jacobsen SM *et al*., 2008).

1.2.4 Biofilms in Human Disease

Human bacterial infections most often lead to acute illnesses, largely treated with a short-term treatment of antibiotics. However, if the infecting bacteria are able to form biofilms, they may cause chronic illness which extends treatment time and can be difficult to cure. In addition, many bacteria produce toxins which may harm the body as well as increase the chance of further colonisation (Bjarnscholt T, 2013).

Staphylococcus aureus can cause relatively harmless skin infections which exhibit as boils or impetigo. However, *S. aureus* can also infect cuts, wounds and medical implants such as artificial hips (Weiser MC & Moucha CS, 2015). While the immune system is able to combat the majority of these infections, *S. aureus* is able to attenuate immune system responses, permitting the formation of biofilm. Once a biofilm has formed and matured, *S. aureus* is even less susceptible to immune responses and medical intervention due to the protection afforded by the biofilm components (Cha JO *et al*., 2013). The bacteria may then enter the bloodstream leading to sepsis and organ failure (McAdow M *et al*., 2011). The most prevalent reference to *S. aureus* in the media is the proliferation of methicillin-resistant *S.*

aureus (MRSA) which has evolved resistances to many frontline drugs such as methicillin and other β-lactam antibiotics (Choo EJ & Chamber HF, 2016). Due to these resistances, and the hardiness of the biofilm, the mortality rate from *MRSA* infection remains high (>60%) even with antibiotic treatment (McCarthy H *et al*., 2015, Rudkin JK *et al*., 2012).

The bacterium *Pseudomonas aeruginosa* is able to colonise the human respiratory tract. In acute lung infections, the immune system of the respiratory tract is able to remove *P. aeruginosa* and prevent the development of biofilms. However, in cases where the tract walls have been damaged by tobacco smoking, occupational exposure or viral disease, *P. aeruginosa* is able to evade weakened immune responses and form biofilms (Murphy TF *et al*., 2008). Another risk factor is cystic fibrosis; a genetic disease which causes thick mucus to be secreted in the lungs. The inability to clear mucus from the respiratory tract hampers the removal of bacteria from the lungs and other primary immune responses and facilitates chronic biofilm-based *P. aeruginosa* infections. *P. aeruginosa* biofilms are difficult to treat, involving high doses of antibiotics or, in extreme cases, lung transplantation. Chronic infection can lead to bronchopneumonia and sepsis if the bacteria enters the bloodstream (Høiby N *et al*., 2010).

E. coli colonises multiple physiological niches in the human body, but is most well-known for its involvement in gastrointestinal disease. Different *E. coli* strains give rise to different forms of disease in the gut but the mechanisms of biofilm formation in the gut are less clear. On one hand Enteroaggregative *E. coli* (EAEC) strains, which cause chronic diarrhoea, have been shown to adopt ordered ‘stacked-brick’ aggregates on the intestinal walls signifying extensive biofilm structure (Kaur P *et al*., 2010). However, the more severe enterohaemorrhagic *E. coli* (EHEC) strains have been shown to adhere to the intestinal walls using type-1 fimbriae, but their ability to produce biofilm components differs greatly,

correlating with variations in pathogenicity (Yeh JH & Chen J, 2004). In addition, the archetypal EHEC strain O157:H7 features a phage insertion in *csgD*, which expresses a transcription factor considered to be a major positive regulator in *E. coli* biofilm formation (the importance of *csgD* is expanded on in Section 1.4.3). The importance of biofilm to *E. coli* gut pathogenesis, as opposed to adherence, is therefore unclear (Uhlich GA *et al*., 2013).

One niche in which *E. coli* biofilm formation has proven to be indispensable to infection is in the urinary tract. Uropathogenic *E. coli* (UPEC) strains are a leading cause of urinary tract infections (UTIs) in humans (Flores-Mireles AL *et al*., 2015). As previously stated, UPEC can form biofilms on the mucosa of the urinary tract and resist the harmful chemical conditions and mechanical forces of urine flow (Salo J *et al*., 2009). Due to these resistances, UTIs are often chronic, requiring extended antibiotic treatment to clear the infection (Jacobsen SM, *et al*., 2008).

1.2.5 Biofilm Stress Resistance

Bacterial biofilm cohesion is maintained by the production of a variety of extracellular structures and polymers which allow strong cell-cell and cell-surface attachment (Ahimou F *et al.,* 2007). These elements are known as extracellular polymeric substances (EPS). The combination of these structures elicits mechanical cohesion and elasticity, maintaining the structure of the biofilm under mechanical stress. Biofilms are capable of retaining water within the EPS, preventing desiccation (Klapper I *et al*., 2002). EPS elements have been shown to resist antibiotic uptake, predation by phagocytes and increase solvent tolerance (Limoli DH *et al*., 2015). Consequently, EPS is essential to the resistances which biofilms display in all settings.

1.2.6 Multi-species Biofilms

The traditional view of bacterial cells is of a free-floating or swimming population in a liquid medium. This outlook has changed as more and more species have been found to adhere to surfaces and form biofilms with other members of their strain or species, especially in the environment (Beloin C *et al.*, 2008). This concept, however, is also an over-simplification. Bacterial species in nature do not typically exist as monocultures and coexist with other species (Flemming H-C *et al*., 2016). Interactions between species can be highly competitive, eliminating the evolutionarily weaker species from the niche, or collaborative, increasing each other's survivability in a medium (Elias S & Banin E, 2012). These interactions are highly complex and as such have not been extensively studied (Yang L *et al*., 2011b).

Streptococcus mutans has been shown to form biofilm on the surface of teeth, promoting the subsequent colonisation of *Actinomyces gerencseriae* and *Lactobacillus plantarum*. This interaction is likely due to biofilm structure produced by the initial biofilm forming species, which helps the adherence of the later colonisers (Filoche SK *et al*., 2004).

Gardnerella vaginalis is linked with bacterial vaginosis, but can be exacerbated by the presence of the UTI-related species *Enterococcus faecalis* and *E. coli*. It has been shown that *E. faecalis* and *E. coli* can infiltrate and incorporate into a mature *G. vaginalis* biofilm, and even increase the overall bacterial load which can be supported. This raises concerns over cross-infection between bacterial vaginosis and UTIs (Castro J *et al*., 2016). As before, this exacerbation is likely to be caused by the combination of EPS components produced by the different species.

A study of biofilms in untreated water revealed that multispecies biofilms exhibited a greater tolerance to chlorine than multi-species planktonic cultures. Strikingly, the concentration of

chlorine required to kill the bacteria in the multispecies biofilm exceeded the amount of chlorine recommended by the World Health Organisation for water treatment. This study also indicated that the mixed bacterial biofilms were far more resistant to chemicals than monoculture biofilms (Schwering M *et al*., 2013).

1.2.7 Biofilms in Biocatalysis

Due to their self-immobilisation ability and protective properties, biofilms have been explored as potential platforms for biocatalysis. The most successful output for biocatalytic biofilms has been in the treatment of wastewater (Qureshi N *et al*., 2005). Contaminated wastewater contains pollutants such as harmful chemicals and heavy metals which must be removed before the water can be recycled. Multi-species biofilms are capable of resisting these hazards and can convert chemicals into less harmful forms. In addition, the biofilm retains a high volume of cells in the reactor, thereby lengthening the amount of time the reactor can be used before it must be replenished. This increases the economic viability of the system. Examples of functions which multi-species biofilms can fulfil include dechlorination (Horber C *et al*., 1998), denitrification (Jesis JS & Owen RW, 1977) and removal of ammonia (Rosa MF *et al*., 1998) and hydrogen sulphide (Koe LCC & Yang F, 2000).

Single-species biofilms can also be exploited for biocatalytic outputs. Haloalkanes represent a polluting side-product in industrial processes and are toxic to many organisms. *Pseudomonas putida* has shown significant natural resistance to the effects of haloalkanes. An artificial strain of *P. putida* was engineered which produced reliable biofilms, and was successfully used to degrade 1-chlorobutane. Additionally, the process exhibited little effect on the health of the bacteria. Furthermore, the biofilm system outcompeted planktonic cultures, indicating the advantages of biofilm-based biocatalysis (Benedetti I *et al*., 2016).

P. putida biofilms have also been employed to produce the industrially-relevant chemicals 1-octanol and styrene oxide. It was found that the process was suitable for upscaling, and it was estimated that 1000 tons of styrene oxide could be produced per year. Furthermore, this process was found to produce a higher yield and reduced waste when compared to planktonic alternatives. Challenges were encountered in maintaining stable biofilm and productivity, but these were tackled by modulating the supply of nutrients to the bacteria (Gross R *et al*., 2012). Development of this process has continued, with particular focus on the bacterium *Pseudomonas taiwanensis* which exhibits stronger biofilm formation and increased chemical tolerance over *P. putida* (Volmer J *et al*., 2014). Nonetheless, more research is required to move this process from the lab to industry. Due to their intrinsic resistant properties, *Pseudomonas* species have been noted as potential candidates for other harsh biocatalytic processes which might damage other organisms (Nikel PI *et al*., 2016).

Zymomonas mobilis biofilms have been employed in the continuous production of ethanol from non-sterilised starch. *Z. mobilis* biofilms were found to be superior to planktonic cultures, and superior even to the traditional ethanol-producing yeast *S. cerevisiae*. This indicates that biocatalytic biofilms may have lucrative outputs in already-established industrial processes (Kunduru MR & Pometto AL 3rd, 1996).

E. coli has also been investigated for its biocatalytic potential. A biofilm-forming strain of *E. coli* overexpressing tryptophan synthase was successfully used to transform 5-haloindole into 5-halo-L-tryptophan, a chemical precursor, at a higher rate than with planktonic cells. This indicates that whole-cell recombinant enzyme biocatalysis is possible in *E. coli*, a well understood and genetically tractable organism. The work presented in this thesis follows on

from the data obtained in that study (Tsoligkas AN *et al*., 2011, Tsoligkas AN *et al*., 2012, Perni S *et al*., 2013).

1.2.8 *Escherichia coli*

Escherichia coli is a Gram-negative gammaproteobacterium native to the lower intestine of many mammals including humans. Some *E. coli* strains adopt a commensal relationship with their host and do not cause disease. Other strains can cause gastrointestinal, renal or uropathogenic infections (Conway T & Cohen PS, 2015). Lab strains of *E. coli*, descended from human commensal isolates, are used heavily in research, molecular biology and biotechnology as they have been found to be relatively fast, inexpensive and safe to grow and use (Huang CJ *et al*., 2012). *E. coli* is capable of forming robust biofilms in multiple ecological niches such as the gut and urinary tract (biotic surfaces) but can also form biofilms in the environment (abiotic surfaces) as a protective strategy (Beloin C *et al*., 2008). *E. coli* biofilms are formed from a multitude of different components depending on strain and conditions, and have been attributed to multiple modes of stress resistance (Limoli DH *et al*., 2015, Conway T & Cohen PS, 2015).

1.3 *E. coli* Biofilm Components

E. coli forms biofilms in a series of stages, depicted in Figure 1.3. These stages are termed ‘reversible attachment’, ‘irreversible attachment’ and ‘3D maturation’. In brief, cells must find an amenable surface, form a strong attachment to that surface and then form a 3D structure growing out from that surface (Beloin C *et al*., 2008). Cells may detach from a mature biofilm and return to planktonic modes of growth, establishing further biofilms elsewhere, and so

biofilm formation is often termed a cycle (Garrett TR *et al*., 2008). As this work focuses primarily on the growth of biofilms, detachment mechanisms will not be covered in this thesis.

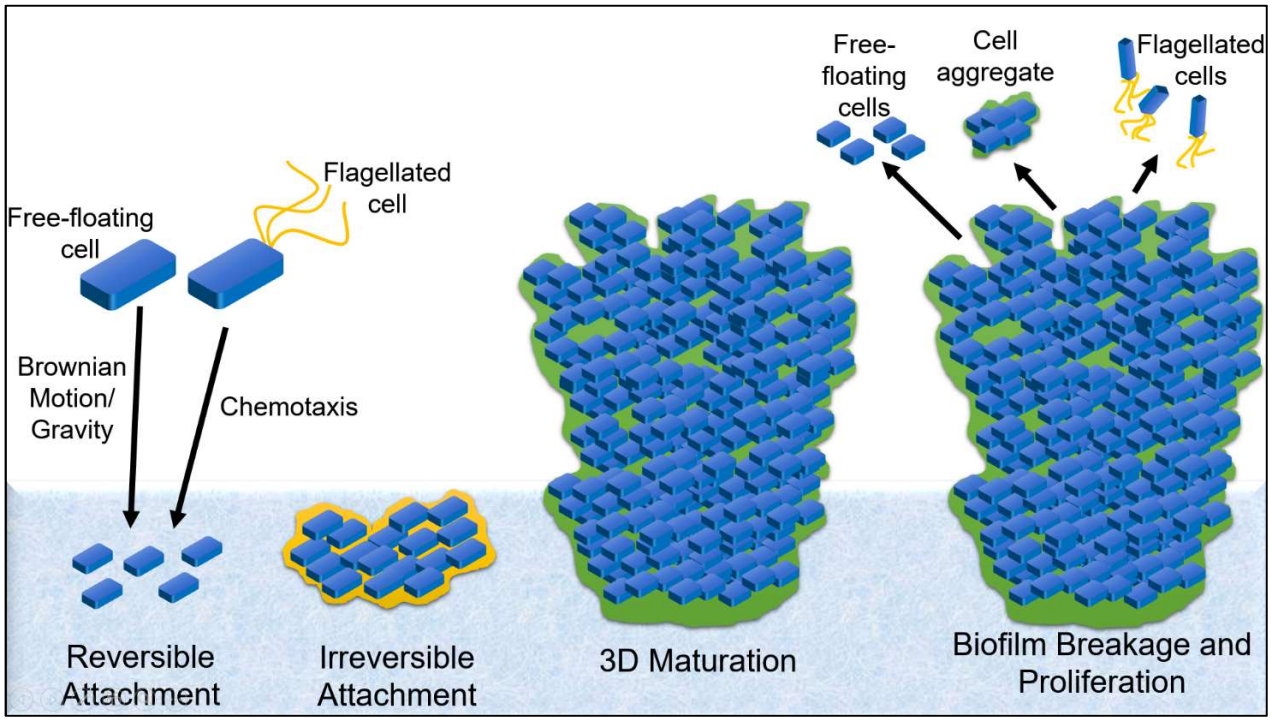

Figure 1.3: *Diagram of* E. coli *biofilm formation. Cells first come into contact with a surface through active or passive means (reversible attachment). The cells then produce proteinaceous EPS (yellow) to anchor the cells to the surface (irreversible attachment). The cells outgrow from the surface forming a 3D structure containing polysaccharide EPS (green) (3D maturation). Cells may then detach from the biofilm through active or passive means, either returning to a planktonic state or forming subsequent biofilms elsewhere (breakage and proliferation).*

1.3.1 Components Involved in Reversible Attachment

In order to form a robust biofilm, *E. coli* cells must first 'find' amenable surfaces by active or passive means. Brownian motion, electrostatic attraction and hydrophobicity allows the opportunity for cells moving in random directions to collide with surfaces and initiate attachment. As this method is based on chance encounter with a surface, it is inefficient and may lead to detachment just as easily. *E. coli* therefore has mechanisms to assist in the initial stages of attachment (Beloin C *et al*., 2008).

Some *E. coli* species produce flagella; proteinaceous, whip-like organelles which propel cells toward stimuli, termed chemotaxis. This allows *E. coli* to detect and move towards surfaces likely to be useful for their survival. As the flagellum may move the cell against flow, this facilitates interaction with surfaces otherwise unreachable through Brownian motion, such as in the folds of the epithelia in the gut (Donlan RM, 2002, Beloin C *et al*., 2008). Flagella have been found to be non-essential in biofilm formation, but provide an advantage in the reversible attachment stage by promoting cell-surface contact (Pratt LA & Kolter R, 1998). In later stages, transcription of flagellar genes is repressed, preventing the formation of new flagella (Guttenplan SB & Kearns DB, 2013). However, flagella have also been found to be an element in mature biofilms, suggesting that they remain part of the biofilm matrix after attachment (Serra DO *et al*., 2013). The exact role of flagella during biofilm growth is therefore unclear.

1.3.2 Components Involved in Irreversible Attachment

Reversible attachment mostly consists of transient, weak interactions between cells and a surface. Irreversible attachment occurs when the bacterium produces materials which stabilise interactions between the cell and the surface, thereby 'anchoring' the cell. In *E. coli*,

irreversible attachment is facilitated by protein factors. A list of the primary components involved in *E. coli* biofilm formation can be found in Table 1.1.

Table 1.1.: E. coli *biofilm components, properties and purpose in biofilm formation.*

	Description	**Interaction**	**Purpose**	**Biofilm Essential?**	**References**
Flagella	Cell-anchored long protein structure	Cell-surface?	Motility, chemotaxis	No	Pratt LA & Kolter R, 1998
Curli Fimbriae	Functional protein amyloid	Cell-cell Cell-surface	Aggregation, surface attachment	Essential for initial attachment	Barnhart MM & Chapman MR, 2010
Type-1 Pili	Cell-anchored long protein structure	Cell-cell Cell-surface	Aggregation, surface attachment	Essential for initial attachment	Schilling JD *et al*., 2001
F Pili	Cell-anchored long protein structure	Cell-cell	Aggregative, horizontal gene transfer	No	May T & Okabe S, 2008
Ag43	Cell-surface displayed protein	Cell-cell	Aggregative	No	van der Woude MW & Henderson IR, 2008
Colanic Acid	Cell-associated, negatively-charged heteropolysaccharide	Cell-cell	Architectural	Essential for 3D development	Limoli DH *et al*., 2015
Cellulose	Secreted, neutral homopolysaccharide	Cell-cell Cell-epithelium	Aggregative, protective	Essential in-host only	Serra DO *et al*., 2013
PNAG	Secreted, positively-charged homopolysaccharide	Cell-cell	Aggregative, Architectural, protective	Essential for 3D development	Limoli DH *et al*., 2015

1.3.2.1 Curli Fimbriae

Curli fimbriae (or thin aggregative fimbriae) are highly aggregated and hydrophobic extracellular amyloid structures which facilitate attachment to hydrophobic surfaces such as laminin in the gut epithelia as well as plastics such as polystyrene (Beloin C *et al*., 2008). Curli aggregates are similar to amyloid accumulations in human neural cells which lead to illnesses such as Alzheimer's disease and Parkinson's disease. However, curli is classified as a 'functional amyloid' which has a defined purpose in bacterial biofilm growth (Evans ML *et al*., 2015). The forces involved in curli amyloid aggregation are very strong and difficult to break with mechanical stress, and have been shown to possess resistance to cleaning chemicals and solvents, suggesting that curli is important in resisting mechanical stress and industrial cleaning techniques (Nguyen PQ *et al*., 2014). Curli produced by an individual cell can aggregate with curli from other cells, thereby forming an aggregate on a surface (Beloin C *et al*., 2008).

The production of curli is facilitated by two operons, *csgBAC* and *csgDEFG*. The regulation of these operons will be discussed in Section 1.4.3. Curli fimbriae are heteropolymers composed of CsgB and CsgA, the minor and major subunits respectively (Barnhart MM & Chapman MR, 2006). CsgB and CsgA are coexpressed with CsgC. CsgC interacts with CsgB and CsgA to prevent amyloid formation in the cytoplasm which would be detrimental to cell function (Evans ML *et al*., 2015). CsgB and CsgA are transported into the periplasm via the Sec apparatus. A nonameric protein complex CsgG forms a diffusion channel in the outer membrane through which CsgB and CsgA are exported. CsgE is a periplasmically-localised protein which appears to have an essential role in mediating this export, potentially as a curli-specific chaperone, but this role has yet to be determined (Shu Q *et al*., 2016). This process is also assisted, through unknown means, by CsgF which is in direct contact

with CsgG. (Nenninger AA *et al*., 2009). Once outside the cell, CsgB acts as a nucleator to induce CsgA amyloid polymerisation (Hammer ND *et al*., 2007).

1.3.2.2 Type 1 Pili

Type 1 pili are long, needle-like extracellular structures of up to 3 μm in length formed of multiple Fim proteins. The tip of a type 1 pilus displays a lectin, FimH, which facilitates attachment to sugar molecules such as mannose. This allows *E. coli* cells to attach to mannose-presenting eukaryotic cells in a host, as well as mannose-containing EPS in biofilms (Beloin C *et al*., 2008). Type 1 pili have been found to be essential for attachment to abiotic surfaces and subsequent biofilm formation, suggesting additional roles than just mannose interaction (Pratt LA & Kolter R, 1998). Type 1 pili genes are expressed from the *fimAICDFGH* operon. This operon is regulated by the action of the recombinases FimB and FimE. FimB and FimE are responsible for inverting a 314 bp section of DNA preceding *fimA*, thereby switching the *fimAICDFGH* operon to an ON or OFF phase (Gally DL *et al*., 1996). This switching determines whether the individual bacterium will produce Type 1 pili, enabling both phenotypes to exist in the same clonal population. This behaviour may allow an *E. coli* population to rapidly adapt to new conditions, depending on whether Type 1 pili-mediated biofilm formation is desirable to the population. FimB is downregulated in stationary phase, indicating temporal control (Dove SL *et al*., 1997). To theorise, the majority of cells which have reached the irreversible attachment stage of biofilm development will be in the ON phase. Further recombination to the OFF phase would be detrimental during biofilm maturation, therefore stationary phase processes active during biofilm maturation repress FimB. This appears to represent a ‘commitment’ to the biofilm mode of growth, and reduced

fim gene variation in the early biofilm stages. Whether *fim* genes continue to be turned on in the later maturation stages is unknown.

1.3.2.3 Antigen 43

Antigen 43 (Ag43) is a mediator for autoaggregation in *E. coli*. Ag43 consists of an α and β domain; the β domain autotransports and anchors the α domain, which is displayed on the surface of the *E. coli* cell (van der Woude MW & Henderson IR, 2008). Ag43 proteins displayed on an *E. coli* cell bind strongly to Ag43 proteins on other cells, thereby forming a close-contact association between the two cells, and allowing the establishment of cellular aggregates in suspension. This aggregation also appears to impair motility (Ulett GC *et al*., 2006). Ag43 also plays an important role in biofilm formation by mediating close interactions between *E. coli* cells in a similar way to the action of curli-mediated aggregation. However, Ag43 does not appear to be involved in the interaction between *E. coli* cells and the gut epithelia, in contrast to curli fimbriae, and appears only to promote cell-cell interaction (de Luna Md *et al*., 2008). Phase variation allows the *E. coli* cell to switch the Ag43 gene, termed *flu*, ON or OFF randomly within a population. After replication, the *flu* promoter will either recruit the methylase Dam or the transcriptional regulator OxyR. Dam methylates adenosine bases in repeat GATC sequences in the *flu* promoter, preventing OxyR binding and leaving the *flu* gene ON. Conversely, binding of OxyR to an unmethylated *flu* promoter prevents the action of Dam methylase, turning the gene OFF. This activation or repression is permanent until the cell replicates, thereby allowing switching again. Switching has been shown to occur once per 1000 cells per generation. Thus, any population of *E. coli* cells may contain ON and OFF cells. Biofilms contain a high proportion of ON cells and therefore the formation of biofilm is an ON-selective process (Chauhan A *et al*., 2013). The purpose of this phase

variation may be similar to the phase variation present in type 1 pili regulation; to allow rapid variation of a population for the purposes of survival (van der Woude MW & Bäumler AJ, 2004).

1.3.2.4 F Pili

F pili (or conjugation pili) allow horizontal gene transfer between bacteria by forming a hollow pilus between cells through which DNA can be transferred. This process allows the rapid transfer of genes within a population, including genes for antibiotic resistance. The apparatus for this process is encoded on the F plasmid which is found in many commensal isolates (Silverman PM & Clarke MB, 2009). However, many lab strains of *E. coli* have been 'cured' of the F plasmid, i.e. lost through several generations of growth in lab conditions, and so cannot perform this transfer (Blattner FR *et al*., 1997). Interestingly however, when the F plasmid is transformed into a poor biofilm-forming lab strain such as K-12, a thicker and more complex biofilm can be produced than without the plasmid. This was found to be due to the stimulation of curli and colanic acid synthesis (colanic acid will be discussed in Section 1.3.3.1). This perhaps sheds light on differences in biofilm development between lab strains and isolates, and the relatively poor biofilms produced by K-12 strains. F pili may represent a structural intercellular element which promotes cell-cell interaction in a similar way to curli and Ag43 autoaggregation, although due to the absence of F pili in lab strains this has not been extensively studied (May T & Okabe S, 2008).

1.3.3 Components Involved in Biofilm Maturation

Biofilm maturation is the development of a three-dimensional biofilm structure, primarily facilitated by polysaccharide factors. Polysaccharides are generally more stable than protein

factors, relying on permanent covalent bonds instead of transient protein interactions, and therefore allow the biofilm to remain intact for longer periods of time (Flemming H-C & Wingender J, 2010). A list of the primary polysaccharide components involved in *E. coli* biofilm formation can be found in Table 1.1.

1.3.3.1 Colanic Acid

Colanic acid (CA) is a negatively-charged heteropolysaccharide composed of galactose, glucuronic acid, fucose and glucose. CA has been noted as being essential to the development of 3D structure in *E. coli* biofilms (maturation), but not involved in initial attachment to surfaces (Danese PN *et al*., 2000, Limoli DH *et al*., 2015). Colanic acid has been shown to protect cells against desiccation, likely by allowing the entrapment of water in the biofilm (Ophir T & Gutnick DL, 1994). The operon encoding the apparatus for colanic acid production is a set of 19-21 genes (reports vary), predicted to be involved in incorporation and polymerisation of saccharide subunits, and transport of the polymer out of the cell (Stevenson G *et al*., 1996). The operon is upregulated by the heterodimer RcsAB, which is in turn regulated by the Rcs phosphorelay, which will be discussed in Section 1.4.6. CA is produced at temperatures below 37°C, indicating an importance to environmental biofilm formation as opposed to biofilm formation in a host (Nassif X *et al*., 1989). CA production has also been shown to be stimulated by the presence of the F plasmid, as with curli, suggesting similar paths of regulation (May T & Okabe S, 2008).

1.3.3.2 Cellulose

Cellulose is a neutral-charge homopolysaccharide of glucose units. Cellulose is the most abundant polymer found on Earth due to its ubiquity in plant cell walls. However, cellulose

is also produced by many bacterial species including *E. coli*. Cellulose has been noted as having a high tensile strength, thereby providing mechanical rigidity to the biofilm (Limoli DH *et al*., 2015). In contrast, cellulose has been shown to provide mechanical elasticity to macrocolony biofilms (large colonies grown on agar plates) (Serra DO *et al*., 2013). Cellulose enhances binding of *E. coli* cells to the host epithelium in the gut (Limoli DH *et al*., 2015). The operons which produce the apparatus necessary for cellulose production are *yhjR-bcsQABZC* and *bcsEFG* (Römling U & Galperin MY, 2015). In *E. coli* lab strains such as K-12, a point mutation has occurred in the *bcsQ* gene creating a premature transcriptional stop site and preventing the expression of downstream genes such as the cellulose synthase subunits BcsA and BcsB. K-12 strains therefore do not produce cellulose (Serra DO *et al*., 2013). As K-12 strains form biofilms outside of a host regardless, cellulose is dispensable for biofilm formation in the environment. Regulation of cellulose synthesis appears to be mainly post-translational, and is dependent on the bacterial messenger molecule cyclic-diguanosine monophosphate, which will be discussed in Section 1.4.3 (Simm R *et al*., 2004).

1.3.3.3 PNAG

Poly-N-acetylglucosamine (PNAG), also termed polysaccharide intercellular adhesin (PIA), is a positively-charged polymer of N-acetylglucosamine subunits. PNAG is essential for biofilm formation in *E. coli* and provides structural cohesion by both cell-cell and cell-surface interaction. PNAG has also been shown to protect against host immune responses and resist antimicrobial drugs (Arciola CR *et al*., 2015). PNAG is polymerised by PgaC and PgaD in a c-di-GMP dependent manner, then partially deacetylated and exported by PgaB through the outer membrane porin PgaA (Little DJ *et al*., 2014). The *pgaABCD* operon is positively

regulated by NhaR in response to sodium-binding, and negatively regulated by OmpR and CsrA (Goller C *et al*., 2006).

1.4 Regulation of Biofilm Formation

1.4.1 c-di-GMP

An essential element in *E. coli* biofilm formation is the bacterial second messenger cyclic dimeric guanosine monophosphate (c-di-GMP) (Hengge R, 2009, Römling U *et al*., 2013). c-di-GMP is synthesised and degraded by two classes of enzyme – diguanylate cyclases (DGCs) and c-di-GMP-specific phosphodiesterases (PDEs) respectively. DGCs and PDEs, working in tandem or globally, fine-tune the level of c-di-GMP within the cell depending on various stimuli. DGCs and PDEs are highly conserved between species highlighting their importance in cellular function. Concentrations of this molecule increase upon entry into stationary phase, leading to the downregulation of motility-related flagellar genes and upregulation of biofilm-related genes (Figures 1.4, 1.5) (Spurbeck RR *et al*., 2012). This increase triggers biofilm formation in *E. coli* (Lindenberg S *et al*., 2013).

1.4.2 DGCs and PDEs in *E. coli*

Lab strain *E. coli* K-12 features 14 identified DGC genes and 17 identified c-di-GMP-specific PDE genes. Other strains of *E. coli* may feature other DGCs and PDEs, suggesting that the fine-tuning of c-di-GMP may be dependent on the ecological niche in which the strain resides. DGCs contain a consensus GGDEF amino acid domain which synthesises c-di-GMP from 2 molecules of guanosine triphosphate (GTP). PDEs contain a consensus EAL amino acid domain which degrades c-di-GMP into pGpG. pGpG is then converted by the

cell into 2 molecules of guanosine monophosphate (GMP) for recycling (Hengge R, 2009). Some proteins feature non-functional or degenerate GGDEF or EAL sequences, resulting in a loss of enzymatic activity. The way in which DGCs and PDEs interact with each other and modulate c-di-GMP activity depends greatly on the pathway in question. Some PDEs have been classified as ‘trigger enzymes’ which release repression of pathways when the correct stimulus is detected, allowing rapid initiation of biofilm formation under certain conditions (Hengge R, 2016).

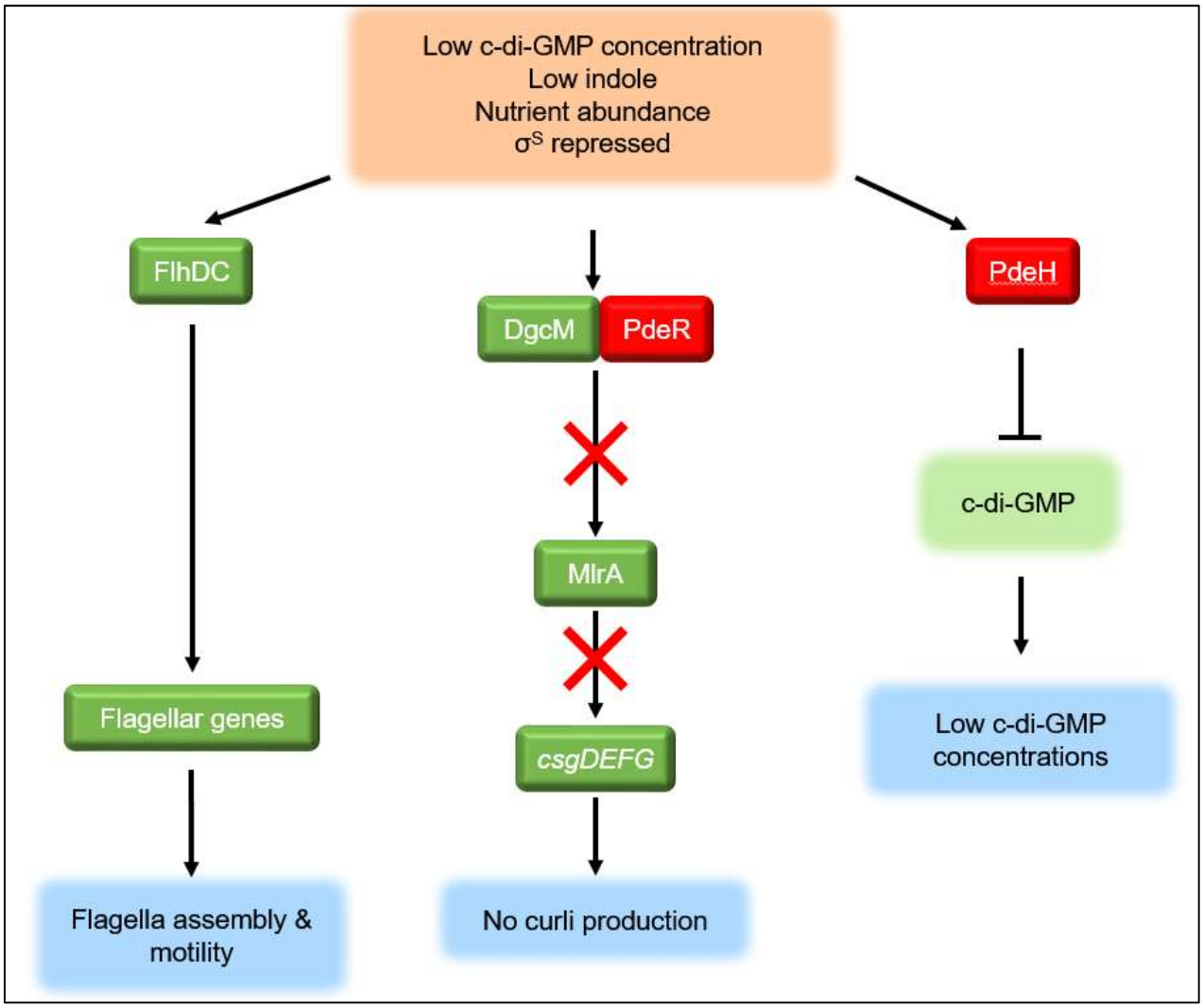

Figure 1.4: *Regulation of* E. coli *K-12 biofilm genes during planktonic exponential phase growth. Abundant resources prevent the activation of biofilm-related genes and maintain motility. c-di-GMP concentrations are low during this phase due to degradation by PdeH. DgcM is repressed by direct interaction with PdeR. sRNA regulation has been omitted for clarity. Green boxes represent factors which positively affect biofilm formation. Red boxes represent factors which negatively affect biofilm formation. Peach boxes represent stimuli which affect biofilm formation. Blue boxes represent the results of these regulatory processes.*

1.4.3 CsgD

CsgD can perhaps be regarded as the ‘master switch’ of biofilm formation in *E. coli*. CsgD is a transcriptional regulator at the centre of a complex network of pathways which all influence the production of biofilm (Figure 1.5). As such, CsgD has been shown to be essential to biofilm formation in *E. coli* (Liu Z *et al*., 2014). CsgD activates the production of the curli subunits from the *csgBAC* operon. CsgD also activates the expression of DgcC (AdrA) which positively regulates cellulose production. AdrA produces c-di-GMP which binds the cellulose synthase complex (BcsA-BcsB), leading to cellulose synthesis (Gualdi L *et al*., 2008). CsgD is more highly expressed in the mid-exponential growth phase but activation of curli expression occurs during stationary phase (Brombacher E *et al*., 2003). Multiple stimuli have been identified for increased curli production, including carbon starvation. CRP-cAMP has been shown to directly activate the expression of CsgD in low glucose conditions, and therefore abundant glucose represses CsgD and curli production (Hufnagel DA *et al*., 2016). In lab conditions, *E. coli* does not produce curli above 32°C; nevertheless curli is still produced by *E. coli* in the mammalian gut which has an internal temperature of approximately 37°C (Olsén A *et al*., 1993). This may represent distinct biofilm formation strategies for cells outside or inside a host (Barnhart MM & Chapman MR, 2006). The transcription factor MlrA directly activates CsgD expression. MlrA is controlled by a trigger PDE complex consisting of DgcM and PdeR. PdeR binds to DgcM when cellular c-di-GMP concentration is low, preventing DgcM from post-translationally activating MlrA (Figure 1.4). When c-di-GMP levels increase, such as in the entry to stationary phase, PdeR begins to bind and degrade c-di-GMP, releasing DgcM and allowing it to bind and activate MlrA and therefore the *csgDEFG* operon (Figure 1.5). Released DgcM also produces c-di-GMP, creating a positive feedback loop (Hengge R, 2016). The *csgDEFG* operon is directly

activated by the EnvZ-OmpR two-component signal transduction system (discussed in Section 1.4.4) (Jubelin G *et al*., 2005). The *csgDEFG* operon is fairly well defined, but possesses myriad overlapping regulatory sites. This complexity indicates that its expression level can be fine-tuned depending on environmental conditions.

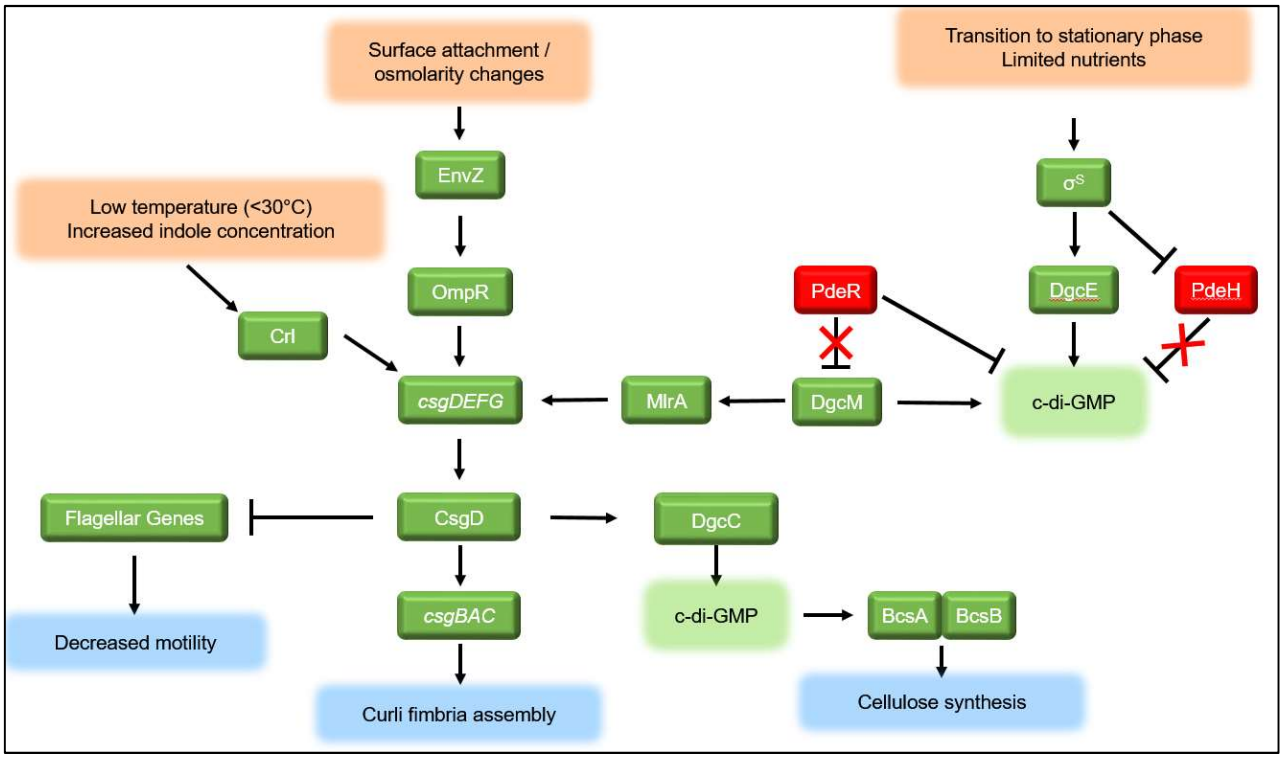

***Figure 1.5**: Biofilm gene regulation during stationary phase and leading into irreversible attachment. As resources are consumed and cell density increases,* E. coli *cells enter stationary phase. The stationary phase sigma factor, σ^S, represses PdeH and activates DgcE, leading to an increase in c-di-GMP concentrations. c-di-GMP occupies PdeR, releasing repression of DgcM. DgcM binds MlrA and activates the expression of CsgD, leading to curli and cellulose expression and flagellar gene repression. CsgD expression is also increased by OmpR and the sigma factor modulator Crl. sRNA regulation has been omitted for clarity. Green boxes represent factors which positively affect biofilm formation. Red boxes represent factors which negatively affect biofilm formation. Peach boxes represent stimuli which affect biofilm formation. Blue boxes represent the results of these regulatory processes.*

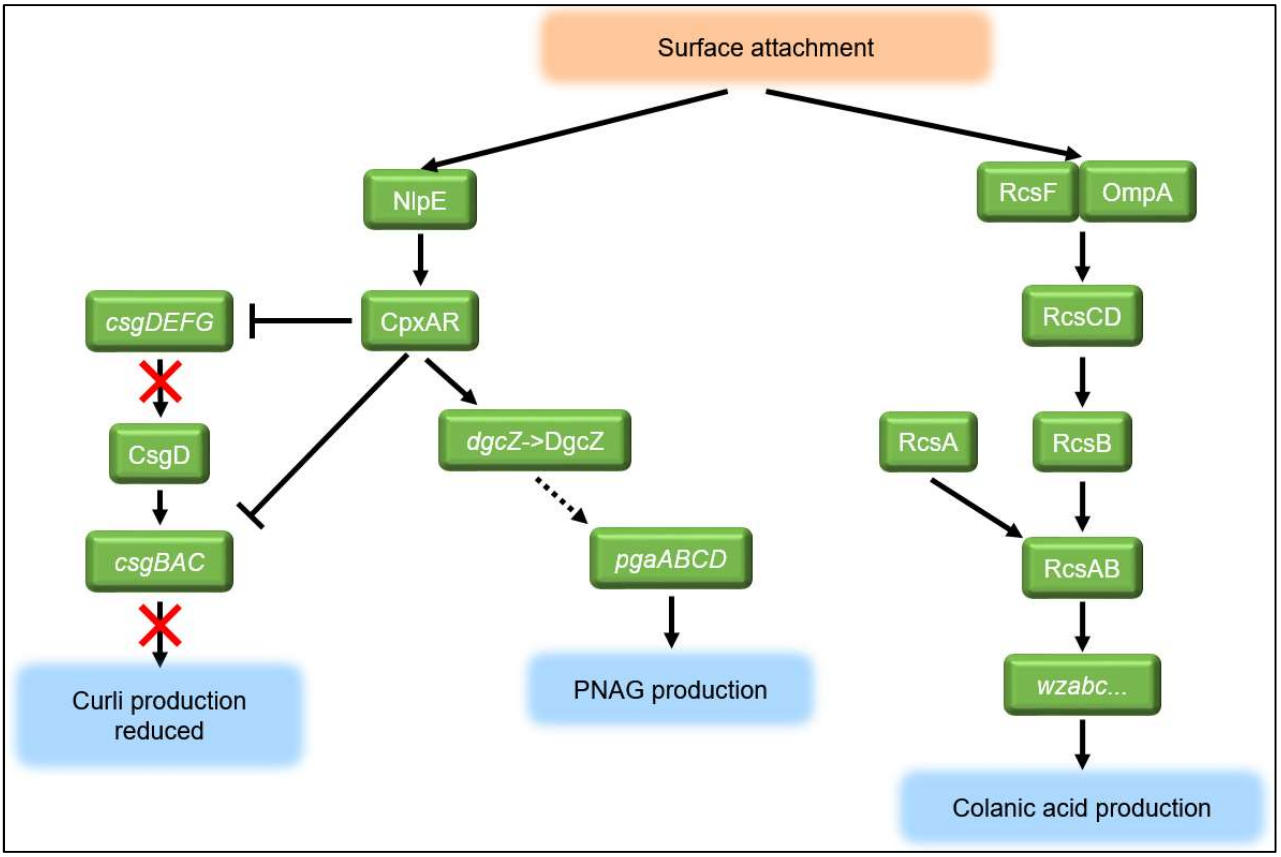

Figure 1.6: *Regulation of biofilm genes during maturation. Surface attachment is detected by NlpE and RcsF/OmpA through uncharacterised mechanisms. NlpE activates the CpxAR system leading to the repression of curli genes and the activation of PNAG production. RcsF/OmpA activates the Rcs phosphorelay, leading to colanic acid production. sRNA regulation has been omitted for clarity.*

1.4.4 The EnvZ-OmpR Two-Component Signal Transduction System

Through unknown mechanisms, the inner membrane protein EnvZ senses changes in osmolarity affecting the cell. EnvZ phosphorylates the transcriptional regulator OmpR. OmpR activates the expression of CsgD, thereby leading to curli production (Jubelin G *et al*., 2005). It has been shown that a mutation in EnvZ (*envZP41L*) increases the efficiency of phosphorylation of OmpR and leads to increased colonisation in a mouse intestine (Adediran J *et al*., 2014). In addition, a mutation in OmpR (termed *ompR234* allele; *ompRL43R*) leads to increased biofilm formation on glass and plastic, theorised to be due to more efficient activation of the CsgD promoter (Vidal O *et al*., 1998). These observations highlight the importance of EnvZ-OmpR activation in biofilm formation, and indicate that changes in osmolarity play a role in biofilm formation.

1.4.5 NlpE and the CpxAR Two-Component Signal Transduction System

The inner-membrane protein CpxA senses and responds to various stimuli including surface adhesion and changes in pH (Batchelor E *et al*., 2005). Detection of surface adhesion requires the outer membrane protein NlpE, but the mechanisms which elicit this response are unclear (Hirano Y *et al*., 2007). CpxA, when stimulated, phosphorylates the transcriptional regulator CpxR. CpxR has a wide regulon including direct roles in activating the multiple antibiotic resistance genes (such as *marA*) and multidrug efflux pumps (Weatherspoon-Griffin N *et al*., 2014). CpxR binds several repression sites in the *csgDEFG* and *csgBAC* promoters. Additionally, CpxR activates the expression of the small RNA RprA which represses *csgD* translation, leading to reduced curli production. These repressions limit production of curli by both pre- and post-transcriptional means, perhaps to prevent toxic curli overproduction (Pringent-Combaret C *et al*., 2001). NlpE and CpxAR positively regulate

the DGC DgcZ, which has been shown to increase the production of PNAG, thus promoting PNAG-mediated 3D maturation (Figure 1.6) (Lacanna E *et al*., 2016). To theorise, CpxR may facilitate temporal control of biofilm component production. By reducing the expression of components involved in irreversible attachment (i.e. curli) and increasing those involved in 3D maturation (PNAG), CpxR triggers the transition from irreversible attachment to 3D maturation.

1.4.6 The RcsCDB Phosphorelay

The Rcs phosphorelay activates in response to changes in osmolarity and cell membrane stress. The outer membrane protein RcsF, in conjunction with OmpA, has also been shown to directly activate the Rcs phosphorelay during envelope stress, though it is unknown if this is the sole activator of the system (Cho SH *et al*., 2014). The Rcs phosphorelay transfers a phosphate group from RcsC to RcsD and then to RcsB. Homodimers of phosphorylated RcsB activate operons involved in envelope stress responses (such as *rpoE*), as well as the cell division proteins FtsA and FtsZ (Majdalani N & Gottesman S, 2005). RcsB may also form heterodimers with specific stress response regulators such as GadE to activate expression of acid stress response genes (Johnson MD *et al*., 2011). With relevance to biofilm formation, RcsB can form a heterodimer with RcsA. RcsAB has an undefined role in repressing *csgDEFG*, thereby reducing curli production, but also in repressing flagellar genes via *flhDC* (Vianney A *et al*., 2005, Fredericks CE *et al*., 2006). These roles appear counterproductive to each other, but interestingly, RcsAB also activates expression of the colanic acid synthesis operon thereby stimulating production of an essential biofilm maturation polysaccharide (Figure 1.6). Furthermore, RcsAB also activates expression of a poorly defined operon *yjbEFGH* which appears to synthesise a polysaccharide not yet

characterised in *E. coli* (Ferrières L *et al*., 2007). The repression of curli production, and the stimulation of polysaccharide production, may indicate that RcsAB provides temporal regulation of biofilm formation, signalling the cell to switch from producing irreversible attachment components to producing maturation polysaccharides, in a similar manner to CpxR.

1.4.7 Small RNAs Affecting CsgD Expression

CsgD expression is regulated by several small RNA sequences which bind to the 5' untranslated region (5' UTR) of the *csgDEFG* transcript (Chambers JR & Sauer K, 2013). RprA, as previously mentioned, is activated by CpxR which also represses the *csgD* promoter. This provides a pre- and post-transcriptional reduction in *csgD* transcripts to reduce overall curli accumulation (Mika F *et al*., 2012). McaS both represses *csgD* and activates *flhDC*, thereby suppressing biofilm formation and activating motility. In rich medium, McaS is highly expressed in the transition from exponential to stationary phase, while in minimal medium, maximal expression occurs in exponential phase (Thomason MK *et al*., 2012). This perhaps explains why biofilms are more readily formed in minimal medium as opposed to nutrient-rich environments, as McaS may repress the transition into the biofilm mode of growth. OmrA and OmrB are OmpR-activated sRNAs which downregulate both curli and flagella synthesis, binding in the same upstream promoter elements as McaS. OmrA and OmrB appear to downregulate the incorporation of outer membrane proteins such as OmpT, in response to environmental stimuli such as changes in osmolarity as evidenced by their activation by OmpR (Bak G *et al*., 2015). This process may be to prevent overloading of the outer membrane with transport proteins. GcvB represses a number of amino acid transporters as well as *csgD*. The role in the modulation of biofilm formation is unclear, but,

as it is produced when amino acids are abundant, may restrict biofilm formation in rich media (Bak G *et al*., 2015).

1.4.8 Indole

Indole is an exported molecule produced by many species of bacteria which has multiple effects on growth and biofilm formation. In *E. coli*, indole is synthesised by the enzyme TnaA which degrades tryptophan into indole, pyruvate and ammonia (Li G & Young KD, 2015). *E. coli* is capable of tolerating high extracellular concentrations of indole, up to around 5mM, and studies have shown that in minimal medium any exogenous tryptophan not needed by the cell for protein synthesis is converted directly into indole (Li G & Young KD, 2013). While pyruvate can be used as a carbon source, indole is actively pumped out of the cell as it cannot be degraded by *E. coli*.

Expression of TnaA, and therefore production of indole, is activated in low glucose conditions by CRP-cAMP, in order to liberate energy from tryptophan when carbohydrate concentrations are low (Li G & Young KD, 2014). In addition, the expression of TnaA is dependent on σ^S and is therefore most highly expressed at the entry into stationary phase (Lacour S & Landini P, 2004). TnaA expression is also upregulated by the TorSTR phosphorelay, in response to the detection of trimethylamine N-oxide (TMAO) (Bordi C *et al*., 2004). TMAO is produced as a by-product of the breakdown of choline and carnitine, often found in meat as it passes through a mammalian digestive tract (Koeth RA *et al*., 2013). The detection of TMAO therefore may signal *E. coli* to produce TnaA to break down excess tryptophan released from the digesting meat proteins. The subsequent production of indole may only be a by-product of this degradation, but indole nevertheless has multiple striking effects on *E. coli* metabolism.

Indole directly affects cell division and growth rate. Indole has been shown to be an ionophore; disrupting the proton gradient across the cytoplasmic membrane. Loss of this proton gradient disrupts the function of MinD, responsible for regulating the formation of the FtsZ ring at the mid-cell, thus restricting cell division. Increasing indole concentrations therefore reduce the growth rate of an *E. coli* population (Chimerel C *et al*., 2012).

TnaA has been shown to directly bind an sRNA produced by ColE1 plasmids, Rcd. Rcd plays a role in stabilising the ColE1 plasmid copies by delaying cell division until all of the plasmids have been properly replicated. Rcd binds TnaA and increases the production of indole by modulating affinity for the substrate tryptophan. This increase in intracellular indole slows cell growth during exponential phase, thereby allowing efficient plasmid replication (Chant EL & Summers DK, 2007, Field CM & Summers DK, 2012). Similar mechanisms may be present in other plasmids to allow efficient replication, although this has not been proven.

In addition to its importance in metabolic modulation, indole is also essential for biofilm formation in *E. coli*. At 30°C, indole activates the expression of Crl, which binds to the RNAP holoenzyme. Crl skews the sigma factor preference of RNAP towards σ^S, thereby increasing expression of σ^S- and stationary phase-related genes such as *csgD* and therefore promotes biofilm formation (Lelong C *et al*., 2007). Promotion of σ^S via Crl leads to the expression of stress response genes such as multidrug transporter genes, and therefore increasing indole concentrations elicit these effects (Hu M *et al*., 2010).

Since metabolic regulation, reduced growth rates, plasmid retention and antibiotic resistance are all hallmarks of biofilms, indole plays an indispensable role in biofilm formation, maturation and survival (Hu M *et al*., 2010).

The question of whether indole should be classified as an inter-cell signalling molecule for *E. coli* has been debated (Hu M *et al*., 2010, Kim J and Park W, 2015). Indole has multiple distinct effects on the growth, metabolism and phenotypes of *E. coli* populations, and is essential in eliciting these effects in a growth-dependent manner. On the other hand, some researchers have noted that the production of indole may only be regarded as a by-product of tryptophan degradation, and levels of indole used in experiments are much higher than would be encountered in natural growth (Kim J and Park W, 2015). Much of the debate stems from the differences in intracellular and extracellular indole concentrations, which have been found to differ greatly over growth phases. Research has found that a high intracellular concentration of indole (~60 mM) can be found only at the entry into stationary phase, before the concentration equilibrates with the lower extracellular concentration (0.5 – 1 mM) (Gaimster H *et al*., 2014, Gaimster H & Summers DK, 2015). More research is clearly needed to understand the natural process of indole concentration variation, but its necessity in eliciting biofilm formation cannot be ignored. An interesting observation is that indole effects on flagellar genes and cell division are more pronounced at 30°C than 37°C, with the inverse being true of the quorum sensing molecule AI-2 (Section 1.4.9). As indole affects a similar subset of genes to AI-2 (biofilm and motility genes), indole may in fact be classified as a quorum sensing molecule, although this has not been confirmed (Lee J *et al*., 2008).

1.4.9 Quorum Sensing

Quorum sensing is the ability of a cell to detect the population density of cells in the same environment, either its own population or other species, and modulate its activity accordingly. *E. coli* produces a quorum sensing molecule known as autoinducer-2 (AI-2).

AI-2 is produced by LuxS, the expression of which is activated by the BarA-UvrY two-component system (Mitra A *et al*., 2016). AI-2 appears to have a greater effect at 37°C than at 30°C, indicating that this molecule is produced when *E. coli* is inside a host organism. AI-2 affects pathways involved with motility and virulence, though whether this effect is direct or indirect is unclear (Lee J *et al*., 2008). One interesting determination is that *E. coli* can move toward high concentrations of AI-2 by chemotaxis (Hegde M *et al*., 2011). AI-2-mediated chemotaxis increases aggregation of cells and also increases biofilm formation (Laganenka L *et al*., 2016). Maximal production of AI-2 occurs during late exponential phase, which is consistent with biofilm regulation mechanisms activating in the entry to stationary phase, thereby promoting the cells to be in close proximity before biofilm formation begins (Ren D *et al*., 2004). As these experiments were performed with free-floating aggregated cells, an interesting question may be whether surface-adhered cells in reversible or irreversible attachment stages use AI-2-mediated chemotaxis to attract and recruit further cells to join the nascent biofilm.

Many bacteria, but not *E. coli*, produce N-acyl-L-homoserine lactones (AHLs), another group of quorum sensing molecules. AHL signalling is predominantly present in Gram-negative bacteria such as *P. aeruginosa* where it is essential for monoculture biofilm formation (Rasamiravaka T *et al*., 2015). Although *E. coli* lacks the enzymes required to produce AHLs, the species is able to respond to the signalling molecule, suggesting that AHLs are additionally used for interspecies signalling (Van Houdt R *et al*., 2006).

Responses to AHL quorum sensing signals are not fully understood in *E. coli*. An AHL-detecting transcription factor has been discovered, termed SdiA (Van Houdt R *et al*., 2006). AHLs have been theorised to have a stabilising effect on the structure of SdiA, rather than affecting DNA-binding (Nguyen Y *et al*., 2015). SdiA activation leads to slower cell division,

mirroring the effect of indole (Shimada T *et al*., 2014). In addition, SdiA positively regulates the *uvrY* gene, which as previously stated activates the expression of LuxS and the production of AI-2 (Suzuki K *et al*., 2002). This suggests that quorum-sensing molecules from other species have a pro-biofilm effect on *E. coli* cells, and indeed the presence of AHL-producing bacteria such as *P. aeruginosa* has been shown to improve biofilm growth in mixed biofilms (Culotti A & Packman AI, 2014). This may indicate a natural tolerance for multi-species biofilm growth.

Most quorum sensing molecules do not display direct effects on cell metabolism, and so indole is not directly considered to be a quorum sensing molecule. Nevertheless, indole has effects on quorum sensing-related pathways (Lee J *et al*., 2007). The AHL-sensing protein SdiA regulates genes which have been shown to be affected by indole concentration, such as motility and biofilm genes, but it has been found that the protein itself does not respond directly to indole, and its activity is repressed by high concentrations of indole. In addition, exogenous indole inhibited AHL detection by SdiA, suggesting that indole and AHL compete for binding to SdiA. It has been theorised that the effect of indole signalling on SdiA-related genes may be indirect, and an uncharacterised intermediary may be present (Sabag-Daigle A *et al*., 2012).

The similar responses observed as a result of AHL or indole binding may represent a mechanism for the bacteria to ‘decide’ what type of biofilm it will need to form to increase survivability in that environment. In the example of *E. coli* and *P. aeruginosa* mixed biofilm, *P. aeruginosa* produces AHLs which bind to *E. coli* SdiA and therefore signal that another species is present and to form a cooperative biofilm accordingly (Culotti A & Packman AI, 2014). Interestingly, indole produced by *E. coli* also reduces the production of *P. aeruginosa* anti-microbial toxins such as pyocyanin, therefore allowing biofilm formation with *P.*

aeruginosa without being harmed by *P. aeruginosa* toxins (Chu W *et al*., 2012). In an *E. coli* monoculture, AHLs are not present and therefore indole and AI-2 are the prevailing molecules promoting monoculture biofilm formation. These observations indicate that quorum sensing is a positive force in biofilm formation and overall survival on a surface.

1.5 Experimental Models for Biofilm Growth

As they are generally regarded as detrimental to industry and medical settings, biofilms have received a significant level of attention in the scientific community. Many of these studies concern the removal of biofilms from real-life systems, and little research has gone into creating systems to form large amounts of functional biofilm material in the lab. Traditional protocols for biofilm development either involve small-scale replicable growth environments such as microtiter plates, or are *in situ* models to mimic an existing system, such as a catheter or a flow cell.

1.5.1 Microtiter Plates

Microtiter plates are plastic or glass trays with multiple 'wells' to contain separate experiments. Microtiter plates are typically inexpensive and disposable. Wells can be coated with different materials and ligands and can have different shapes and sizes depending on experimental necessity. In biofilm studies, this allows the researcher to determine the effect of many different conditions on biofilm development in the same experiment. The ability to perform multiple repeat experiments also increases the overall level of accuracy. Microtiter plates are often used in medical biofilm research, as attachment to plastic or glass can be a useful indicator of biofilm development, and can be quantified using simple techniques such

as crystal violet staining (Macia MD *et al*., 2014, Coffey BM & Anderson GG, 2014). The disadvantages of this model, aside from the small-scale of biofilm development, are that the size and shape of the wells does not allow visualisation of the biofilm by microscopic methods, as much of the biofilm adheres to the walls of the wells at the air liquid-interface (O'Toole GA, 2011).

1.5.2 Calgary Biofilm Device

The Calgary Biofilm Device consists of a microtiter plate with pegs attached to the lid. Biofilm is formed on the pegs as well as the well walls. The lid and pegs can then be transferred to another plate, allowing easy manipulation and movement of the biofilm into other media. This has been used to test antimicrobials, by growing a biofilm on pegs in one plate, then transferring the pegs to an antimicrobial-containing plate. The Calgary Biofilm Device also allows for microscopy techniques to visualise the biofilm, such as by removing individual pegs and preparing them for scanning electron microscopy (Ceri H *et al*., 1999, Ali L *et al*., 2006).

1.5.3 Flow Cells

To simulate conditions in industrial water-flow systems, researchers have employed flow cells. A flow cell is a chamber with an inlet and outlet whereby a medium or culture is pumped through, allowing bacterial cells to attach and develop biofilms inside the cell. Flow cells are often used to test the functionality of cleaning fluids such as bleach or small-molecule biofilm removal effectors. Flow cells are generally used for environmental contaminants which can form biofilms in flow, such as *Pseudomonas* species (Gupta S *et al*., 2011). Additionally, simulated urinary catheters can be tested in much the same way (Azevado AS *et al*., 2016).

Flow cells can be built with viewing ports to allow visualisation of the growing biofilm. Nevertheless, flow cells can be difficult to build, operate and clean, since biofilms are of course encouraged to grow inside them. In addition, the materials required to build a flow cell limit the number of repeat experiments which can be performed (Sternberg C & Tolker-Nielsen T, 2006).

1.5.4 CDC Biofilm Reactor

The CDC Biofilm Reactor is a device for generating biofilms on removable and manipulatable coupons. The Reactor consists of a cylindrical vessel into which rods are inserted holding the coupons. These coupons typically face the middle of the vessel, where a rotating fan maintains a constant movement of media, and bacterial cells, towards the coupons. The vessel has inputs and outputs, allowing media to flow through the device depending on experimental need. Multiple coupons can be inserted into the reactor, increasing reproducibility. When coupons are removed after biofilm generation, they can be easily analysed by quantitative techniques such as crystal violet staining or imaging techniques such as light/electron microscopy (Goeres DM *et al*., 2005, Gilmore BF *et al*., 2010). The primary disadvantage of the Reactor is its cost, exceeding £1000 in some cases (Biosurface Technologies Corporation website). In addition, the reactor can only contain one ‘experiment’ at a time, limiting the number of experiments which can be performed. The Reactor is also a bulky piece of equipment, and although the device can be autoclaved, it is difficult to maintain aseptic conditions when adding media or the bacteria being tested.

1.5.5 Spin Coated Engineered Biofilms

One method developed specifically for biocatalytic biofilm research is the Spin Coated Engineered Biofilm (SCEB). In brief, an *E. coli* culture was centrifuged onto an amenable surface to promote initial attachment. The surface was then transferred to a conical flask containing minimal medium and grown for 7-10 days. Robust biofilm was noted after 6 days in the medium and was shown to a have a high degree of structural cohesion. Additionally, a biocatalytic reaction was proven to function within the biofilm with a higher yield than for planktonic cultures (Tsoligkas A *et al*., 2011, Tsoligkas A *et al*., 2012, Perni S *et al*., 2013).

1.6 A Multipurpose Biocatalytic Biofilm

Biofilms are a natural construct with many desirable traits in the field of biocatalysis. The work presented in this thesis was an attempt to develop and test a multipurpose biocatalytic biofilm which may express multiple recombinant enzymes for different biocatalytic reactions. This biofilm platform was termed a plug-and-play system, in that a plasmid expressing a biocatalytic enzyme could be transformed into the putative bacterium and form robust biofilm quickly and reproducibly. The following section describes the rationale employed in choosing a bacterial platform for this purpose.

1.6.1 Strain Candidates for an *E. coli* Biocatalytic Biofilm

E. coli is a widely-used industrial species which is simple to grow and has been extensively characterised. In addition, *E. coli* is capable of expressing and maintaining high concentrations of recombinant enzymes (Overton TW, 2014). *E. coli* strains vary widely in terms of biofilm-forming ability, and therefore the choice of *E. coli* strain is very important

(Reisner A *et al*., 2006, Beloin C *et al*., 2008). Three distinct *E. coli* strains were chosen for use in this work, based on previously noted biofilm-forming ability.

1.6.1.1 PHL644

E. coli K-12 was first isolated in 1922 from a patient suffering from diphtheria, and maintained in agar stab cultures for many years (Neidhardt FC *et al*., 1996). K-12 strains are widely used in labs due to their relative safety and ease of growth and maintenance. However, K-12 strains are considered poor in terms of biofilm formation on abiotic and biotic surfaces due to the loss of native F plasmids, mutation of the *yhjR-bcsQABZC* operon leading to loss of cellulose production and other potential mutations caused by decades of growth in labs (Reisner A *et al*., 2006, May T & Okabe S, 2008, Serra DO *et al*., 2013). In brief, many K-12 strains have become so acclimatised to growth on agar plates that they have lost their intrinsic abilities to form robust biofilm naturally. PHL644 is derived from MC4100, a K-12 derivative. A useful reference for defining the differences between standard K-12 strains and MC4100 can be found in Peters JE *et al*. (2003). PHL644 was developed by Vidal O *et al* (1998) by screening for K-12 mutants which were able to colonise glass and polystyrene surfaces efficiently. A mutation was detected in the *ompR* gene, whereby a leucine at position 43 was replaced by an arginine (L43R). This mutation, termed the *ompR234* allele, was later found to increase the efficiency of OmpR binding to the *csgDEFG* promoter and therefore lead to a higher activation of curli gene expression (Pringent-Combaret C *et al*., 2001). Several strains containing this mutation created and described by Vidal O *et al* (1998) led to an increase in biofilm formation on both glass and polystyrene, including PHL644. PHL644 was also used in previous work from Tsoligkas *et al* (2011) so it was decided to continue using this strain in this work.

MC4100, and therefore PHL644, is derived from MG1655, an archetypal K-12 strain. MC4100 (and PHL644) features a mutation in *flhD*, which along with FlhC, forms the flagellar gene regulator. Consequently, MC4100, and thus PHL644, do not produce flagella. The question of whether PHL644 produces type-1 pili is unclear. PHL644 features deletions in *fimB* and *fimE*; recombinases which switch the pili-producing *fimAICDFGH* promoter from an ON to an OFF conformation (and vice versa) in a phase-variation mechanism (Section 1.3.2.2). Deletion of these recombinase genes therefore leaves the *fimAICDFGH* operon in an ON or OFF mode, meaning that a population of PHL644 cells may contain cells of both phases. Finally, as previously stated, PHL644 does not produce cellulose in its biofilms (Serra DO *et al*., 2013). Assuming no other mutations or deletions affecting biofilm formation, PHL644 biofilms likely contain curli, type 1 pili, colanic acid and PNAG.

1.6.1.2 BL21 Star (DE3)

E. coli BL21 Star (DE3) is a derivative of the widely-used, industrially relevant BL21(DE3). BL21 and BL21(DE3) are derived from a B/r isolate strain (Wood WB, 1966, Studier FW & Moffatt BA, 1986). BL21(DE3) features a DE3 insertion element which allows the expression of the viral T7 RNA polymerase under the control of a *lacUV5* IPTG-inducible promoter. The T7 RNA polymerase is able to express genes from T7 promoters on transformed recombinant plasmids. BL21 Star (DE3) further features a mutation in RNAseE, reducing mRNA degradation. These mutations give BL21 Star (DE3) the ability to produce large amounts of recombinant protein, and is therefore widely-used as an RPP platform. The base strain BL21 also features mutations in the proteases OmpT and Lon in order to reduce degradation of recombinant proteins (ThermoFisher Scientific, Catalogue No. C601003). One of the targets of the Lon protease is RcsA which binds RcsB to activate CA gene

expression. A deletion in *lon* has been shown to stabilise RcsA and allow more CA production in other *E. coli* strains, perhaps leading to increased biofilm production potential in BL21 Star (DE3) (Stout V *et al*., 1991). BL21 Star (DE3) has been cured of the F plasmid and has been shown to be non-motile, but the strain produces cellulose unlike PHL644 (Marisch K *et al*., 2013). All other biofilm-related genes are presumably intact.

1.6.1.3 Nissle 1917

E. coli Nissle 1917 is a probiotic gut-dwelling isolate strain which has the ability to outcompete and eliminate pathogenic *E. coli* strains. Although Nissle 1917 is a gut bacterium, it is closely related to the uropathogenic strain CFT073 (Hancock V *et al*., 2010). Despite possessing many of the same genes and virulence factors, Nissle 1917 is known to be non-pathogenic to humans and somewhat beneficial in maintaining a healthy gut flora and protecting against infection. Nissle 1917 is therefore often considered a probiotic strain (Gronbach K *et al*., 2010). As an example, Nissle 1917 has been shown to inhibit the growth and pathogenicity of both O157:H7 and O104:H4 EHEC strains (Mohsin M *et al*., 2015). Nissle 1917 is capable of forming a robust biofilm in the gut, but its development on abiotic surfaces has not been well characterised. Lab strains of Nissle 1917 do not carry an F plasmid, but are motile and produce cellulose (Adediran J *et al*., 2014). Interestingly, cellulose production in Nissle 1917 is not dependent on CsgD and DgcC as with K-12 strains of *E. coli*, indicating a striking variance in biofilm regulation (Monteiro C *et al*., 2009).

1.6.2 Candidate Solid Surfaces for *E. coli* Biofilm Formation

E. coli is normally associated with the colonisation of biotic surfaces such as the intestinal lumen and the urinary tract wall, but it has been shown in multiple studies that *E. coli* may

colonise many abiotic surfaces additionally (Beloin C *et al*., 2008). Abiotic surfaces such as glass, plastics and metals can vary greatly in composition, structure and chemistry, and it is therefore important to understand the biofilm-promoting properties of the surfaces used in this project (Berne C *et al*., 2015, Ryu J-H & Beuchat LR, 2005). As biofilm growth on different surfaces varies between strains, it is important to screen multiple materials for their ability to support *E. coli* biofilm.

1.6.2.1 Glass

Glass is composed primarily of silicate compounds such as silicon dioxide. Glass used in laboratories generally falls under two categories, soda-lime or borosilicate. Soda lime glass is a mixture of silicon dioxide and calcium oxide, whereas borosilicate glass is a mixture of silicon dioxide and boron trioxide. Borosilicate glass has a greater resistance to heat than soda-lime, and is used extensively in lab equipment such as beakers and flasks, but consumable items such as microscope slides and cover slips are predominantly made of soda-lime (Mauro JC *et al*., 2014). In this project, soda-lime microscope slides were employed to determine whether soda-lime glass was a suitable substrate for growth of a biocatalytic biofilm.

The chemical composition of any glass is a covalent network of silicon and oxygen with free ions of calcium or boron to maintain the solid structure and charge balance. The extensive silicon-oxygen bonding results in a hydrophilic surface, easily forming hydrogen bonds with water molecules in surrounding media (Donlan RM, 2002). In *E. coli* planktonic culture experiments, biofilms may form on glass flasks or tubes at the air-liquid interface. The formation of curli fimbriae has also been linked to attachment to glass surfaces (Castonguay

MH *et al*., 2006). It was therefore theorised that biofilm would form on glass surfaces in these experiments.

1.6.2.2 Polystyrene (PS)

The plastic PS is a homopolymer of styrene residues, generally used in the lab for disposable plasticware such as petri dishes. PS is considered brittle compared to other plastics and may allow water vapour and oxygen to pass through (Yousif E & Haddad R, 2013). In terms of chemical properties, benzene residues displayed on the surface of the polymer make the material hydrophobic, i.e. repellent to water (Thormann E *et al*., 2008). As the surface of the intestinal mucosa is generally considered to be hydrophobic, it was theorised that a hydrophobic surface might improve the initial attachment of *E. coli* (Qin X *et al*., 2008). Further to this, *E. coli* curli fimbriae produce amyloid structures which are hydrophobic so it was theorised that this would be the primary means of attachment to plastics (Patel J *et al*., 2011, Pawar DM *et al*., 2005). In this project, polystyrene surfaces were obtained by cutting square petri dishes; details of which can be found in Section 2.2.4.1.

1.6.2.3 Polycarbonate (PC)

PC plastics can be made from a variety of monomers including bisphenol A (BPA). In general, these polymers are much less brittle than polystyrene and have a higher heat tolerance (M2 Scientifics website, Lab Plastics Guide). A concern about the stability of polycarbonate materials has arisen as it has been found that BPA may leach into water and have aberrant effects on organisms (Le HH *et al*., 2008). PC is considered to be slightly less

hydrophobic than PS but much more hydrophobic than soda-lime glass. In this project, polycarbonate was bought as sheets and cut to necessary sizes in the lab (Section 2.2.4.1).

1.6.2.4 Stainless Steel (SS)

SS is an alloy of steel and chromium used in various 'wet' settings due to its low corrosiveness (BSSA website, FAQs). In industry, stainless steel is used to make pipework and liquid containers and is resistant to the action of chemicals passing through. SS is generally polished to decrease resistance, but is a rugose material which may contain microscopic structures of >1 μm (Laopornpichayanuwat W *et al*., 2011). Hydrophobicity of SS is variable, and depends on surface roughness; in general, rougher SS leads to increased hydrophobicity (Bernardes PC *et al*., 2010). These structural properties allow bacteria to attach and form biofilm, which is a major problem in industrial pipework (Rodriguez A *et al*., 2008, Nan L *et al*., 2015). Increased surface roughness has been directly linked with increased biofilm formation (Garcia S *et al*., 2016, Pons L *et al*., 2011, Zhang H *et al*., 2005). However, these biofilm-promoting properties may be desirable for a biofilm biocatalyst.

1.6.2.5 Polytetrafluoroethylene (PTFE)

PTFE is a homopolymer of tetrafluoroethylene residues which is known for its strong hydrophobicity, higher than both PC and PS (Carbone EAD *et al*., 2009). PTFE is most well-known by the brand name Teflon (Chemours), and is used to coat cookware such as frying pans, giving the surface a 'non-stick' property which makes cleaning easier. Suspensions of PTFE are also sometimes used as dry lubricants, as PTFE displays very little friction with other materials. The displayed fluorine residues of the polymer impart strong hydrophobicity

to the surface, allowing water to pass across PTFE-coated surfaces without 'wetting' (Biswal NR & Paria S, 2012). An important application for PTFE is in the coating of urinary tract catheters, preventing bacteria from attaching to the catheter walls (Lam TB *et al*., 2014, Lawrence EL & Turner IG, 2005). This property may appear to be counter-intuitive when developing a biofilm biocatalyst, but this material was explored to test whether increased hydrophobicity was a positive or negative force in biofilm formation in the strains analysed. PTFE tape, commonly known as 'Plumber's Tape' due to its use in making pipework watertight, was used in these experiments due to its malleability and ease of handling. Other desirable properties of this material include its high melting point (over 300°C) and low reactivity; and could therefore be easily sterilised by autoclaving and would not leach into the culture medium.

1.6.3 Impact of Biofilm Architecture on Biocatalysis

E. coli biofilms have been noted to adopt 3D 'mushroom-shaped' structures with voids or 'channels' in between, presumably to allow the transfer of nutrients into or out of the biofilm (Reisner A *et al*., 2003). From a biocatalysis point-of-view, these channels may allow the movement of reactants into the biofilm and products out of the biofilm. Fewer channels, or a more compact structure may therefore restrict the ability of the biofilm to take up nutrients or reactants or release secreted compounds or products. It was noted in a fungal *Cunninghamella elegans* biofilm biocatalyst that excessive biofilm thickness reduced biocatalytic activity (Amadio J *et al*., 2013). It was theorised that this was due to reduced metabolic activity caused by reduced oxygen penetration into the biofilm. In any biocatalytic biofilm, it is likely that the majority of the biocatalytic activity occurs in cells inhabiting the apical areas as these are most exposed to the reaction buffer. It would therefore be logical

that restricting biofilm thickness would create a more efficient biocatalyst. However, it might also be suggested that a thinner biofilm may be weaker in terms of mechanical strength and chemical resistance and may not be able to withstand multiple reaction cycles and retain biocatalytic efficiency. Due to the documented weakness of some *E. coli* strains in forming biofilms in abiotic conditions, it was posited in this study that a thicker biofilm would be easier to analyse, manipulate and determine biocatalytic potential (Reisner A *et al*., 2003). Thus, many of the experiments in this study focused on improving biofilm abundance and mature architecture.

1.7 Research Techniques Employed in this Work

1.7.1 Reporter Gene Technology

Transcriptional reporters are regularly employed in molecular biology to understand the transcriptional regulation of operons without having to directly measure the production of a transcript or protein product. A standard reporter construct consists of the promoter of the operon in question fused to a reporter gene. Measuring the level of the reporter gene product gives the level of activation of the promoter (Schenborn E & Groskreutz D, 1999).

Reporter proteins must be easily detectable and measurable, and must have little effect on the cell overall. The traditional reporter protein used by molecular biologists is *E. coli* LacZ or β-galactosidase, and is used in a test known as the β-galactosidase assay (Miller JH, 1972). LacZ catalyses the degradation of lactose into galactose and glucose, but can also catalyse the degradation of ortho-nitrophenyl-β-galactoside (ONPG) into ortho-nitrophenol and galactose. Ortho-nitrophenol is yellow in colour, thus the rate at which it is produced can be measured colourimetrically. The reaction rate has a direct relationship with the

number of LacZ molecules present, thus a faster reaction rate indicates that more LacZ was produced, and accordingly the promoter had a higher degree of activation. The primary disadvantage of LacZ as a reporter is that cells containing the reporter construct must be lysed or permeabilised to access the LacZ molecules, and so the level of production cannot be measured over time without performing additional experiments (Griffith KL & Wolf RE Jr, 2002, Schenborn E & Groskreutz D, 1999).

Green fluorescent protein (GFP) was initially isolated from the jellyfish *Aequorea victoria*, and has become an important tool in molecular biology (Schenborn E & Groskreutz D, 1999, Gerdes HH & Kaether C, 1996). Wild-type GFP glows green when excited by ultraviolet (UV) radiation. GFP requires oxygen to form its fluorophore domain, but does not require any other cofactors or reactants to function, and can be detected within living cells without the need for lysis or other disruptive techniques (Enterina JR *et al*., 2015, Zuverink M & Barbieri JT, 2015). Variants of GFP have been created to cater to specific experimental uses. Enhanced GFP (eGFP) contains a P64L and a S65T mutation which decrease protein maturation time, enhance emission of green light and shift the excitation maximum to 488 nm, allowing blue light to be used in assays (Yang TT *et al*., 1996, Cinelli RA *et al*., 2000). This is more desirable in many experiments as blue light is safer for researchers and cells alike and has a decreased risk of photobleaching the fluorescent protein than higher-energy UV radiation. The disadvantages of standard GFP include its long half-life (approximately 24 hours) and its dependence on oxygen to form its fluorophore. GFP has been shown to be malleable in countering these issues. As an example, GFP can be fused to a tag which promotes faster degradation of the protein, which limits accumulation and increases the accuracy of time-sensitive assays (Miller WG *et al*., 2000).

As single-cell fluorescence can be easily detected by flow cytometry, eGFP was employed as the reporter gene of choice in this work. Details of the construction of reporters used in this project can be found in Section 2.1.2.

1.7.2 Confocal Laser Scanning Microscopy (CLSM)

CLSM is an extension of fluorescence microscopy. In brief, a sample is exposed to a laser which excites fluorophores within the material. The fluorophores emit light which is constrained through a pinhole. The pinhole filters out any light which is not at the 'plane' being focused on at that time, giving a 2D image without interference from other planes. Computer reconstruction can then be employed to produce a 3D image from multiple planes in which the inner strata of a 3D object can be explored (Pawley J, 2006). Biofilms are 3D architecturally-structured arrangements of bacteria and EPS, and therefore the ability to view the internal structure of a biofilm is essential to characterising the physical nature of a biofilm biocatalyst (May T & Okabe S, 2008, Beloin C *et al*., 2008). CLSM has already been used extensively for imaging biofilms (Harrison JJ *et al*., 2006, Cerca N *et al*., 2012).

1.7.3 Flow Cytometry

A flow cytometer is employed to detect specific properties of cells in a culture. By constraining the movement of a cell culture through a narrow flow cell, single cells can be analysed as they pass through detectors. In flow cytometric analyses, an excitation laser is directed at a cell passing through the flow cell. The scattering of this laser is detected by the device, which gives data on the size and granularity of the cell. Additionally fluorescence intensity, either from fluorescent proteins produced by the cell or dyes added to bind specific cellular components, is also detected. Flow cytometry is normally associated with the

analysis of eukaryotic cells, such as mammalian cell lines, but can be adapted to analyse bacterial cells (Ambriz-Aviña V *et al*., 2014, Wyre C & Overton TW, 2014). As bacterial biofilms may contain a mixture of cells in different metabolic states, flow cytometry allows detection of variation within a biofilm by single-cell analyses. Recently, molecular timers were successfully used to detect variable metabolic rates in an *E. coli* biofilm, employing flow cytometry (Besharova O *et al*., 2016). In this project, flow cytometry facilitated the detection of GFP expression within cultures transformed with reporter plasmids. This also permitted the detection of subpopulations producing different levels of GFP, indicating variable levels of expression, which would have been impossible using standard fluorescence detection techniques such as a fluorometer.

1.8 Project Aims

1. Develop a reliable means of generating *E. coli* biofilm which can be analysed using quantitative and imaging techniques.
2. Optimise biofilm generation by modulating surface, growth conditions or *E. coli* strain.
3. Characterise the expression of curli fimbriae during biofilm formation using reporter gene technology.
4. Utilise DGC-overexpressing plasmids to modulate biofilm formation and determine effects on biofilm architecture and curli fimbriae expression.
5. Utilise recombinant biocatalysis enzymes to determine whether the developed biofilms are capable of performing biocatalysis processes.

Chapter 2

Materials and Methods

Unless otherwise stated, all solutions produced in this project were made with deionised water.

2.1 General Microbiological Practices

2.1.1 Bacterial Strains

Table 2.1: *List of E. coli strains used in this study with notable genotypes and properties.*

Strain	Genotype	Notes	Reference
E. coli MC4100	*araD139 Δ(argF-lac)U169 rpsL150 relA1 flbB5301 deoC1 ptsF25 rbsR*	Derivative of the K-12 strain MG1655.	Peters JE *et al*., 2003
E. coli PHL644	MC4100 *malA-kan ompR234*	Strain directly engineered to overactivate OmpR. Derived from MC4100.	Vidal O *et al*., 1998
E. coli BL21 Star (DE3)	F- *ompT hsdS*$_B$ (r_B^-, m_B^-) *galdcmrne*131 (DE3)	Industrially-relevant strain for recombinant protein production. B/r strain.	Wood WB, 1966, Studier FW & Moffat BA, 1986
E. coli Nissle 1917	Isolate strain	Strain known for its ability to outcompete biofilms of pathogenic *E. coli* species.	Hancock V *et al*., 2010
E. coli DH5α	F- Φ80*lacZ*ΔM15 Δ(*lacZYA-argF*) U169 *recA1 endA1 hsdR17* (rk-, mk+) *phoA supE44* λ-thi-1 *gyrA96 relA1*	Strain which produces high stable levels of recombinant plasmids. Used for plasmid maintenance.	Taylor RG *et al*., 1993. Purchased from ThermoFisher.

Table 2.1 lists the *Escherichia coli* strains used in this study. Bacteria were maintained on 2.8% Nutrient Agar (Oxoid) plates. Plates were incubated statically at 30°C for 20 hours for growth, then stored at 4°C. Bacterial plates were stored for a maximum of 1 month. For long term stocks, bacterial cultures were frozen at -80°C in 25% glycerol (ThermoFisher) / 75% phosphate buffered saline (PBS, Sigma-Aldrich) for a maximum of 12 months.

2.1.2 Plasmids

Table 2.2 lists the plasmids used in this study and their origins. The novel plasmid pJLC-A was designed in this work as a gene reporter for the *csgBAC* promoter. MC4100 was used as the template genome for the promoter sequence (GenBank: HG738867.1). The entire 754 bp intergenic sequence between the *csgBAC* and *csgDEFG* open reading frames (ORF) was taken as the promoter region for the reporter (Figure 2.1). The native ribosome binding site sequence of *csgBAC* (AGGGTGACAAC) was replaced with an optimised binding site with the sequence AGGAAACAGCT (O'Neill GP *et al*., 1986) in order to increase translation efficiency. This sequence was fused to the sequence encoding eGFP (Zhang G *et al*., 1996) followed by (at the C-terminus) a sequence encoding an AANDENYALVA amino acid tag, and then 2 terminator codons. AANDENYALVA tags have been shown to reduce the half-life of eGFP to approximately 60 minutes (Miller WG *et al*., 2000). The reporter therefore expressed eGFP-AANDENYALVA from the *csgBAC* promoter. The construct was flanked by an EcoRI site at the 5' end and a HindIII site at the 3' end to allow subsequent subcloning of the full reporter. The linear reporter construct was synthesised by GeneArt (ThermoFisher) as a complete circularised plasmid termed pJLC-A. This plasmid featured a pBR322 origin of replication and a *bla* antibiotic resistance marker. These features were incompatible with many of the plasmids intended to be used in this study, and so the reporter

construct was subcloned into pPROBE'-TT (purchased from Addgene) using the EcoRI and HindIII restriction endonuclease sites (restriction endonucleases purchased from NEB). pPROBE'-TT (Addgene) featured a *tetR* resistance marker and a pBBR1 origin of replication which were compatible with the other plasmids used in this work. The resulting novel plasmid was termed pJLC-T. A plasmid map was not created for pJLC-T as the full plasmid sequence for pPROBE'-TT was not included with the Addgene listing. However, the sequence of the reporter construct is presented in Section 2.1.2.1. pT7-CsgD, pYdaM, pYddV and pYaiC are described and utilised in Chapter 4. pSTB7, pSG22 and pQR801 are described and utilised in Chapter 5.

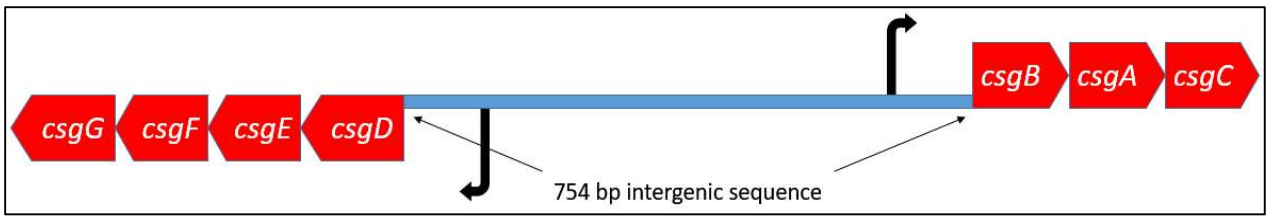

Figure 2.1: *Diagram of the intergenic sequence used for the* csgBAC *reporter construct. Red – genes, blue – intergenic sequence, black – transcriptional start sites.*

Table 2.2: *List of plasmids used in this study with properties and sources.*

Plasmid	Features	Purpose in Study	Source/Reference
pJLC-A	*bla* pBR322	Expression of eGFP-AANDENYALVA from the *E. coli* MC4100 *csgBAC* promoter.	This study, synthesised by GeneArt
pPROBE-TT'	*tetR* pBBR1	Backbone for pJLC-T.	Addgene, Miller WG *et al*., 2000
pJLC-T	*tetR* pBBR1	P*csgBAC*-eGFP-AANDENYALVA gene reporter construct.	This study, subcloned from pJLC-A.
pT7-CsgD	*bla* pBR322	IPTG-induced overexpression of CsgD via T7 system.	Brombacher E *et al*., 2006, gift from Regina Hengge (Humboldt-Universität, Berlin).
pYdaM	*bla* *Kan* pBR322	Constitutive overexpression of DgcM (aka YdaM) via *lac* promoter.	Tagliabue L *et al*., 2010, gift from Paolo Landini (Università degli Studi di Milano).
pYddV	*bla* *kan* pBR322	Constitutive overexpression of DgcO (aka YddV) via *lac* promoter.	Tagliabue L *et al*., 2010, gift from Paolo Landini (Università degli Studi di Milano).
pYaiC	*bla* pSC101	IPTG-induced overexpression of DgcC (aka YaiC/AdrA) via *lac* promoter.	Tschowri N *et al*., 2009, gift from Regina Hengge (Humboldt-Universität, Berlin).
pSTB7	*bla* pBR322	Constitutive expression of *Salmonella enterica* serovar Typhimurium TrpBA via deregulated *trp* promoter.	Kawasaki H *et al*., 1989.
pSG22	*bla* pBR322	IPTG-induced overexpression of *Pseudomonas fluorescens* PrnA.	Rebecca Goss, University of St. Andrews (collaboration).
pQR801	*kan* pBR322	IPTG-induced overexpression of *Chromobacterium violaceum* CV2025 via T7 system.	Kaulmann U *et al*., 2007, gift from John Ward (University College London).

2.1.2.1 Base Sequence of Reporter Construct for pJLC-A and pJLC-T (Insert Only)

GAATTCGATGAAACCCCGCTTTTTTTATTGATCGCACACCTGACAGCTGCCTCTAAAATAGAAGCACCAG
AAGTACTGACAGATGTTGCACTGCTGTGTGTAGTAATAAATCAGCCCTAAATGGGTAAAATATAAAACTA
ATGGATTACATCTGATTTCAATCTAGCCATTACAAATCTTAAATCAAGTGTTAAACATGTAACTAAATGTAA
CTCGTTATATTAAAATGTTAACCTTAAGGTTTTATTAAGTTTAGAAATGATAGAAAAGTTGTACATTTGGTT
TTTATTGCACAATTTTAAAAAATCATACAAATGGTGATAACTTACTAATAATGCATATAAAAAATATTTCGG
TGTAGTCCTTTCGTCATGTAAAACGTTCTTGTTTTTTCTCCACACCTCCGTGGACAATTTTTTACTGCAAA
AAGACGAGGTTTGTCACGGCTTGTGCGCAAGACATATCGCAGCAATCAGCGACGGGCAAGAAGAATGA
CTGTCTGGTGCTTTTTGATAGCGGAAAACGGAGATTTAAAAGAAAACAAAATATTTTTTTGCGTAGATAAC
AGCGTATTTACGTGGGTTTTAATACTTTGGTATGAACTAAAAAAGAAAAATACAACGCGCGGGTGAGTTA
TTAAAAATATTTCCGCAGACATACTTTCCATCGTAACGCAGCGTTAACAAAATACAGGTTGCGTTAACAA
CCAAGTTGAAATTTAATTTCTTAAATGTACGACCAGGTCCAGGAAACAGCTATGAGTAAAGGAGAAGAAC
TTTTCACTGGAGTTGTCCCAATTCTTGTTGAATTAGATGGTGATGTTAATGGGCACAAATTTTCTGTCAGT
GGAGAGGGTGAAGGTGATGCAACATACGGAAAACTTACCCTTAAATTTATTTGCACTACTGGAAAACTAC
CTGTTCCATGGCCAACACTTGTCACTACTTTGACTTATGGTGTTCAATGCTTTTCAAGATACCCAGATCAT
ATGAAACGGCATGACTTTTTCAAGAGTGCCATGCCCGAAGGTTATGTACAGGAAAGAACTATATTTTTCA
AAGATGACGGGAACTACAAGACACGTGCTGAAGTCAAGTTTGAAGGTGATACCCTTGTTAATAGAATCG
AGTTAAAAGGTATTGATTTTAAAGAAGATGGAAACATTCTTGGACACAAATTGGAATACAACTATAACTCA
CACAATGTATACATCATGGCAGACAAACAAAAGAATGGAATCAAAGTTAACTTCAAAATTAGACACAACA
TTGAAGATGGAAGCGTTCAACTAGCAGACCATTATCAACAAAATACTCCAATTGGCGATGGCCCTGTCC
TTTTACCAGACAACCATTACCTGTCCACACAATCTGCCCTTTCGAAAGATCCCAACGAAAAGAGAGACCA
CATGGTCCTTCTTGAGTTTGTAACAGCTGCTGGGATTACACATGGCATGGATGAACTATACAAAAGGCC
TGCAGCAAACGACGAAAACTACGCTTTAGTAGCTTAATAAAAGCTT

Reference – Orange: restriction endonuclease sites; EcoRI upstream and HindIII downstream. Black: *csgBAC-csgDEFG* intergenic sequence; considered as *csgBAC* promoter region. Purple: optimised RBS sequence. Green: eGFP ORF. Blue: sequence encoding AANDENYALVA tag. Red: termination codons.

2.1.2.2 DNA Sequence Alignment of *csgBAC* Promoters

The full intergenic sequences of *csgBAC-csgDEFG* were obtained for *E. coli* MC4100 (GenBank: HG738867.1), BL21(DE3) (GenBank: CP001509.3) and Nissle 1917 (GenBank: CP007799) from the NCBI nucleotide database. MC4100 was used to represent the PHL644 sequence; BL21(DE3) was used to represent the BL21 Star (DE3) sequence. The intergenic sequence lengths were as follows: MC4100 754 bp, BL21(DE3) 754 bp, Nissle 1917 752 bp. Sequences were aligned using Multiple Sequence Comparison by Log Expectation (MUSCLE) from http://www.ebi.ac.uk/Tools/msa/muscle. MC4100 and BL21(DE3) were found to have 100% sequence identity using the Percent Identity Matrix tool. Nissle 1917 was found to have 98.8% sequence identity to either MC4100 or BL21(DE3). Sequence alignments are presented in Section 8.1 as supplementary material.

2.1.3 Chemically-Competent Cell Preparation for Transformations

100 mM $CaCl_2$ (ThermoFisher) and 100 mM $CaCl_2$ + 15% glycerol solutions were prepared and autoclaved to sterilise. These solutions were stored at 4°C. When needed, these solutions were transferred to an ice box. All following steps were performed aseptically. 400 µL of 5 mL overnight bacterial culture in Luria-Bertani (LB) Broth (Miller formulation; 10 g/L tryptone (Sigma-Aldrich), 5 g/L yeast extract (Oxoid), 10 g/L NaCl (ThermoFisher)) was used to inoculate 40 mL of LB broth in a 250 mL conical flask. Cultures were grown to an OD_{600} of 0.3-0.5. Cultures were transferred to sterile 50 mL centrifuge tubes, kept on ice for 20 minutes, then centrifuged at 1683 RCF at 4°C for 15 minutes. The supernatant was decanted and discarded and the pellet was gently resuspended in 4 mL sterile ice-cold 100 mM $CaCl_2$ and left on ice for 20 minutes. Cultures were centrifuged again under the same conditions. The supernatant was decanted and discarded and the pellet was gently

resuspended in 2 mL sterile ice-cold 100 mM $CaCl_2$ + 15% glycerol. Cultures were gently transferred into ice-cold 1.5 mL microcentrifuge tubes in 200 µL aliquots. Microcentrifuge tubes were transferred directly from ice into a -80°C freezer. Competent stocks were stored for a maximum of 12 months.

2.1.4 Chemically-Competent Cell Transformation

Aliquots of 200 µL of competent cells were removed from the -80°C freezer directly onto ice. All following steps were performed aseptically. Aliquots were thawed and 50 µL was transferred into a sterile microcentrifuge tube. 0.5 µL of plasmid stock was added gently. Cells and plasmid were allowed to mix for 20 minutes on ice. The transformation tube was heat-shocked by direct transfer from ice into a 42°C heat block for 1 minute. The tube was then transferred back into the ice for 1 minute after which 700 µL of LB was added. Tubes were incubated in a heat block at 37°C and 600 RPM for 1 hour to allow heat-shock recovery. Transformations and appropriate controls were spread onto nutrient agar with appropriate selective antibiotics (carbenicillin (Melford) 100 µg/mL in water, tetracycline (Sigma-Aldrich) 10 µg/mL in 70% ethanol/30% water, kanamycin (Sigma-Aldrich) 50 µg/ml in water). Selective plates were incubated statically at 30°C for 20 hours, unless otherwise stated. Although the standard incubation temperature for *E. coli* is 37°C, it was noted that 30°C produced fewer satellite colonies. It also was theorised to be beneficial to grow the cells at the temperature which they would be exposed to in the biofilm generators, i.e. 30°C thus reducing the time needed to acclimatise to new conditions. Colonies resulting from transformations were restreaked onto fresh nutrient agar plates with appropriate antibiotics to ensure selection. Transformation plates were stored at 4°C for up to 2 weeks, then discarded.

2.1.5 Plasmid Maintenance

Transformed *E. coli* DH5α cultures were grown in sterile glass test tubes with 5 mL of LB with appropriate antibiotics. Cultures were incubated at 30°C and 150 RPM for 18 hours. Plasmids were extracted from the cultures using a QIAprep Spin Miniprep Kit (QIAGEN) and eluted into molecular biology-grade water. Plasmids were stored in microcentrifuge tubes at -20°C for up to 6 months.

2.2 Biofilm Generation Practices

2.2.1 Overnight Cultures for Biofilm Experiments

Overnight cultures of bacteria were grown in sterile glass test tubes in 5 mL of LB with appropriate antibiotics. When using two antibiotics simultaneously, as in experiments using two plasmids, concentrations were reduced to 50 µg/mL carbenicillin and 5 µg/mL tetracycline. Cultures were incubated for 18 hours at 30°C and 150 RPM. When required, cultures were transferred to 15 mL centrifuge tubes and centrifuged at 1683 RCF for 15 minutes to pellet the cells. The supernatant was then poured off and replaced with 5 mL of sterile PBS. The OD_{600} was measured and the culture was centrifuged again, the supernatant poured off and a volume of PBS added to adjust the cell culture to an OD_{600} of 1.

2.2.2 Biofilm Growth Media

In all cases, antibiotics were omitted from biofilm growth media to prevent any adverse effects on biofilm formation. Standard M63 minimal medium consisted of 100 mM KH_2PO_4 (Sigma-Aldrich), 15 mM $(NH_4)_2SO4$ (Sigma-Aldrich), 1 mM $MgSO_4$ (ThermoFisher), 1.8 µM

$FeSO_4$ (Sigma-Aldrich) and 10 mM D-glucose (ThermoFisher). The primary medium used for the growth of biofilms in this study was termed M63+ and consisted of 100 mM KH_2PO_4, 15 mM $(NH_4)_2SO_4$, 1 mM $MgSO_4$, 1.8 µM $FeSO_4$, 10 mM D-glucose and 17 mM sodium succinate (ThermoFisher). M63+ was prepared thusly. A 500 mL '5X stock' solution comprising 500 mM KH_2PO_4 (32.02 g), 75 mM $(NH_4)_2SO_4$ (4.96 g) and 85 mM sodium succinate (11.48 g) was mixed and the pH was adjusted to 7 using potassium hydroxide (Sigma-Aldrich). This was sterilised by autoclaving and stored at room temperature. $MgSO_4$ was prepared as a stock concentration of 100 mM and then autoclaved and stored at room temperature. $MgSO_4$ was prepared separately to prevent reactions with KH_2PO_4 during autoclaving. A 1.8 mM stock concentration of $FeSO_4$ was prepared and filter sterilised using a 0.22 µm filter. This was stored at 4°C and away from light. A 1 M stock concentration of D-glucose was prepared and filter sterilised. This was stored at 4°C.

As an example, 70 mL M63+ was prepared thusly in the following volumes: 14 mL '5X stock', 700 µL 100 mM $MgSO_4$, 70 µL 1.8 mM $FeSO_4$, 700 µL D-glucose, 54.53 mL sterile deionised water. Solutions were assembled aseptically and inoculated immediately. Solutions were examined daily and discarded if contamination, precipitation or other indications of detrimental effects were apparent. Any changes to the final M63+ composition are noted in the appropriate experiment descriptions. Succinic acid and potassium succinate were both purchased from ThermoFisher.

2.2.3 Biofilm Generation Platforms

2.2.3.1 Preparation of Coupons for Use in the Biofilm Generators

Standard glass cover slips (SLS) were washed with ethanol to remove residues, dried, then autoclaved to sterilise. After use, these coupons were discarded. Polystyrene (PS) coupons were obtained by cutting square Petri dishes (SLS) with a scalpel into 22 x 32 mm coupons. These coupons were washed and soaked in ethanol for >2 hours to sterilise, then dried before insertion into 6-Well Plates. After use, these coupons were discarded. Polycarbonate (PC) sheets were purchased (RS Components) and cut into 22 x 32 mm coupons. These coupons were washed and soaked in ethanol for >2 hours to sterilise, then dried before insertion into 6-Well Plates. After use, these coupons were discarded. PS and PC coupons were not autoclaved due to concerns that heat would either melt or warp the coupons. 304-grade stainless steel (SS) coupons were prepared by the University of Birmingham Mechanical Engineering Workshop to dimensions of 22 mm x 32 mm. Stainless steel coupons were washed with acetone (ThermoFisher) and ethanol to remove residues, dried, then autoclaved to sterilise. After use in biofilm experiments, SS coupons were washed thoroughly with acetone, ethanol and deionised water and reused. Glass microscope slides (ThermoFisher) (75 mm x 25 mm) were washed with ethanol, dried, and sterilised by autoclaving. After use, these coupons were discarded. PTFE-wrapped microscope slides were prepared by wrapping PTFE thread seal tape (12 m length x 12 mm width x 0.075 mm depth; RS Components part number 0512238) around a glass microscope slide to cover the entire surface on both sides. An image of a finished slide can be seen in Figure 2.2. These were washed with deionised water, dried, and then sterilised by autoclaving. After use, these coupons were discarded. At all points, forceps used for manipulation of the coupons were

washed in ethanol and then lit using a Bunsen burner to sterilise and maintain aseptic conditions, and repeated between coupons to prevent cross-contamination.

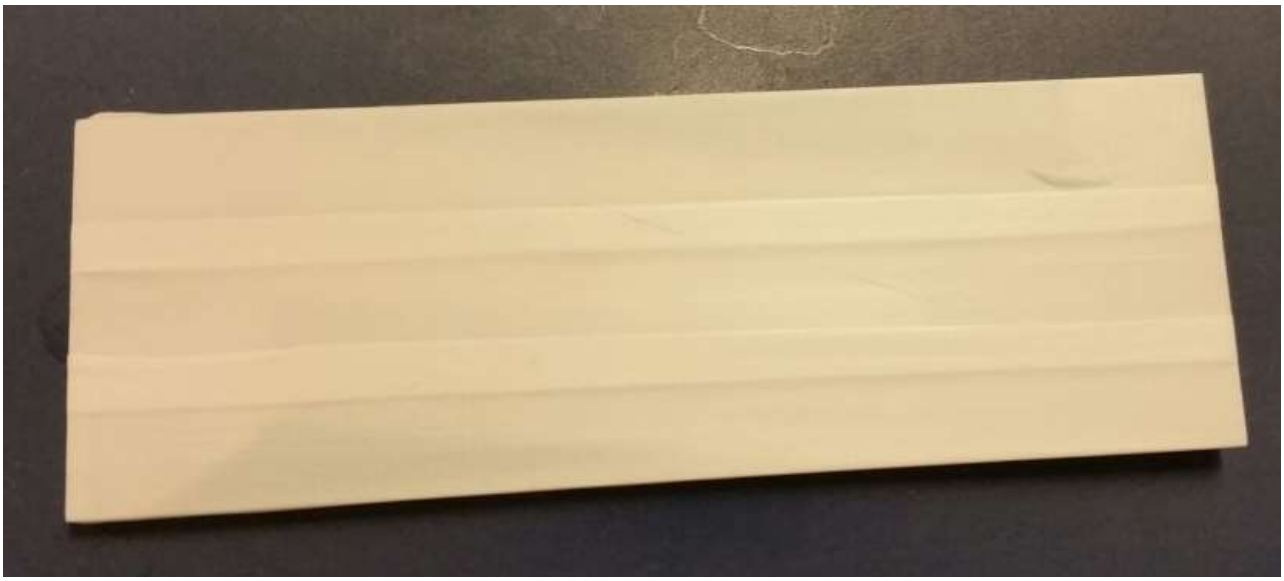

Figure 2.2: *Photograph of a glass microscope slide wrapped with PTFE tape. The tape was wrapped length-wise to cover the entire surface of the slide. Details of cleaning and application as a biofilm-forming surface can be found in Section 2.2.3.1.*

2.2.3.2 Contact Angle Measurement

Contact angle determination was used to infer the relative hydrophobicity of materials used in this study. A small drop of deionised water was dripped onto each material coupon from a hypodermic needle suspended approximately 20 cm above the coupon. An image of the droplet on the surface was obtained and the angle at which it contacted the surface was measured using ImageJ. A narrower angle indicated that the water droplet interacted strongly with the coupon, indicating hydrophilicity. A wider angle indicated that the water droplet was repelled by the coupon, indicating hydrophobicity. All measurements were performed three times with independent coupons.

2.2.3.3 Preparation of the 6-Well Plate Biofilm Generator

Polystyrene 6-well microplates (ThermoFisher) were purchased sterile and all steps involving these plates were performed under aseptic conditions. For biofilm growth, a 22 mm x 32 mm coupon was inserted into each of the wells which rested at a diagonal angle of approximately 30°. Previously described M63+ medium, and a 100x dilution of overnight culture, was added to each well to a volume of 10 mL. The plates were incubated in a MaxQ orbital shaker with an orbit of 19 mm. All 6-Well Plate experiments were performed at 30°C and 70 RPM for 3 days.

2.2.3.4 Preparation of the Duran Bottle Biofilm Generator

A polyurethane bung was inserted into a 100 mL Duran Bottle (without screw-top lid) to retain aseptic conditions in the experiments, and maximise gas transfer for growing cells. The Duran Bottle was then sterilised by autoclaving. All steps after this point were performed in aseptic conditions. M63+ and a 100X dilution of overnight culture was added to the Duran Bottle to a final volume of 70 mL, and a coupon was inserted into the bottle at an angle of approximately 70°. The Duran Bottles were incubated in a MaxQ orbital shaker with an orbit of 19 mm. All Duran Bottle experiments were performed at 30°C and 70 RPM for 3 days unless otherwise noted in specific experimental sections.

2.3 Biofilm Analysis Techniques

2.3.1 Quantification of Biofilm Growth by Crystal Violet Staining

2.3.1.1 6-Well Plate Method

10 µL of 1% Crystal Violet (CV) solution (Sigma-Aldrich) was added to each well of the 6-Well Plate biofilm generator and left to stain for 1 hour at 30°C and 70 RPM. The staining concentration of CV in each well was 0.001%. Stained coupons were then removed with tweezers and washed three times by submersion in PBS to remove non-adhered cells. The coupons were then inserted into a new, clean 6-Well Plate with 10 mL of 95% ethanol (ThermoFisher) in each well for 30 minutes at room temperature and 70 RPM to destain. The coupons were then discarded, the destain solution was mixed, and the absorbance at 580 nm of the destain solution was measured using a spectrophotometer using 95% ethanol as a zero value.

2.3.1.2 Duran Bottle Method

70 µL of 1% Crystal Violet solution was added directly to a biofilm generation bottle and left to stain at 30°C and 70 RPM for 1 hour. The staining concentration in each bottle was 0.001%. The stained coupon was removed and washed three times by submersion in PBS to remove non-adhered cells. The stained coupon was inserted into a 50 mL centrifuge tube with 35 mL of 95% ethanol for 30 minutes to destain. Coupons were then removed and discarded, and the destain tube was vortexed to ensure homogenous concentration of CV. The absorbance at 580 nm of the destain solution was measured using a spectrophotometer using 95% ethanol as a zero value.

2.3.2 Confocal Laser Scanning Microscopy (CLSM)

All steps in the preparation of biofilm samples for imaging were performed carefully and gently to prevent damage to the biofilm. A biofilm-coated coupon was removed from a 6-Well Plate or Duran Bottle and washed three times by submersion in PBS to remove non-adhered cells. The coupon was then placed biofilm-coated-side-up on a clean microscope slide. 20 µL of 200 µM SYTO™ 62 (ThermoFisher) was applied to the biofilm-coated surface of the coupon. SYTO™ 62 is a fluorescent, membrane-permeable nucleic acid stain and so binds the DNA of cells in the biofilm. SYTO™ 62 was left to bind in dark conditions to prevent photobleaching for 15 minutes. A 22 mm x 32 mm glass cover slip was gently applied to the top of the area to be viewed, then the sample was immediately transferred to the CLSM device – a Leica TCS SPE Confocal Laser Scanning Microscope. A small drop of immersion oil was applied to the top of the cover slip, and then the sample was set on the microscope stage. All images in this study were obtained using a 40X oil-immersion lens, as this was found to produce the clearest images while retaining a wide field. SYTO™ 62 was excited by a 635 nm laser and emission was detected in the range of 670 nm to 690 nm. All images exhibited in this thesis display SYTO™ 62 fluorescence as red. Images were captured and manipulated using the Leica Application Suite X software. To generate 3D images, an automated Z-stack scan was set up for each sample to capture the entire visible thickness of the biofilm. Number of scans was dependent on thickness, but scans were set 2 µm apart in all cases. Top-down and side-view images were created using maximum projection renders of the 3D image stack rotated at either 90° or 0° at the Y axis. Scale bars were added using the software to ensure correct scaling. Brightness of images was enhanced when necessary.

2.3.3 Flow Cytometry

Planktonic bacterial suspensions were analysed by removing 100 µL aseptically and diluting with PBS to approximately 1000 cells per microliter. No dye was applied to the sample as only the levels of green fluorescent protein were analysed. Flow cytometry analysis was performed using a BD Accuri C6 Flow Cytometer. Samples were run at 14, 35 or 66 µL per minute as appropriate until 25000 events were collected. Cell size was measured by the device using the forward scatter detector, the output of which was termed FSC. An FSC threshold was set at 12000 to eliminate non-cellular material; this threshold was based on direct observation of *E. coli* cell size variation. Sample excitation was performed using a 488 nm laser. Fluorescence emission was detected using a 533/30 nm filter, the output of which was termed FL1.

The mean fluorescence of samples of untransformed PHL644 and BL21 Star (DE3) over a period of 24 hours was measured as between 190 and 210 units with very little variation. The threshold for GFP production was set at 575, as at least 99.86% of the population was below this threshold at all times. Cells counted below this threshold were determined to be GFP-negative and inferred to be not producing *csgBAC* transcript. Cells counted above this threshold were determined to be GFP-positive and inferred to be producing *csgBAC* transcript. Values for the percentage of GFP-positive cells and the level of fluorescence produced were transcribed from the statistical analysis section of the Accuri C6 software, termed ‘Statistics’.

A full discussion of the rationale for this analysis method is presented in Section 3.4.

2.4 Biocatalysis Practices

2.4.1 Halogenase/pSG22 Reaction Protocols

2.4.1.1 Halogenase Reaction Buffer

The reaction buffer for the halogenase reactions was composed of 100 mM KH_2PO_4, 20 mM NaCl and 2 mM L-tryptophan, and was adjusted to pH7 using potassium hydroxide. The buffer was sterilised using a 0.22 µm vacuum filtration system. Until needed, halogenase buffer was stored at 4°C in dark conditions. Before use, halogenase buffer bottles were returned to room temperature in a water bath in dark conditions.

2.4.1.2 High Performance Liquid Chromatography (HPLC)

All HPLC activities presented here were performed in the School of Chemistry, University of Birmingham. HPLC analysis was performed using a Shimadzu Prominence LC 20 machine with a C18 reversed-phase column (ThermoFisher). HPLC-grade methanol and water (ThermoFisher) were acidified with 0.1% methanoic acid (Sigma-Aldrich), and used as resolving solvents. The solvent gradient, run at 1 mL/minute, is detailed in Table 2.3. Samples were analysed for absorbance at 280 nm.

Table 2.3: *HPLC solvent gradients used to analyse samples containing tryptophan, indole, 7-chloroindole and 7-chloro-L-tryptophan.*

Time (minutes)	**Percentage of Solvent B: Methanol**	**Percentage of Solvent A: Water**
0-0.5	10	90
0.5-12.5	10 to 95	90 to 5
12.5-15	95	5
15-16	95 to 10	5 to 90
16-21	10	90

2.4.1.3 Calibration Graphs

Tryptophan, indole and 7-chloroindole were run as calibration standards in the following concentrations: 1 mM, 0.5 mM, 0.25 mM and 0.125 mM. 2 mM was initially used but the absorbance reading was found to exceed the linear range of the calibration. 0.0625 mM was also found to be outside of the linear range, except for 7-chloroindole, which was included on the calibration graph. 7-chloro-L-tryptophan could not be obtained for calibration due to high cost. Samples were diluted with HPLC-grade water as necessary and then readjusted during calibration. Retention times for the 3 chemicals were as follows: tryptophan at 4.9 minutes, indole at 10.5 minutes, 7-chloroindole at 12.4 minutes. Calibration standards were performed in triplicate and calibration graphs are presented in Figure 2.3.

2.4.1.4 Halogenase Reaction – Planktonic Cells

PHL644 pSG22 and BL21 Star (DE3) pSG22 planktonic cells were grown in 70 mL M63+ (+100 µM IPTG) in 100 mL Duran bottles without coupons for 3 days at 30°C and 70 RPM. Cultures were then transferred to centrifuge tubes, centrifuged at 1683 RCF for 15 minutes, resuspended in PBS, and the OD_{600} was measured using a spectrophotometer using deionised water as a zero value. The suspension was centrifuged again, then resuspended in halogenase reaction buffer to an OD_{600} of 1 and inserted into clean, sterile 100 mL Duran bottles. Reactions were performed at 30°C and 70 RPM for 24 hours. 500 µL samples were taken every 2 hours for 0-8hrs and then at 24hrs. Samples were filtered (0.22 µm) to remove cells before transfer into glass HPLC tubes. HPLC tubes were stored at 4°C in dark conditions for a maximum of 2 days until analysis.

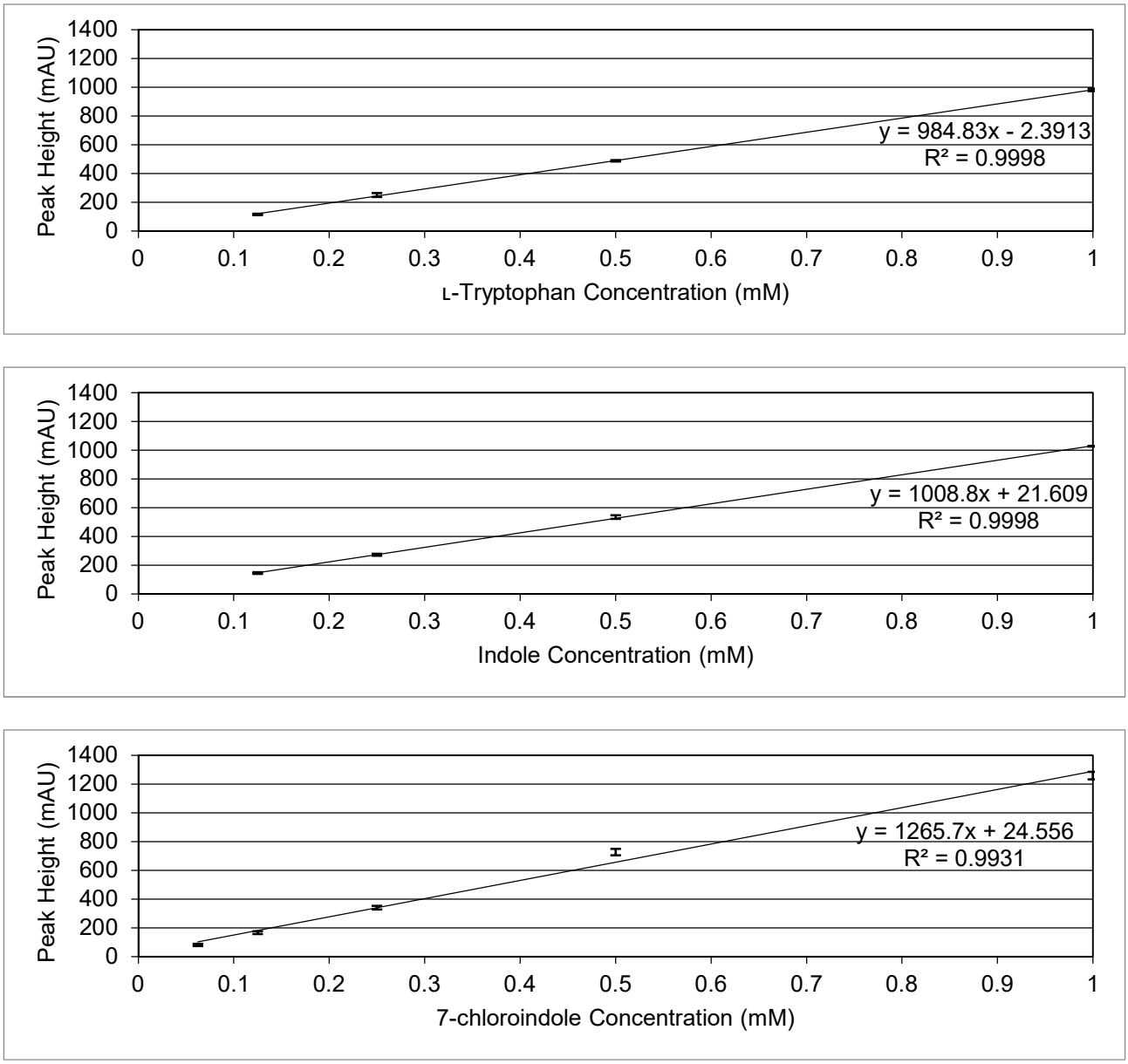

Figure 2.3: *Calibration graphs for L-tryptophan, indole and 7-chloroindole. Error bars represent 1 standard deviation from the mean of three independent reactions.*

2.4.1.5 Halogenase Reaction – Biofilms

PHL644 pSG22 and BL21 Star (DE3) pSG22 biofilm cells were grown in 70 mL M63+ (+100 µM IPTG) in 100 mL Duran bottles on PTFE coupons for 3 days at 30°C and 70 RPM. Biofilms were removed under aseptic conditions and washed 3 times by submersion in PBS.

Biofilms were then placed into clean, sterile 100 mL Duran bottles containing 70 mL halogenase reaction buffer. Reactions were performed at 30°C and 70 RPM for 24 hours. 500 µL samples of the reaction buffer were taken every 2 hours for 0-8hrs and then at 24hrs. Samples were filtered (0.22 µm) to remove cells before transfer into glass HPLC tubes. HPLC tubes were stored at 4°C in dark conditions for a maximum of 2 days until analysis.

2.4.2 Transaminase/pQR801 Reaction Protocols

2.4.2.1 Transaminase Reaction Buffer and Calibration

Transaminase reaction buffer consisted of 100 mM KH_2PO_4, 2 mM (S)-(-)-α-methylbenzylamine (Sigma-Aldrich), 2 mM sodium pyruvate (Sigma-Aldrich) and was adjusted to pH 7 using potassium hydroxide. For acetophenone concentration calibration, the buffer was prepared with added 0.1, 0.05, 0.025, 0.0125 or 0.00625 mM acetophenone. The calibration standards were analysed using a spectrophotometer at 245 nm using deionised water as a zero value, and is presented in Figure 2.4.

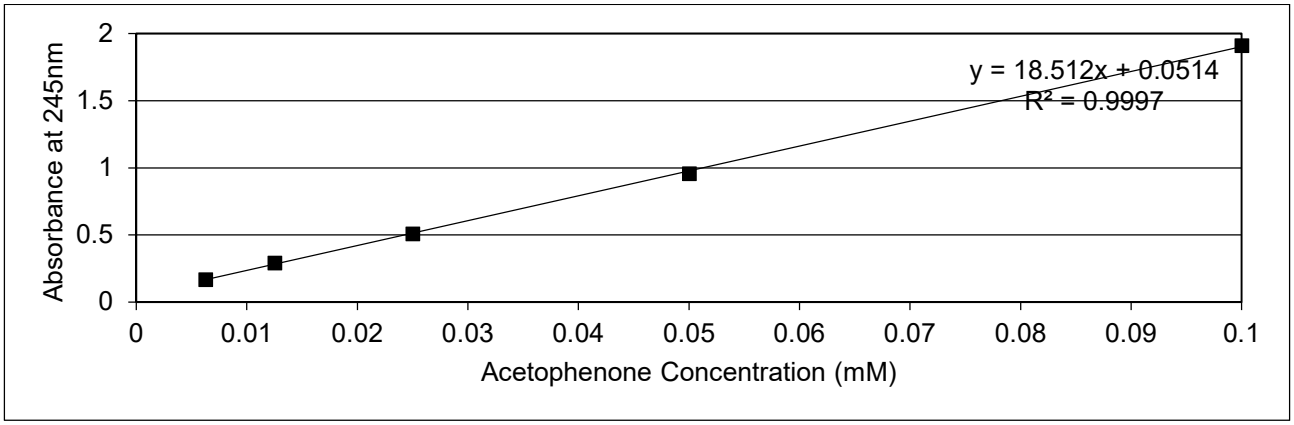

Figure 2.4: *Calibration graph for variable acetophenone concentrations in transaminase reaction buffer. Error bars represent 1 standard deviation from the mean of three independent samples.*

2.4.2.2 Transaminase Reaction – Planktonic Cells

BL21 Star (DE3) pQR801 and BL21 Star (DE3) were grown in 100 mL Duran bottles in M63+ (without antibiotic) at 30°C and 70 RPM for 3 days (with 100 µM IPTG to induce CV2025 expression). Cultures were then centrifuged at 1683 RCF for 15 mins, washed with PBS, centrifuged again, then resuspended in reaction buffer and adjusted to an OD_{600} of 1. Resuspended cultures were inserted into clean, sterile 100 mL Duran Bottles. Reactions were performed at 30°C and 70 RPM. 500 µL samples were taken every 2 hours for 0-8hrs and then at 24hrs. These samples were diluted as necessary, then filtered (0.22 µm) and immediately analysed with a spectrophotometer at 245 nm using deionised water as a zero value.

2.4.2.3 Transaminase Reaction – Biofilms

BL21 Star (DE3) pQR801 and BL21 Star (DE3) were grown in 100 mL Duran bottles in M63+ at 30°C and 70 RPM for 3 days (with 100 µM IPTG to induce CV2025 expression). A PTFE-wrapped microscope slide was inserted from the start to provide a surface for biofilm formation. The PTFE-wrapped slide was then removed, washed twice by submersion in PBS, then inserted into a clean sterile 100 mL Duran bottle containing the previously described reaction buffer. Reactions were performed at 30°C and 70 RPM. 500 µL samples were taken every 2 hours for 0-8hrs and then at 24hrs. These samples were diluted as necessary, then filtered (0.22 µm) and immediately analysed with a spectrophotometer at 245 nm using deionised water as a zero value.

Chapter 3

Development of a Biofilm Biocatalyst

3.1 Necessities of a Biocatalytic Biofilm

A list of necessary properties for the novel biofilm biocatalyst was posited. These properties would ensure that the biofilms would be stable, grow reliably and perform biocatalytic reactions efficiently. The biofilm should:

1. be robust on a solid surface

Mechanical robustness is essential to maintain the 3D structure of a biofilm after washing, being moved or after exposure to reaction conditions (Billings N *et al*., 2015). Any instability in the biofilm may decrease the viability of biocatalytic processes due to a loss of functional biomass. Attachment to a solid removable surface, as opposed to a membrane or the walls of a microtiter well, allows the biofilm to be easily moved from one medium into another, in this case from a biofilm generation medium into a reaction buffer. A simple test of robustness was performed by submerging the biofilm in PBS to remove unattached cells before analysis by CV staining or CLSM. A more robust biofilm would have greater cohesive properties and so fewer unattached cells would be observed in microscope images. Attachment to the surfaces tested in this work was to be analysed by CV staining and CLSM imaging.

2. contain a substantial biomass of cells

The number of recombinant cells present not only affects the biocatalytic potential of the biofilm, but also increases the overall stability and robustness of the biofilm on the surface. This was to be measured using CV staining.

3. be inexpensive and simple to grow and use

Due to the costs involved in purchasing reaction precursors as well as purifying the products of any reactions, it was considered beneficial to keep the overall costs of the biofilm biocatalyst model low. Model simplicity was also essential, as applying complexity to a biofilm-forming system may lead to increased variability in structure and also reaction efficiency.

4. have a 3D structure defined by the cell population and not by random aggregation

A biofilm requires a functional 3D structure determined by its growth patterns to allow flow of nutrients or reaction components in or out of the cells (Beloin C *et al.*, 2008). An aggregate of bacteria is composed of cells attached to each other randomly without structure and so cannot be considered to be a functional biofilm under these criteria. Biofilm microstructure was to be analysed using CLSM imaging.

5. retain plasmids and express enzymes necessary for biocatalytic functions

In order to operate as a multifunctional platform, the cells must be able to transform and maintain various recombinant biocatalysis plasmids. The cells must then retain the plasmids through biofilm formation so encoded recombinant enzymes can be expressed for biocatalysis. These aspects will be focused on in Chapter 5.

6. be able to perform biocatalytic functions with a high degree of efficiency and yield

The biofilm must be able to take up reactants from the reaction buffer to facilitate the desired reaction. The biofilm must then transport the product out of the cell and out of the biofilm to

ensure efficient conversion of the product in question and also reclamation of the product from the buffer. These aspects will be focused on in Chapter 5.

As noted in Section 1.5, many of the techniques employed to grow catalytic biofilms in prior studies, such as the CDC device, are expensive and require specialised equipment to operate. It was therefore decided to develop a novel platform to fulfil the above criteria.

3.2 Methods for Developing a Biofilm Biocatalyst

3.2.1 6-Well Plate Method

6-well polystyrene plates were initially employed in this study to test surfaces for biofilm formation. Specific details about the plates used in this work can be found in Section 2.2.3.2. To facilitate both quantification and imaging using CLSM, a 22 x 32 mm coupon (composed of different materials) was inserted into the well and used as the surface for biofilm formation (Figure 3.1). This strategy also allowed the coupon, and therefore the biofilm, to be removed and transferred to other containers as necessary. The coupon rested at a diagonal angle across the well, at approximately 30° elevation. Liquid medium and bacterial culture were added to the well to a total volume of 10 mL, which covered approximately half of the coupon. It should be noted that while 22 x 22 mm coupons were also employed, which lay horizontally at the bottom of the well, this led to poor biofilm growth which was easily washed off by submersion in PBS. Details of media and inoculation procedures can be found in Section 2.3. The plates were incubated in an orbital shaker at 30°C and 70 RPM unless otherwise stated. These conditions were initially used by Tsoligkas A *et al*. (2011) to grow engineered biofilms, but will be examined later in this chapter. It was theorised that the rotation would

aid in the development of initial attachment by ‘pushing’ the cells toward the diagonally situated surface of the coupon. It has been demonstrated previously that shear may promote biofilm formation (Liu Y & Tay JH, 2002, Park A *et al*., 2011). However, the rotation was kept relatively low compared to standard planktonic culturing conditions in conical flasks (150-200 RPM) to prevent mechanical damage to the biofilm by sloughing. The 6-Well Plate method was employed for many of the initial material characterisation experiments in this project, specifically glass, PS, PC and SS (Section 1.6.2). However, a problem was encountered when the material PTFE was investigated (Section 1.6.2.5). PTFE tape was wrapped around a glass cover slip and inserted into a well as stated before. Instead of remaining at a diagonal angle in the well when the growth medium was added, the PTFE coupon floated on top of the liquid and was therefore unusable in the experiment. This is likely due to the hydrophobicity of PTFE and the low mass of the cover slip. In order to overcome this issue, as well as to increase the volume of biofilm produced in the experiment, a second technique was developed.

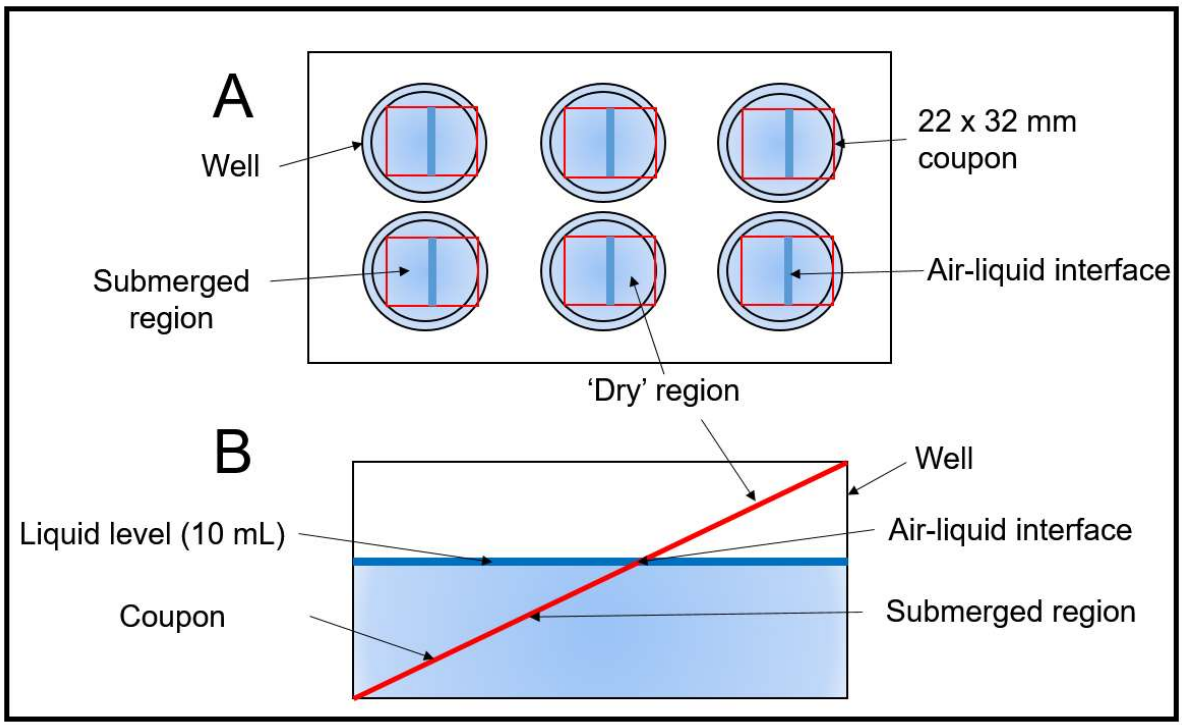

Figure 3.1: *Diagram of the 6-Well Plate biofilm generator. A represents a top-down view of the generator. B represents a side-view of a single well. For a full description of how the generator was prepared see Section 2.2.3.2.*

3.2.2 Duran Bottle Method

The Duran Bottle Method was used to compare biofilm development on glass microscope slides and PTFE-wrapped microscope slides (Figure 3.2). A glass microscope slide or PTFE-wrapped microscope slide was inserted into a 100 mL Duran bottle. Comparably-sized coupons could not be obtained for the other materials. The slide rested at an angle of approximately 65°, though this varied slightly (± 5°) due to imperfections in the slide or the bottle. Unlike PTFE-wrapped cover slips, PTFE-wrapped microscope slides did not float in the medium. Growth medium and bacterial suspension was added to a total volume of 70 mL which covered approximately half of the slide. Culturing conditions (30°C, 70 RPM) were kept identical unless otherwise stated. A polyurethane foam bung was inserted into the bottle

to allow gas transfer and to maintain an aseptic environment. Full details of the preparation of a Duran Bottle biofilm generator can be found in Section 2.2.3.3.

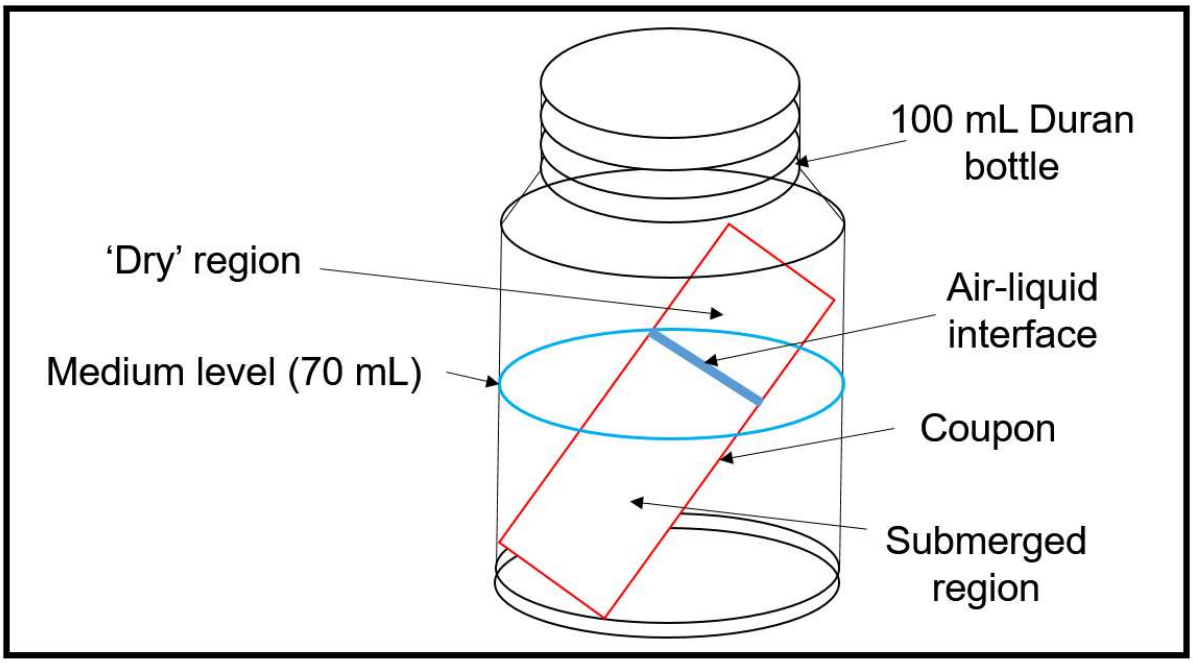

Figure 3.2: *Diagram of the Duran Bottle biofilm generator. Polyurethane bung has been omitted for clarity. For a full description of how the generator was prepared see Section 2.2.3.3.*

3.3 Characterisation of *E. coli* Biofilm Growth on Varied Materials

Several different materials were investigated for their ability to support biofilm growth. Bacteria such as *Pseudomonas* spp. and *Legionella* spp. are known for their ability to colonise a wide range of abiotic surfaces in various medical and industrial settings. However, *E. coli*, and specifically the lab strains employed in many biological research experiments are not known for forming robust biofilms on abiotic surfaces (Beloin C *et al*., 2008). It was therefore important to screen for materials which were amenable to growing *E. coli* biofilms.

3.3.1 Glass

E. coli PHL644, BL21 Star (DE3) and Nissle 1917 biofilms were grown using the 6-Well Plate method. Biofilms were grown in 10 mL M63+ medium on a glass cover slip at 30°C and 70 RPM for 3 days. Biofilms were analysed using CV staining and CLSM. CLSM was performed at least twice on at least 2 areas of each biofilm, and then a representative image was chosen.

As shown by CV staining (Figure 3.3), BL21 Star (DE3) and Nissle 1917 both displayed mean A_{580} values which were higher than PHL644, yet within 1 standard deviation of PHL644 indicating that these three strains produced a very similar amount of biofilm on the glass cover slip. This was surprising, as PHL644 has been specifically engineered to produce robust biofilms, and would be expected to produce more biofilm than the other strains (Vidal O *et al*., 1998). This suggests that the non-K-12 strains (BL21 Star (DE3) and Nissle 1917) are as competent at forming biofilms on glass as an engineered K-12 derivative (PHL644).

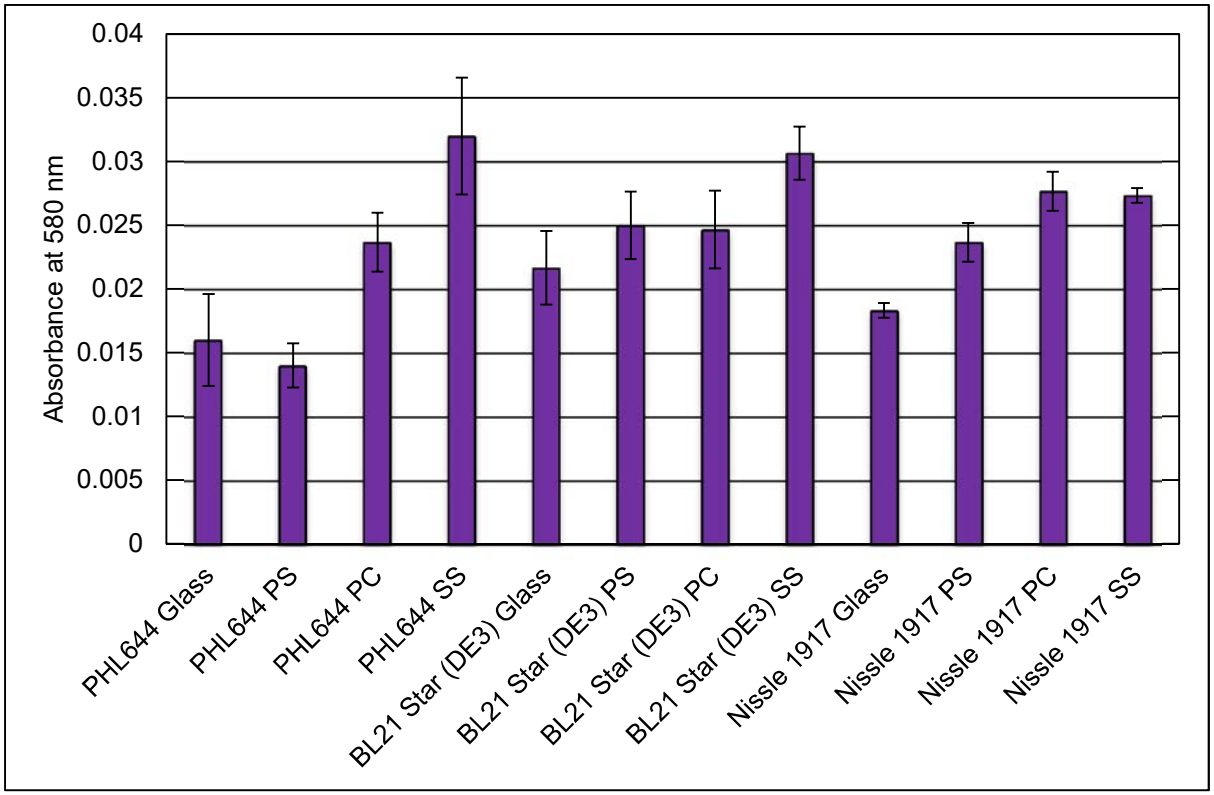

Figure 3.3: *Graph comparing CV retention of PHL644, BL21 Star (DE3) and Nissle 1917 on glass, polystyrene (PS), polycarbonate (PC) and stainless steel (SS) coupons. Experiments were performed using the 6 Well Plate method. Error bars represent 1 standard deviation from the mean of 3 independent cultures.*

CLSM images reveal, in all strains, that biofilms at the air-liquid interface were thicker and better defined than submerged areas on glass (Figure 3.4). PHL644 interface biofilms formed distinct 3D 'mushroom-shaped' structures which grew out from the surface. In contrast, submerged PHL644 biofilms adhered to the glass surface but showed little defined outgrowth compared to interface biofilms. BL21 Star (DE3) biofilms were similar to PHL644 in terms of the differences between the interface and submerged areas, but were generally thicker than PHL644 in both areas. Nissle 1917 interface biofilms appeared more random, less defined and thinner than either PHL644 or BL21 Star (DE3). Additionally, submerged

Nissle 1917 biofilms were sparser and showed no appreciable 3D outgrowth from the surface. PHL644 interface biofilms reached a consistent maximum thickness of ~40 μm, while submerged biofilms varied from ~40 to ~15 μm. BL21 Star (DE3) interface biofilms were thicker, reaching a consistent maximum of ~60 μm, while submerged biofilms reached a fairly consistent 30 μm. Nissle 1917 biofilms did not exceed 20 μm at either the interface or submerged areas.

In this experiment, the growth of *E. coli* biofilm on glass appears to be highly strain-dependent, with the three strains showing distinct morphological phenotypes when observed by confocal microscopy. However, all three strains were unable to produce a consistent biofilm in terms of thickness at both the air-liquid interface and the submerged areas. These data may indicate that conditions such as air exposure and desiccation encountered at the air-liquid interface may lead *E. coli* cells to form specific types of biofilm, perhaps better suited to survival in those conditions. Analysis of the ECM components present in interface and submerged biofilms may confirm this, but was not possible in this study.

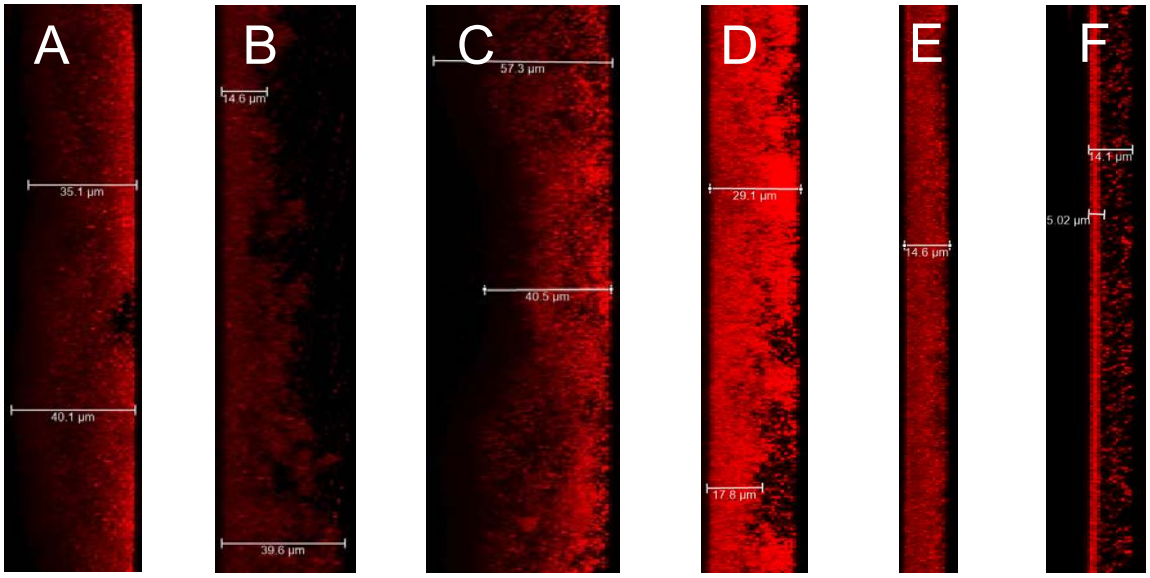

Figure 3.4a: *Representative side-view CLSM images of PHL644, BL21 Star (DE3) and Nissle 1917 biofilms on glass coupons grown using the 6-Well Plate method. A – PHL644 interface biofilm. B – PHL644 submerged biofilm. C – BL21 Star (DE3) interface biofilm. D – BL21 Star (DE3) submerged biofilm. E – Nissle 1917 interface biofilm. F – Nissle 1917 submerged biofilm. In all images, the base of the biofilm is on the left.*

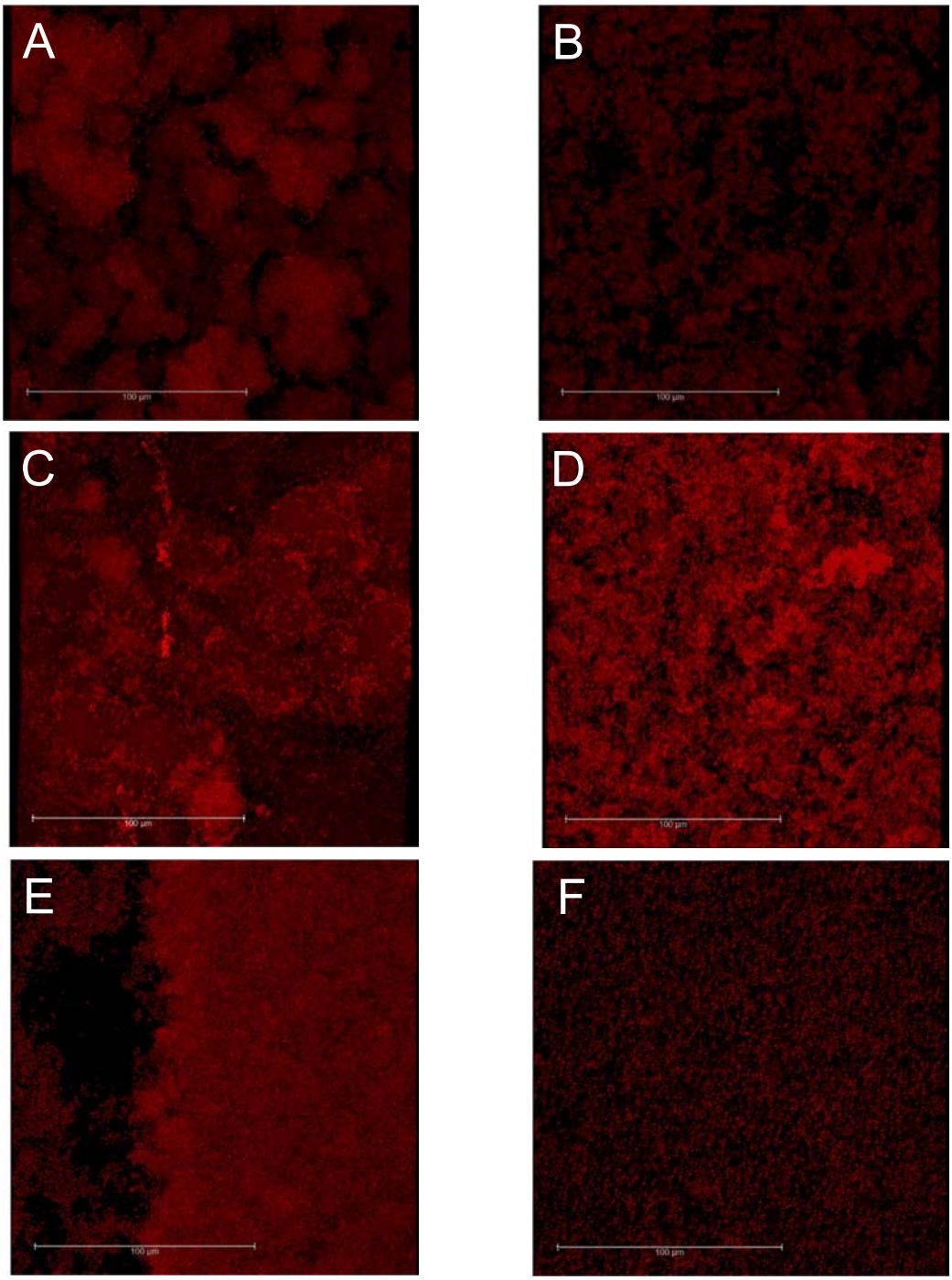

Figure 3.4b: *Representative top-down view CLSM images of PHL644, BL21 Star (DE3) and Nissle 1917 biofilms on glass coupons grown using the 6-Well Plate method. A – PHL644 interface biofilm. B – PHL644 submerged biofilm. C – BL21 Star (DE3) interface biofilm. D – BL21 Star (DE3) submerged biofilm. E – Nissle 1917 interface biofilm. F – Nissle 1917 submerged biofilm.*

3.3.2 Polystyrene and Polycarbonate

E. coli PHL644, BL21 Star (DE3) and Nissle 1917 biofilms were grown using the 6-well plate method. Biofilms were grown in 10 mL M63+ on a polystyrene or polycarbonate coupon at 30°C and 70 RPM for 3 days. Preparation of the coupons is described in Section 2.2.4.1. Biofilms were analysed using CV staining.

PHL644 showed a slight decrease in mean A_{580} on polystyrene compared to glass, but within 1 standard deviation (Figure 3.3). However, PHL644 had a statistically significant (more than 1 standard deviation) increase in A_{580} on the polycarbonate coupon. This indicates that PHL644 forms more biofilm on polycarbonate than glass or polystyrene. BL21 Star (DE3) displayed slight non-significant increases for both polystyrene and polycarbonate, indicating that these materials did not provide a better surface for BL21 Star (DE3) biofilm formation than glass. Nissle 1917 displayed a significant increase in A_{580} on polystyrene compared to glass, but with an even greater increase on polycarbonate, indicating that polycarbonate provides a better surface for Nissle 1917 biofilm development than glass or polystyrene. The reasons for this are unclear, but may be linked to the ECM components produced by the different strains.

3.3.3 Stainless Steel

E. coli PHL644, BL21 Star (DE3) and Nissle 1917 biofilms were grown using the 6-well plate method. Biofilms were grown in 10 mL M63+ on a stainless steel coupon at 30°C and 70 RPM for 3 days. Biofilms were analysed using CV staining.

PHL644 and BL21 Star (DE3) biofilms on stainless steel both displayed significant increases (more than 1 standard deviation) in A_{580} over glass, polystyrene or polycarbonate, indicating that stainless steel provided the best surface for biofilm formation for these strains of the

materials tested (Figure 3.3). Nissle 1917 biofilm on stainless steel did not display a significant A_{580} increase over polycarbonate, indicating that stainless steel and polycarbonate were equally suited to providing a surface for Nissle 1917 biofilm formation. Nissle 1917 displayed the lowest mean A_{580} of the three strains, but was within 1 standard deviation of PHL644 (but not of BL21 Star (DE3)), indicating that all three strains produced a similar amount of biofilm on stainless steel.

3.3.4 Polytetrafluoroethylene (PTFE)

As previously stated, a second biofilm generation technique, the Duran Bottle method, was required for testing PTFE. To ensure fair testing, PTFE-wrapped glass microscope slides were tested against uncovered glass microscope slides to compare biofilm formation on PTFE and glass. Comparable coupons could not be obtained for polystyrene, polycarbonate or stainless steel.

E. coli PHL644, BL21 Star (DE3) and Nissle 1917 biofilms were grown using the Duran Bottle method. Biofilms were grown in 70 mL M63+ on a glass microscope slide or a PTFE-wrapped glass microscope slide at 30°C and 70 RPM for 3 days. Biofilms were analysed using CV staining and CLSM.

As shown by Figure 3.5, PHL644 biofilms on PTFE showed a dramatic 15-fold increase in A_{580} over glass. Increases were also seen for BL21 Star (DE3) and Nissle 1917, albeit to a far lesser extent; approximately 2-fold and 1.5-fold respectively, with BL21 Star (DE3) producing more biofilm than Nissle 1917 (more than 1 standard deviation). While BL21 Star (DE3) and Nissle 1917 attained a similar A_{580} on PTFE (within 1 standard deviation), as with glass cover slips, PHL644 attained a level approximately half of these values. This indicates that PHL644 has a disadvantage in attaching to glass microscope slides compared to BL21

Star (DE3) and Nissle 1917, but not to glass cover slips. This is likely due to material differences between cover slips and microscope slides, or in biofilm components such as cellulose which is produced by BL21 Star (DE3) and Nissle 1917 but not by PHL644.

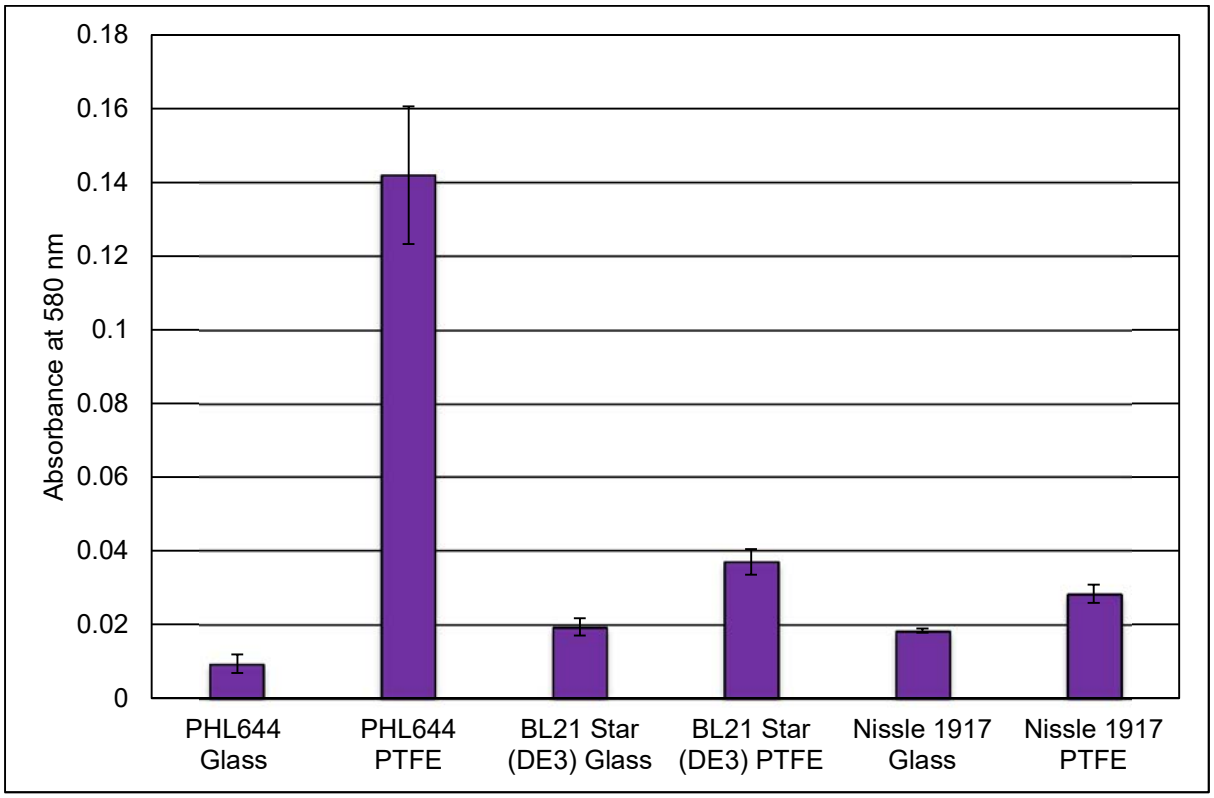

Figure 3.5: *Graph comparing CV retention of PHL644, BL21 Star (DE3) and Nissle 1917 biofilms on glass microscope slides and PTFE-wrapped microscope slides. Experiments were performed using the 100 mL Duran Bottle method. Error bars represent 1 standard deviation from the mean of 3 independent cultures.*

Biofilms grown on glass and PTFE showed striking differences in terms of microstructure. Figure 3.6 shows that PHL644 biofilms grown on glass microscope slides were very poor, and did not exceed 25 µm (Figure 3.6a). While some outgrowth could be observed at the interface, the structures mostly took the form of small sparse aggregates (Figure 3.6b). In contrast, PHL644 interface biofilms on PTFE revealed extremely thick structures of more

than 260 µm, with submerged areas comparably reaching more than 200 µm (Figure 3.6c). The actual thickness of the PHL644 biofilms is unknown, as the confocal images do not appear to have a defined point where the biofilm is in contact with the PTFE surface. This is likely due to either poor Syto 62 dye penetration or poor laser penetration. Importantly, both interface and submerged PHL644 biofilms showed extensive outgrowth and defined 3D structure, indicating consistent growth in both areas, in contrast to glass (Figure 3.6e).

BL21 Star (DE3) biofilms on glass reached a consistent thickness of around 45 µm at both the interface and submerged regions (Figure 3.6a). BL21 Star (DE3) biofilms on PTFE displayed consistent thicknesses of ~130 µm at the interface region and ~80 µm at the submerged region (Figure 3.6d). Interestingly, BL21 Star (DE3) did not display the same distinctive mushroom-shaped outgrowths and produced generally flatter and smoother biofilms than PHL644 (Figure 3.6e). This may be due to differing ECM components, as BL21 Star (DE3) produces cellulose, while PHL644 does not. These differences in morphology were not apparent in the 6-Well Plate experiments as perhaps these differences can only be noted in thicker biofilms.

Nissle 1917 biofilms on glass and PTFE were extremely thin (<20 µm) and displayed little outgrowth (Figure 3.6d). Many unattached, moving cells were observed in the images suggesting that the structures produced had little cohesion (Figure 3.6e). This suggests that glass and PTFE are not amenable to biofilm formation by Nissle 1917.

These increases indicate that PTFE is a more amenable surface to biofilm formation by PHL644, BL21 Star (DE3) and Nissle 1917 than glass, but PHL644 benefitted the most from this material.

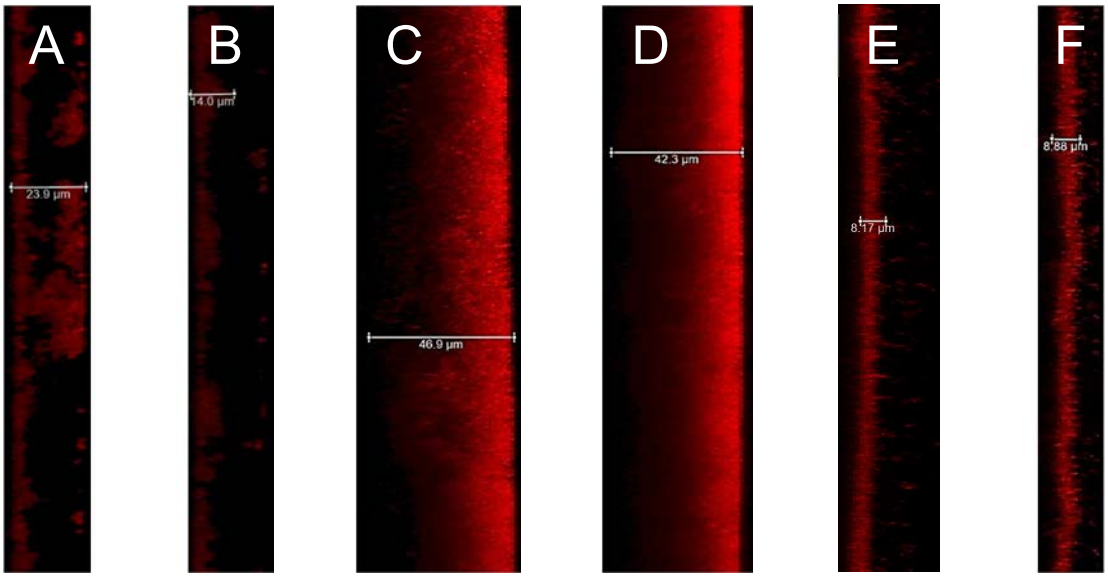

Figure 3.6a: *Representative side-view CLSM images of PHL644, BL21 Star (DE3) and Nissle 1917 biofilms on glass microscope slides grown using the Duran Bottle method. A – PHL644 interface biofilm. B – PHL644 submerged biofilm. C – BL21 Star (DE3) interface biofilm. D – BL21 Star (DE3) submerged biofilm. E – Nissle 1917 interface biofilm. F – Nissle 1917 submerged biofilm. In all images, the base of the biofilm is on the left.*

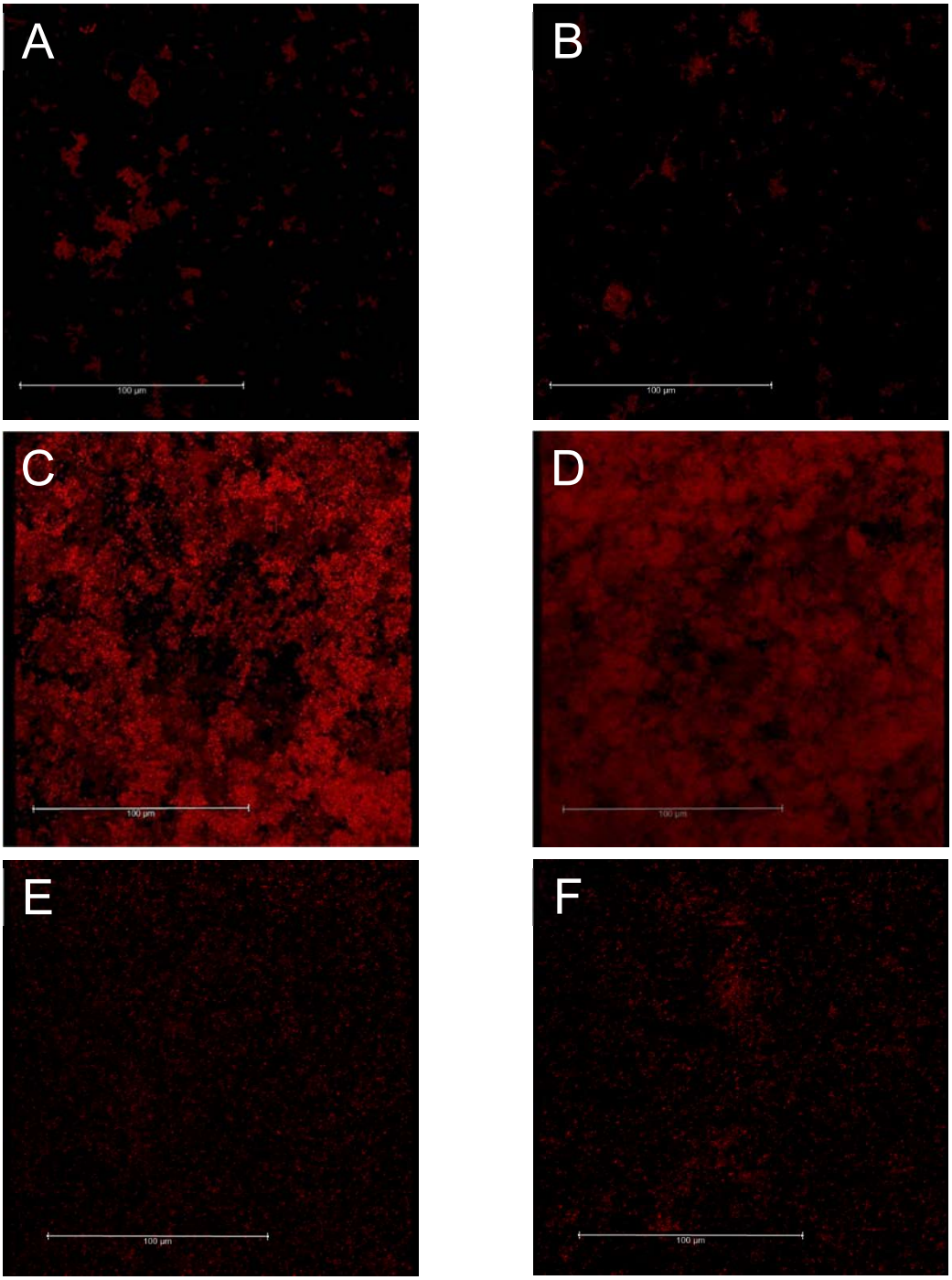

Figure 3.6b: *Representative top-down-view CLSM images of PHL644, BL21 Star (DE3) and Nissle 1917 biofilms on glass microscope slides grown using the Duran Bottle method. A – PHL644 interface biofilm. B – PHL644 submerged biofilm. C – BL21 Star (DE3) interface biofilm. D – BL21 Star (DE3) submerged biofilm. E – Nissle 1917 interface biofilm. F – Nissle 1917 submerged biofilm.*

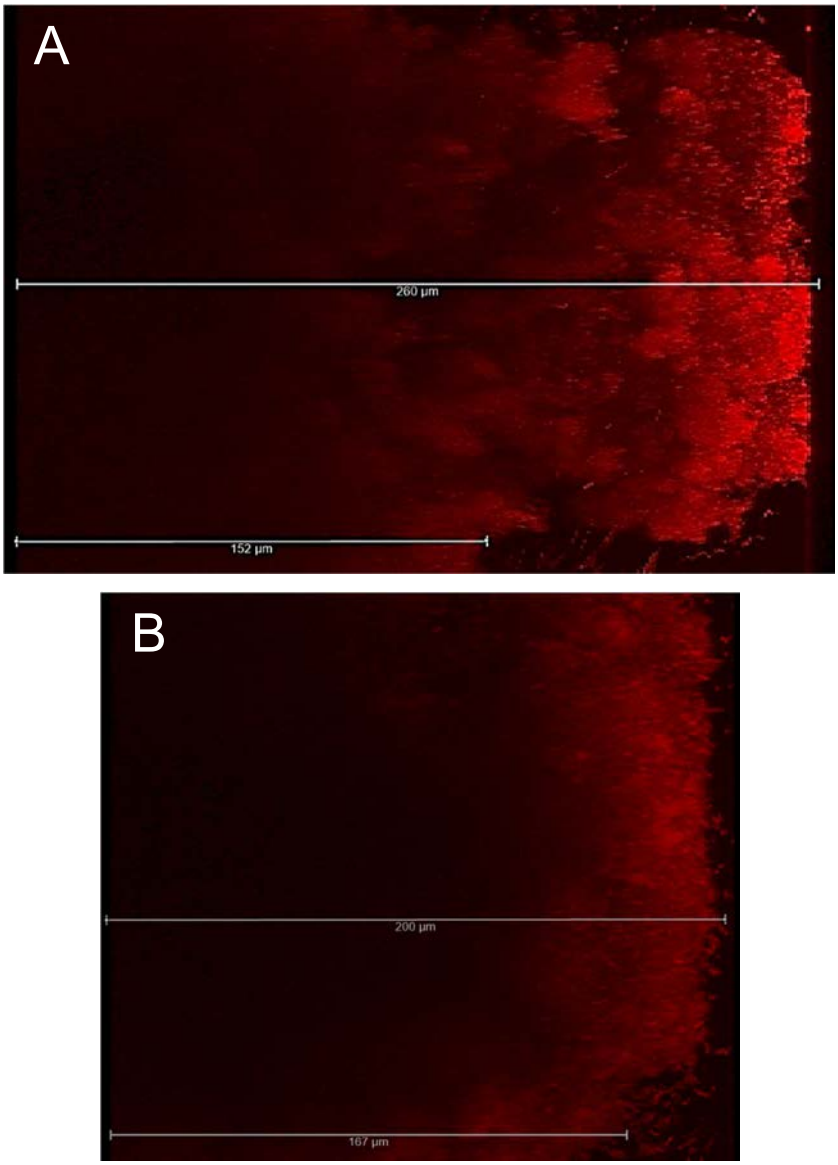

Figure 3.6c: *Representative side-view CLSM images of PHL644 biofilm on PTFE-wrapped microscope slides grown using the Duran Bottle method. A – PHL644 interface biofilm. B – PHL644 submerged biofilm. In all images, the base of the biofilm is on the left.*

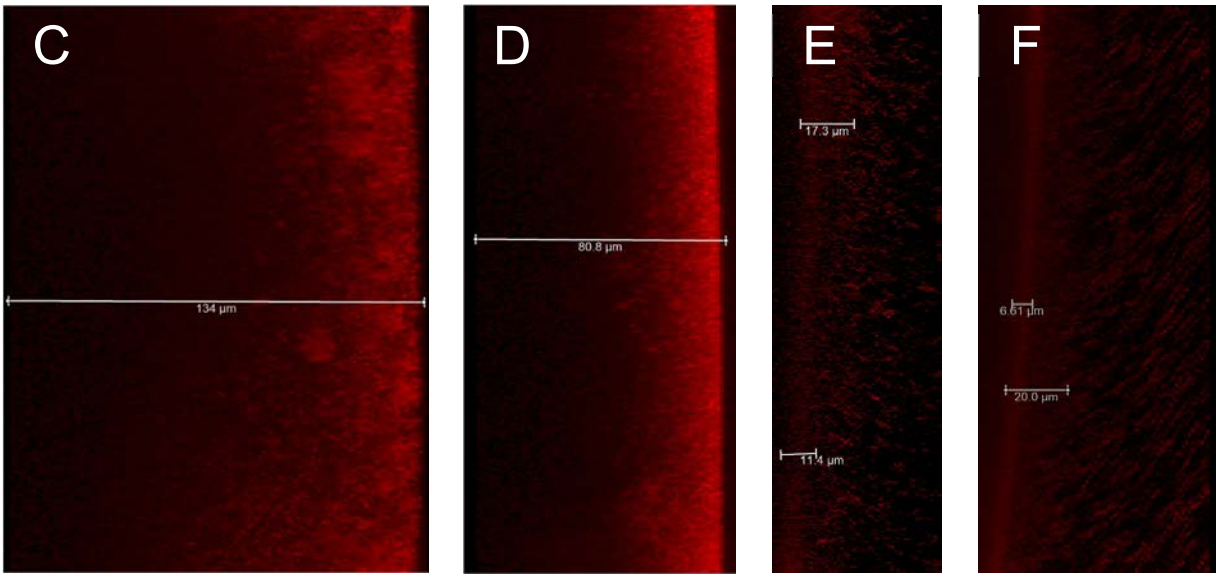

Figure 3.6d: *Representative side-view CLSM images of BL21 Star (DE3) and Nissle 1917 biofilms on PTFE-wrapped microscope slides grown using the Duran Bottle method. C – BL21 Star (DE3) interface biofilm. D – BL21 Star (DE3) submerged biofilm. E – Nissle 1917 interface biofilm. F – Nissle 1917 submerged biofilm. In all images, the base of the biofilm is on the left.*

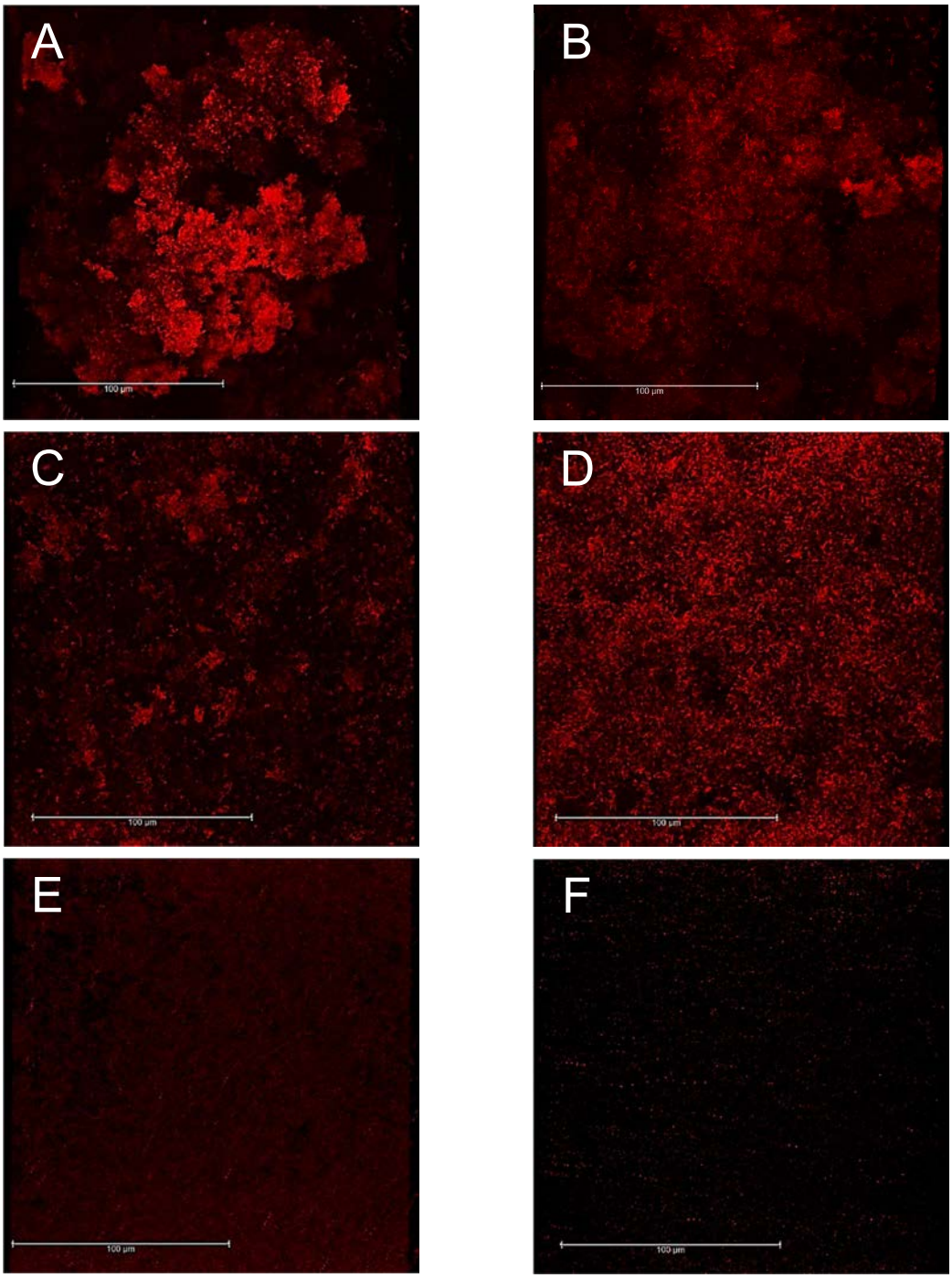

Figure 3.6e: *Representative top-down-view CLSM images of PHL644, BL21 Star (DE3) and Nissle 1917 biofilms on PTFE-wrapped microscope slides grown using the Duran Bottle method. A – PHL644 interface biofilm. B – PHL644 submerged biofilm. C – BL21 Star (DE3) interface biofilm. D – BL21 Star (DE3) submerged biofilm. E – Nissle 1917 interface biofilm. F – Nissle 1917 submerged biofilm.*

3.3.5 Conclusions on Material Screening

Biofilms grown on glass, PS, PC and SS displayed similar phenotypes in terms of biofilm abundance, microstructure and material coverage. Nevertheless, none of these materials could produce a robust biofilm in the submerged region. SS facilitated a slight increase in colonisation of the submerged region, likely due to the inherent rugosity of SS materials, but not to the extent of PTFE. The discovery that PTFE was highly amenable to producing not only a thicker PHL644 or BL21 Star (DE3) biofilm but a biofilm which covered the entire surface was therefore a great step forward in determining a surface suitable for the biofilm biocatalyst. As PTFE is used in urinary catheters to prevent the attachment of UTI-related bacteria such as *E. coli*, it was somewhat surprising that all three strains displayed increased colonisation of a PTFE surface (Lam TB *et al*., 2014). However, the orbital mechanical forces applied to the biofilms grown in the Duran Bottle method may permit repeated reversible attachment events where a continual non-recycling system might wash away reversibly-attached bacteria. Despite the observed increases in biofilm formation, questions remained as to why PTFE increased biofilm formation so radically with PHL644. As such, the following experiments were designed to answer this question.

3.3.6 Hydrophobicity and Contact Angle Measurement

PHL644 overproduces curli fimbriae due to the *ompR234* allele (Pringent-Combaret C *et al*., 2001). It was questioned as to whether the increases in biofilm development could be attributed to increased interaction between curli fimbriae and the surface substrate. Curli proteins are highly hydrophobic due to multiple β-sheet folds (Stefani M, 2004). A more hydrophobic surface would therefore be expected to have stronger interactions with curli than a more hydrophilic surface.

In order to determine the relative hydrophobicity of a surface, a method known as contact angle analysis was employed. A small drop of deionised water was dripped onto each material coupon from a hypodermic needle approximately 20 cm above the coupon. An image of the droplet on the surface was obtained and the angle at which it contacted the surface was measured. A narrower angle indicated that the water droplet interacts strongly with the coupon, indicating hydrophilicity. A wider angle indicated that the water droplet is repelled by the coupon, indicating hydrophobicity.

Table 3.1 lists the contact angle measurements noted for the materials used in these experiments. PTFE displayed the highest contact angle measurement at 113°, and was therefore the most hydrophobic substrate used in the experiment. Glass displayed the lowest contact angle measurement at 43° and was therefore the least hydrophobic. PS, PC and SS contact angles were in the range of 80° to 90°, indicating more hydrophobicity than glass but less hydrophobicity than PTFE. This likely explains how these materials were able to exhibit increased biofilm formation over glass, but not to the extent of PTFE, as noted in Figure 3.5. Hydrophobicity was therefore shown to be a factor in the formation of *E. coli* biofilms, at least with these strains tested, which is complemented by previous data (Patel J *et al*., 2011). However, other research suggests that bacterial biofilm formation is more dependent on surface chemical groups than solely hydrophobicity, and that biofilm formation cannot be predicted by contact angle data alone (Hook AL *et al*., 2012). More extensive analysis could provide insight into how *E. coli* strains interact with these surfaces. Nevertheless, hydrophobic PTFE was proven to promote extensive biofilm formation in these experiments.

Table 3.1: *Comparison of contact angles observed for deionised water droplets on materials tested in this study. Mean and standard deviation values derived from 3 independent tests.*

Material	Mean Contact Angle	Standard Deviation
Glass	43°	±1.53°
PS	85°	±3.51°
PC	84°	±2.52°
SS	89°	±1.73°
PTFE	113°	±3.06°

3.3.7 Comparison of PHL644 and MC4100 Biofilm Formation

To determine whether the *ompR234* allele was essential to PHL644 biofilm formation on PTFE, PHL644 was compared against its parent strain MC4100. MC4100 and PHL644 biofilms were grown using the Duran Bottle method. Biofilms were grown in 70 mL M63+ on either a glass microscope slide or a PTFE-wrapped microscope slide at 30°C and 70 RPM for 3 days. Biofilms were analysed using CV staining and CLSM. From this point, all representative images were taken from submerged areas of the biofilm as there was found to be no observable difference in biofilm morphology between the interface and submerged areas.

As shown by Figure 3.7, PHL644 displayed no significant increase in A_{580} (within 1 standard deviation) on glass compared to MC4100. However, PHL644 displayed an increase in A_{580} of 6.5 fold on PTFE over MC4100.

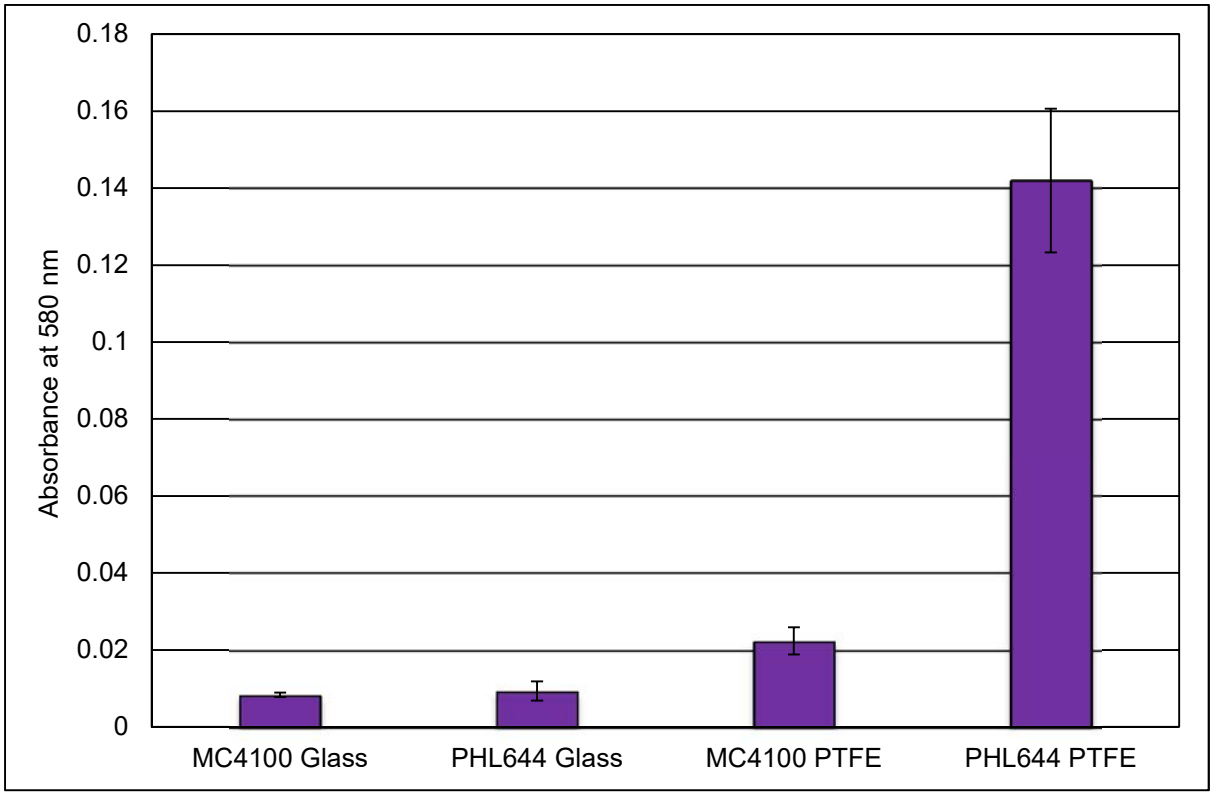

Figure 3.7: *Graph comparing CV retention of MC4100 and PHL644 on glass microscope slides and PTFE-wrapped microscope slides. Experiments were performed using the Duran Bottle method. Error bars represent 1 standard deviation from the mean of 3 independent cultures.*

Figure 3.8 reveals that MC4100 grew an extremely thin (<15 μm), sparse biofilm on glass with little aggregation. On PTFE, MC4100 displayed more aggregation and some outgrowth (~25 μm) but was much thinner and sparser than PHL644 on PTFE (~200 μm). On glass, PHL644 appears to aggregate more than MC4100, likely due to the effect of overproduced curli fimbriae. However, this overproduction does not seem to assist in biofilm growth on glass, as with PTFE.

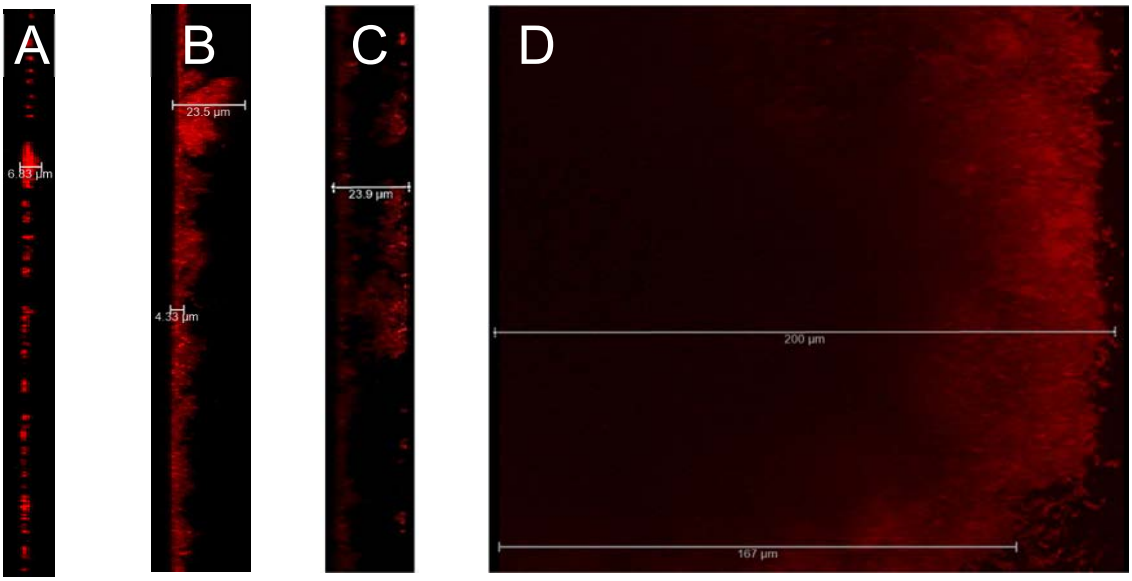

Figure 3.8a: *Representative side-view CLSM images of MC4100 and PHL644 biofilms grown on either glass microscope slides or PTFE wrapped microscope slides using the Duran Bottle method. A – MC4100 biofilm on glass. B – MC4100 biofilm on PTFE. C – PHL644 biofilm on glass. D – PHL644 biofilm on PTFE. In all images, the base of the biofilm is on the left.*

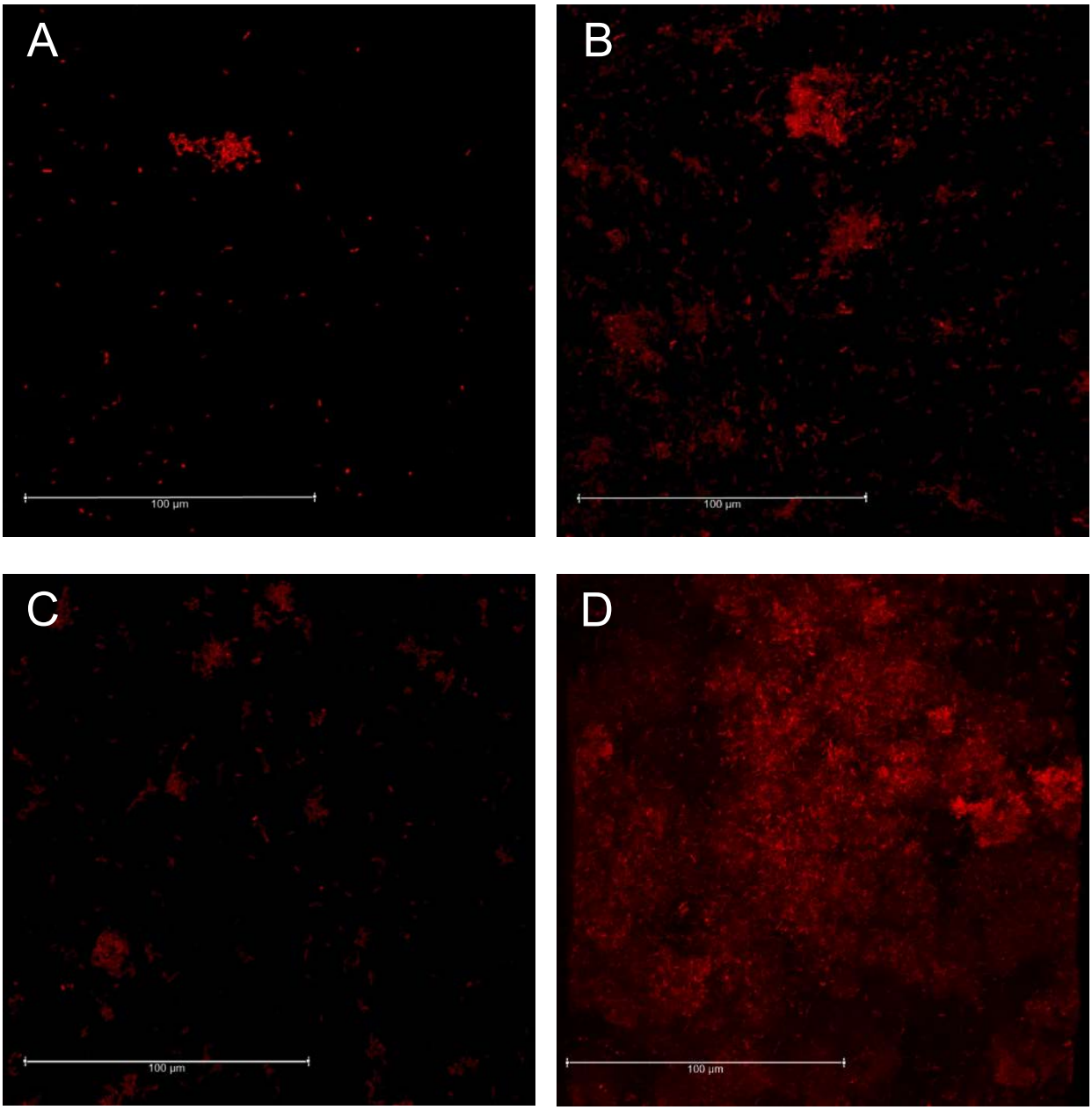

Figure 3.8b: *Representative top-down-view CLSM images of MC4100 and PHL644 biofilms grown on either glass microscope slides or PTFE wrapped microscope slides using the Duran Bottle method. A – MC4100 biofilm on glass. B – MC4100 biofilm on PTFE. C – PHL644 biofilm on glass. D – PHL644 biofilm on PTFE.*

These results indicate that the *ompR234* allele increased biofilm formation on PTFE (a hydrophobic material), but had little effect on biofilm formation on glass (a hydrophilic material) in this model. This is most likely due to the overproduction of hydrophobic curli fimbriae allowing stronger interactions with PTFE. Further experiments could include inserting the *ompR234* allele into BL21 Star (DE3) and Nissle 1917 to determine whether similar benefits could be achieved in these strains. Interestingly, MC4100 biofilm formation was increased on PTFE over glass, though not to the extent of PHL644, indicating that it is more competent in colonising PTFE. This suggests that MC4100 possesses limited formation ability, but less than PHL644, BL21 Star (DE3) or Nissle 1917 when compared to Figure 3.5.

The evidence presented here highlights the fact that PTFE was capable of producing the most abundant, thickest and most consistent *E. coli* biofilms of the materials tested in this study. As such, PTFE was chosen as the 'ideal' surface for the biofilm biocatalyst. It was suggested during the study that a nano-structured superhydrophobic surface would be more consistent in terms of biofilm formation than the consumer-grade PTFE tape used herein. However, PTFE tape was deemed to be suitable in this work due to its inexpensiveness and ease of handling.

3.3.8 Development of *E. coli* Biofilm Over Time

It was decided to image the developing biofilms over 3 days to investigate how PHL644 and BL21 Star (DE3) biofilms formed and what changes in morphology could be observed during this period. Nissle 1917 was omitted from all further experiments due to poor biofilm formation under these conditions compared to PHL644 and BL21 Star (DE3).

PHL644 and BL21 Star (DE3) biofilms were grown using the Duran Bottle method. Biofilms were grown in 70 mL M63+ on a PTFE-wrapped microscope slide at 30°C and 70 RPM for 3 days. Biofilms were analysed using CV staining and CLSM at 24, 48 and 72 hours.

Figure 3.9 shows that the largest increases in biofilm formation in PHL644 and BL21 Star (DE3) occurred between 24 and 48 hours. After 24 hours, PHL644 biofilm reached an A_{580} of 0.034, compared to BL21 Star (DE3) at 0.017. PHL644 increased to an A_{580} of 0.109 after 48 hours, an increase of ~3.2 fold. BL21 Star (DE3) increased to 0.03 after 48 hours, an increase of 1.75 fold.

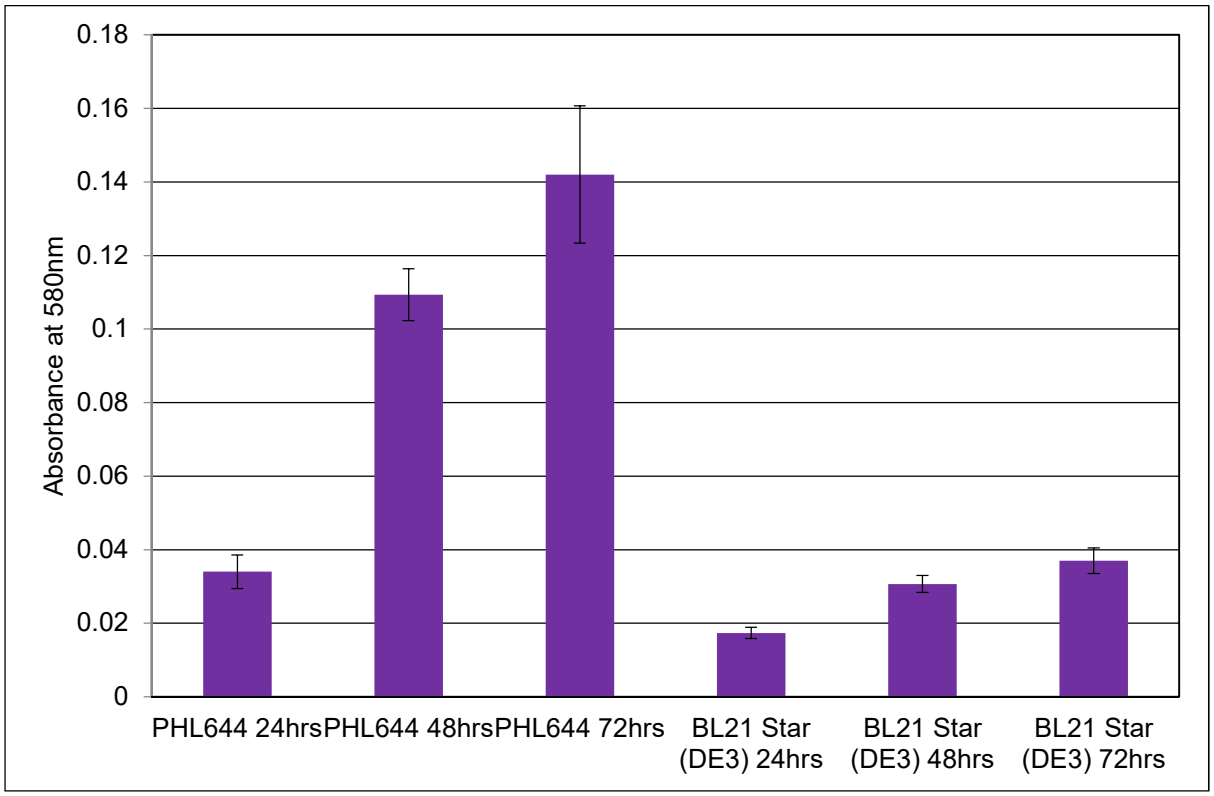

Figure 3.9: *Graph comparing CV retention of PHL644 and BL21 Star (DE3) biofilms on PTFE-wrapped microscope slides over 3 days using the Duran Bottle method. Error bars represent 1 standard deviation from the mean of 3 independent cultures.*

Figure 3.10 reveals the thickness of the biofilm increased over the 3 days in all cases. After 24 hours, PHL644 biofilm reached a maximum thickness of ~120 μm. After 48 hours, this level increased to between ~130 and ~170 μm, and then to over 200 μm after 72 hours. Comparatively, BL21 Star (DE3) reached a maximum thickness of ~30 μm after 24 hours, increasing to ~50 μm after 48 hours, and then to ~80 μm after 72 hours. The increase in maximum thicknesses of these biofilms do not follow the same pattern as the CV staining data, suggesting that biofilm thickness may be less consistent over the entire surface than the CLSM images indicate. Another possibility is that the level of staining by CV does not have a linear relationship with the thickness of the biofilm, and different ECM components produced at different times may bind different amounts of CV stain. This would require extensive analysis of the composition of the biofilm ECM to test and thus could not be performed in this study.

The morphologies adopted may give some insight into the process of biofilm maturation. In both strains, biofilms grown for 24 and 48 hours appear rougher and less compact than at 72 hours, suggesting that biofilm maturation involves a smoothing of the biofilm architecture with a more compact structure. This form of maturation may lead to an overall strengthening of the biofilm matrix as well as reducing possible mechanical damage from flow forces. It is unknown whether this maturation effect may be seen in other techniques of biofilm growth, but is nevertheless an interesting concept. It would be beneficial to observe the biofilms in growth more frequently to provide a clearer picture of formation. It would also be of interest to grow the biofilms for a longer period to determine if any other maturation processes may be observed.

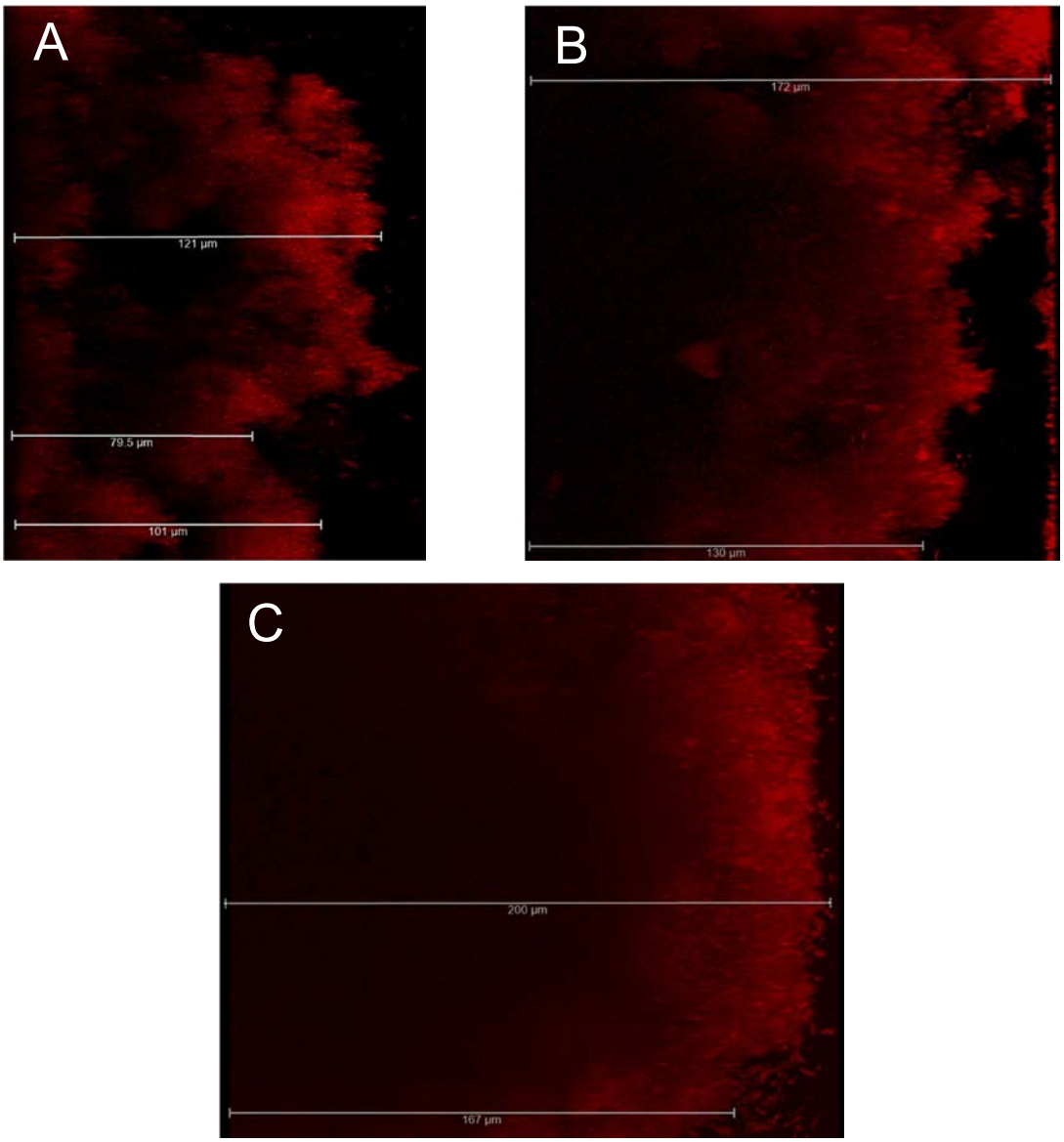

Figure 3.10a: *Representative side-view CLSM images of PHL644 biofilms on PTFE-wrapped microscope slides over 3 days using the Duran Bottle method. A – 24 hour PHL644 biofilm. B – 48 hour PHL644 biofilm. C – 72 hour PHL644 biofilm. In all images, the base of the biofilm is on the left.*

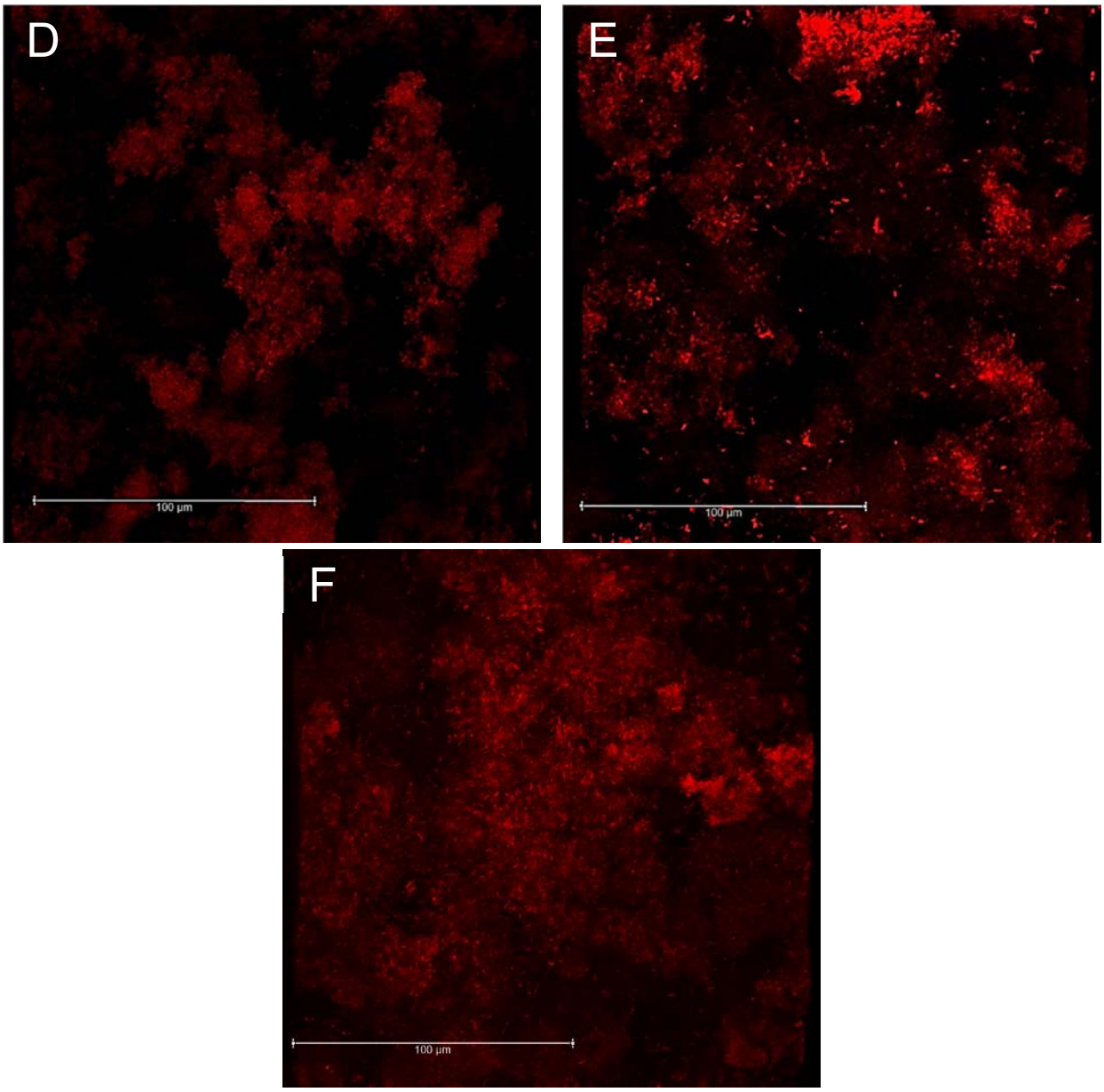

Figure 3.10b: *Representative top-down-view CLSM images of PHL644 biofilms on PTFE-wrapped microscope slides over 3 days using the Duran Bottle method. A – 24 hour PHL644 biofilm. B – 48 hour PHL644 biofilm. C – 72 hour PHL644 biofilm.*

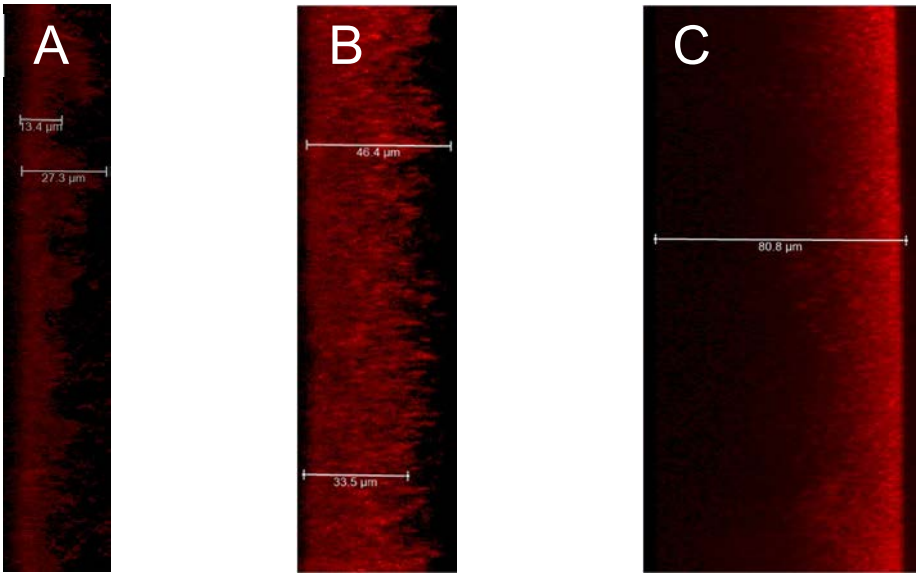

Figure 3.10c: *Representative side-view CLSM images of BL21 Star (DE3) biofilms on PTFE-wrapped microscope slides over 3 days using the Duran Bottle method. A – 24 hour BL21 Star (DE3) biofilm. B – 48 hour BL21 Star (DE3) biofilm. C – 72 hour BL21 Star (DE3) biofilm. In all images, the base of the biofilm is on the left.*

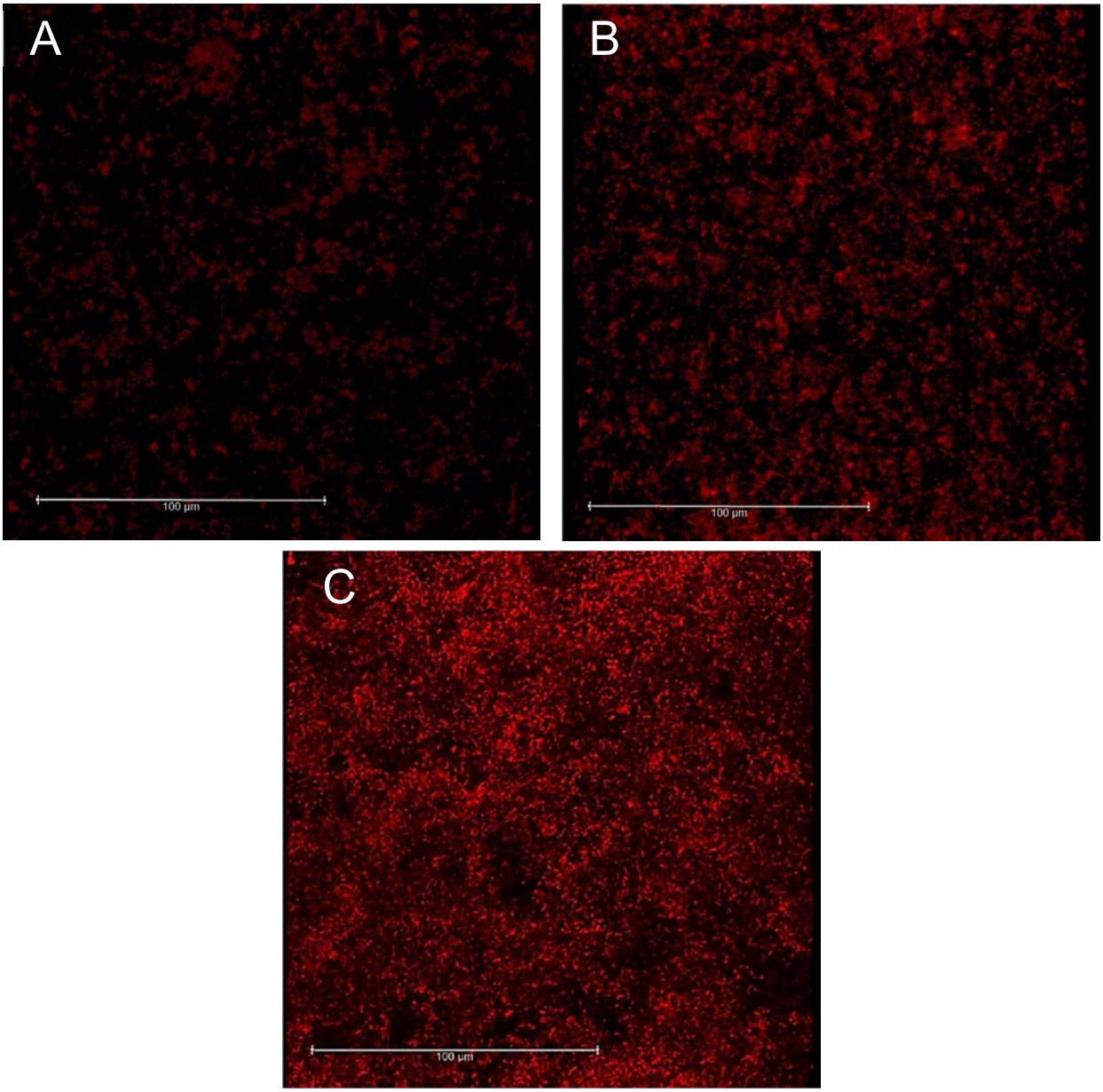

Figure 3.10d: *Representative top-down-view CLSM images of BL21 Star (DE3) biofilms on PTFE-wrapped microscope slides over 3 days using the Duran Bottle method. A – 24 hour BL21 Star (DE3) biofilm. B – 48 hour BL21 Star (DE3) biofilm. C – 72 hour BL21 Star (DE3) biofilm.*

3.3.9 Effect of Growth Medium on Biofilm Formation

The choice of growth medium is important to biofilm generation. Studies have shown that an abundance of nutrients such as glucose can directly inhibit biofilm-forming mechanisms, and that minimal media with limited resources such as M63 and M9 stimulate *E. coli* to produce biofilms (Hufnagel DA *et al*., 2016, Jackson DW *et al*., 2002, Naves P *et al*., 2008). Despite this, other studies have found the correlation between biofilm formation and media composition to be less clear-cut and highly dependent on strain (Reisner A *et al*., 2006). To determine the effect of media composition on the biofilm forming strains used in this study, PHL644 biofilms were grown in either LB (a rich medium) or M63+ (a minimal medium).

PHL644 biofilms were grown using the Duran Bottle method. Biofilms were grown in 70 mL LB or M63+ on a PTFE-wrapped microscope slide at 30°C and 70 RPM for 3 days. Biofilms were analysed using CV staining and CLSM.

As shown by Figure 3.11, PHL644 biofilms grown on PTFE in LB reached an A_{580} approximately 1/3 of the value for M63+, suggesting that despite the increased nutrient content, this did not lead to increased biofilm formation.

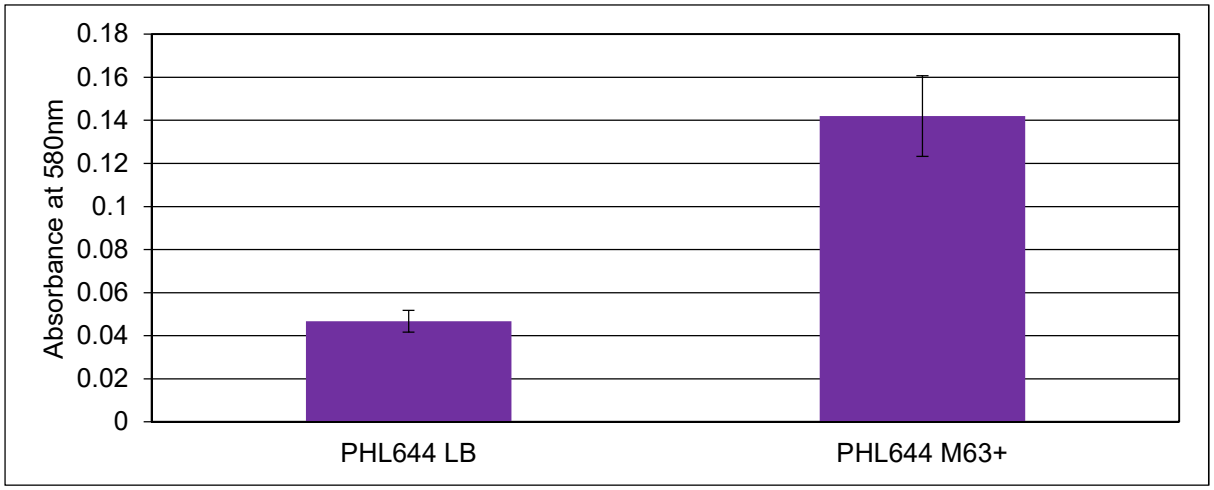

Figure 3.11: *Graph comparing CV retention of PHL644 biofilms grown on PTFE-wrapped microscope slides in either LB or M63+ medium using the Duran Bottle method. Error bars represent 1 standard deviation from the mean of 3 independent cultures.*

Figure 3.12 reveals that PHL644 biofilms grown in LB medium did not exceed 70 µm in thickness, compared to >200 µm for M63+, and did not display the architectural structures seen for PHL644 biofilms grown in M63+.

These data indicate that M63+ supports the formation of thicker, more structured PHL644 biofilms than LB. The reasons for this likely follow the findings of previous studies, that a rich medium contains abundant nutrients which repress biofilm-forming pathways (Jackson DW *et al*., 2002, Hufnagel DA *et al*., 2016). Of interest is the observation that the biofilms grown in LB using the Duran Bottle method appear less compact and do not display the defined structures seen for ones grown in M63+. It may be beneficial to observe the LB-grown biofilms over time to determine how this particular morphology has formed, and suggest any differences to M63+-grown biofilms.

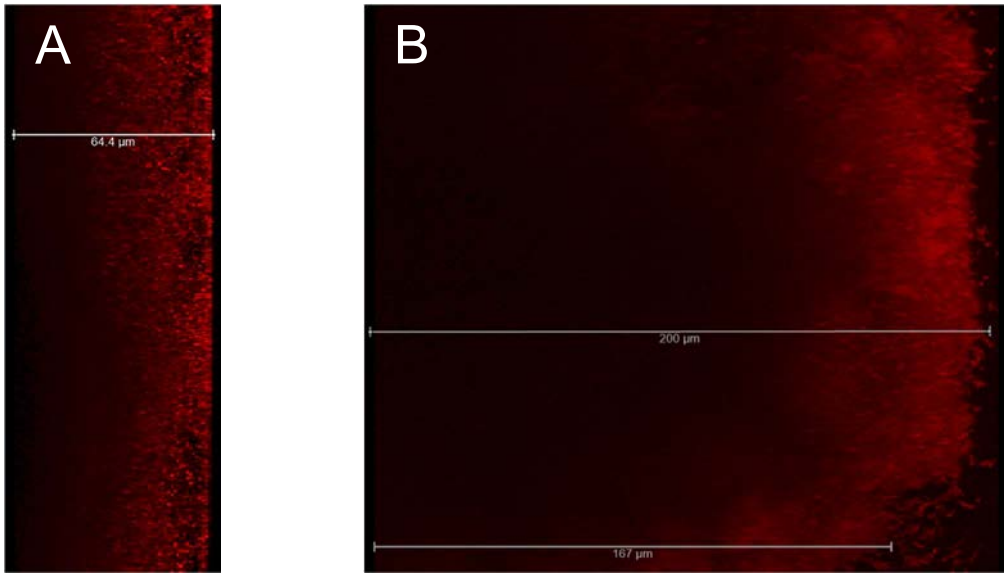

Figure 3.12a: *Representative side-view CLSM images of PHL644 biofilms grown on PTFE-wrapped microscope slides in either LB or M63+ medium using the Duran Bottle method. A – PHL644 biofilm grown in LB medium. B – PHL644 biofilm grown in M63+ medium. In all images, the base of the biofilm is on the left.*

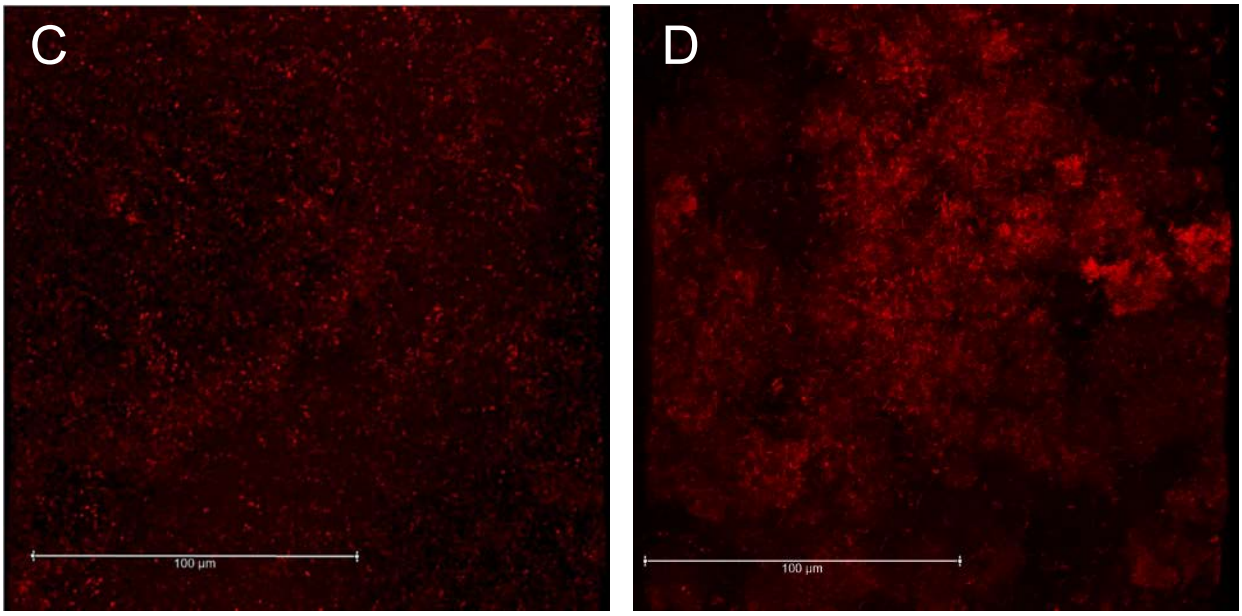

Figure 3.12b: *Representative top-down-view CLSM images of PHL644 biofilms grown on PTFE-wrapped microscope slides in either LB or M63+ medium using the Duran Bottle method. A – PHL644 biofilm grown in LB medium. B – PHL644 biofilm grown in M63+ medium.*

3.3.10 Effect of Glucose on Biofilm Formation

As described in Section 1.4.3, glucose has an inhibitory effect on biofilm formation and CsgD expression in *E. coli* through repression of the cAMP-CRP activator (Jackson DW *et al*., 2002, Hufnagel DA *et al.*, 2016). It is therefore logical to keep the concentration of glucose low in a biofilm-formation medium. To determine the effect of glucose elicits on biofilm formation in the model described in this chapter, M63+ was modified to contain varying concentrations of glucose.

PHL644 biofilms were grown using the Duran Bottle method. Biofilms were grown in 70 mL M63+ on a PTFE-wrapped microscope slide at 30°C and 70 RPM for 3 days. M63+ was

modified to contain either 0 mM, 1 mM, 10 mM or 100 mM glucose. Biofilms were analysed using CV staining.

As shown in Figure 3.7, a high concentration of glucose (100 mM) had a negative effect on biofilm formation and reduced the measured A_{580} by approximately 4.5 fold compared to 10 mM. The level of CV retention for 100 mM glucose was in fact within 1 standard deviation of the level observed for 1 mM glucose, suggesting that glucose abundance is as detrimental to biofilm formation as glucose deficiency. When glucose was omitted from the medium (0 mM), an extremely low A_{580} was noted, despite the fact that 17 mM sodium succinate (a secondary carbon source) was still present in the media. This suggests that the presence of glucose is essential to biofilm growth in this medium. 10 mM glucose gave the highest A_{580} and was thus determined to be a suitable concentration for biofilm growth.

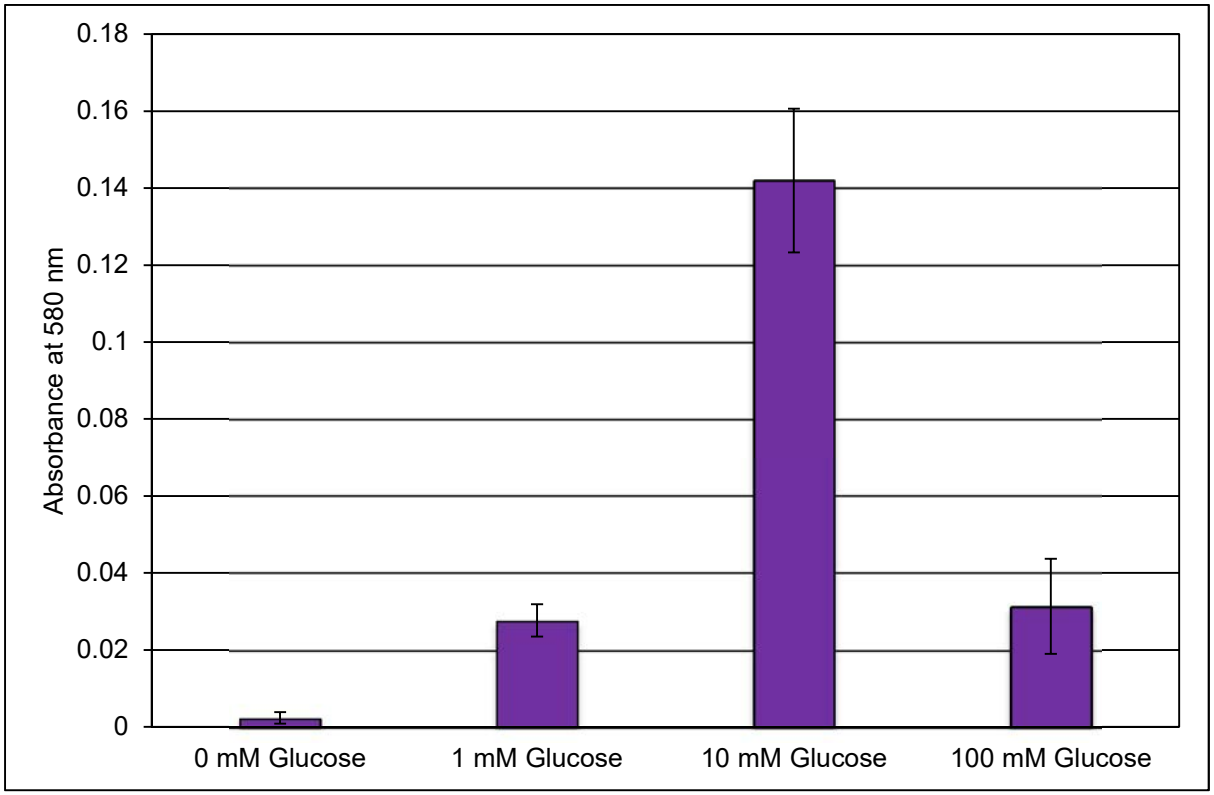

Figure 3.13: *Graph comparing CV retention of PHL644 biofilm grown on PTFE-wrapped microscope slides in M63+ with varying concentrations of glucose using the Duran Bottle method. Error bars represent 1 standard deviation from the mean of 3 independent cultures.*

3.3.11 Effect of Succinate, Potassium and Sodium on Biofilm Formation

In previous work, 17 mM potassium succinate was added to standard M63 to create a novel biofilm formation medium (Tsoligkas A *et al*., 2011). This addition was intended to provide a secondary carbon source which would enhance the growth of the cells and the biofilm matrix. Succinate ions feed directly into the citric acid cycle of *E. coli* and as such do not increase the level of intracellular glucose, thereby preventing catabolite repression of biofilm-formation pathways (Hufnagel DA *et al*., 2016). It was decided to test whether another source of succinate ions would create a better biofilm-producing medium. This idea was derived from the finding that the *pgaABCD* operon (responsible for the production of

the ECM component PNAG) is activated by the transcriptional regulator NhaR, which is activated by sodium ions (Cerca N *et al*., 2008). It was therefore hypothesised that sodium succinate instead of potassium succinate would improve *E. coli* biofilm growth by increasing the production of PNAG.

PHL644 biofilms were grown using the Duran Bottle method. Biofilms were grown in 70 mL M63+ on a PTFE-wrapped microscope slide at 30°C and 70 RPM for 3 days. M63+ was modified to contain either 0 mM succinate, 17 mM succinic acid, 17 mM potassium succinate or 17 mM sodium succinate. Biofilms were analysed using CV staining.

As shown by Figure 3.14, 17 mM sodium succinate elicited the greatest increase in A_{580} over standard M63 (no succinate, 10 mM glucose), by approximately 3.5 fold. 17 mM succinic acid increased biofilm over standard M63 by approximately 2 fold. Both potassium succinate and sodium succinate were superior to succinic acid, suggesting that both cations had positive effects, with sodium as the strongest. It was noted that when succinate ions were omitted (0 mM succinate), a biofilm was still produced, in contrast to the removal of glucose. This indicates that glucose is an essential component in this biofilm growth model, while succinate is a beneficial supplement.

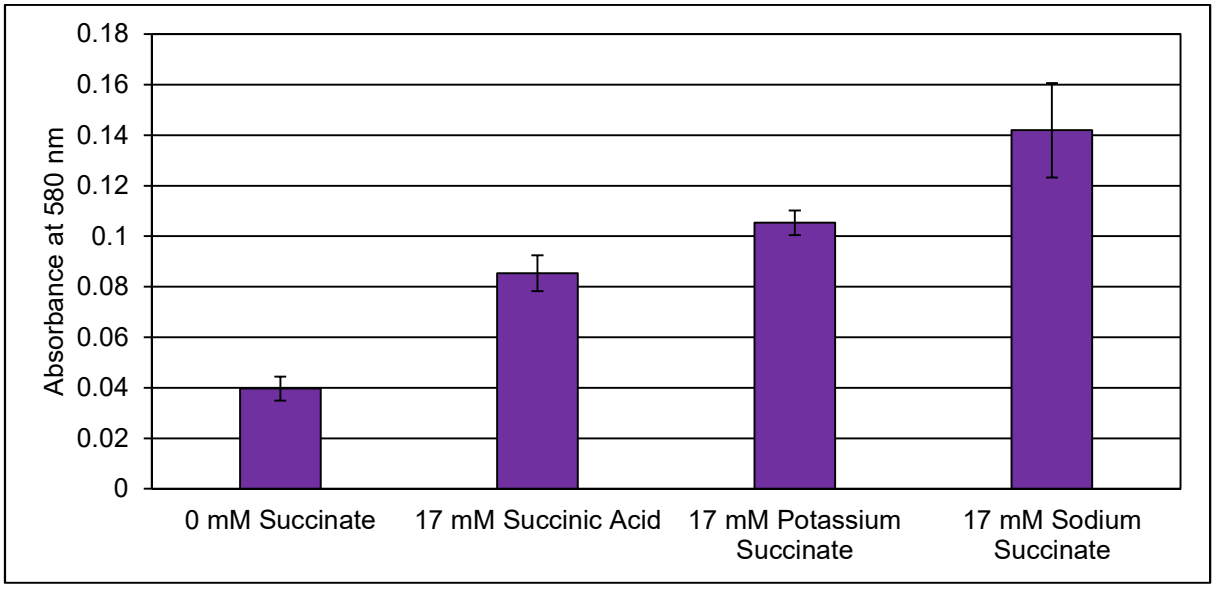

Figure 3.14: *Graph comparing CV retention of PHL644 biofilms grown on PTFE-wrapped microscope slides in M63+ with varying sources of succinate ions (with standard 10 mM glucose) using the Duran Bottle method. Error bars represent 1 standard deviation from the mean of 3 independent cultures.*

It is clear that the addition of succinate to standard M63 is beneficial to increasing biofilm formation in PHL644, likely by increasing available resources for population growth and forming carbon-based biofilm components such as polysaccharides. It is also clear that sodium and potassium have further positive effects on biofilm formation. In the case of sodium, this is likely due to the effects on PNAG production as previously stated. The effect of potassium is less clear however, as M63 medium already contains 100 mM potassium phosphate (and is adjusted to pH7 with potassium hydroxide) and therefore additional potassium ions would not be expected to have any effects. To theorise, additional potassium ions may affect the osmotic balance of the media and have biofilm-promoting effects on the *E. coli* cells, as noted by previous studies (Beloin C *et al*., 2008, Francez-Charlot A *et al*., 2005). This observation may warrant further study, but due to time constraints, was not

explored in this work. Sodium succinate was deemed to be the best succinate source for M63+, and was therefore used in all instances of M63+.

3.3.12 Effect of Temperature on Biofilm Formation

Various studies have shown that *E. coli* biofilm formation is affected by temperature (Rühs PA *et al*., 2013, Uhlich GA *et al*., 2014, Adnan M *et al*., 2010). *E. coli* is most well-known for colonising the mammalian gut, which maintains a temperature of 37°C. However, *E. coli* can also survive outside of a host, at temperatures below 37°C. As such, it was decided to determine an optimal temperature for biofilm formation on the PTFE surface.

PHL644 biofilms were grown using the Duran Bottle method. Biofilms were grown in 70 mL M63+ on a PTFE-wrapped microscope slide at either 25°C, 30°C or 37°C and 70 RPM for 3 days. Biofilms were analysed using CV staining.

As shown by Figure 3.15, PHL644 biofilms grown at 30°C exhibited the greatest A_{580}. Biofilms grown at 25°C and 37°C were both reduced in A_{580} compared to 30°C, but surprisingly 37°C produced the least biofilm of the three temperatures. *E. coli* typically forms a biofilm in a host gut at 37°C, but specific biofilm-promoting stimuli found in a host may be missing from this model. In addition, there may be significant differences between the biotic surface of a host gut and the abiotic surfaces used in these experiments, and different biofilm formation factors may be produced at different temperatures. 30°C was therefore determined to be a suitable temperature for growing the biofilm biocatalyst.

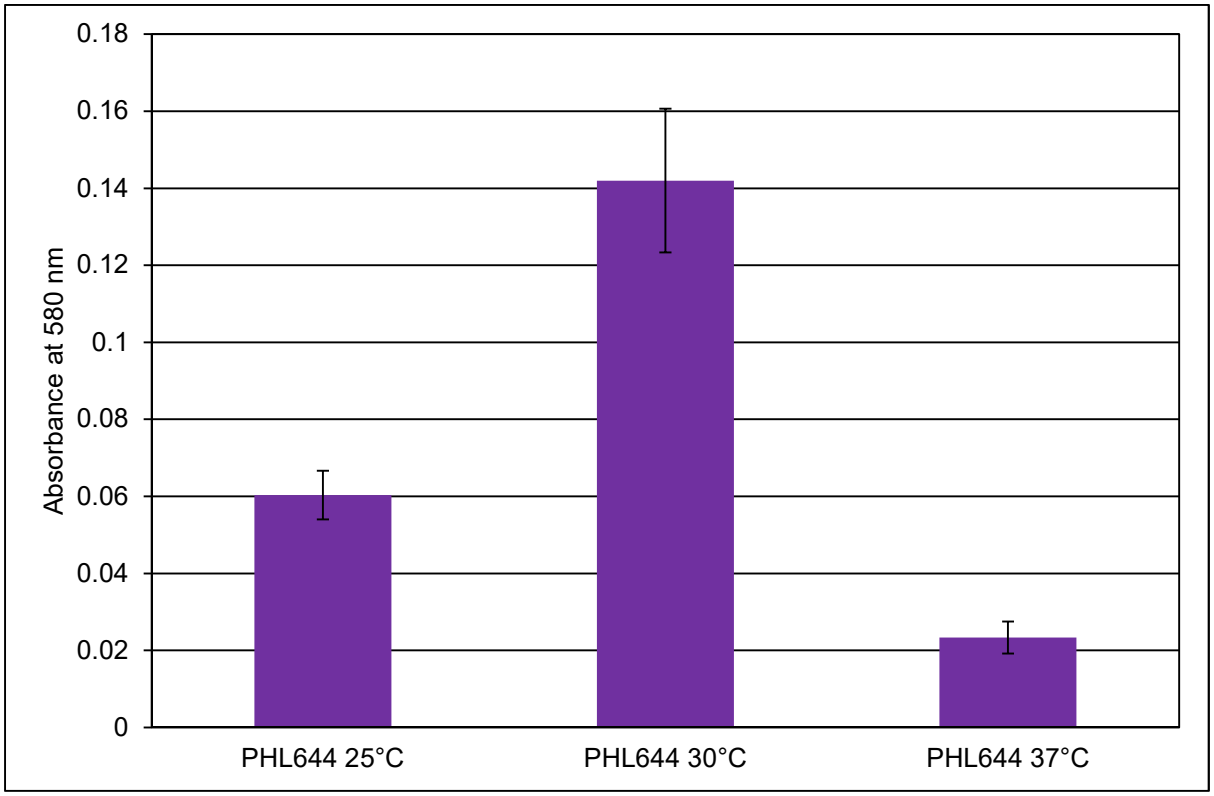

Figure 3.15: *Graph comparing CV retention of PHL644 biofilms on PTFE-wrapped microscope slides in varying temperatures using the Duran Bottle method. Error bars represent 1 standard deviation from the mean of 3 independent cultures.*

3.3.13 Effect of Incubation Speed on Biofilm Formation

As previously stated (Section 3.1), the biofilms presented in this study were grown in an orbital shaker under a relatively slow rotation speed to allow the cells to move towards and attach to the surface but also to prevent mechanical shearing of the biofilm as it grew. It was decided to determine an ideal rotation speed for this purpose.

PHL644 biofilms were grown using the Duran Bottle method. Biofilms were grown in 70 mL M63+ on a PTFE-wrapped microscope slide at 30°C and either 0, 35, 70 or 150 RPM for 3 days. These experiments were all performed in a Thermo MaxQ 4000 series orbital shaker with an orbit of 19 mm. Biofilms were analysed using CV staining.

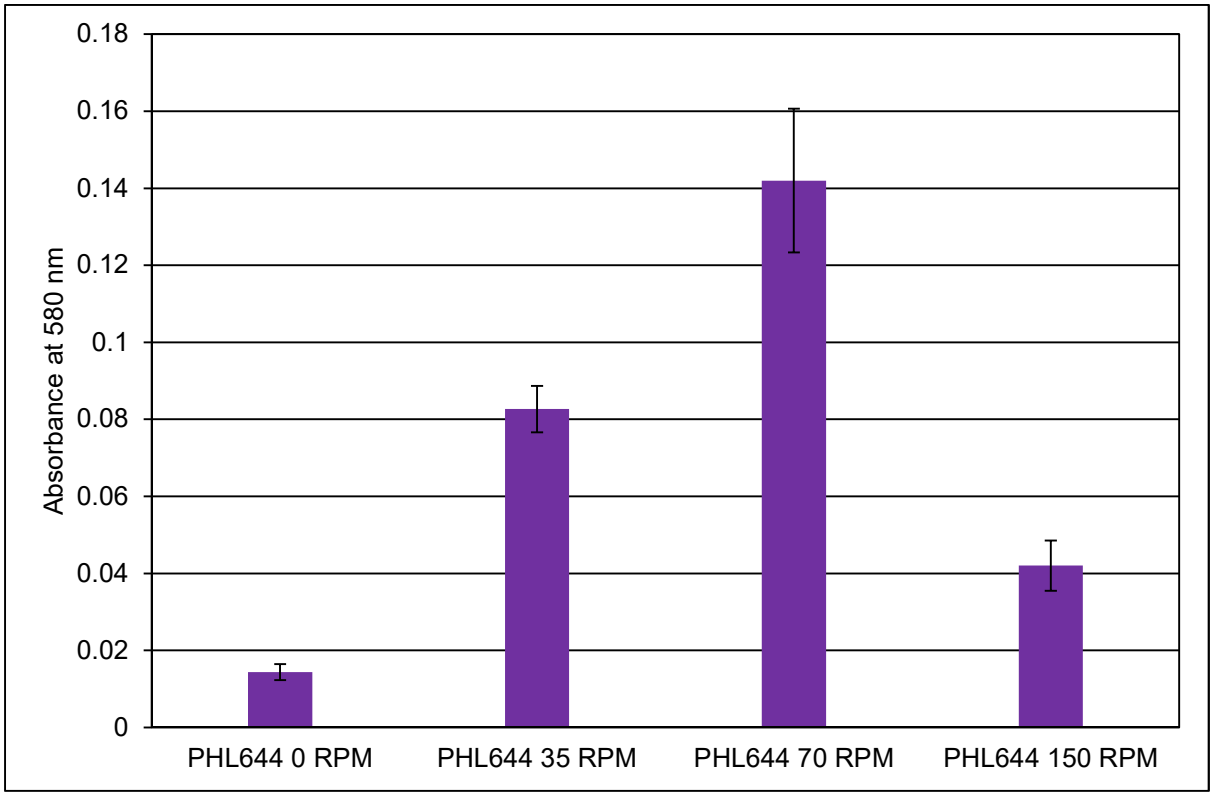

Figure 3.16: *Graph comparing CV retention of PHL644 biofilms grown on PTFE-wrapped microscope slides under varying rotation speeds using the Duran Bottle method. Error bars represent 1 standard deviation from the mean of 3 independent cultures.*

As shown by Figure 3.16, 70 RPM facilitated the greatest biofilm growth on the PTFE surface. A rotation speed of 0 RPM led to an exceptionally low A_{580}, suggesting that at least some movement of the culture is necessary to form a substantial biofilm. Biofilms grown at 150 RPM reached an A_{580} which was ~1/3 of those grown at 70 RPM, suggesting that this speed may damage the nascent biofilm as it grows, or that it reduces the success of attachment events in early stages. It has been shown that increasing shear forces can be used to enhance biofilm growth in wastewater biofilm development (Liu Y & Tay JH, 2002) as well as in flow cell models (Park A *et al*., 2011). The mechanical stress caused by higher rotation speeds in the Duran Bottle model likely selects for mechanically stronger biofilms

as the shear forces would remove weaker biofilms from the surface. A stronger biofilm would provide a stronger foundation for the formation of a thicker biofilm, and therefore, a higher recorded A_{580}. However, as shown by 150 RPM, there is a limit to the shear forces which the biofilm can tolerate. 70 RPM was therefore determined to be a suitable rotation speed for generation of the biofilm biocatalyst.

3.4 Reporter Experiments

3.4.1 Construction of Gene Reporter Plasmids

As stated in Chapter 1, curli fimbriae are an essential element in the attachment and development of *E. coli* biofilms. It was therefore postulated that the analysis of curli expression within the biofilm model described herein could provide insight into a major biofilm factor. Reporter technology and flow cytometry (described in Section 1.7.1) were employed to facilitate this analysis.

In this project, a reporter construct plasmid was designed for the *csgBAC* promoter, encoding the curli protein subunits (Section 1.3, 1.4). The construct was synthesised to allow more precise control over the DNA sequence. Full reporter construct sequence and construction details can be found in Section 2.1.2.

MC4100 was used as the template genome for the reporter as the primary biofilm-forming strain used in this work was PHL644, its derivative strain. To ensure the construct would be suitable for use in other strains, a multiple sequence alignment test was performed to compare the *csgBAC* promoter sequences in the strains to be tested. The MC4100 *csgBAC* promoter sequences was found to have 100% sequence identity with the representative BL21(DE3) sequence and 98.8% identity with the Nissle 1917 sequence. A description of

how this test was performed can be found in Section 2.1.2.2. Full promoter sequences in alignment can be found in Section 8.1.

The complete MC4100 intergenic sequence between *csgBAC* and *csgDEFG* was fused with the gene sequence for the reporter protein eGFP, at the translational start point of *csgBAC*. The ribosome binding site upstream of the translational start site was replaced with an 'ideal' ribosome binding site to improve translation, which has been performed in other transcriptional assay research. The eGFP ORF was further fused at the C-terminus with a sequence encoding an AANDENYALVA amino acid sequence tag. This protein tag targets the protein for degradation by ClpA and ClpX and reduces the half-life of eGFP from 24 hours to 60 minutes, allowing more precise detection of temporal gene expression (Purcell O *et al*., 2012, Miller WG *et al*., 2000). EcoRI and HindIII restriction endonuclease sites were inserted flanking the construct to allow subsequent subcloning. The construct was synthesised by GeneArt (Thermo Fisher Scientific) and inserted into a *bla*/pBR322 vector, termed pJLC-A. Due to incompatibilities with other *bla*/pBR322 plasmids used in this project, the insert was further subcloned into pPROBE'-TT (Addgene), with *tetR*/pBBR1 elements. The resulting reporter construct was termed pJLC-T. Initial experiments with pJLC-A and pJLC-T revealed that pJLC-A produced very low levels of GFP, perhaps due to the lower copy number of pBR322 origins or the reduced half-life of eGFP-AANDENYALVA. pJLC-T produced more GFP and was generally easier to measure than pJLC-A. As such, pJLC-T was the construct chosen for the transcriptional assays described in this section.

An important note is that no fluorescence was detected when pJLC-T was transformed into Nissle 1917. As Nissle 1917 also produced a poor biofilm in the conditions developed in this chapter, this strain was not used in these experiments. Transcriptional assays were performed with PHL644 and BL21 Star (DE3) only. All assays using the pJLC-T plasmid

were performed without antibiotic as it was felt that antibiotics may adversely affect the biofilm-forming potential of the *E. coli* strains.

3.4.2 Determination of a Baseline Fluorescence for Analysing Flow Cytometry Data

Flow cytometry allows the analysis of single cells within large populations of bacteria, as well as distinguishing between subpopulations within the overall population. *E. coli* cells naturally produce a low level of green fluorescence due to native cellular materials. By determining the mean fluorescence produced by untransformed *E. coli* cells, a threshold was established to discriminate between cells which were or were not producing GFP in cells transformed with pJLC-T. These are designated in this work as GFP-positive or GFP-negative. This have an indication of which cells possessed active *csgBAC* promoters and were therefore producing curli proteins in a potentially heterogeneous population.

A caveat with this determination is that some cells may have lost their plasmids and can be miscounted as GFP-negative pJLC-T cells. As antibiotic supplements were omitted from all growth media there is no way to distinguish between plasmid-free and GFP-negative cells.

To establish this threshold, untransformed PHL644 and BL21 Star (DE3) cultures were grown in 70 mL M63+ at 30°C and 70 RPM for 24 hours. A PTFE-wrapped microscope slide was inserted so that a growing biofilm would be present. The OD_{600} of the planktonic culture was measured every 2 hours. 100 µL of the planktonic culture was removed every 2 hours for flow cytometry analysis, and diluted with PBS when necessary.

Figure 3.17 displays an example of the histogram output from the flow cytometry analysis of untransformed PHL644 after 24 hours. The mean fluorescence of this sample was measured as 190 units. Thus, the threshold for GFP production was set at 575. 99.86% of the population was below this threshold, with 0.14% analysed above this threshold; these

are likely to be outliers or miscounted events. Mean green fluorescence in untransformed cells did not exceed 210 units at any point over a 24 hour period and so were omitted from subsequent fluorescence graphs. Cells counted below this threshold were determined as GFP-negative and therefore any fluorescence was as a result of natural fluorophores. Cells counted above this threshold, when analysing cells containing a fluorescent reporter plasmid, were determined to be GFP-positive as increased fluorescence intensity could only be a result of GFP production. To summarise, in cells containing pJLC-T, cells producing more than 575 units of fluorescence were determined to be producing curli genes (GFP-positive), and those below 575 units were determined to be non-productive (GFP-negative). Figure 3.17 shows this thresholding in practice in two planktonic PHL644 pJLC-T culture samples (this experiment will be described in Section 3.4.2). After 4 hours, 2 distinct populations have emerged, one above the 575 threshold and the other below. In this example, 73.8% of the total population is considered to be GFP-positive while 26.2% is considered to be GFP-negative. After 24 hours, this has changed to 97.5% GFP-positive and 2.5% GFP-negative. As stated before, this 2.5% may be made up of GFP-negative or plasmid-free cells. However, since this number has decreased by approximately 10-fold between 4 and 24 hours, it can be suggested that most of this percentage below the 575 threshold is made up of GFP-negative cells rather than plasmid free cells. The implications of this data will be expanded upon in subsequent sections. However, this application of data analysis exhibits the strengths of flow cytometry as a useful tool in understanding the variations in gene expression in complex populations.

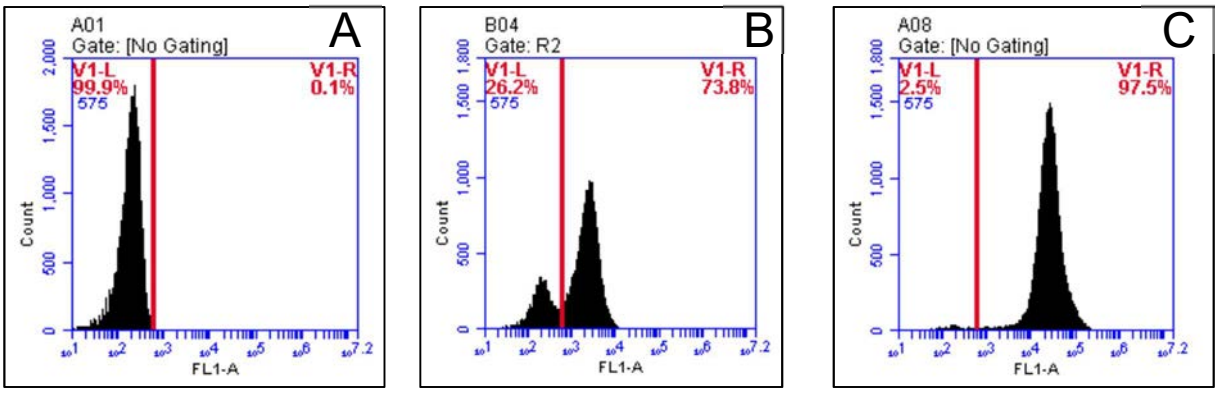

Figure 3.17: *Flow cytometry histograms of planktonic E. coli cultures in M63+ medium grown using the Duran Bottle method. A – PHL644 at 24 hours. B – PHL644 pJLC-T at 4 hours. C – PHL644 pJLC-T at 24 hours. Red line represents applied threshold at 575 units. Percentages displayed in graphs were taken from statistical data rather than graph outputs.*

3.4.3 *csgBAC* Expression in Planktonic *E. coli* Cells

In this work, the production of curli fimbriae was shown to be important to the development of an *E. coli* biofilm on PTFE. Understanding the regulation of the *csgBAC* operon in a biofilm-forming population was thus considered important in understanding how these procedures may be improved. Growth rate and fluorescence were observed in planktonic cells transformed with the pJLC-T plasmid. This data was then compared against data obtained for PTFE-attached cells to determine how curli gene regulation was affected by attachment (Section 3.4.4). Planktonic experiments were performed in both PHL644 pJLC-T and BL21 Star (DE3) pJLC-T.

3.4.4 Growth of Planktonic *E. coli* Cells transformed with the pJLC-T Plasmid

PHL644 pJLC-T and BL21 Star (DE3) pJLC-T cultures, and their untransformed variants, were grown in 70 mL M63+ at 30°C and 70 RPM for 24 hours. A PTFE-wrapped microscope slide was inserted so that a growing biofilm would be present, despite the experiment focusing on planktonic cells only. The OD_{600} of the planktonic culture was measured every 2 hours using a spectrophotometer. 100 µL of the planktonic culture was removed every 2 hours for flow cytometry analysis, and diluted with filtered PBS when necessary.

As shown by Figure 3.18, the presence of pJLC-T reduced the maximum OD_{600} of both PHL644 and BL21 Star (DE3) after 24 hours. This was not unexpected as the replication of plasmids has been shown before to have direct effects on *E. coli* growth (Klumpp S *et al*., 2009). As stated in Section 1.4.8, plasmids may directly interfere with cell division apparatus to halt cell fission until the plasmid has been sufficiently replicated to its desired copy number. In this experiment, all transformed and untransformed cultures exhibited a lag phase of very slow growth for approximately 10 hours, likely due to acclimatisation to the M63+ medium. After 12 hours, the untransformed PHL644 and BL21 Star (DE3) grew more quickly than the pJLC-T-containing cultures, with a fairly consistent increase to an OD of approximately 1.2 and 1.4 respectively. PHL644 pJLC-T and BL21 Star (DE3) pJLC-T growth rates increased more gradually after 12 hours, reaching a similar, but still reduced, growth rate after 22 hours. After 24 hours, the OD_{600} of the cultures reached 1 and 0.9 respectively. This indicates that the presence of pJLC-T has a slight negative effect on overall growth in both PHL644 and BL21 Star (DE3), but not to any substantial degree.

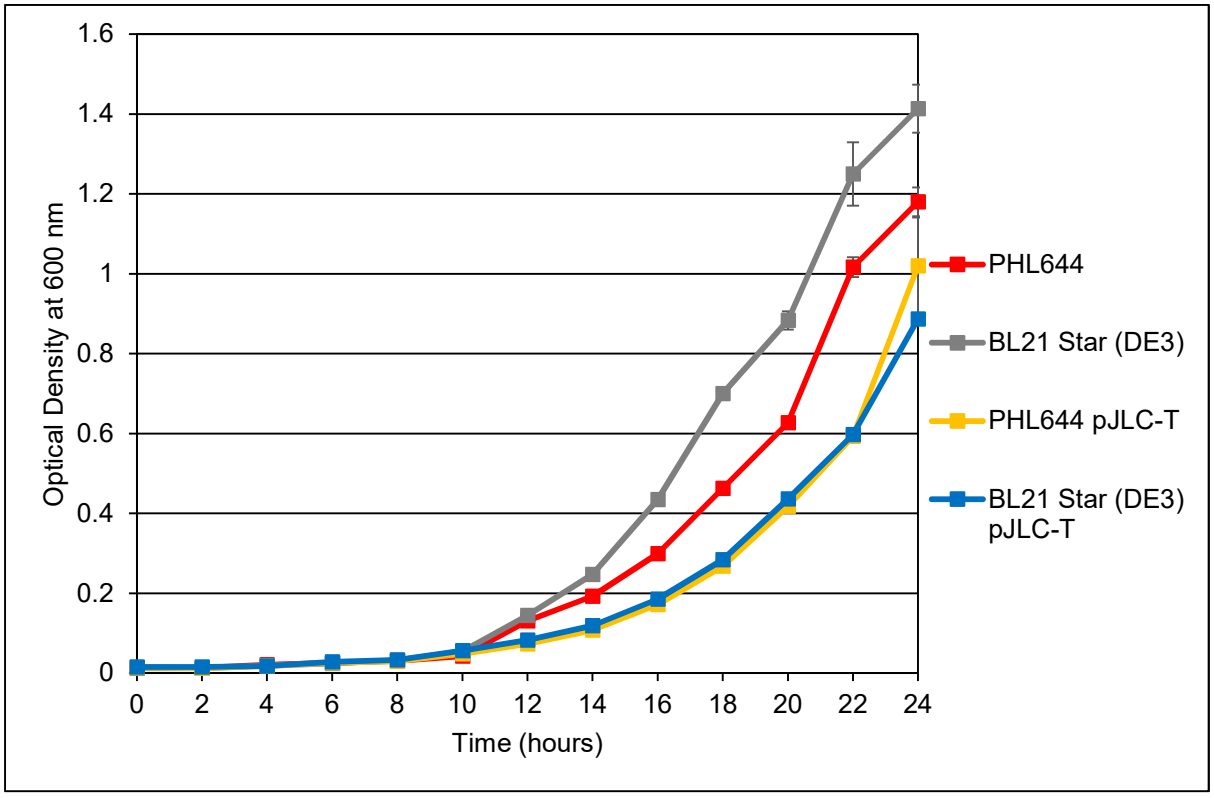

Figure 3.18: *Growth curves for PHL644 pJLC-T and BL21 Star (DE3) pJLC-T and their untransformed variants. Cultures were grown in M63+ (30°C, 70 RPM) for 24 hours in 100 mL Duran bottles. OD_{600} measurements were taken every 2 hours. Error bars represent 1 standard deviation from the mean of three independent cultures.*

3.4.5 *csgBAC* Expression in Planktonic *E. coli* Cells

Flow cytometry allows the analysis of individual cells within a diverse population. Using the pJLC-T reporter plasmid, green fluorescence is a marker of *csgBAC* promoter activation while green fluorescence intensity is a marker of the level of expression from that promoter i.e. how much transcript is produced. Figure 3.19 presents the percentage of the sample population considered to be cells emitting green fluorescence as a result of GFP expression. These GFP-producing cells are termed 'activated' in this work. The population of activated PHL644 at 0 hours is in the minority, at 40%. However, this quickly increases to 67% after

2 hours, and then to >80% after 4 hours. This suggests a rapid activation of the PHL644 *csgBAC* promoter in M63+. This percentage remains consistent until 8 hours, after which it increases to >96% after 12 hours and remains above 95% for the rest of the experiment. BL21 Star (DE3) pJLC-T has a higher activated population than PHL644 pJLC-T for most of the experiment, beginning at 81% at 0 hours. However, this level remains the same for 2 hours, and then increases to 97% after 12 hours which remains consistent until the end of the experiment.

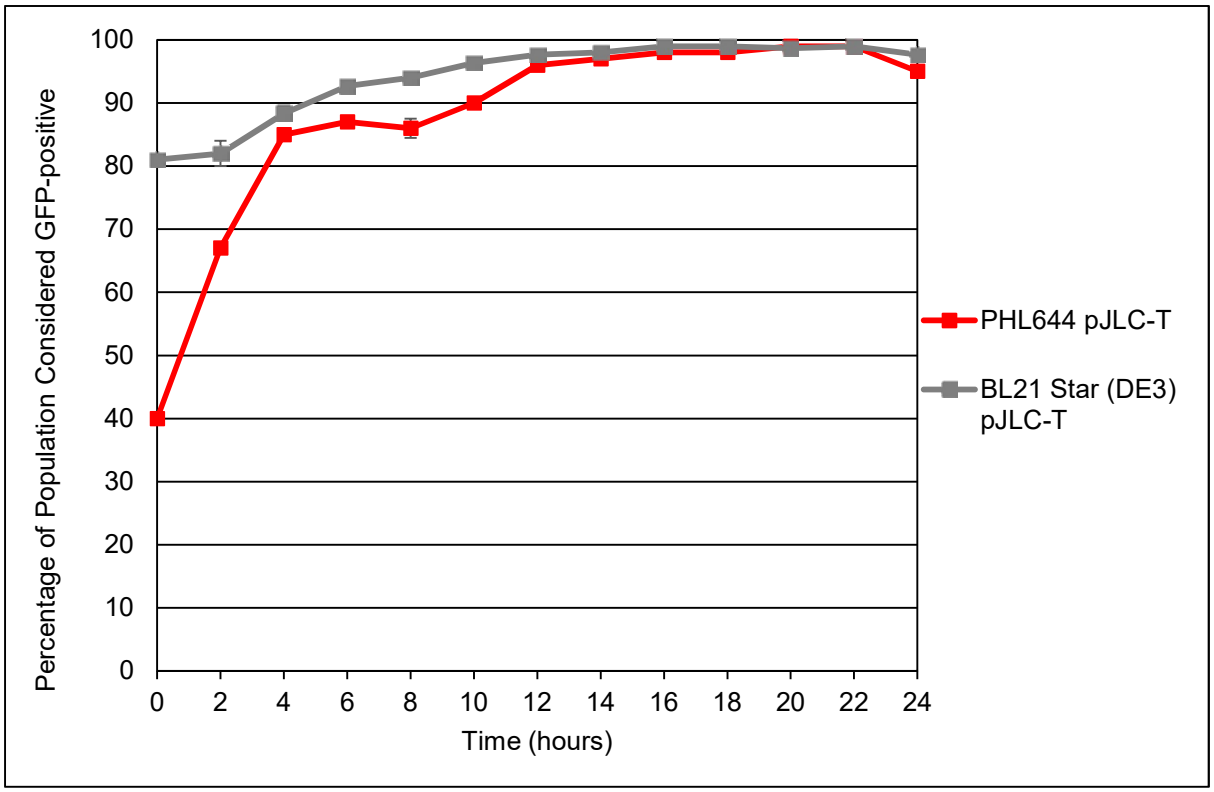

Figure 3.19: *Graph comparing percentages of planktonic PHL644 pJLC-T and BL21 Star (DE3) pJLC-T cells considered GFP-positive over 24 hours. Error bars represent 1 standard deviation from the mean of 3 independent cultures.*

Figure 3.20 presents the mean green fluorescence of the overall population over the 24 hour experiment. PHL644 pJLC-T features a gradual increase from ~5000 to ~12000 units over the first 6 hours. This level does not increase significantly between 6 and 8 hours (within 1 standard deviation). After this point, the level increases fairly consistently until ~33000 units at 16 hours. From 16 to 18 hours, this level does not increase. After 18 hours, intensity increases quickly again until 22 hours where it reaches ~50000 units. BL21 Star (DE3) pJLC-T displays a very similar pattern to PHL644 pJLC-T, but is slightly higher in intensity at most points. Importantly, both strains have points where the fluorescence intensity does not increase significantly, indicating that GFP is produced at the same rate that it is degraded. These points, at 6-8 hours and 16-18 hours in both strains, may represent points where negative feedback prevents the increasing production of curli genes. Interestingly, the 6-8 hour time point aligns with the end of the lag growth phase posited in Figure 3.18, after which growth rates increase quickly. However, no such noticeable correlation occurs between 16 and 18 hours, when growth rates are still high but fluorescence intensity reaches a plateau. It is likely that these points of consistent intensity represent regulation points where GFP production, and therefore *csgBAC* transcription, is reduced or halted. This suggests that, in planktonic cultures of PHL644 and BL21 Star (DE3) in these conditions, the level of curli fimbriae expression rises over time but is regulated at defined points, perhaps to prevent overproduction of amyloid material at key growth points.

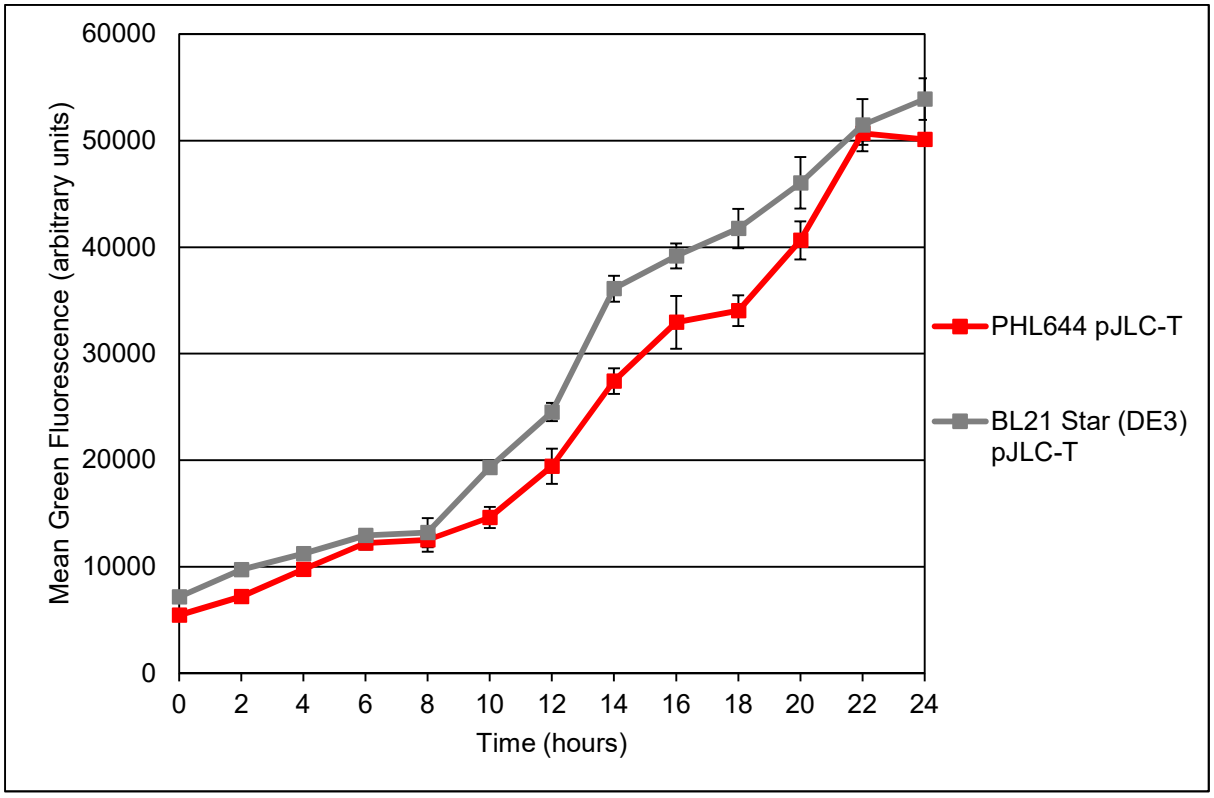

Figure 3.20: *Graph comparing mean green fluorescence intensities of planktonic PHL644 pJLC-T and BL21 Star (DE3) pJLC-T cultures over 24 hours. Error bars represent 1 standard deviation from the mean of 3 independent cultures.*

These data suggest surprising insights into how PHL644 and BL21 Star (DE3) act in a planktonic medium. PHL644 possesses the *ompR234* allele which increases the activity of the OmpR activator on the promoter for CsgD expression (Pringent-Combaret C *et al*., 2001). Increased CsgD would be expected to lead to increased expression of CsgBAC proteins. However, BL21 Star (DE3), which does not feature the *ompR234* allele, maintains a level of expression higher than or equal to PHL644. This may indicate that BL21 Star (DE3) features mutations of its own which allow for the increased production of curli fimbriae. However, the reverse may be true, that K-12 strains feature uncharacterised mutations limiting their ability to produce biofilms, and the *ompR234* allele restores this function. As

shown by Section 3.3.4, PHL644 produces far more biofilm that BL21 Star (DE3) on PTFE. The data presented in this section suggests that this increased biofilm-forming potential cannot be directly linked to the amount of curli fimbriae produced by the cell. Nevertheless, this data suggests that growth of *E. coli* cells in the biofilm-forming conditions utilised in this work leads to a high percentage of cells within the planktonic population which produce curli fimbriae, increasing the likelihood of strong interactions with a hydrophobic surface.

3.4.6 *csgBAC* Expression in Biofilm-Phase *E. coli* Cells

After determining how *csgBAC* expression was affected by growth in planktonic culture, an experiment was designed to compare planktonic and biofilm-phase expression in *E. coli* cells, as it was theorised that curli gene expression may differ between the modes of growth. PHL644 pJLC-T cultures were grown in 70 mL M63+ in 100 mL Duran Bottles at 30°C and 70 RPM for 24 hours. A PTFE-wrapped microscope slide was inserted to allow cell attachment. Every 2 hours, a PTFE slide was removed, washed twice by submersion in PBS, inserted into a centrifuge tube containing 35 mL PBS and vortexed to resuspend attached cells. The PTFE-wrapped slide was then discarded and the vortexed suspension was analysed using flow cytometry. As such, a bottle was set up for each time point. It should be noted that this experiment was performed with PHL644 pJLC-T only as an insufficient number of BL21 Star (DE3) pJLC-T cells for flow cytometry could be recovered using these methods. Additionally, insufficient cells could be obtained at the 0 and 2 hour time points for PHL644 pJLC-T, and thus this data was omitted. This method is dependent on the number of cells that have attached to the surface and suggests that little cell attachment occurs during the first 2 hours of the experiment.

Figure 3.21 reveals that fewer biofilm cells exhibit GFP expression than planktonic cells throughout the course of the experiment. After 4 hours, the percentage of GFP-positive planktonic cells reached 85%, while GFP-positive biofilm cells reached only 65%. Planktonic cells remained above 90% activated from 10 hours until 24 hours. Biofilm cells did not exceed 90% activation at any point and in fact decreased from 87% to 78% from 20 to 24 hours. This suggests that the *csgBAC* promoter is not active in all cells adhered to the PTFE surface.

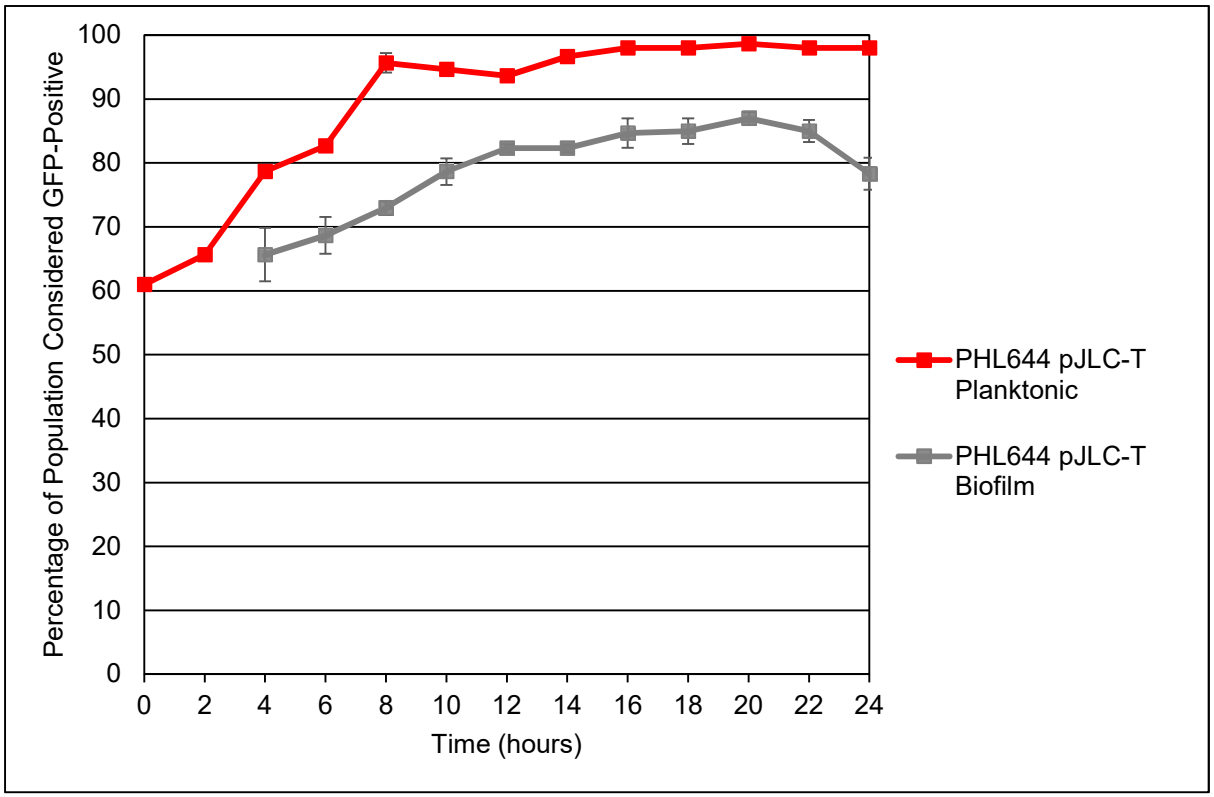

Figure 3.21: *Graph comparing percentages of planktonic and biofilm PHL644 pJLC-T cells considered GFP-positive over 24 hours. Error bars represent 1 standard deviation from the mean of 3 independent cultures.*

Figure 3.22 shows that, from 4-12 hours, biofilm cells express more GFP than planktonic cells, suggesting that cells expressing more curli proteins are more likely to adhere to the PTFE surface. However, the level of expression between 8 and 18 hours becomes erratic and only continues to increase after 18 hours. This period aligns with the end of lag phase in planktonic culture, and suggests that negative regulation occurs during this period, preventing the accumulation of GFP. In contrast, planktonic cell *csgBAC* expression consistently rises during this period. After 18 hours, both planktonic and biofilm cell GFP expression rise consistently and are statistically similar until 22 hours (within 1 standard deviation).

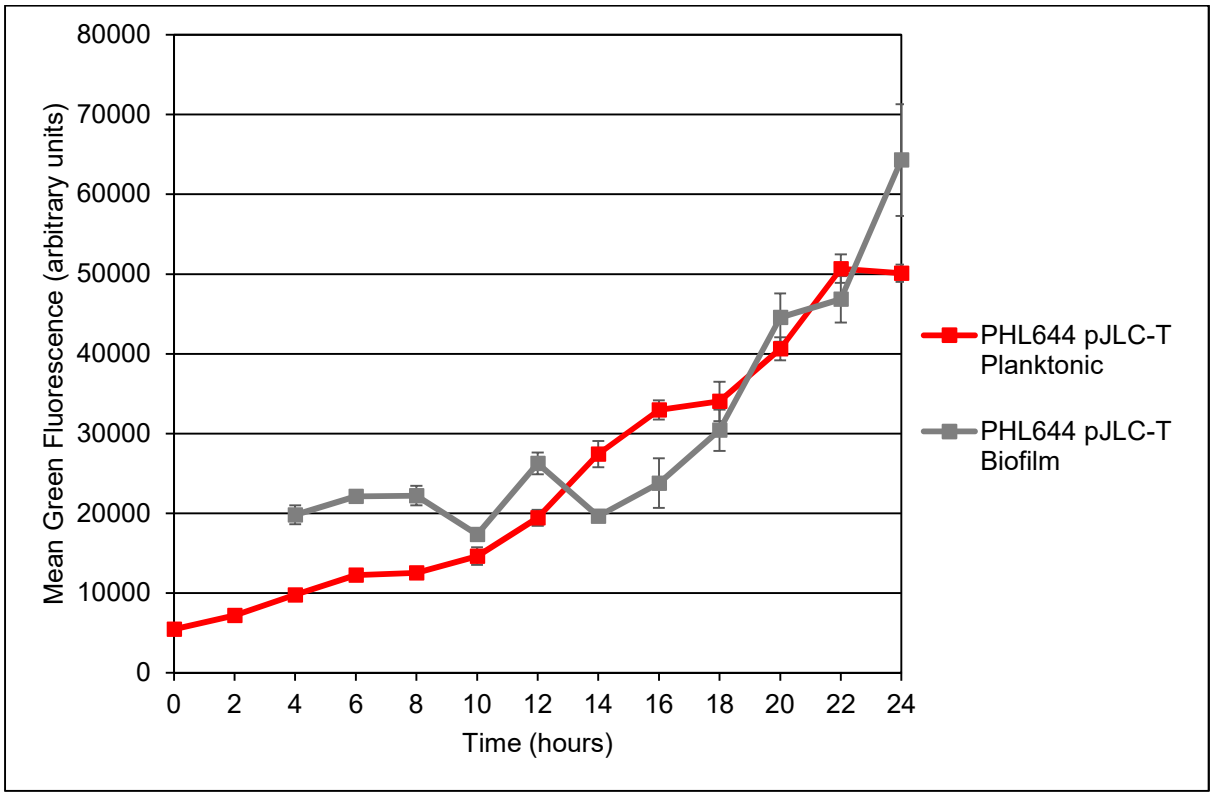

Figure 3.22: *Graph comparing the mean green fluorescence intensities of planktonic and biofilm PHL644 pJLC-T cultures over 24 hours. Error bars represent 1 standard deviation from the mean of 3 independent cultures.*

The implications of these data sets are complex. To theorise, cells producing more curli proteins would be more amenable to attaching to the PTFE surface in the early stages of reversible and irreversible attachment as a result of strong hydrophobic interactions. However, once irreversible attachment has been established, curli proteins do not need to be continually expressed, and the overproduction of amyloid proteins can be toxic to the cell. Downregulation caused by surface-sensing, by regulators such as CpxR, therefore represses redundant expression of *csgBAC* (Otto K & Silhavy TJ, 2002). As shown by CLSM images (Figure 3.10), PHL644 biofilms form structures with a maximum thickness of over 100 μm on PTFE in 24 hours. It has been shown that strong CsgD gene expression occurs in the outer layers of *E. coli* K-12 biofilms and is reduced near the surface, indicating that curli protein expression is reduced at the point of attachment (Serra DO *et al*., 2013). It is likely that the population of biofilm-associated GFP-negative cells seen in Figure 3.20 were irreversibly attached to the surface and therefore in state of curli repression. The GFP-positive cells are more likely to be attached to the biofilm by cell-cell interaction than by direct cell-surface interaction, and continue to produce curli proteins to strengthen their attachment to the biofilm. Additionally, it would take time to degrade any accumulated GFP produced before repression occurred. Once these cells are irreversibly attached to the biofilm, they likely repress curli gene expression, thereby becoming GFP-negative cells. This theory explains why the percentage of GFP-positive cells in the biofilm cell samples never exceeds 87%, as curli-producing cells interact with the nascent biofilm, become irreversibly attached, and then repress curli production, leading to a mixed population in terms of curli production as shown by Figure 3.21. As planktonic cells are not associated with the surface, they retain their curli expression and continue to seek an amenable surface for attachment.

This may explain why the level of curli expression in planktonic cells continues to rise, as these cells are producing as much curli as possible to attach to any surface they can find. To test this, the biofilm cells would need to be imaged every 2 hours to determine the point at which the biofilm began to form 3D structures on the surface, and compare that data to the flow cytometry data presented here. Due to resource limitations, this could not be done in this study. Additionally, the biofilm cells could be counterstained with a nucleic acid stain such as Syto 62 to determine which cells were GFP-positive or GFP-negative and therefore display which cells were producing curli proteins. This was attempted, but it was quickly discovered that the confocal microscope used in this study was not able to precisely determine the intensity of green fluorescence from individual cells. Perhaps with a more sensitive confocal microscope, this would be feasible.

Chapter 4

Modulation of the Biocatalytic Biofilm via Molecular Biology Techniques

As shown by Chapter 3, the combination of the Duran Bottle method and a PTFE surface was extremely useful in quantifying and imaging *E. coli* biofilms. To that end, it was decided to apply several plasmids which have been linked to modulating biofilm formation to the biofilm-producing cells in order to determine their effects in this model. Additionally, using the pJLC-T plasmid, the biofilm-modulating plasmids' direct effects on curli gene expression could be observed. These data would then inform further decisions to alter the biofilm-forming strains to be more effective at their task.

4.1 Effect of Biofilm-Modulating Plasmids on *E. coli* Biofilm Formation

4.1.1 Overexpression of CsgD via pT7-CsgD

pT7-CsgD was created to determine the effects of constitutive CsgD expression on biofilm formation (Brombacher E *et al*., 2006). The plasmid was found to promote biofilm formation in a temperature- and media-dependent manner. An overview of the effects of CsgD in *E. coli* can be found in Section 1.4.3. Specifically, 30°C and M9 minimal medium were found to produce the greatest increases in biofilm formation. As these conditions are similar to the ones developed in Chapter 3 of this study, this plasmid was theorised to be able to increase biofilm formation in this model.

pT7-CsgD expresses CsgD from a T7 promoter. Normally, proteins are expressed from this promoter using the T7 RNA polymerase which is expressed in specialised strains such as BL21 Star (DE3). However, it was noted in the original study that this plasmid constitutively produces a low level of CsgD in strains which did not possess the T7 RNAP (Brombacher E *et al*., 2006). This is likely due to non-specific transcription from the native *E. coli* RNAP.

pT7-CsgD was transformed into PHL644 and BL21 Star (DE3). Nissle 1917 was omitted from all further experiments due to time constraints, as well as the poor biofilm formation exhibited in Chapter 3. As an additional note, Nissle 1917 is known for its strong gut biofilm formation and thus improving its colonisation abilities may lead to unforeseen, potentially hazardous side effects.

PHL644 pT7-CsgD and BL21 Star (DE3) pT7-CsgD biofilms were grown using the Duran Bottle method. Biofilms were grown in 70 mL M63+ on a PTFE-wrapped microscope slide at 30°C and 70 RPM for 3 days. Biofilms were analysed using CV staining and CLSM. All CLSM images are of the submerged region of the biofilm.

As shown by Figure 4.1, pT7-CsgD increased the A_{580} of PHL644 by nearly 2-fold, albeit with an extremely wide standard deviation. pT7-CsgD reduced the A_{580} of BL21 Star (DE3) by a third. CsgD directly activates the production of curli proteins and therefore constitutive production of CsgD would be expected to increase surface attachment and biofilm initiation. However, as shown by Chapter 3, the fact that BL21 Star (DE3) produced more *csgBAC* than PHL644 did not lead to increased biofilm formation. As pT7-CsgD reduces biofilm formation in BL21 Star (DE3) it can be suggested that curli overproduction is actually detrimental to biofilm formation. However, the opposite appears true for PHL644, where pT7-CsgD is beneficial to increasing biofilm abundance on a surface. The implications of these data are therefore unclear, but may imply that certain biofilm components are more important to certain strains than others, for instance curli may be important to PHL644 biofilm formation while being less important to BL21 Star (DE3).

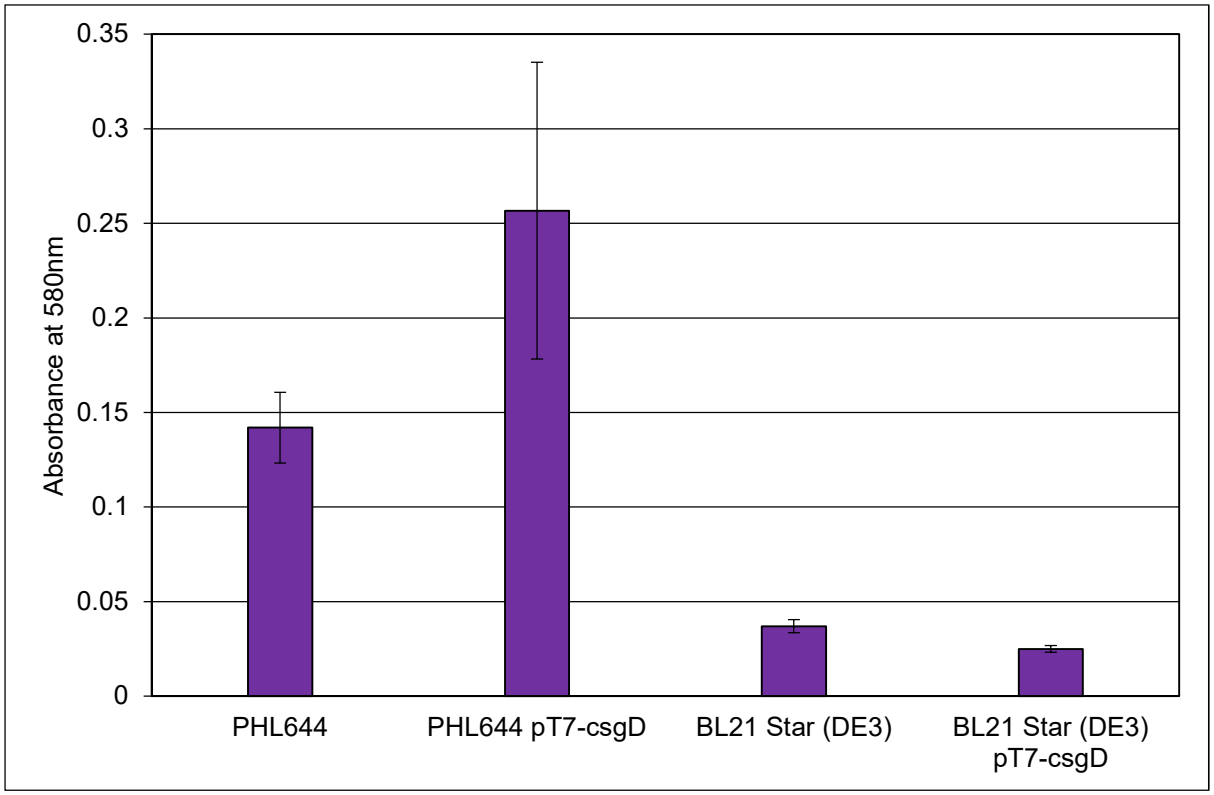

Figure 4.1: *Graph comparing CV retention of PHL644 pT7-CsgD and BL21 Star (DE3) pT7-CsgD biofilms to their untransformed counterparts. Biofilms were grown using the Duran Bottle method. Error bars represent 1 standard deviation from the mean of 3 independent cultures.*

Figure 4.2 shows the observed morphology of biofilms produced by PHL644 pT7-CsgD and BL21 Star (DE3) pT7-CsgD. PHL644 pT7-CsgD exceeded 200 µm in thickness, as with PHL644, but lacked the characteristic architecture observed for the untransformed strain, such as mushroom-shaped outgrowth. Instead, the biofilm appeared much more compact but featured loose cells moving across the surface. This suggests that the cells have aggregated extensively but have not grown in the standard PHL644 manner. BL21 Star

(DE3) pT7-CsgD displays a sparse biofilm with many unattached cells indicating poor, loose biofilm development, complementing the CV data in Figure 4.1.

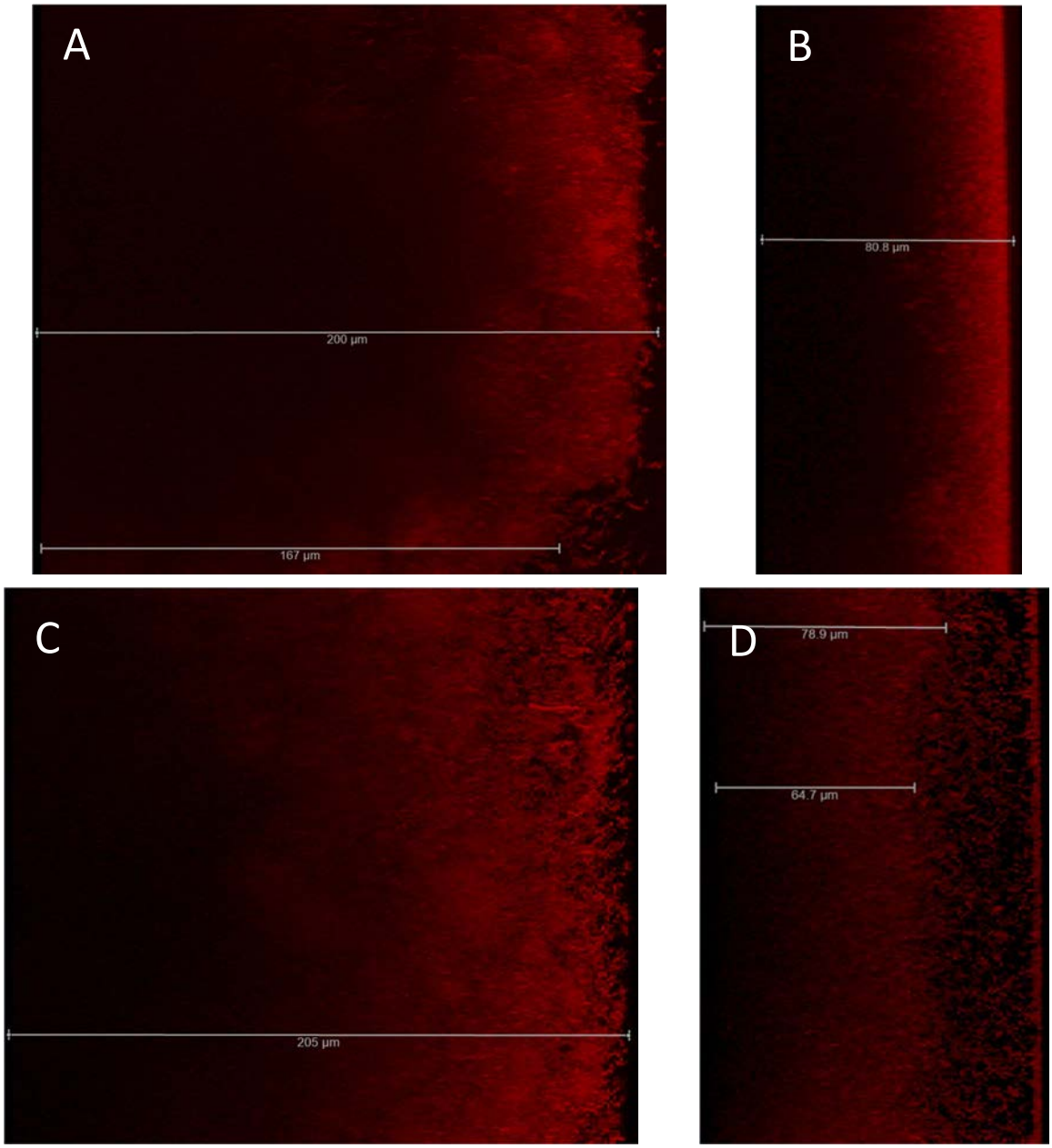

Figure 4.2a: *Representative side-view CLSM images of PHL644 pT7-CsgD and BL21 Star (DE3) pT7-CsgD biofilms and their untransformed counterparts. Biofilms were grown using the Duran Bottle method. A – PHL644. B – BL21 Star (DE3). C – PHL644 pT7-CsgD. D – BL21 Star (DE3) pT7-CsgD. In all images, the base of the biofilm is on the left.*

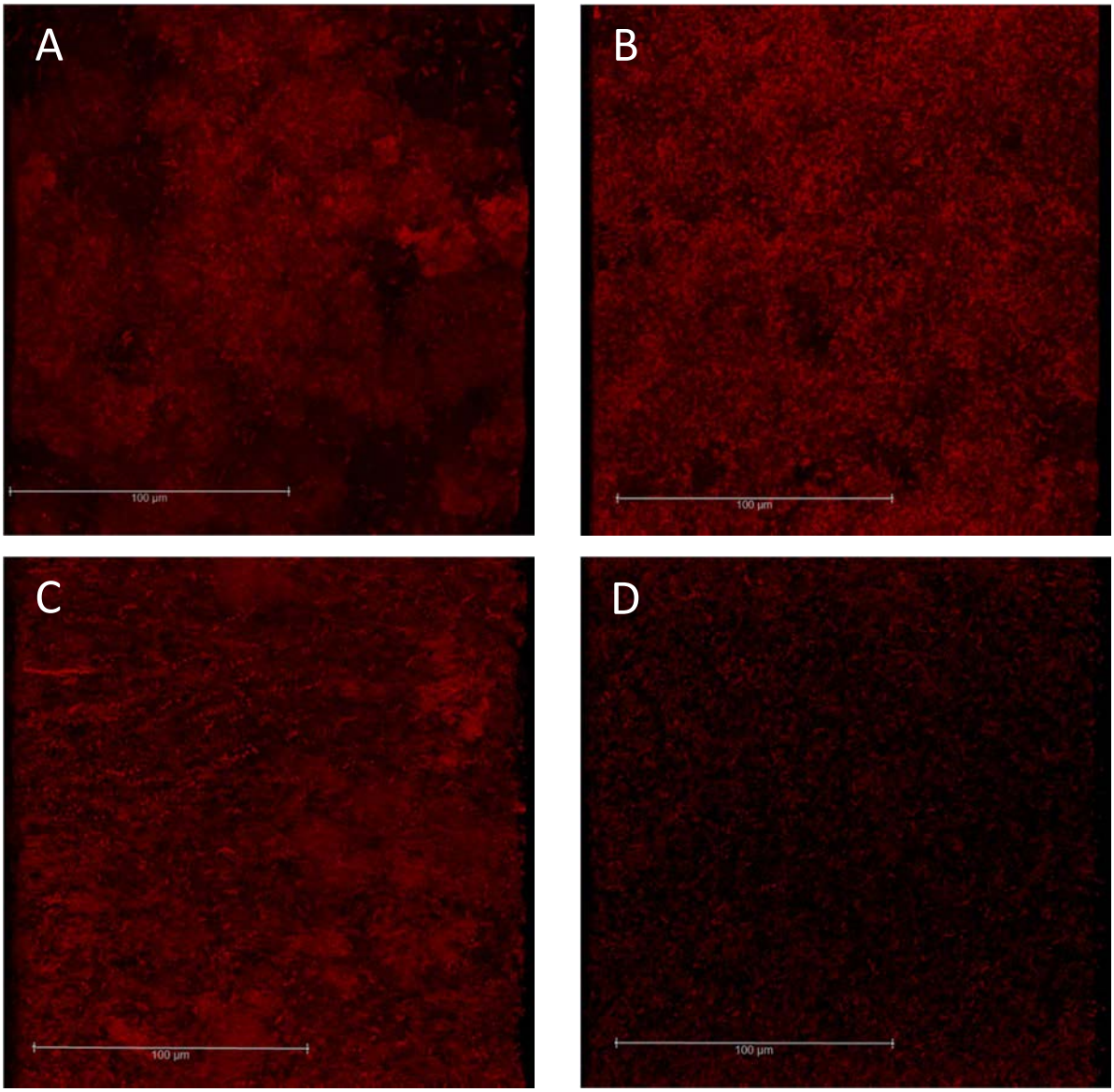

Figure 4.2b: *Representative top-down-view CLSM images of PHL644 pT7-CsgD and BL21 Star (DE3) pT7-CsgD biofilms and their untransformed counterparts. Biofilms were grown using the Duran Bottle method. A – PHL644. B – BL21 Star (DE3). C – PHL644 pT7-CsgD. D – BL21 Star (DE3) pT7-CsgD.*

These results indicate that while pT7-CsgD may increase attachment of PHL644 to PTFE, the plasmid does not support the growth of structured biofilm, such as was seen with the untransformed strains. Increased production of curli fimbriae would logically increase attachment to a hydrophobic surface. However, as suggested in Chapter 3, *E. coli* may downregulate expression of curli proteins upon attachment to a surface. pT7-CsgD bypasses this downregulation by constitutively expressing CsgD, allowing the continued expression of the curli proteins CsgBAC. This likely leads to a more compact, aggregated biofilm. The observation of non-attached cells in PHL644 pT7-CsgD and BL21 Star (DE3) pT7-CsgD biofilms after washing with PBS indicates that this mode of biofilm growth is not necessarily more robust than the untransformed strains, as strong attachment would be expected to hold the biofilm together. Polysaccharides such as colanic acid are likely to be more important than curli in providing biofilm robustness and ordered structure. However, colanic acid production has an inverse regulation to CsgD (Section 1.4.3). If curli genes are not downregulated at the correct time, colanic acid may not be able to perform its function in forming a structured 3D biofilm. Instead, cells continue to produce curli, becoming more and more aggregated without structure. This may explain the less structured biofilm observed for PHL644 pT7-CsgD, but this does not explain the reduction in biofilm thickness and aggregation observed for BL21 Star (DE3) pT7-CsgD, and suggests that increased CsgD levels did not lead to increased aggregation. Extensive analysis of the transcriptomes of cells in this mode of growth would need to be performed to analyse the effects of pT7-CsgD in these strains. However, the compact nature of biofilms produced with pT7-CsgD likely decreases efficient mass transfer between the media and the deeper cells. This effect would obstruct uptake of both nutrients and biocatalysis reactants in a biofilm biocatalyst.

Combined with the reduction in thickness of BL21 Star (DE3) biofilms, pT7-CsgD was considered to be detrimental to biofilm formation in this model.

4.1.2 Overexpression of DgcM (YdaM) via pYdaM

DgcM is a DGC involved in the regulation of CsgD expression. A description of this pathway can be found in Section 1.4.3. In brief, DgcM binds to the PDE PdeR when c-di-GMP concentrations are low. When c-di-GMP concentrations are increased, such as in the entry to stationary phase, PdeR begins to degrade c-di-GMP and releases DgcM. DgcM binds to MlrA which activates the expression of the *csgDEFG* operon (Lindenberg S *et al*., 2013). CsgD leads to production of curli genes as well as cellulose production via DgcC (Brombacher E *et al*., 2003). Aside from direct effects on curli and cellulose production, DgcM overexpression has been shown to increase production of PNAG (Tagliabue L *et al*., 2010). It was therefore expected that DgcM overexpression would lead to increased biofilm formation in the biofilm-forming strains PHL644 and BL21 Star (DE3) tested in this work. In this study, DgcM was expressed from pYdaM (Tagliabue L *et al*., 2010). DgcM was expressed from a deregulated *lac* promoter, resulting in constitutive expression of DgcM.

pYdaM was transformed into PHL644 and BL21 Star (DE3). PHL644 pYdaM and BL21 Star (DE3) pYdaM biofilms, and their untransformed variants, were grown using the Duran Bottle method. Biofilms were grown in 70 mL M63+ on a PTFE-wrapped microscope slide at 30°C and 70 RPM for 3 days. Biofilms were analysed using CV staining and CLSM. All CLSM images are of the submerged region of the biofilm.

As shown by Figure 4.3, pYdaM had a negative effect on *E. coli* biofilm growth. The mean A_{580} of PHL644 pYdaM was less than half of the untransformed strain, indicating less abundant biofilm on the PTFE surface. For BL21 Star (DE3) pYdaM, the mean A_{580}

appeared reduced but was within 1 standard deviation of untransformed BL21 Star (DE3). However, this result had a comparatively wide standard deviation, indicating more variability in biofilm formation. The reduction in A_{580} in PHL644 and the increase in variability in BL21 Star (DE3) are both negative effects as a reliable biofilm biocatalyst requires a large biomass of cells with as little variability in abundance as possible.

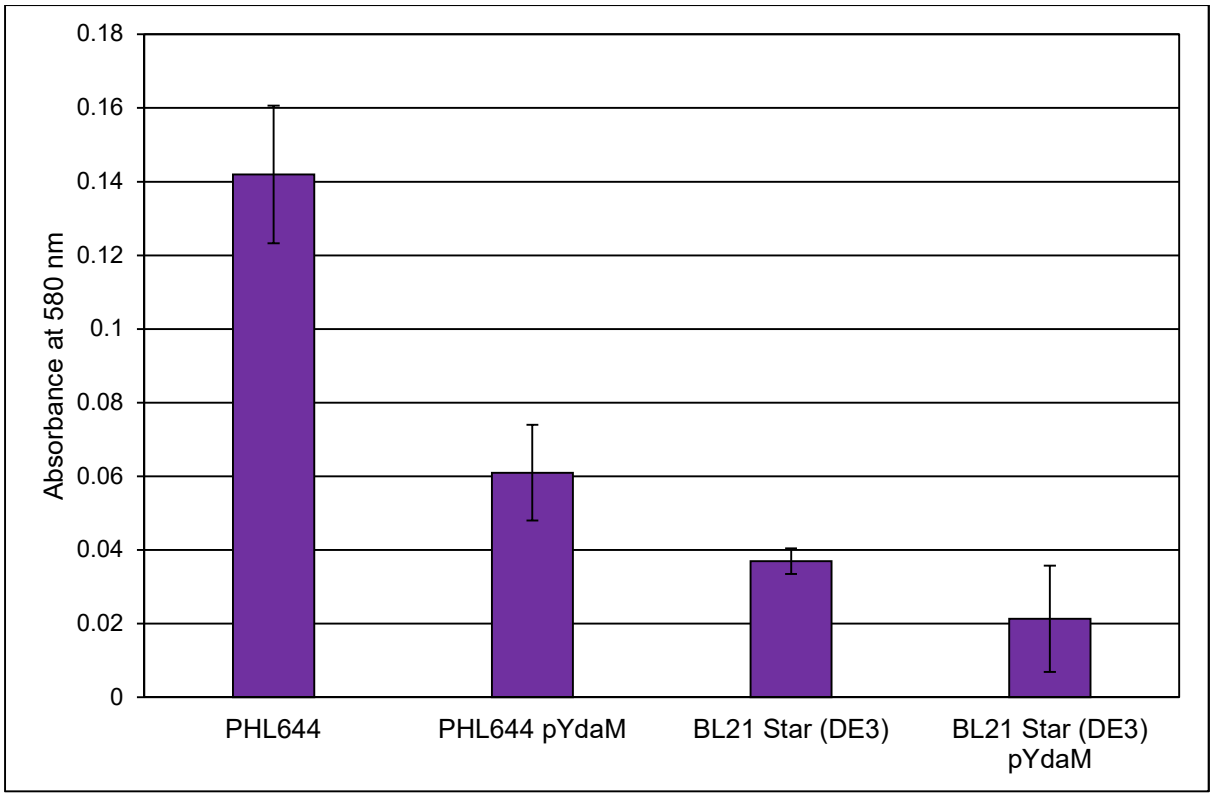

Figure 4.3: *Graph comparing CV retention of PHL644 pYdaM and BL21 Star (DE3) pYdaM biofilms to their untransformed counterparts. Biofilms were grown using the Duran Bottle method. Error bars represent 1 standard deviation from the mean of 3 independent cultures.*

The images shown in Figure 4.4 suggest that pYdaM also has a negative effect on biofilm architecture. PHL644 pYdaM grew a 3D-developed biofilm with a maximum thickness of less than 60 μm; a clear reduction compared to the >200 μm observed for untransformed PHL644. Nevertheless, the PHL644 pYdaM biofilm displayed some of the characteristic

outgrowth features observed for PHL644. BL21 Star (DE3) pYdaM grew an extremely thin biofilm of less than 15 μm, compared to the untransformed strain at ~80 μm. No 3D-development could be observed, and many unattached cells were noted in the image. This indicates that the biofilm had poor cohesion. The observed unattached cells may also contribute to the increased variability in A_{580} seen in Figure 4.2.

As DgcM is a promoter of biofilm growth in *E. coli* due to its modulation of CsgD expression, it would be expected that overexpression would further promote biofilm formation. However, as shown by the results of this study, pYdaM had negative effects on biofilm formation in PHL644 and BL21 Star (DE3). As with pT7-CsgD, increased production of curli genes may not be beneficial to the growth of the biofilm. Chapter 3 of this study suggests that curli genes are downregulated on adhesion to a PTFE surface, indicating that some degree of control must be applied at the correct time to allow biofilm formation. pYdaM may prevent this control, allowing the further production of CsgD when it would normally be repressed. As shown by the results of this section, this control appears critical for these biofilm-forming strains. Of interest is the effect pYdaM has on curli gene expression, which will be explored in Section 4.2.

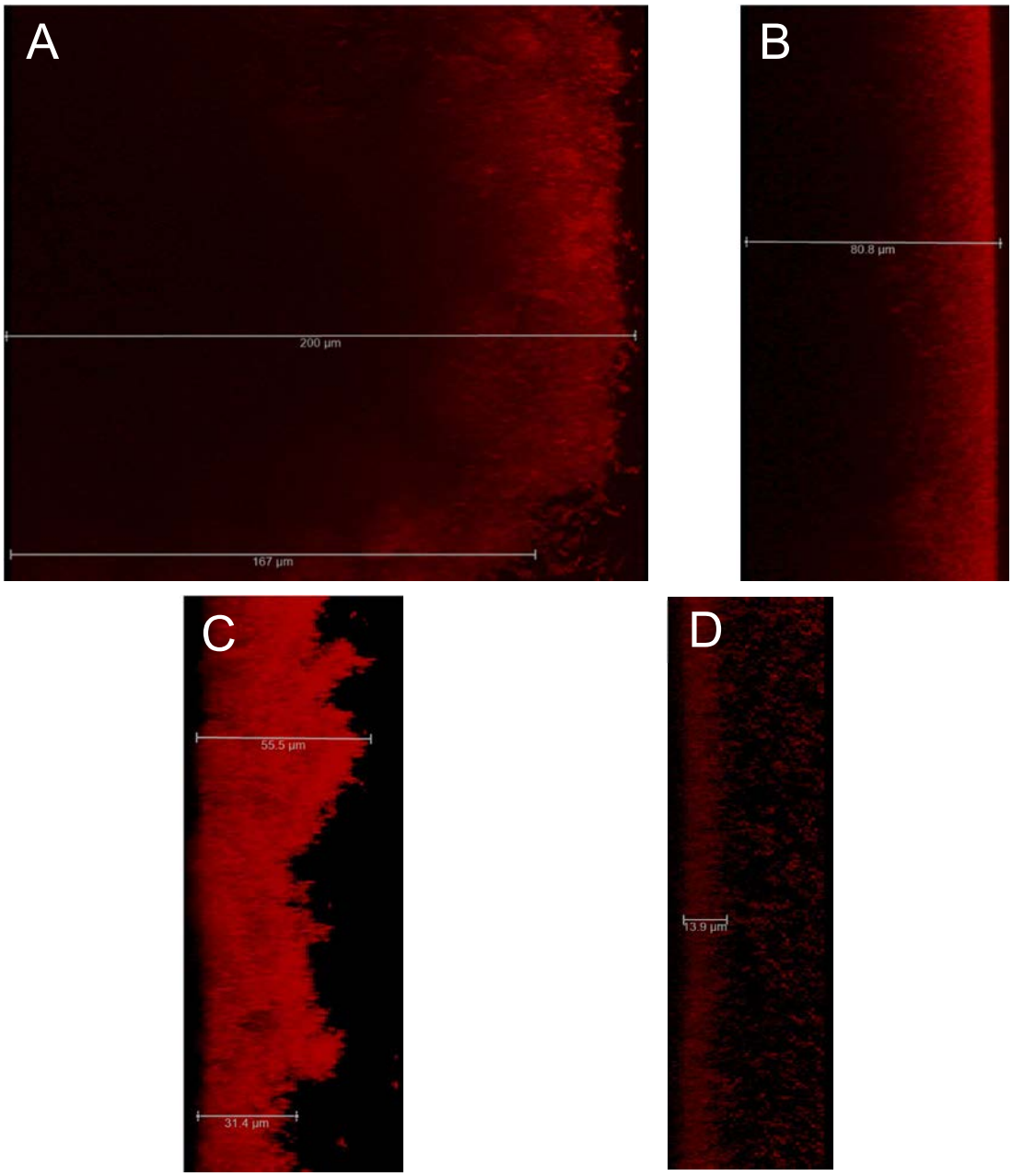

Figure 4.4a: *Representative side-view CLSM images of PHL644 pYdaM and BL21 Star (DE3) pYdaM biofilms and their untransformed counterparts. Biofilms were grown using the Duran Bottle method. A – PHL644 biofilm. B – BL21 Star (DE3) biofilm. C – PHL644 pYdaM biofilm. D – BL21 Star (DE3) pYdaM biofilm. In all images, the base of the biofilm is on the left.*

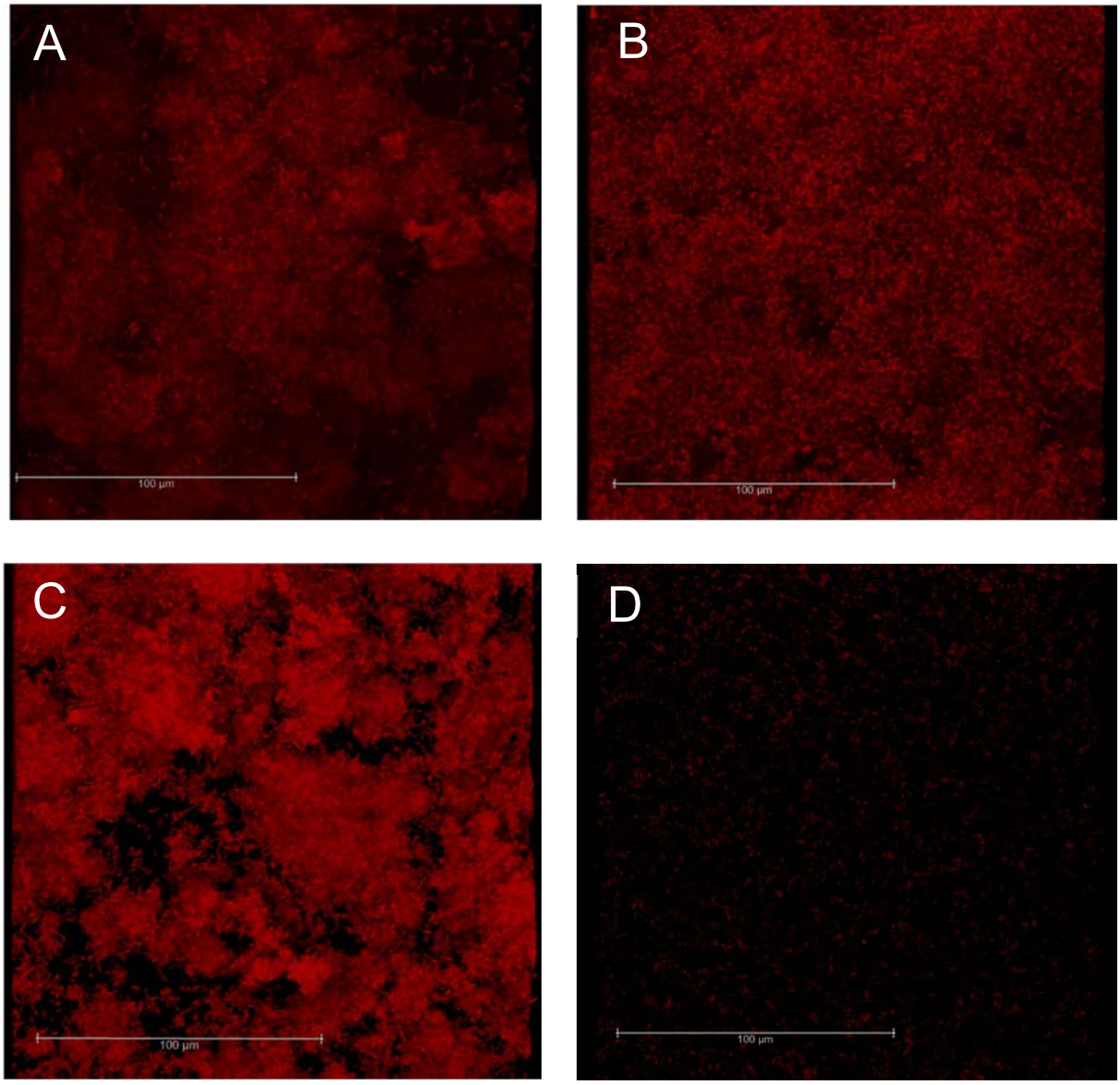

Figure 4.4b: *Representative top-down-view CLSM images of PHL644 pYdaM and BL21 Star (DE3) pYdaM biofilms and their untransformed counterparts. Biofilms were grown using the Duran Bottle method. A – PHL644 biofilm. B – BL21 Star (DE3) biofilm. C – PHL644 pYdaM biofilm. D – BL21 Star (DE3) pYdaM biofilm.*

4.1.3 Overexpression of DgcO (DosC/YddV) via pYddV

DgcO is a DGC which is linked to the production of the ECM polysaccharide PNAG. PNAG production and export is facilitated by the *pgaABCD* operon. DgcO is able to detect the presence of oxygen via a haem group, which modulates its production of c-di-GMP. DgcO forms a complex with PdeO, a phosphodiesterase which also features a haem group, as well as the mRNA-processing enzyme PNPase. In an aerobic environment, oxygen binds to DgcO and PdeO, activating PDE activity while repressing DGC activity. The reduction in c-di-GMP concentrations inactivates PNPase, preventing it from degrading the *pgaABCD* mRNA. Thus, PNAG is produced in aerobic environments. In anaerobic environments, DgcO is activated while PdeO is repressed, and c-di-GMP is produced by DgcO. PNPase is activated by local c-di-GMP which degrades the *pgaABCD* transcript. Thus PNAG is not produced in anaerobic environments (Tagliabue L *et al*., 2010). This may indicate why *E. coli* forms poor biofilms in anaerobic conditions as PNAG has been shown to be essential to biofilm growth. Logically, overexpression of DgcO would be expected to have a negative effect on biofilm formation as in this pathway c-di-GMP production has a negative effect on PNAG production. However, studies have shown that DgcO overexpression increases biofilm abundance (determined by crystal violet staining), and so the effects are unclear (Méndez-Ortiz MM *et al*., 2006). It was therefore decided to test DgcO overexpression in the biofilm-forming strains used in this study. DgcO was expressed from pYddV (Tagliabue L *et al*., 2010). DgcO was expressed from a deregulated *lac* promoter, resulting in constitutive expression of DgcO.

pYddV was transformed into PHL644 and BL21 Star (DE3). PHL644 pYddV and BL21 Star (DE3) pYddV biofilms, and their untransformed variants, were grown using the Duran Bottle method. Biofilms were grown in 70 mL M63+ on a PTFE-wrapped microscope slide at 30°C

and 70 RPM for 3 days. Biofilms were analysed using CV staining and CLSM. All CLSM images are of the submerged region of the biofilm.

As shown by Figure 4.5, pYddV had a negative effect on biofilm abundance. pYddV reduced the mean A_{580} of PHL644 by approximately a quarter, and BL21 Star (DE3) by nearly three quarters, indicating that pYddV had a greater negative effect on BL21 Star (DE3). In comparison to pYdaM, the standard deviations of pYddV-transformed cultures were not increased to any great extent, indicating less variation in the results.

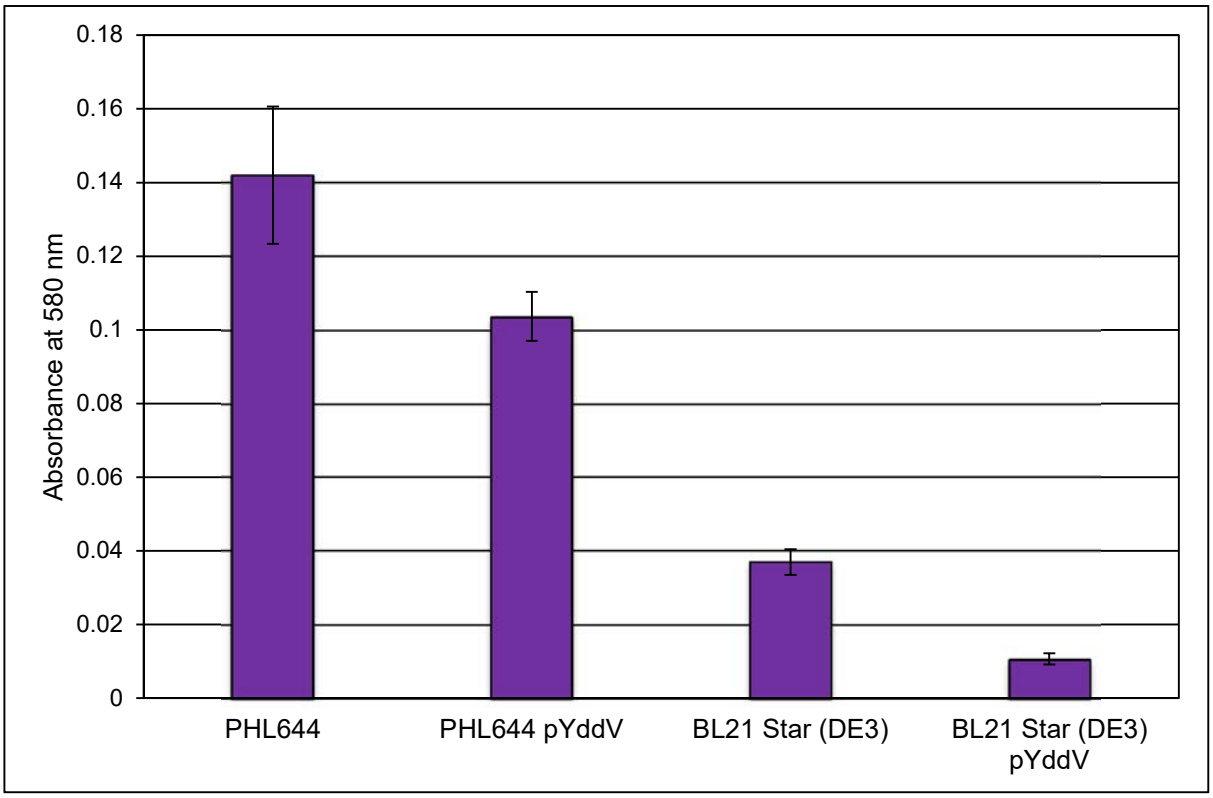

Figure 4.5: *Graph comparing CV retention of PHL644 pYddV and BL21 Star (DE3) pYddV biofilms to their untransformed counterparts. Biofilms were grown using the Duran Bottle method. Error bars represent 1 standard deviation from the mean of 3 independent cultures.*

Figure 4.6 shows that pYddV has striking effects on biofilm formation in PHL644. PHL644 pYddV biofilms were less than 40 μm in thickness and featured compact, rounded structures in comparison to the far deeper mushroom-shaped architecture of the untransformed PHL644. Importantly, between these structures was a mesh of elongated, filamentous *E. coli* cells measuring between 10 and 50 μm (indicated on the image). This mesh appeared to be without defined structure. BL21 Star (DE3) pYddV biofilms were thin with little 3D outgrowth, similar to BL21 Star (DE3) pYdaM biofilms, but did not feature many visible free-floating cells. In contrast to PHL644, no cell elongation was noted in BL21 Star (DE3) pYddV biofilms.

These results indicate, once again, that DGC overexpression can have negative effects on biofilm formation, despite what would be expected. The compact structures observed for PHL644 pYddV may indicate that this plasmid increases aggregation of the *E. coli* cells, rather than leading to better attachment and 3D growth. The extreme cell elongation observed in this strain complements previous data which shows that overexpression of DgcO has a negative effect on cell division (Méndez-Ortiz MM *et al*., 2006), which noted that cell division was inhibited in 85% of cell culture overexpressing DgcO. Cell elongation occurs when cells grow to the size necessary for binary fission, but are unable to divide due to interference with the cell division apparatus. The individual cells continue to grow leading to long chains of *E. coli* cells. The CLSM images shown in this work do not have sufficient resolution to determine whether the elongated cells are at least partially septated, thus it is not possible to theorise at which stage cell division in inhibited. As DgcO is linked to the production of a specific biofilm component, PNAG, it would not be expected to be related to cell division. However, DgcO and PdeO exert control on the PNPase mRNA-processing enzyme, and thus other pathways may be further controlled by this mechanism. DgcO may

therefore confer stationary phase oxygen dependence on multiple cell functions, of which biofilm formation is only one. Elongation effects were not seen for BL21 Star (DE3) pYddV biofilms. To speculate, BL21(DE3) and thus BL21 Star (DE3) feature a mutation in the important oxygen-sensing transcription factor FNR, responsible for anaerobic survival mechanisms, and this may be the reason why elongation was not noted in BL21 Star (DE3) pYddV, that FNR may play a role in DgcO-mediated cell division inhibition (Pinske C *et al*., 2011). This area has not been explored thoroughly and would of course require extensive analysis of the pathways surrounding oxygen-dependence, cell division and biofilm formation, and as such was not explored in this study. Instead, it was determined that the pYddV plasmid was unsuitable for improving the growth of the *E. coli* biofilm biocatalyst as it both reduced biofilm abundance and interfered with normal cell division. An analysis of the effect of pYddV on the *csgBAC* promoter will be presented in Section 4.2.

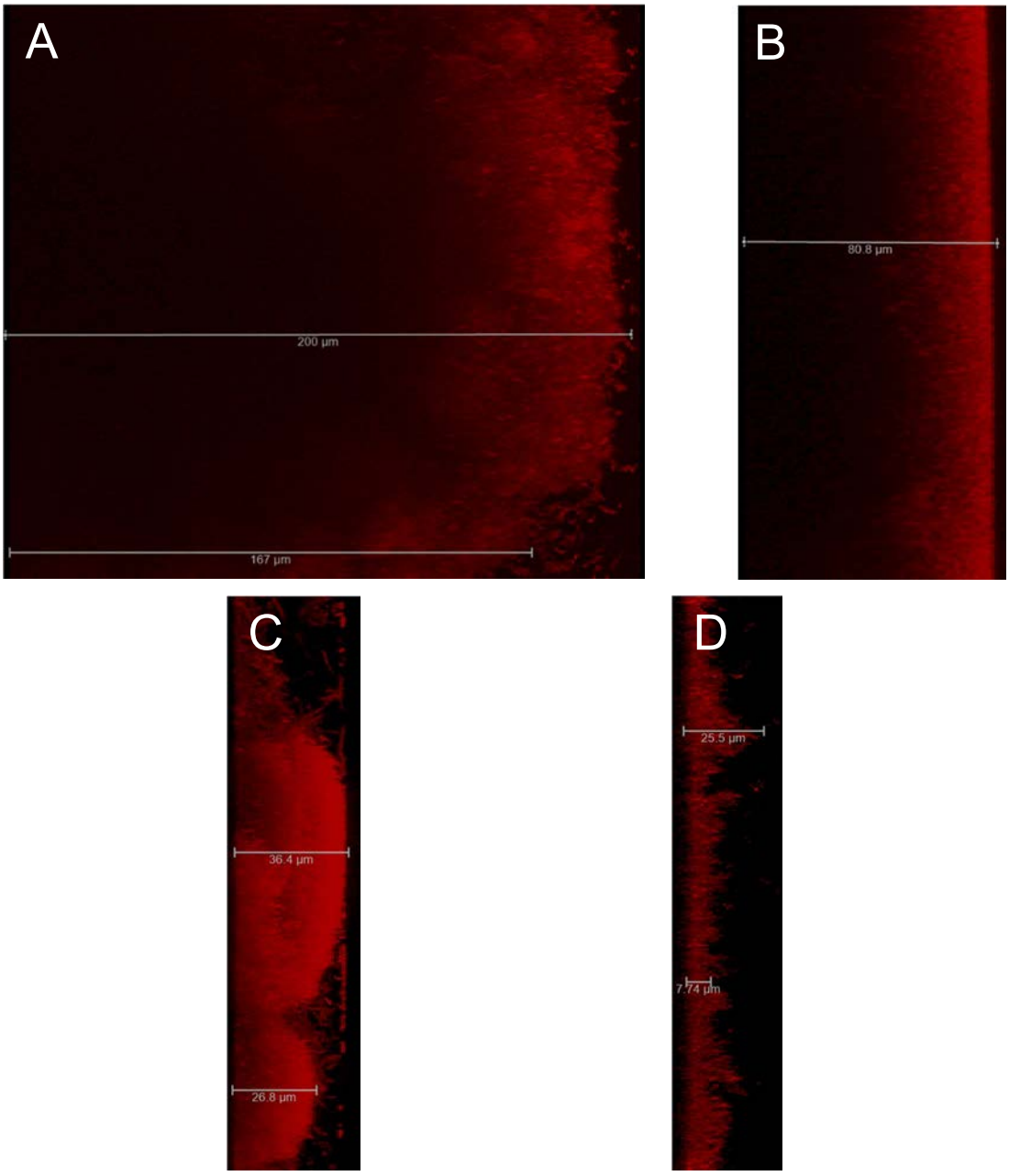

Figure 4.6a: *Representative side-view CLSM images of PHL644 pYddV and BL21 Star (DE3) pYddV biofilms and their untransformed counterparts. Biofilms were grown using the Duran Bottle method. A – PHL644 biofilm. B – BL21 Star (DE3) biofilm. C – PHL644 pYddV biofilm. D – BL21 Star (DE3) pYddV biofilm.*

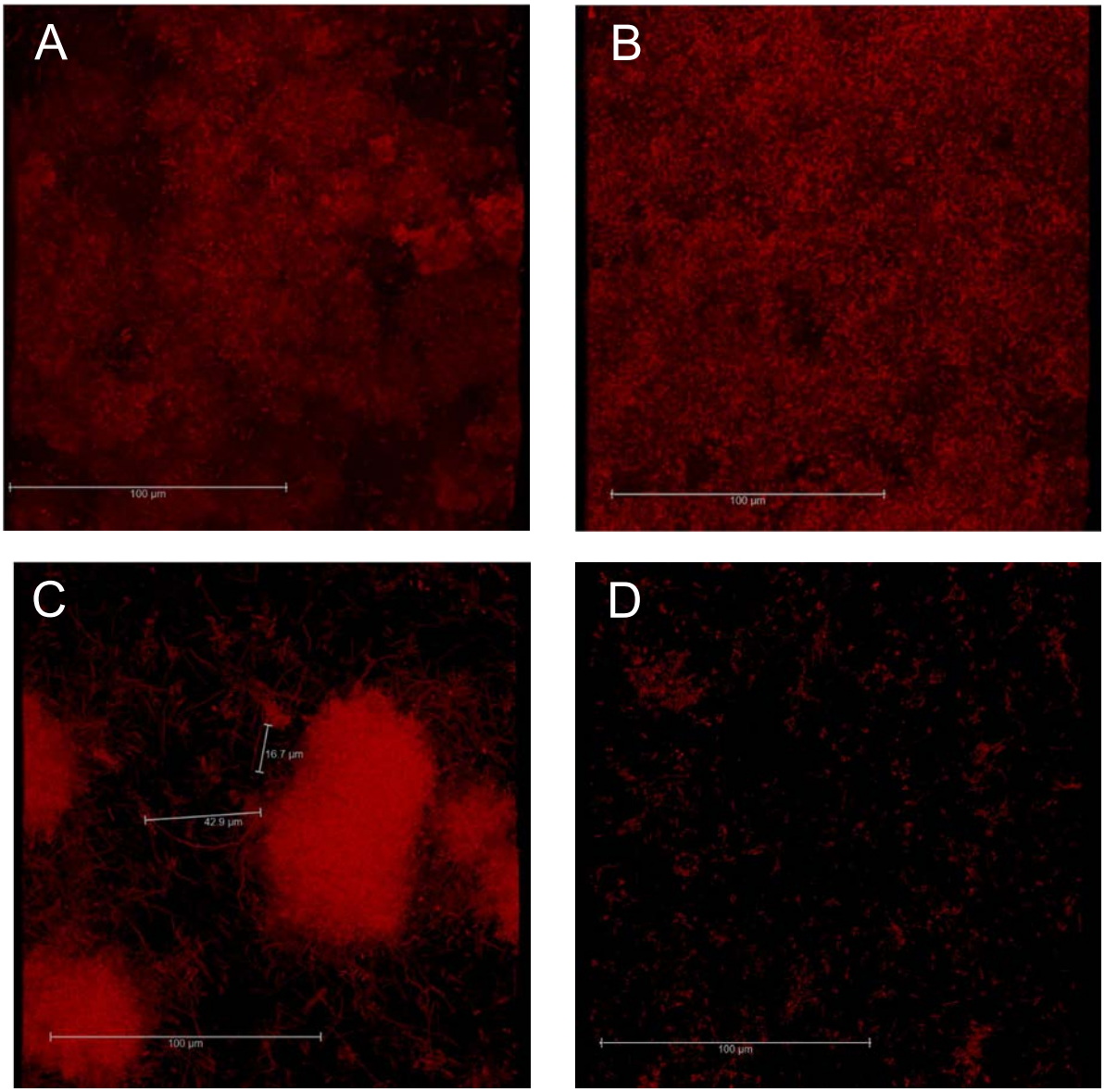

Figure 4.6b: *Representative top-down-view CLSM images of PHL644 pYddV and BL21 Star (DE3) pYddV biofilms and their untransformed counterparts. Biofilms were grown using the Duran Bottle method. A – PHL644 biofilm. B – BL21 Star (DE3) biofilm. C – PHL644 pYddV biofilm; additional scale bars show length of elongated E. coli cells. D – BL21 Star (DE3) pYddV biofilm.*

4.1.4 Overexpression of DgcC (AdrA/YaiC) via pYaiC

DgcC produces c-di-GMP for the activation of the cellulose synthase enzyme complex BcsAB, thus leading to the production of cellulose as a biofilm component. DgcC expression is activated by CsgD in stationary phase, linking curli and cellulose production. It has been shown that curli and cellulose are co-produced as part of the biofilm matrix, in a synergistic relationship (Saldaña Z *et al*., 2009). PHL644, as a derivative of the K-12 strain MC4100, does not produce cellulose due to a mutation in the cellulose gene operon. BL21 Star (DE3) is assumed to produce cellulose, and as such DgcC overexpression was expected to lead to increased biofilm abundance via cellulose overproduction. However, DgcC produces c-di-GMP, which was expected to also increase the level of biofilm abundance in PHL644. DgcC was expressed from pYaiC (Tschowri N *et al*., 2009). DgcC was expressed from a *lac* promoter, resulting in IPTG-dependent expression of DgcC.

pYaiC was transformed into PHL644 and BL21 Star (DE3). PHL644 pYaiC and BL21 Star (DE3) pYaiC biofilms, and their untransformed variants, were grown using the Duran Bottle method. Biofilms were grown in 70 mL M63+ on a PTFE-wrapped microscope slide at 30°C and 70 RPM for 3 days. 100 µM IPTG was added from inoculation to all cultures to induce expression of DgcC from pYaiC. Biofilms were analysed using CV staining and CLSM. All CLSM images are of the submerged region of the biofilm.

Figure 4.7 shows that PHL644 pYaiC featured a higher mean A_{580} than PHL644, but was within 1 standard deviation of the untransformed strain indicating no significant increase. BL21 Star (DE3) pYaiC was significantly increased over BL21 Star (DE3), by approximately 2-fold. These data indicate that pYaiC had positive effects on biofilm abundance, in contrast to pYdaM and pYddV.

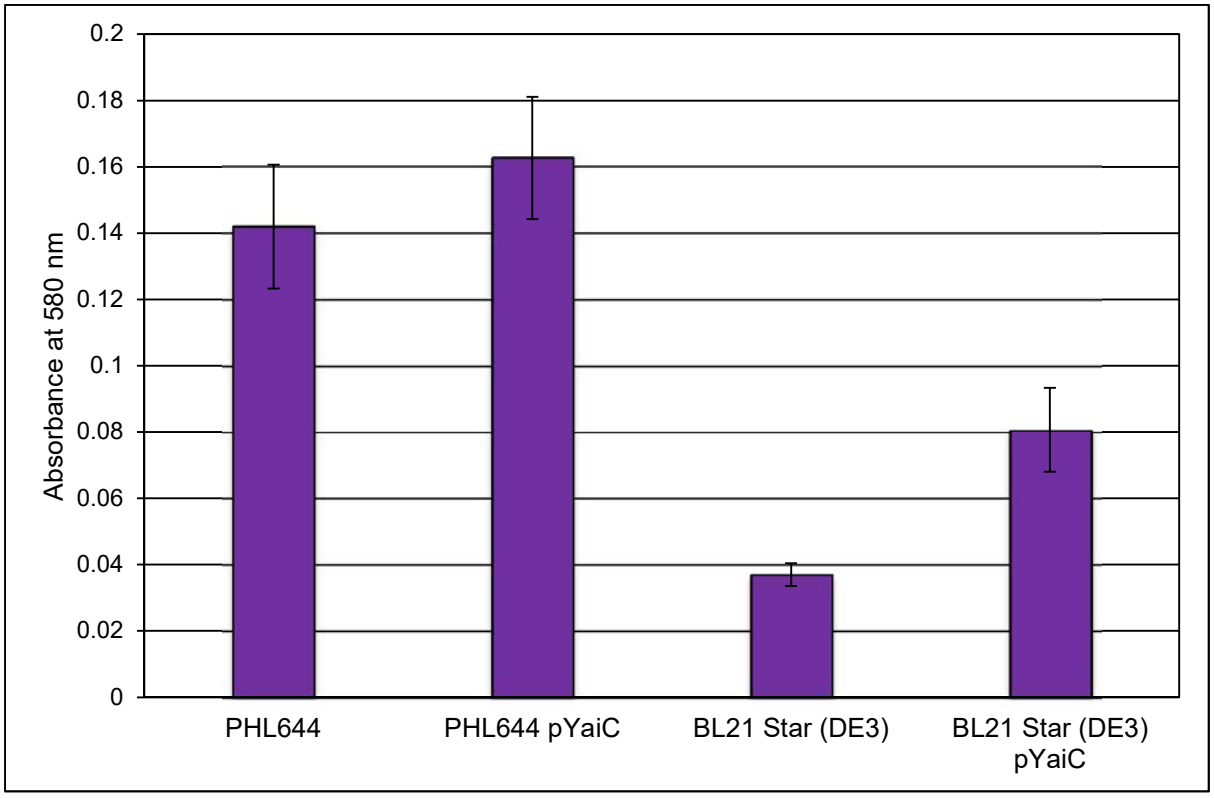

Figure 4.7: *Graph comparing CV retention of PHL644 pYaiC and BL21 Star (DE3) pYaiC biofilms to their untransformed counterparts. Biofilms were grown using the Duran Bottle method. Error bars represent 1 standard deviation from the mean of 3 independent cultures.*

Figure 4.8 shows that PHL644 pYaiC biofilms (80 µm) were slightly thinner than PHL644 biofilms (>200 µm vs 175 µm), and appeared rougher. Specifically, the instances of 3D outgrowth were less well defined than the mushroom structures observed for the untransformed strain. BL21 Star (DE3) pYaiC biofilms on the other hand were thicker than BL21 Star (DE3), but as with PHL644, were more sparsely structured. Interestingly, BL21

Star (DE3) pYaiC biofilms were of a similar maximum thickness to untransformed PHL644 (~200 µm), indicating a beneficial effect on BL21 Star (DE3).

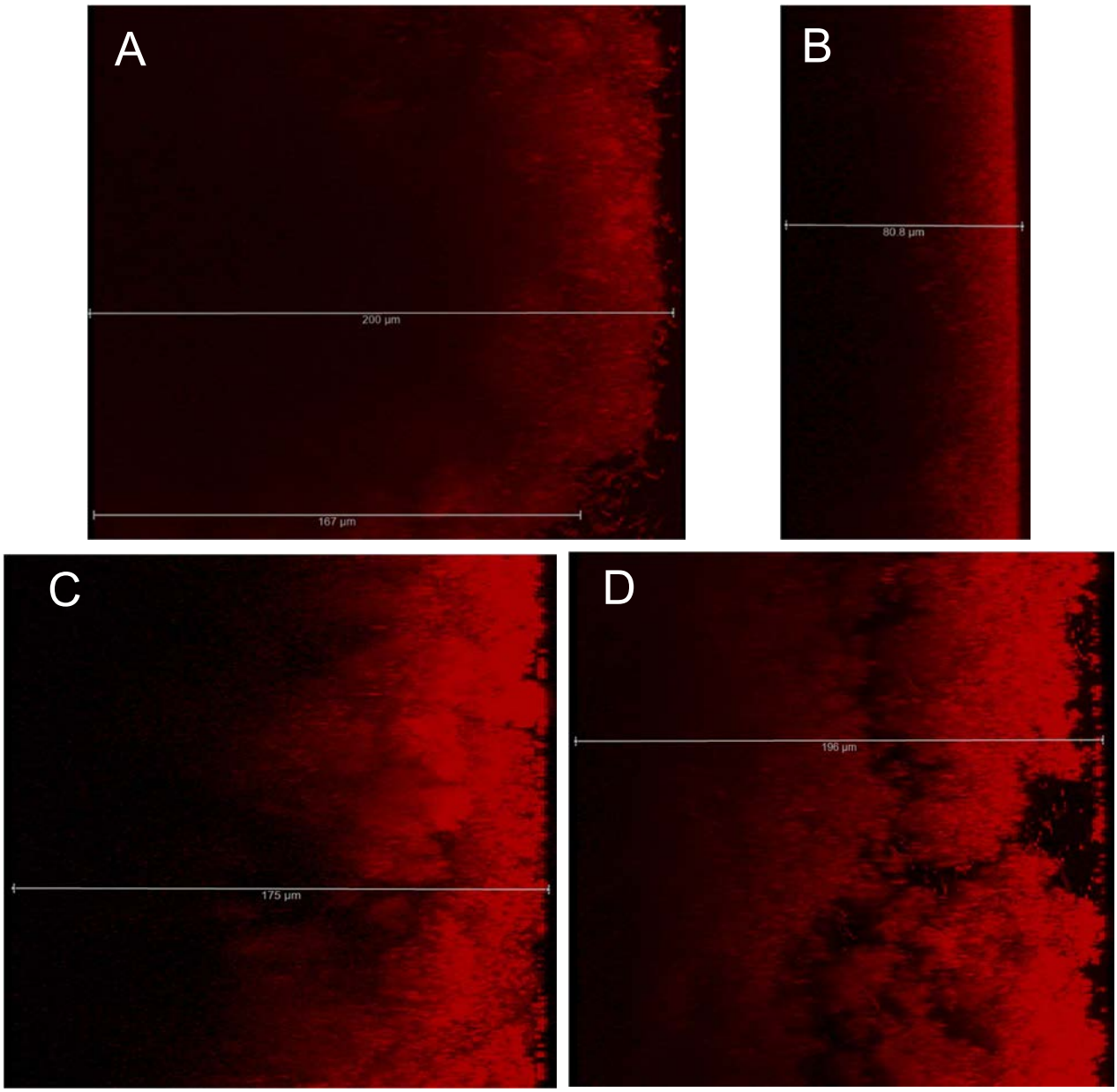

Figure 4.8a: *Representative side-view CLSM images of PHL644 pYaiC and BL21 Star (DE3) pYaiC biofilms and their untransformed counterparts. Biofilms were grown using the Duran Bottle method. A – PHL644 biofilm. B – BL21 Star (DE3) biofilm. C – PHL644 pYaiC. D – BL21 Star (DE3) pYaiC.*

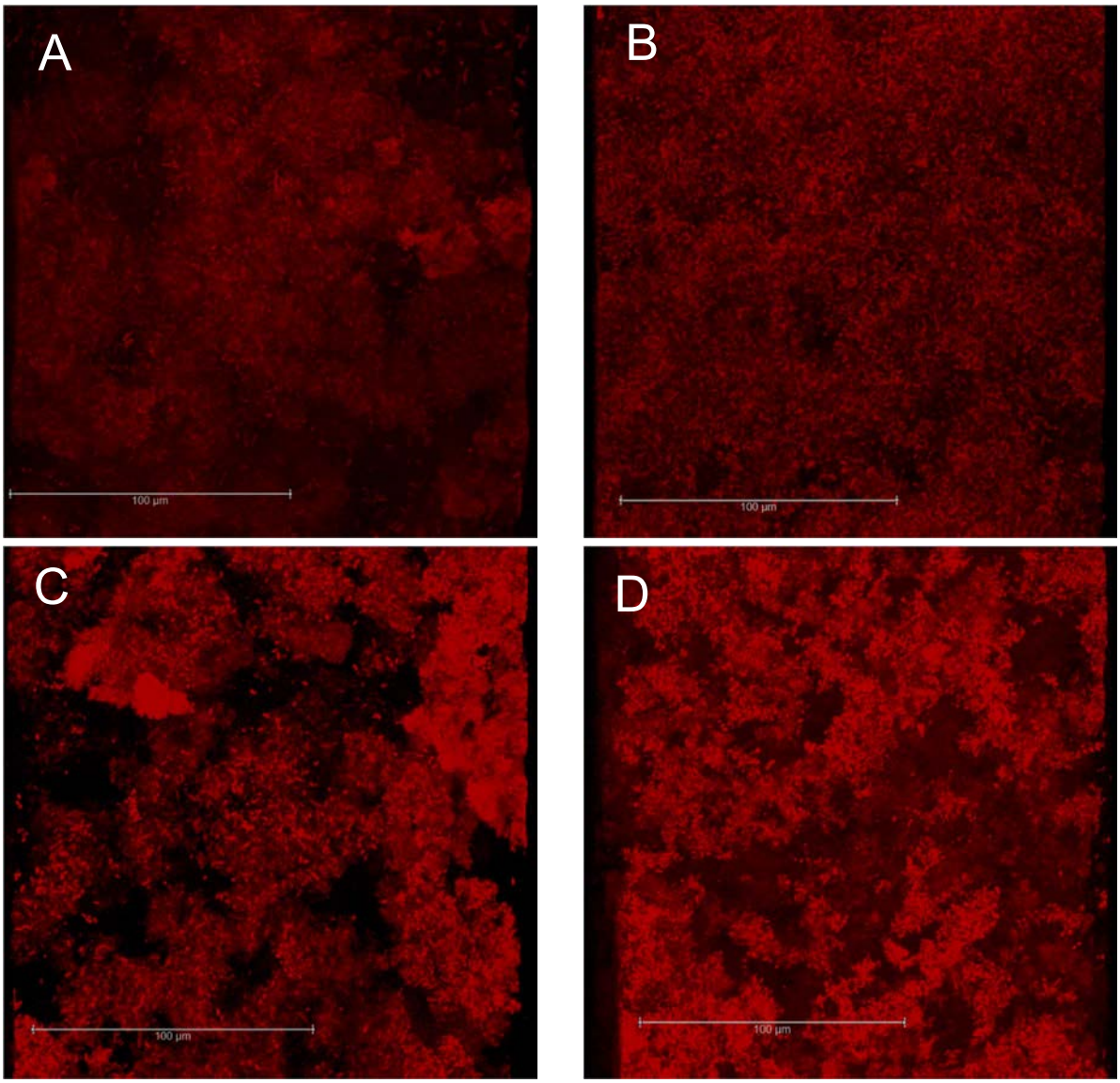

Figure 4.8b: *Representative side-view CLSM images of PHL644 pYaiC and BL21 Star (DE3) pYaiC biofilms and their untransformed counterparts. Biofilms were grown using the Duran Bottle method. A – PHL644 biofilm. B – BL21 Star (DE3) biofilm. C – PHL644 pYaiC. D – BL21 Star (DE3) pYaiC.*

PHL644 pYaiC biofilm formation was not significantly affected by DgcC overexpression, and displayed only a small reduction in maximum thickness. However, BL21 Star (DE3) biofilm formation was significantly promoted suggesting that the positive effects noted for BL21 Star (DE3) pYaiC are due to the effect of DgcC on cellulose production; BL21 Star (DE3) produces cellulose while PHL644 does not. Furthermore, the additional c-di-GMP expected to have been produced by DgcC overexpression had little effect on PHL644 biofilm formation in contrast to BL21 Star (DE3), suggesting either that PHL644 is at peak biofilm-forming capability in terms of c-di-GMP stimulation, or that DgcC has a local effect on cellulose production rather than a global effect on biofilm formation. This would also complement the mechanisms deduced for DgcM and DgcO, in that some DGCs may be specific to certain pathways. In conclusion, pYaiC was determined to have statistically significant positive effects on biofilm formation in BL21 Star (DE3) but not PHL644. A further step in this work may be to mutate the genomic DgcC promoter in BL21 Star (DE3) or another cellulose-producing *E. coli* strain to increase transcription of DgcC and therefore increase BL21 Star (DE3) biofilm formation without the need for pYaiC. This could not be completed in this study due to time and funding constraints, but may be an avenue of interest for developing BL21 Star (DE3) as a biofilm biocatalyst.

4.2 Analysis of Growth Rate and Curli Gene Expression in Strains Containing the Biofilm-Modulation Plasmids

It was decided to determine whether the plasmids in Section 4.1 affected the growth rates and curli gene expression of *E. coli*. This would allow comparisons to be drawn to the previously shown untransformed strain data, as well as suggest explanations for the data observed in Section 4.1.

PHL644 and BL21 Star (DE3) were transformed with pJLC-T (Section 3.4). The resulting transformed strains were made competent again and transformed with either pYdaM, pYddV or pYaiC. pT7-CsgD was not analysed due to time constraints. All transformed strains were grown planktonically using the Duran Bottle method. Cultures were grown in 70 mL M63+ at 30°C and 70 RPM for 24 hours. A PTFE-wrapped microscope slide was inserted to allow the presence of a growing biofilm, even though the focus was on planktonic cells. 100 μM IPTG was added from inoculation to all cultures to induce expression of DgcC from pYaiC, and was kept in all cultures as a control. OD_{600} was measured every 2 hours using a spectrophotometer beginning at 0 hours. Samples for flow cytometry were removed every 2 hours and diluted as necessary in sterile PBS, and then immediately analysed.

Due to time constraints, only planktonic cells could be analysed in this experiment.

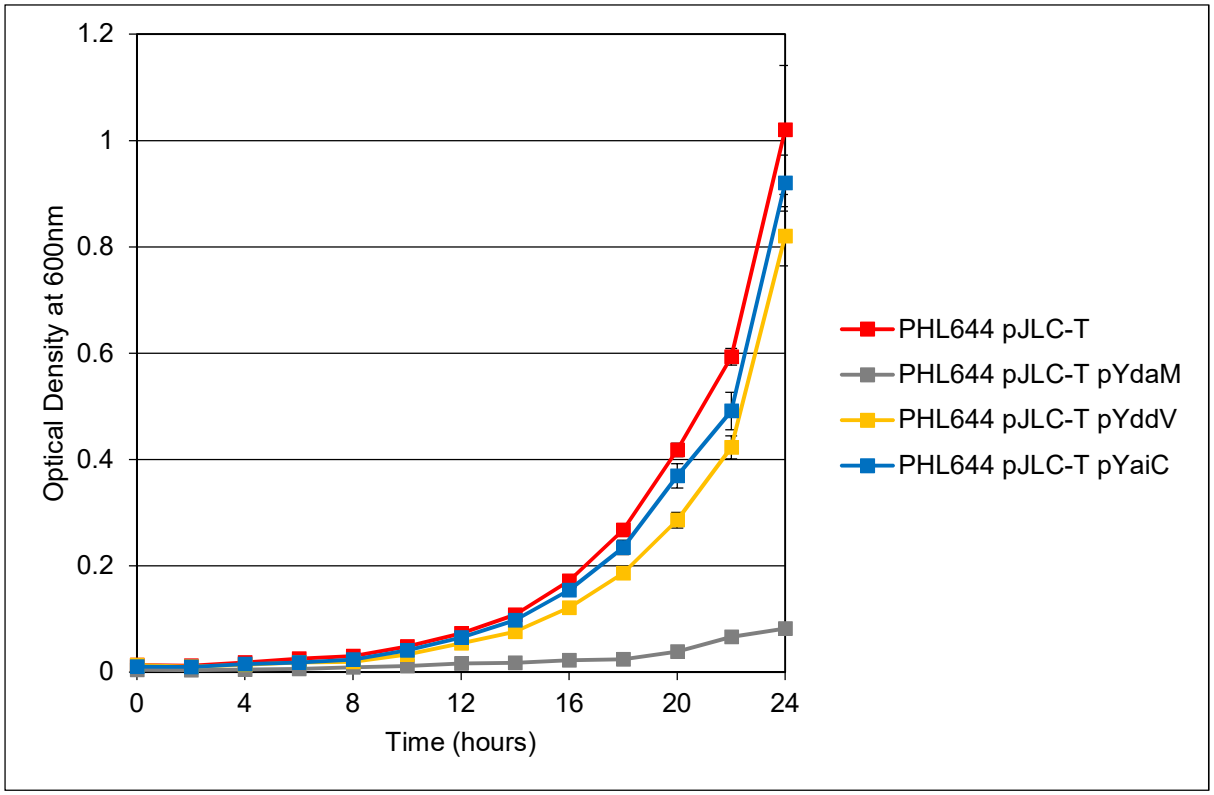

Figure 4.9: *Planktonic growth curves for PHL644 pJLC-T transformed with pYdaM, pYddV and pYaiC. Cultures were grown using the Duran Bottle method. OD_{600} measurements were taken every 2 hours. Error bars represent 1 standard deviation from the mean of three independent cultures.*

Figure 4.9 displays the OD results obtained for PHL644 pJLC-T with either pYdaM, pYddV or pYaiC. PHL644 pJLC-T pYddV and PHL644 pJLC-T pYaiC show slight reductions in mean OD_{600} compared to PHL644 pJLC-T between 14 and 22 hours but by 24 hours these results are within 1 standard deviation of each other. This indicates that pYddV and pYaiC do not significantly affect PHL644 pJLC-T growth rate, and that the metabolic burden of maintaining 2 multi-copy plasmids does not have any substantial observable negative effect on growth. However, the data observed for PHL644 pJLC-T pYdaM indicates that pYdaM severely restricts the growth of this strain compared to PHL644 pJLC-T. After 24 hours, this

strain reached an OD_{600} of only 0.082 compared to 1.02 in PHL644 pJLC-T. These data show that the overexpression of DgcM is detrimental to growth in PHL644 pJLC-T.

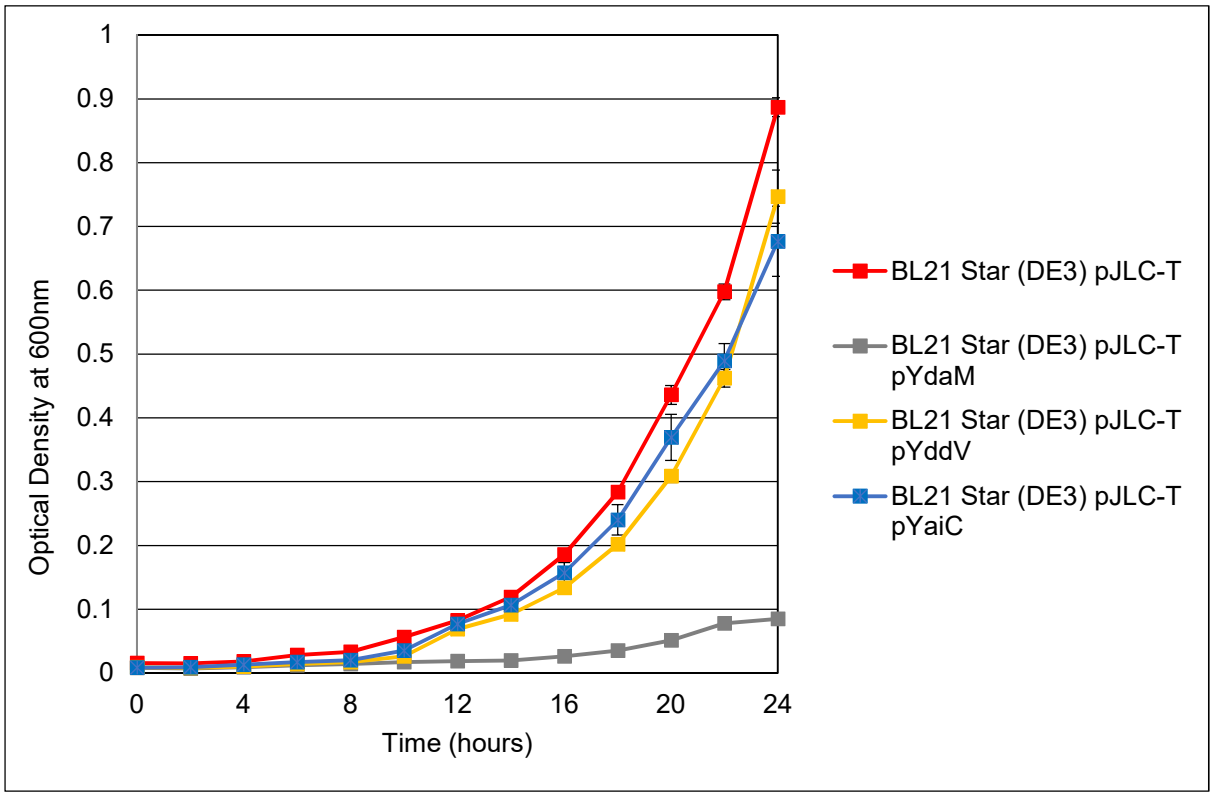

Figure 4.10: *Planktonic growth curves for BL21 Star (DE3) pJLC-T transformed with pYdaM, pYddV and pYaiC. Cultures were grown using the Duran Bottle method.* OD_{600} *measurements were taken every 2 hours. Error bars represent 1 standard deviation from the mean of three independent cultures.*

Figure 4.10 displays the OD results obtained for BL21 Star (DE3) pJLC-T with either pYdaM, pYddV and pYaiC. Once again pYddV and pYaiC have slight negative effects on growth compared to BL21 Star (DE3) pJLC-T, although these effects are statistically significant compared to PHL644 pJLC-T. The result for BL21 Star (DE3) pJLC-T pYdaM complements that of PHL644 pJLC-T pYdaM with a severe reduction in maximum OD_{600} after 24 hours

from 0.887 to 0.085. This indicates that both strains encounter detrimental growth effects when transformed with pYdaM.

Figure 4.11 displays the percentage of cells considered to be GFP-positive in the strain PHL644 pJLC-T when transformed with pYdaM, pYddV or pYaiC. PHL644 pJLC-T pYaiC exhibited the fastest overall activation, increasing from 49% at 0 hours to 95% after 2 hours, indicating that DgcC overexpression led to rapid activation of the *csgBAC* promoter. PHL644 pJLC-T pYddV maintained similar percentages to PHL644 JLC-T, indicating little effect on *csgBAC* promoter activation. pYdaM caused the *csgBAC* promoter to be more slowly activated, reaching 90% after 14 hours. As *csgBAC* is activated during stationary phase, this may indicate that the slower growth rate observed in Figure 4.10 leads to delayed activation of curli genes. After 24 hours, all strains reached >95% activation, indicating that no plasmid had a long-term negative effect on PHL644 pJLC-T curli gene activation.

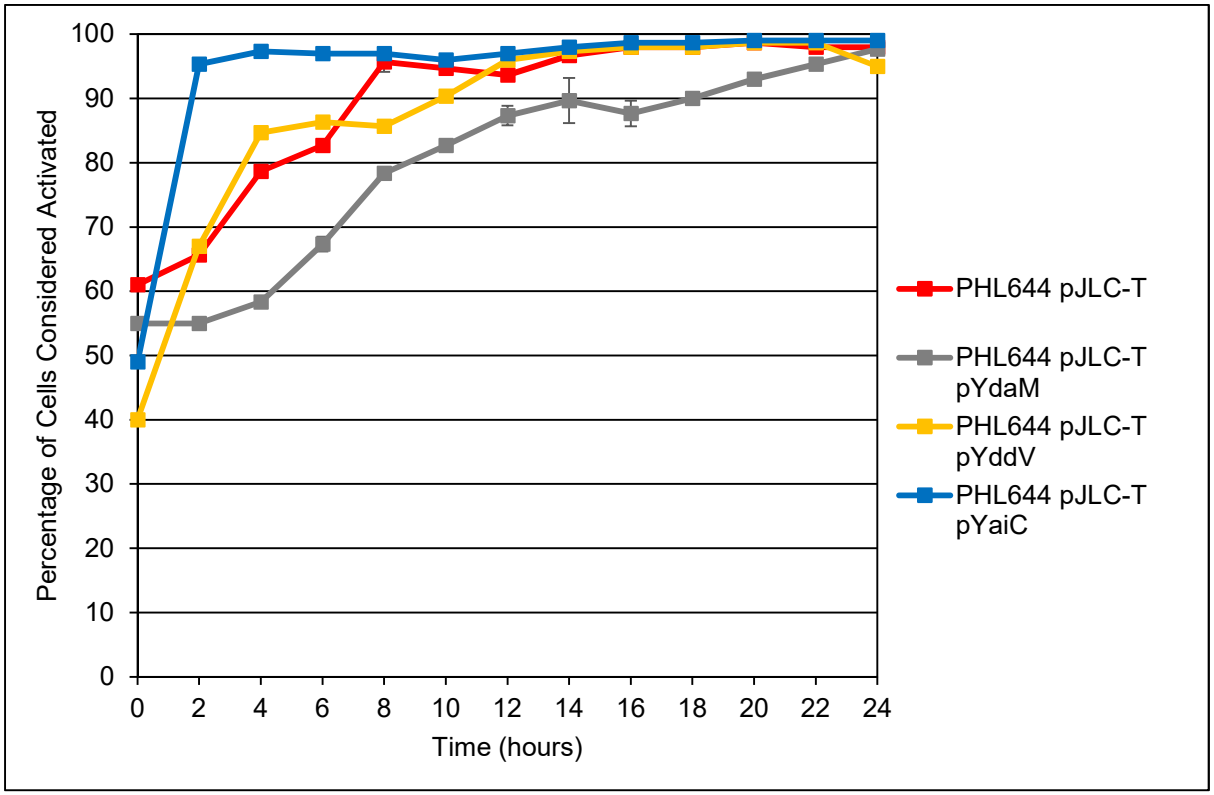

Figure 4.11: *Graph comparing percentages of planktonic PHL644 pJLC-T (and transformed with pYdaM, pYddV and pYaiC) cells considered GFP-positive over 24 hours. Threshold for GFP-positive/negative determination was set at 575 units. Error bars represent 1 standard deviation from the mean of 3 independent cultures.*

Figure 4.12 displays the percentage of cells considered to be GFP-positive in the strain BL21 Star (DE3) pJLC-T when transformed with pYdaM, pYddV or pYaiC. All strains showed extremely similar patterns of activation after 4 hours until the end of the experiments, indicating that pYdaM did not have a negative effect on *csgBAC* promoter activation at any point during the experiment. Interestingly, the strains containing 2 plasmids displayed 0 hours activation percentages of between 30% and 40%, in contrast to BL21 Star (DE3) pJLC-T at 81%. The reason for this is unclear and is only slightly mirrored in PHL644. However, the overnight cultures for BL21 Star (DE3) pJLC-T contained tetracycline, while

the overnight cultures for BL21 Star (DE3) pJLC-T transformed with pYdaM, pYddV and pYaiC contained both tetracycline and carbenicillin. It is possible that carbenicillin, or the combination of both antibiotics, had a repressive effect on *csgBAC* expression which was relieved when transferred into M63+ with no antibiotic. This effect bears little relevance to this study, but suggests further experiments into the expression of curli genes, and therefore biofilm formation, in antibiotic-containing environments.

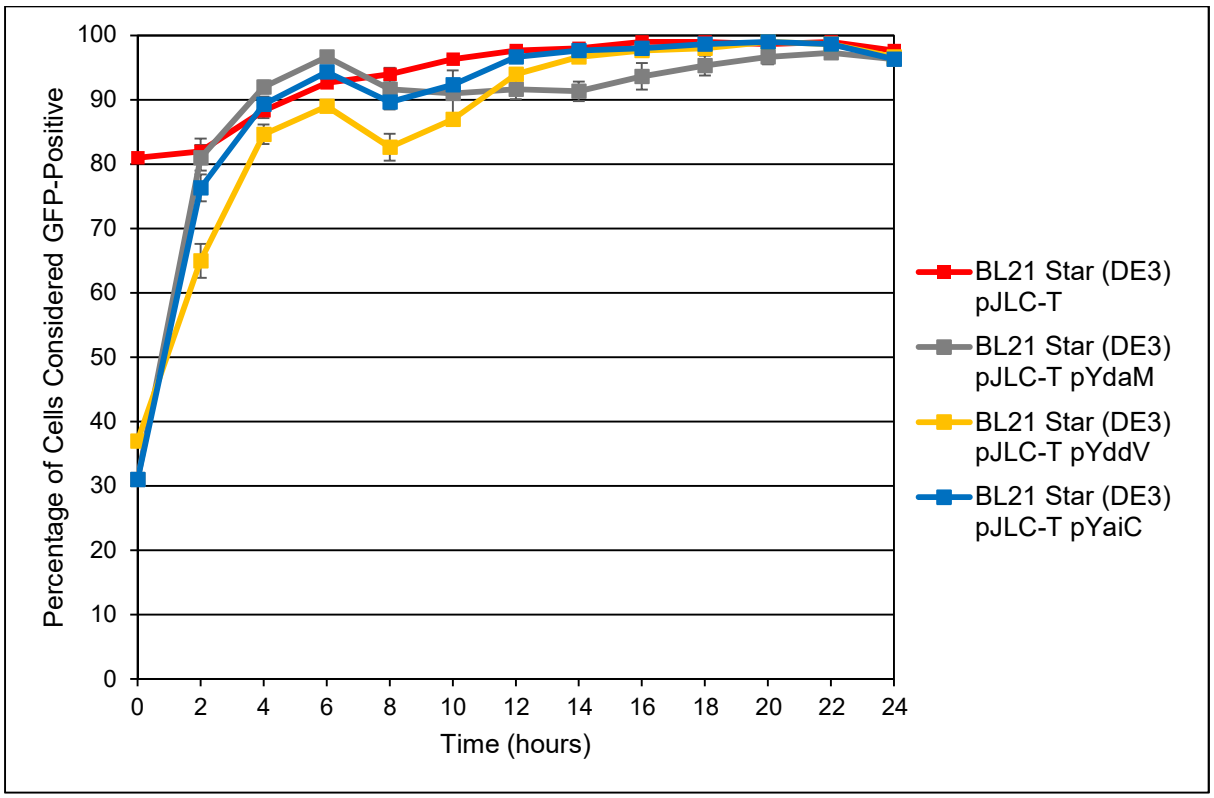

Figure 4.12: *Graph comparing percentages of planktonic BL21 Star (DE3) pJLC-T (and transformed with pYdaM, pYddV and pYaiC) cells considered GFP-positive over 24 hours. Threshold for GFP-positive/negative determination was set at 575 units. Error bars represent 1 standard deviation from the mean of 3 independent cultures.*

Figure 4.13 shows the mean green fluorescence of PHL644 pJLC-T with either pYdaM, pYddV or pYaiC. PHL644 pJLC-T pYdaM expression levels appear to rise in accordance with PHL644 pJLC-T until 14 hours. This level then decreases and remains between 30000 and 20000 until the end of the experiment, while PHL644 pJLC-T fluorescence levels increase to ~50000 units. This indicates that DgcM overexpression has a negative effect on *csgBAC* expression in PHL644 pJLC-T. pYddV had an even stronger negative effect, with a maximum fluorescence not exceeding 12000 throughout the experiment, indicating that DgcO overexpression had a strong negative effect on *csgBAC* expression. pYaiC had the opposite effect. Between 4 and 10 hours, PHL644 pJLC-T pYaiC exhibited a statistically significant (more than 1 standard deviation) higher mean fluorescence than PHL644 pJLC-T, and again after 16 hours until the end of the experiment, at a maximum of ~80000 units. This indicates that DgcC overexpression strongly promoted *csgBAC* expression in PHL644 pJLC-T.

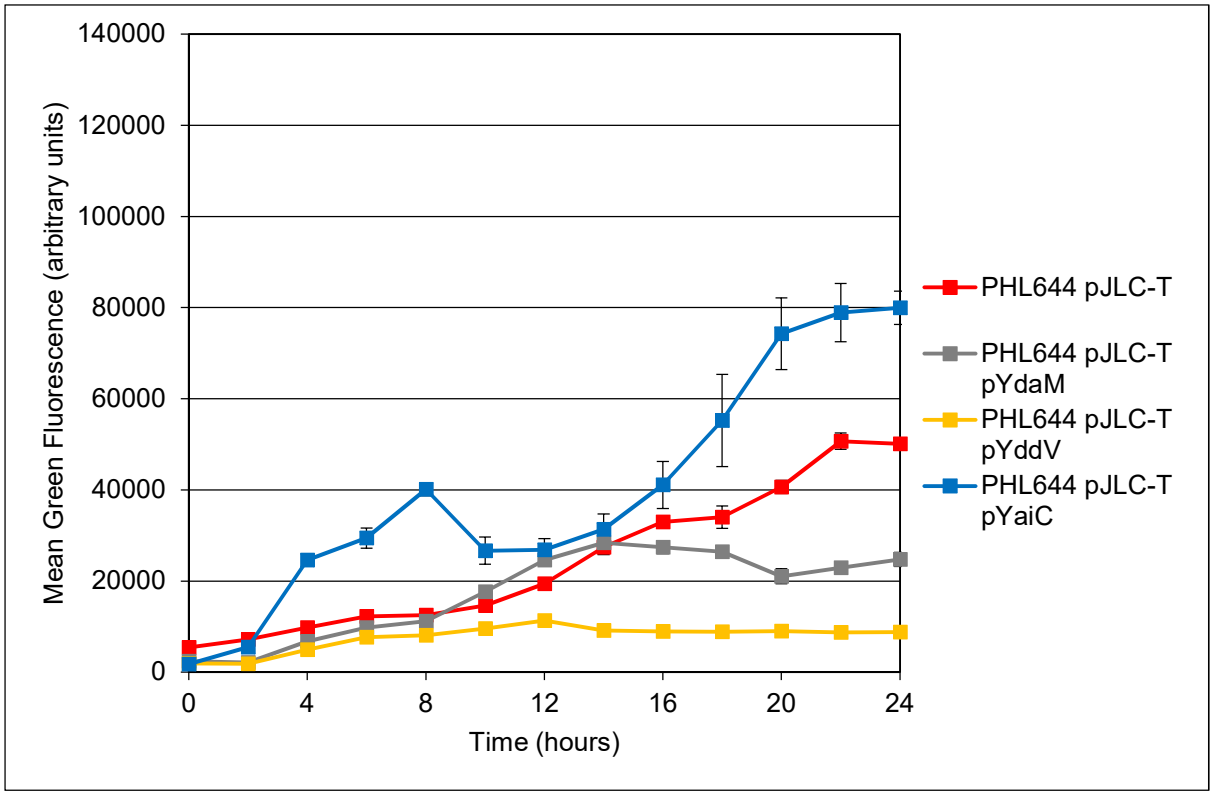

Figure 4.13: *Graph comparing mean green fluorescence intensities of planktonic PHL644 pJLC-T (and transformed with pYdaM, pYddV and pYaiC) cultures over 24 hours. Error bars represent 1 standard deviation from the mean of 3 independent cultures.*

Figure 4.14 shows the mean green fluorescence of BL21 Star (DE3) pJLC-T with either pYdaM, pYddV or pYaiC. As with PHL644 pJLC-T, pYdaM and pYddV had overall negative effects on BL21 Star (DE3) pJLC-T *csgBAC* expression. Interestingly, the level of expression in BL21 Star (DE3) pJLC-T pYdaM was actually higher than BL21 Star (DE3) pJLC-T from 4 to 8 hours, but then began to decrease and maintain a level between 18000 and 24000. BL21 Star (DE3) pJLC-T pYaiC *csgBAC* expression was higher than BL21 Star (DE3) pJLC-T in the periods 6 to 8 hours and 16 to 24 hours, reaching a maximum of ~110000 units, far in excess of BL21 Star (DE3) pJLC-T at ~54000 units. As with PHL644, pYaiC was shown to positively affect *csgBAC* expression.

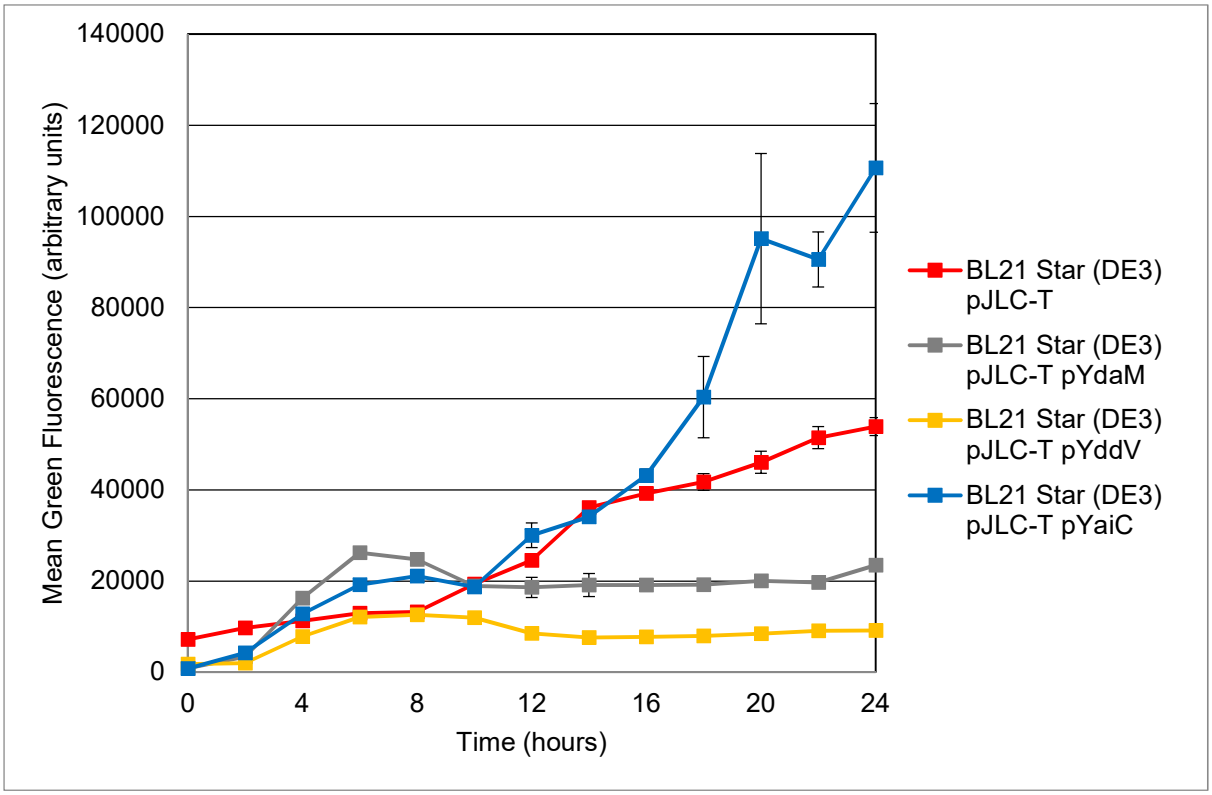

Figure 4.14: *Graph comparing mean green fluorescence intensities of planktonic BL21 Star (DE3) pJLC-T (and transformed with pYdaM, pYddV and pYaiC) cultures over 24 hours. Error bars represent 1 standard deviation from the mean of 3 independent cultures.*

The data presented in this section suggests that the overexpression of DgcM and DgcO are not conducive to increased curli production. In both PHL644 and BL21 Star (DE3), overexpressed DgcM and DgcO reduce the amount of curli gene transcription but not the maximum percentage of activated cells in the population. This indicates that the effects of these overexpressed enzymes attenuate the level of curli gene production and not the initial activation of the genes involved. In contrast DgcC overexpression, in both tested strains, led to increased curli gene production. Interestingly, DgcC overexpression led to more rapid activation of curli genes in PHL644 but not BL21 Star (DE3). These results are likely due to strain differences, but nevertheless reveal that DgcC modulation may lead to increased curli

production in *E. coli* and may be a useful target for strain engineering. These results will be discussed further in Section 6.2.

Chapter 5

Use of *E. coli* Biofilms in Biocatalysis

The initial aim of this project was to develop an *E. coli* strain and simple biofilm-generation method which would be able to accept a biocatalysis plasmid, form a biofilm and perform a biocatalytic task efficiently. This platform was referred to as a 'plug-and-play' biofilm biocatalyst. To prove that the biofilm biocatalyst would be effective in a variety of biocatalytic tasks, three separate enzymes, and therefore reactions, were chosen for testing. The enzymes were chosen based on previously proven biocatalytic potential, simplicity of analysis and industrial value.

5.1 Synthesis of 5-chloro-L-tryptophan using Tryptophan Synthase (TrpBA)

Tryptophan synthase (TrpBA) produces tryptophan from indole and L-serine (Figure 5.1). The tryptophan synthase complex is a tetramer of 2 TrpA and 2 TrpB subunits, known as the α and β subunits respectively. Tryptophan synthase requires pyridoxal-5'-phosphate (PLP) as a cofactor, which is produced and regenerated in the *E. coli* cell (Lane AN & Kirschner K, 1991). While the production of enantimoerically pure L-tryptophan would be beneficial, this work attempted to use tryptophan synthase to produce 5-chloro-L-tryptophan from 5-chloroindole and L-serine. 5-chloro-L-tryptophan can be used as a precursor for pharmaceutical compounds, making it a valuable compound in its enantiopure form (Perni S *et al*., 2013). This had previously been presented in in a spin-coated *E. coli* biofilm biocatalyst and thus was chosen as a base from which to develop the work further (Tsoligkas AN *et al*., 2011).

Chemical synthesis of tryptophan leads to a mixture of L- and D- forms which reduces the yield of functional L-tryptophan. Due to the specificity of TrpBA, enzymatic synthesis

produces only L-tryptophan from indole and therefore is preferable to chemical synthesis (Chen CH *et al*., 2014). In turn, TrpBA will only produce 5-chloro-L-tryptophan from 5-chloroindole.

Possible caveats with this reaction which were considered beforehand involved the dependence of *E. coli* biofilm formation on indole synthesis. Since an overexpression of TrpBA may disrupt this process, effects may be seen on cell growth and most importantly, biofilm formation (Section 1.4.8). These effects were specifically tested for in this experimental section.

In *E. coli* and *Salmonella* spp., TrpB and TrpA are cotranscribed as the polycistronic operon *trpLEDCBA*. The tryptophan leader sequence, *trpL*, contains mRNA regulatory elements which decrease operon expression when tryptophan-charged tRNA is abundant and tryptophan synthesis is thus not required (Landick R *et al*., 1990). While TrpE, TrpD and TrpC are required for the *de novo* synthesis of tryptophan from chorismic acid, the TrpBA complex is sufficient for indole to L-tryptophan conversion (Rodriguez A *et al*., 2014, Kawasaki H *et al*., 1987). The plasmid pSTB7 used in this experiment featured the native *Salmonella enterica* serovar Typhimurium *trpLEDCBA* promoter followed by a truncated *trpC* and full length *trpB* and *trpA*. This construct eliminates the *trpL* regulatory sequence, as well as *trpE* and *trpD*, resulting in constitutive expression of TrpBA (Kawasaki H *et al*., 1987).

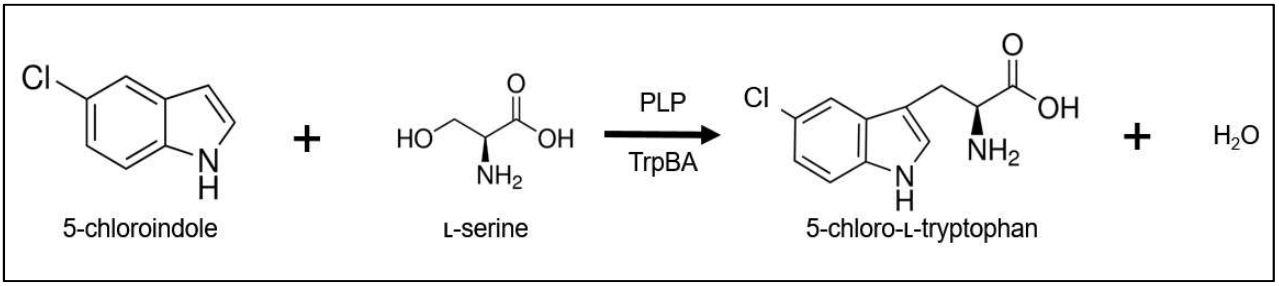

Figure 5.1: *Formation of 5-chloro-L-tryptophan from 5-chlorindole by TrpBA.*

5.1.1 Effect of pSTB7 on Agar Plate Colony Growth

Initially, pSTB7 was transformed into *E. coli* PHL644 and BL21 Star (DE3) using project-standard plating conditions (30°C) on nutrient agar for 20 hours (with 100 µg/mL carbenicillin). However, while all other plasmids used in this project enabled growth at this temperature, cells containing pSTB7 produced no colonies at 30°C. Transformations with this plasmid were therefore grown on agar plates at 37°C for 18 hours, which produced abundant colonies. Thus, pSTB7 negatively affects colony forming ability at 30°C, but not at 37°C. This will be discussed in Section 5.1.5.

5.1.2 Effect of pSTB7 on Planktonic Growth Rate

Growth performance of PHL644 pSTB7 and BL21 Star (DE3) pSTB7 and their untransformed variants in minimal medium was measured through optical density (OD). *E. coli* cultures were grown in 100 mL Duran bottles in 70 mL M63+ at 30°C and 70 RPM for 24 hours. This was to simulate conditions found in 100 mL Duran bottle biofilm generators. The OD of cultures was measured at 600 nm every 2 hours using a spectrophotometer. Despite the poor growth of pSTB7-containing cells on agar plates at 30°C, this temperature was chosen due to it being the optimal temperature for biofilm growth in the untransformed strains as previously shown (Section 3.3.12).

As shown in Figure 5.2, growth of PHL644 pSTB7 and BL21 Star (DE3) pSTB7 was severely repressed as compared to untransformed cultures. While untransformed cultures of PHL644 and BL21 Star (DE3) were able to reach an OD_{600} of approximately 1.2 and 1.4 respectively after 24 hours, strains transformed with pSTB7 were unable to exceed 0.06. This demonstrates that pSTB7 inflicts a severe growth disadvantage on both strains at 30°C.

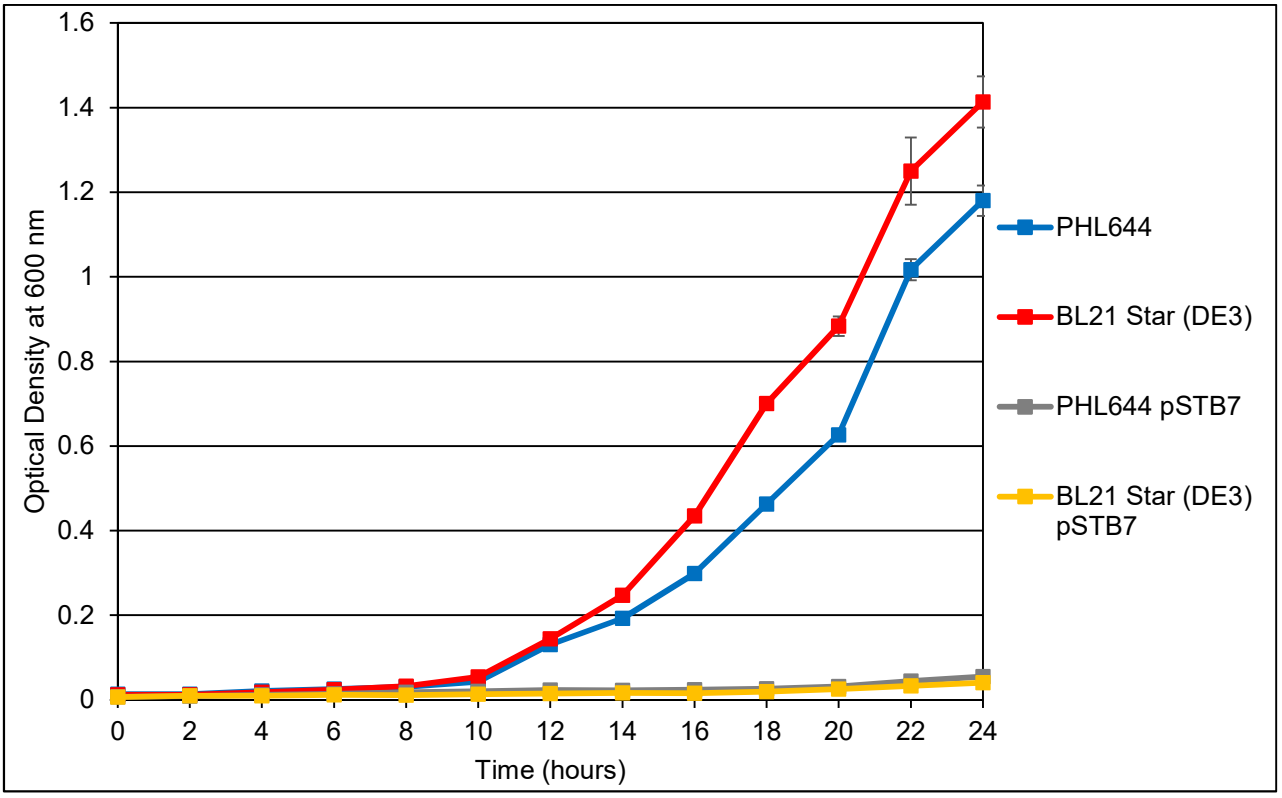

Figure 5.2: *Growth curves for PHL644, BL21 Star (DE3), and their pSTB7-transformed variants. Cultures were grown in M63+ (30°C, 70 RPM) for 24 hours.* OD_{600} *measurements were taken every 2 hours. Error bars represent 1 standard deviation from the mean of three independent cultures.*

5.1.3 Effect of pSTB7 on *csgBAC* Promoter Activity

PHL644 and BL21 Star (DE3) were sequentially transformed with pJLC-T and pSTB7 to determine the effect of pSTB7 on *csgBAC* transcriptional regulation. These cultures were compared against PHL644 pJLC-T and BL21 Star (DE3) pJLC-T. Cells were grown planktonically at 30°C at 70 RPM in M63+ for 24 hours. 100 µL samples were removed every 2 hours, diluted in PBS as required, and analysed using an Accuri C6 flow cytometer. 25000 events were analysed per sample. The FL1-A channel was used to determine green fluorescence.

As shown in Figure 5.3, PHL644 pJLC-T pSTB7 and BL21 Star (DE3) pJLC-T pSTB7 displayed severely reduced fluorescence intensities compared to PHL644 pJLC-T and BL21 Star (DE3) pJLC-T throughout the experiment, with a maximum mean fluorescence of <10000 compared to >50000 shown by both PHL644 pJLC-T and BL21 Star (DE3) pJLC-T after 24 hours. Figure 5.4 indicates the percentage of cells considered GFP-positive during the experiment. PHL644 pJLC-T pSTB7 maintained a relatively constant percentage of GFP-positive cells between 76% and 83% over 24 hours, indicating that most of the population had an active *csgBAC* promoter, despite producing a very low level of GFP (Figure 5.3). BL21 Star (DE3) pJLC-T pSTB7 displayed a GFP-positive population of between 41% and 53% for the first 10 hours of the experiment, then quickly increased between 10 and 12 hours to 73%. This may indicate a rapid regulatory change between 10 and 12 hours, possibly linked to the increase in growth rate at this time noted by Figure 5.2. Between 12 and 24 hours, the percentage increased to 82%, matching PHL644 pJLC-T pSTB7. These data display an interesting difference between the percentage of a population with an active *csgBAC* promoter and how much GFP is actually being produced.

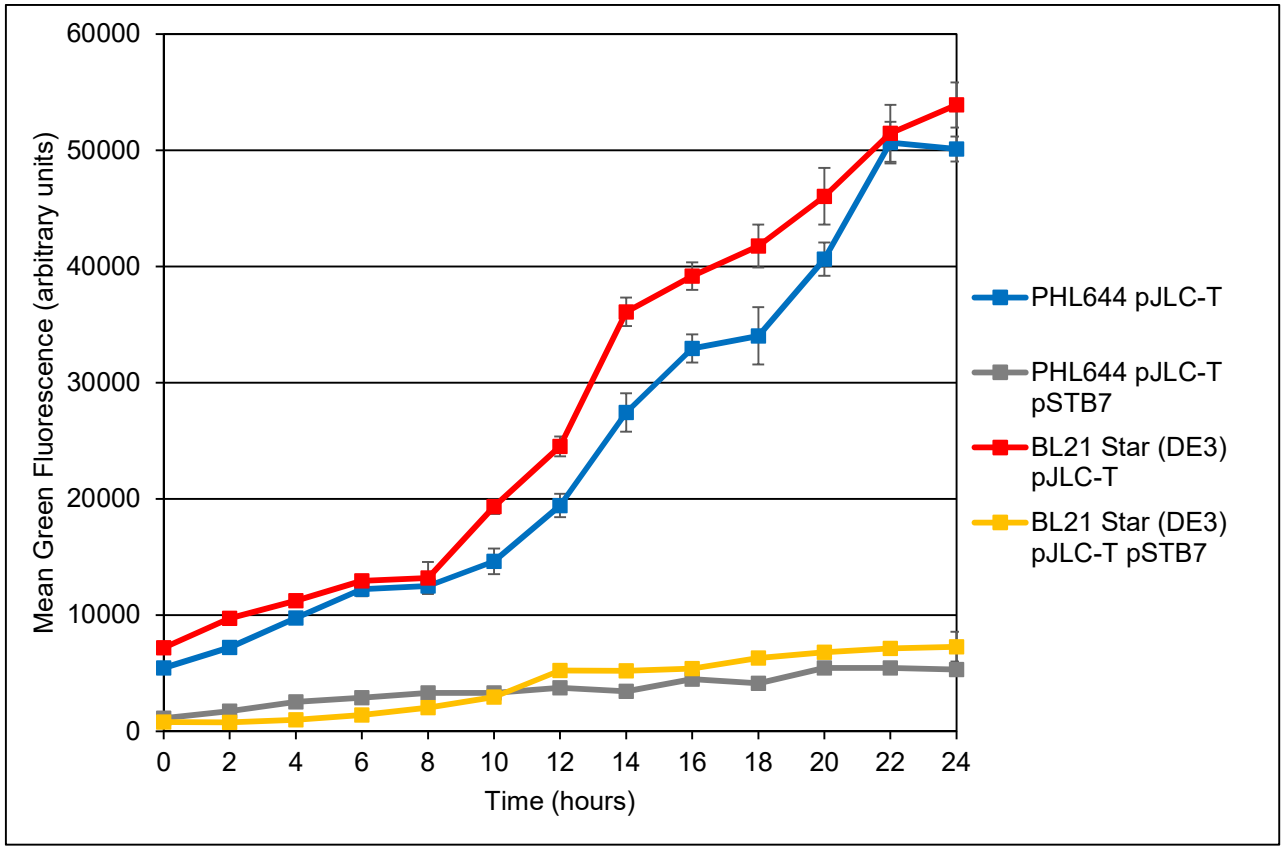

Figure 5.3: *Mean green fluorescence intensity of PHL644 pJLC-T and BL21 Star (DE3) pJLC-T, and their pSTB7-transformed variants. Cultures were grown in M63+ (30°C, 70 RPM) for 24 hours. Flow cytometry samples were taken every 2 hours. Error bars represent 1 standard deviation from the mean of three independent cultures.*

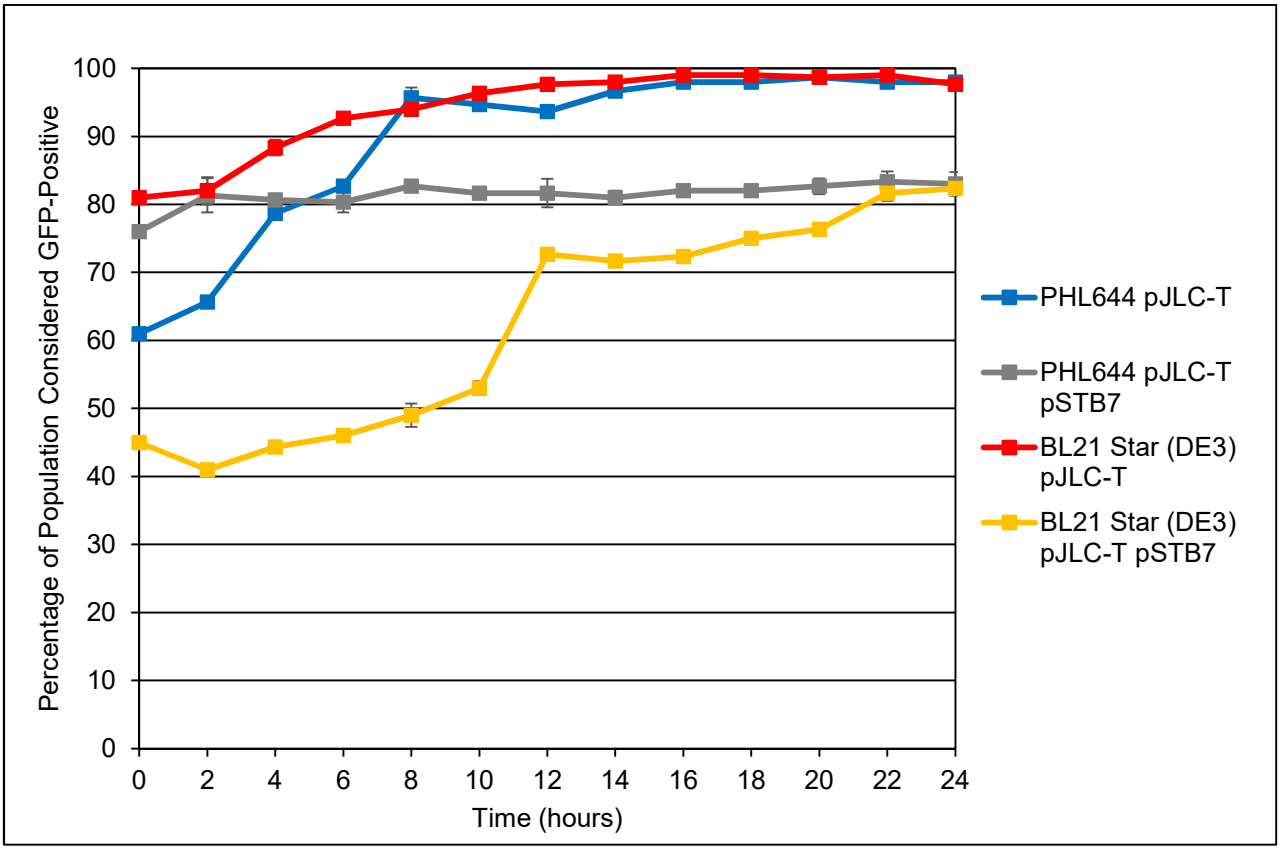

Figure 5.4: *Percentage of cells considered GFP-positive for PHL644 pJLC-T and BL21 Star (DE3) pJLC-T, and their pSTB7-transformed variants. Cultures were grown in M63+ (30°C, 70 RPM) for 24 hours. Flow cytometry samples were taken every 2 hours. Error bars represent 1 standard deviation from the mean of three independent cultures.*

5.1.4 Effect of pSTB7 on Biofilm Formation

PHL644 pSTB7 and BL21 Star (DE3) pSTB7 were analysed for biofilm formation ability and compared to their untransformed variants. PHL644 pSTB7 and BL21 Star (DE3) pSTB7 biofilms were grown using the Duran Bottle method. Biofilms were grown in 70 mL M63+ on a PTFE-wrapped microscope slide at 30°C and 70 RPM for 3 days. Biofilms were analysed using CV staining and CLSM. All CLSM images are of the submerged region of the biofilm.

As indicated by CV staining (Figure 5.5), biofilm development of pSTB7-containing cells was reduced compared to untransformed PHL644 and BL21 Star (DE3). Crystal violet stain retention was reduced by approximately 17 fold for PHL644. BL21 Star (DE3) retention was reduced by nearly half, indicating a less pronounced effect than on PHL644, but a detrimental effect nonetheless. In addition, CLSM revealed sparsely scattered cells on the surface with no 3D structure and very little aggregation (Figure 5.6). pSTB7 therefore has an extremely detrimental effect on biofilm formation.

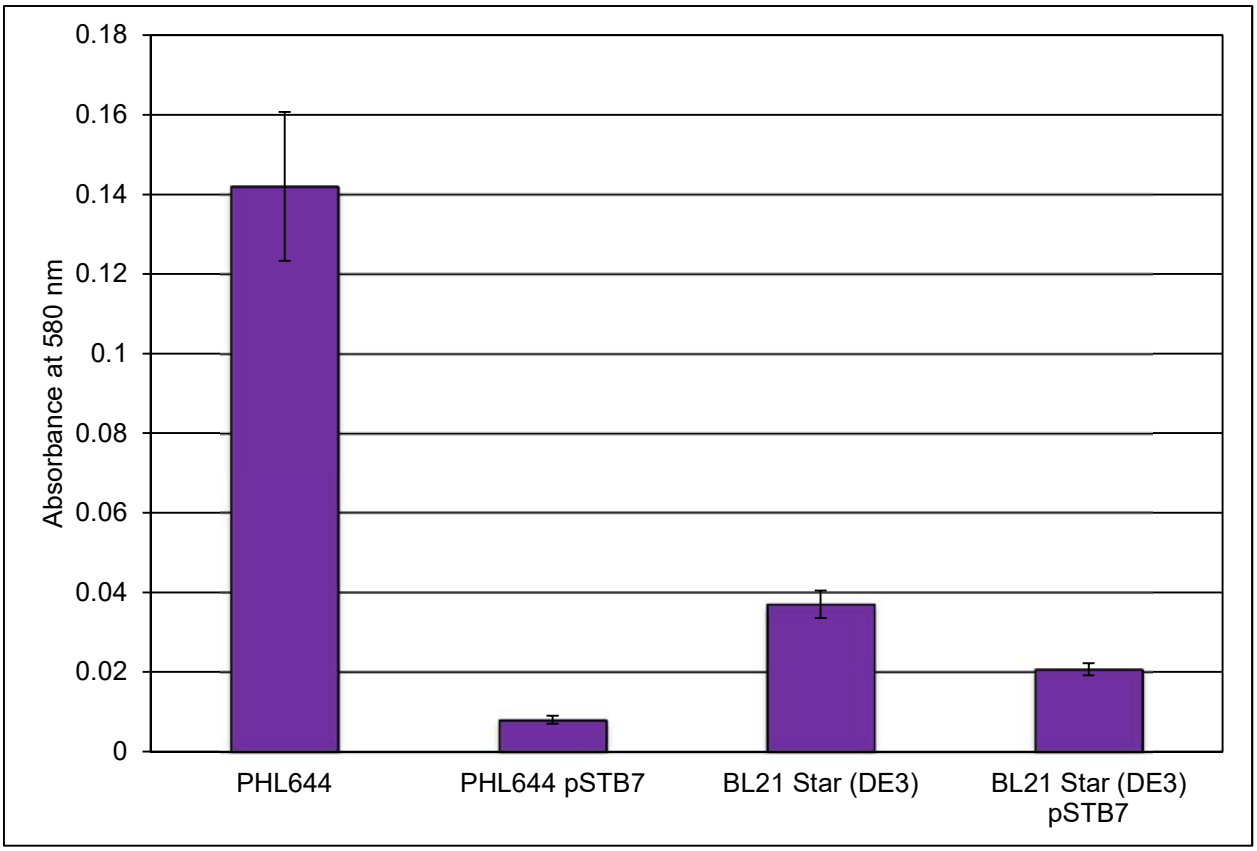

Figure 5.5: *Graph of crystal violet retention for PHL644, BL21 Star (DE3) and their pSTB7-transformed variants. Error bars represent 1 standard deviation from the mean of three independent cultures. Biofilms were grown using the Duran Bottle method.*

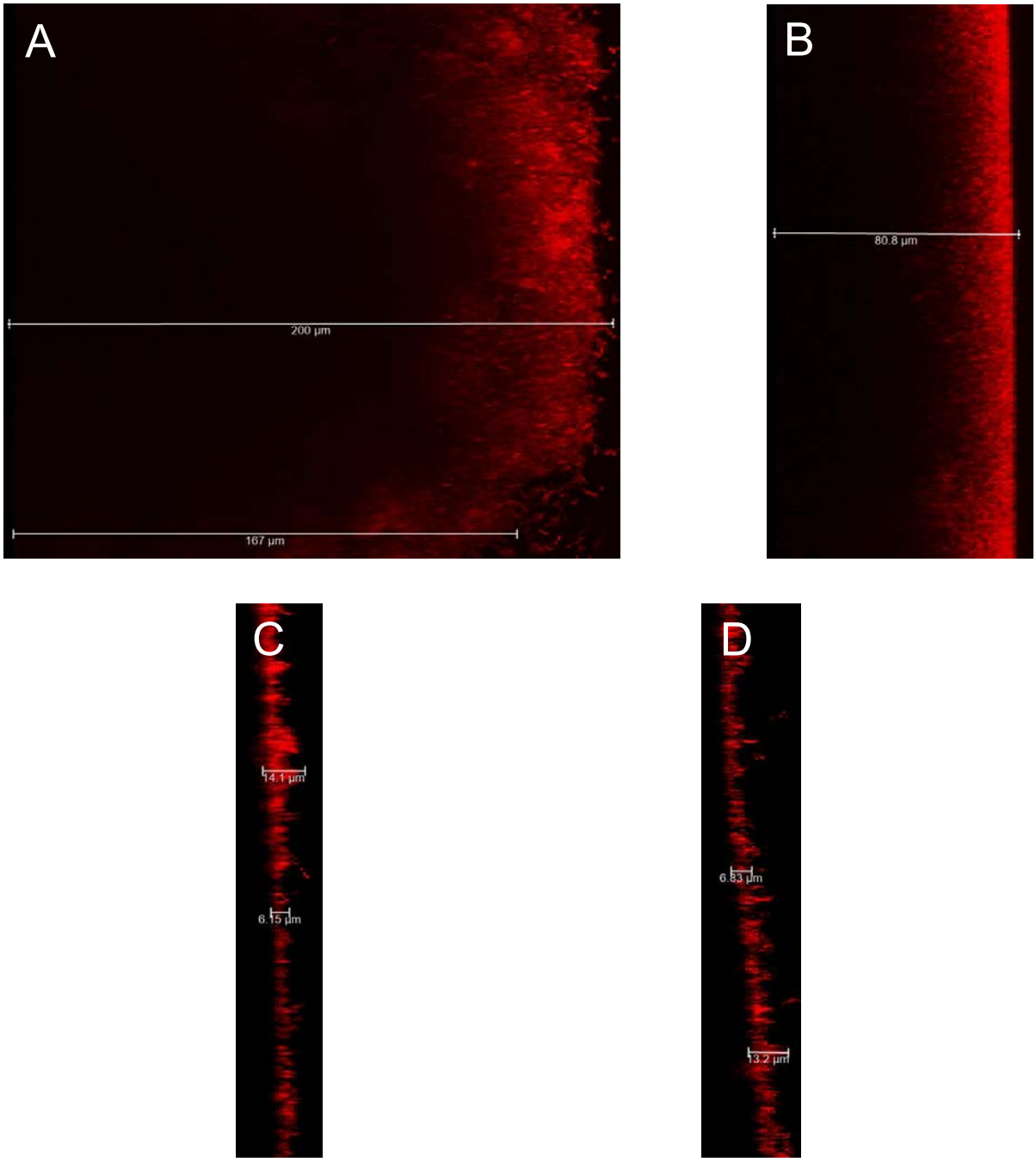

Figure 5.6a: *Representative side-view CLSM images of PHL644 pSTB7 and BL21 Star (DE3) pSTB7 biofilms and their untransformed counterparts. Biofilms were grown using the Duran Bottle method. A – PHL644 biofilm. B – BL21 Star (DE3) biofilm. C – PHL644 pSTB7 biofilm. D – BL21 Star (DE3) biofilm. In all images, the base of the biofilm is on the left.*

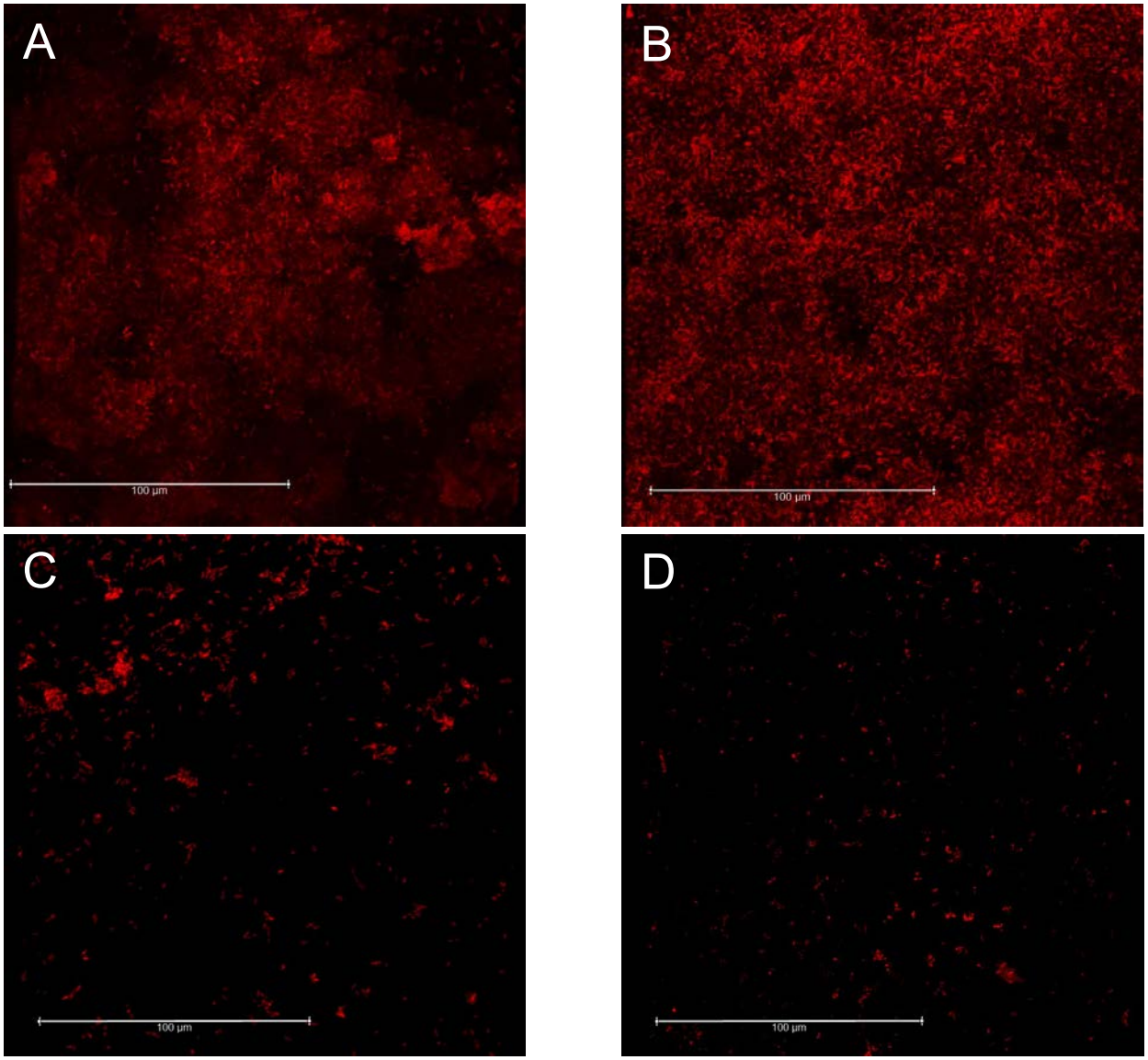

Figure 5.6b: *Representative top-down-view CLSM images of PHL644 pSTB7 and BL21 Star (DE3) pSTB7 biofilms and their untransformed counterparts. Biofilms were grown using the Duran Bottle method. A – PHL644 biofilm. B – BL21 Star (DE3) biofilm. C – PHL644 pSTB7 biofilm. D – BL21 Star (DE3) pSTB7 biofilm.*

5.1.5 Discussion

As previously stated (Section 1.4.8), the production of indole from tryptophan is of extreme importance to the *E. coli* cell in both normal cell function and biofilm development, and plays a major role in the progression into stationary phase at 30°C, but to a lesser extent at 37°C (Hu M *et al*., 2011, Gaimster H & Summers D, 2015, Lee J *et al*., 2008). Constitutive overexpression of recombinant TrpBA from pSTB7 likely prevents the accumulation of indole at the onset of stationary phase by converting indole back into tryptophan, presumably at a higher rate than the native TnaA-mediated reverse reaction can function. Indole accumulation has been shown to have wide effects on metabolism, motility, biofilm formation and general multicellular activities (Hu M *et al*., 2011, Lee J *et al*., 2008). pSTB7 may block these effects, likely explaining both a lack of biofilm growth on PTFE, as well as a lack of colony-forming ability on agar at 30°C. At 37°C, the quorum sensing molecule AI-2 has a greater effect than indole on a similar subset of genes and likely permits biofilm or colony growth (Lee J *et al*., 2008). This data gives the tentative suggestion that indole operates similarly to a quorum sensing molecule at 30°C, in a comparable manner to AI-2 at 37°C, and is not, as has been suggested, merely a metabolic byproduct (Kim J & Park W, 2015, Hu M *et al*., 2010). Further research, such as direct quantification of intracellular and extracellular indole levels, is required before this can be established, but this may indicate a discrepancy between *E. coli* biofilm research conducted at different temperatures.

As shown by reporter gene studies, the *csgBAC* promoter is activated in PHL644 pJLC-T pSTB7 and BL21 Star (DE3) pJLC-T pSTB7 during the 24 hour experiment, but with a severely reduced transcription level indicating a negative effect on biofilm formation. This again can likely be explained by a disrupted intracellular indole concentration. Indole is required for the activation of Crl, which shifts the sigma factor preference of RNA polymerase

from σ^D to σ^S, and leads to increased curli production during stationary phase (Section 1.4.8) (Lelong C *et al*., 2007). A reduction in intracellular indole could therefore prevent this response, suggesting that pSTB7 reduces surface attachment by reducing transcription from the *csgBAC* promoter. As before, direct determination of indole concentrations would be key to proving this theory, as well as directly linking this to the Crl protein.

In conclusion, it was decided that pSTB7 and the tryptophan synthase reaction were unsuitable for use in testing the biofilm biocatalyst, as even the most basic requirement, the formation of a biofilm, was not possible. Moving forward, it may be more beneficial to clone the TrpBA sequence into an inducible plasmid, instead of the constitutive pSTB7, thereby preventing the overexpression of TrpBA before it is required for biocatalysis. However, leaky expression may still lead to some of the same effects seen in this study.

5.1.6 Comparison to Previous Work (Tsoligkas A *et al*., 2011)

As noted, the starting point for this work was the data presented in Tsoligkas A *et al*. (2011) which successfully produced a biofilm biocatalyst capable of performing the tryptophan synthase reaction. To reiterate the methodology developed by Tsoligkas, this biofilm biocatalyst was created by growing PHL644 pSTB7 in half-strength LB until an OD_{600} of 2 was reached. The culture was then transferred into a large centrifuge bottle with a poly-L-lysine-coated glass microscope slide set on the bottom. By centrifuging the bottle at 1851 g for 10 minutes, the cells were 'spin-coated' onto the slide, thereby creating an artificially-immobilised population of PHL644 pSTB7 on the surface associated with the positively-charged poly-L-lysine. The slide was then removed from the centrifuge bottle and transferred to a 500 mL conical flask (flat on the bottom of the flask) containing M63 medium supplemented with 17 mM potassium succinate, 10 mM glucose and 100 µg/mL ampicillin.

The flasks containing the spin-coated biofilm biocatalyst were incubated at 70 RPM and 30°C for 7 days, during which time the biofilm matured and produced EPS. The spin-coated biofilm biocatalyst was then used in biocatalysis assays. This protocol was subsequently used by Perni S *et al*., (2013).

Despite efforts by researchers in this lab, it was not possible to effectively replicate these results and develop a substantial biofilm. Biofilms created using this method were typically poorly adhered to the slide surface, and the act of removing the slide from the M63 culturing medium often led to almost complete removal of visible biofilm. What biofilm could be imaged by CLSM was very thin (<20 μm) with little developed 3D structure. Possible explanations for these observations compared to the work of Tsoligkas include uncontrollable variations in purchased chemical batches, different water purification methods or possibly different equipment such as glassware. However, the ubiquity of these issues in research settings suggest that it may be very difficult to reproduce the data reported by Tsoligkas A *et al*. (2011).

The results presented in Section 5.1 of this thesis show that pSTB7 was detrimental to planktonic growth and biofilm formation in M63 medium in both PHL644 and BL21 Star (DE3), which stands in contrast to the biofilms observed in Tsoligkas A *et al*. (2011). However, atomic force microscopy data (AFM) shown in Tsoligkas A *et al*. (2011) and Tsoligkas A *et al*. (2012) indicates little biofilm growth until the 5th day of the 7 day maturation, and then a rapid increase between 5 and 6 days, suggesting that biofilm growth was ‘triggered’ during this period. Additionally, the antibiotic used to maintain the pSTB7 plasmid was ampicillin which can be rendered ineffective in under 24 hours on agar plates, due to the secretion of β-lactamase enzymes, leading to the formation of satellite colonies. To hypothesise, when the bacteria were first spin-coated onto the slide, they were inhibited

in terms of biofilm growth by the presence of pSTB7, maintained by the necessity for ampicillin resistance. When the ampicillin in the M63 medium became ineffective, pSTB7 would then be gradually lost over a period of several days due to the lack of antibiotic selective pressure. Once the detrimental actions of pSTB7 were lost by at least some members of the population, a biofilm could then be formed by PHL644 cells lacking pSTB7, thereby leading to the AFM results noted in Tsoligkas A *et al*. (2011). This may explain why biofilm growth was reduced in the 3 days of growth used in this study. The fact that the biofilm was able to perform biocatalysis suggests that some of the cells still contained pSTB7; embedded in the biofilm but able to take up 5-chloroindole and release 5-chloro-L-tryptophan.

In spite of this hypothesis, there were multiple differences between the methodologies employed in Tsoligkas *et al*. (2011) compared to this work which may have led to the conflicting observations seen in these data. Tsoligkas *et al*. (2011) created spin-coated biofilms on poly-L-lysine-coated glass slides in contrast to naturally-formed biofilms on PTFE. Ampicillin was employed throughout their experiments, whereas carbenicillin (which is less easily broken down than ampicillin) was substituted at the overnight growth phase and omitted from the biofilm growth medium in this data. Half-strength LB was used for overnight cultures instead of full strength LB. Lastly, the biofilms presented in Tsoligkas A *et al*. (2011) were matured for 7 days instead of 3 days. Nevertheless, the natural biofilm biocatalysts presented in this thesis were able to successfully create a substantial biofilm in all cases (as will be shown in Sections 5.2 and 5.3) except with pSTB7, indicating a significant issue with pSTB7 in facilitating a biocatalysis reaction. It should be noted that the planktonic growth issues noted in this work were not reported (or perhaps not investigated) in Tsoligkas A *et al*. (2011), which used half-strength LB as an overnight culturing medium.

It may therefore be of benefit to explore the effect of different media on pSTB7-transformed *E. coli* cells, as another medium may suppress the negative effects of pSTB7 on growth and biofilm formation, allowing the growth of a biofilm in similar conditions.
The feasibility of future experiments using pSTB7 in an *E. coli* biofilm biocatalyst is therefore unclear. This issue will be discussed in Section 6.3.

5.2 Formation of 7-chloro-L-tryptophan using Tryptophan Halogenase (PrnA)

Halogenation is used in many bacterial species to create a wide variety of complex secondary metabolites such as antibiotics (Latham J *et al*., 2017). Productive halogenation requires that the halogen group be added at a specific point on the target molecule. Chemical synthesis may halogenate several non-specific points on a molecule, thereby reducing the functionality of the product (Latham J *et al*., 2017). Enzymatic production is thus preferred. In *Lechevalieria aerocologines*, the halogenase RebH converts L-tryptophan into 7-chloro-L-tryptophan which is a precursor for the production of an antibiotic termed Rebeccamycin (Yeh E *et al*., 2005). Despite its use by the bacterium as an antibiotic, Rebeccamycin has shown promise as an anti-cancer drug in humans, and the production of high-purity, high-yield 7-chloro-L-tryptophan is desired in pharmaceutical settings. In *Pseudomonas fluorescens*, the halogenase PrnA performs an identical reaction, producing 7-chloro-L-tryptophan for the synthesis of pyrrolnitrin, an antifungal compound (Keller S *et al*., 2000). Halogenation performed by RebH and PrnA requires L-tryptophan and NaCl and is dependent on $FADH_2$ and oxygen (Dong C *et al*., 2005) (Figure 5.7). Enzymatic formation of 7-chloro-L-tryptophan not only ensures specific halogenation of the 7-position of L-

tryptophan, but also retains the chiral identity of the L-tryptophan molecule, thereby ensuring product specificity.

In these experiments, *Pseudomonas fluorescens* PrnA was expressed from the vector pSG22, under the control of a pT7lac promoter. Plasmids featuring pT7 and pT7lac promoters are generally expressed in strains containing the DE3 insert, such as BL21(DE3) and BL21 Star (DE3), which produce the T7 RNA polymerase. However, these plasmids often exhibit non-induced expression of proteins due to non-specific interaction with the T7 promoter by native RNA polymerase. As such, it was theorised that PHL644 would still produce a low level of PrnA despite not featuring a DE3 insert and the T7 polymerase.

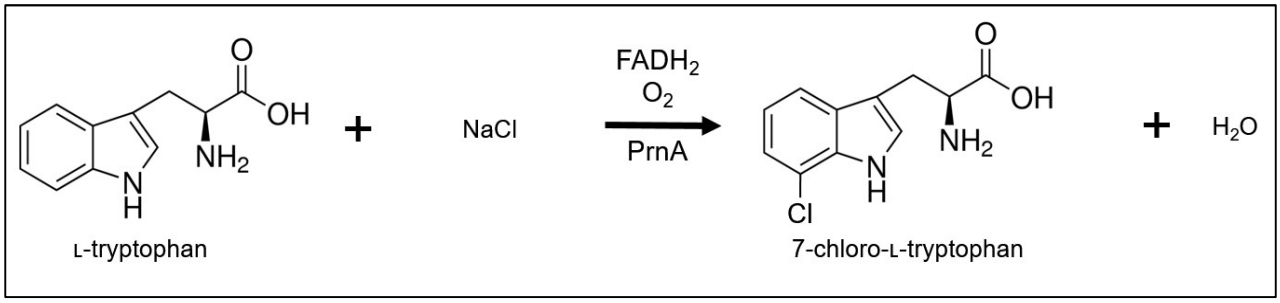

Figure 5.7: *Formation of 7-chloro-L-tryptophan from L-tryptophan by PrnA.*

5.2.1 Effect of pSG22 on Planktonic Growth Rate

pSG22 was transformed into *E. coli* PHL644 and BL21 Star (DE3) using project standard methods (Section 2.1.4). It should be noted that transformants containing pSG22 grew normally on agar plates at 30°C unlike pSTB7, indicating that the pSG22 plasmid did not have an observable effect on colony growth at this temperature.

PHL644 pSG22 and BL21 Star (DE3) pSG22, and their untransformed variants, were grown in 100 mL Duran bottles in 70 mL of M63+ at 30°C and 70 RPM for 24 hours. 100 µM IPTG

was added to both cultures to induce transcription of PrnA from pSG22 and to ensure a fair test between the cultures, despite the fact that IPTG would not affect induction in PHL644. OD was measured at 600 nm using a spectrophotometer every 2 hours.

As compared to untransformed PHL644 and BL21 Star (DE3), pSG22 extended the lag-growth phase of both strains. (Figure 5.8). PHL644 reached a maximal OD_{600} of 1.18 after 24 hours, which was reduced to 0.94 by pSG22. Maximal OD_{600} of BL21 Star (DE3) reached 1.41 after 24 hours, which was reduced to 0.77 by pSG22, a reduction of nearly half. This indicates that the presence of pSG22 has a slight negative effect on the lag-phase growth of both strains, likely due to plasmid maintenance, or expression of PrnA. This effect is common in RPP, as the production of recombinant proteins consumes resources needed for growth mechanisms. Nevertheless, the growth rate becomes very similar to untransformed strains after 18 hours, indicating that the effect of pSG22 is markedly less pronounced than that of pSTB7.

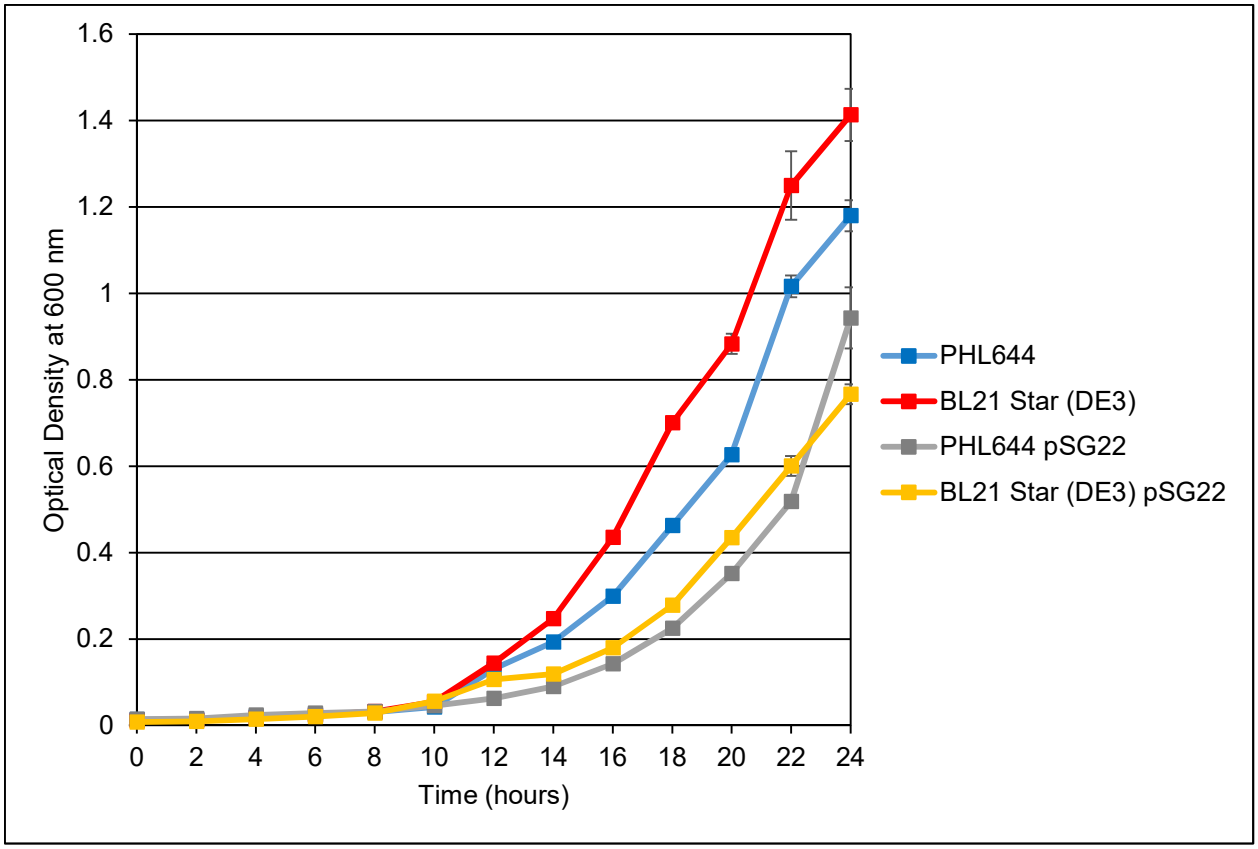

Figure 5.8: *Growth curves for PHL644, BL21 Star (DE3), and their pSG22-transformed variants. Error bars represent 1 standard deviation from the mean of three independent cultures.*

5.2.2 Effect of pSG22 on *csgBAC* Promoter Activity

E. coli PHL644 and BL21 Star (DE3) were sequentially transformed with pJLC-T and pSG22 to determine the effect of pSG22 on curli gene regulation. These were compared against PHL644 pJLC-T and BL21 Star (DE3) pJLC-T. Cells were grown in 100 mL Duran bottles with 70 mL M63+ at 30°C and 70 RPM for 24 hours. 100 µM IPTG was added as before to induce PrnA production. 100 µL samples were taken every 2 hours, and diluted as necessary in PBS for analysis using an Accuri C6 flow cytometer.

PHL644 pJLC-T pSG22 exhibited an extremely similar pattern of green fluorescence to PHL644 pJLC-T, indicating that the presence of pSG22 did not have any strong effect on

curli gene expression (Figure 5.9). BL21 Star (DE3) pJLC-T pSG22 green fluorescence significantly exceeded (more than 1 standard deviation) BL21 Star (DE3) pJLC-T between 4 and 8 hours, and also between 18 and 22 hours. This suggests that pSG22 has a slight positive effect on curli gene expression, although inconsistent, potentially due to the activation of stress genes due to the overexpression of PrnA. However, pSG22 does not have a noticeably detrimental effect on curli gene expression in either strain.

In Figure 5.10, BL21 Star (DE3) pJLC-T pSG22 displayed a severely reduced initial GFP-positive population of 34% at 0 hours, compared to BL21 Star (DE3) pJLC-T at 81%. However, this level quickly rose to match BL21 Star (DE3) pJLC-T after 6 hours and maintained a similar GFP-positive population afterwards. Explanations for this effect may include the presence of carbenicillin in the overnight cultures, which may have a detrimental effect on curli gene expression; quickly eliminated when the cells are transferred into M63+ without antibiotic. This also mirrors effects seen for other *bla* plasmids in in this work (Section 4.2). Interestingly, the same effect is not seen for PHL644 pJLC-T pSG22, which exhibits an initial green-positive population of 88%, exceeding the 61% for PHL644 pJLC-T. However, the levels become extremely similar after 8 hours. The discrepancy between PHL644 and BL21 Star (DE3) may highlight the differences in biofilm regulation between the strains. Nevertheless, in all cases the activated population percentages rise above 90% after 8 hours indicating a strong activation of curli genes within the population and that pSG22 had no appreciable negative effect after this point.

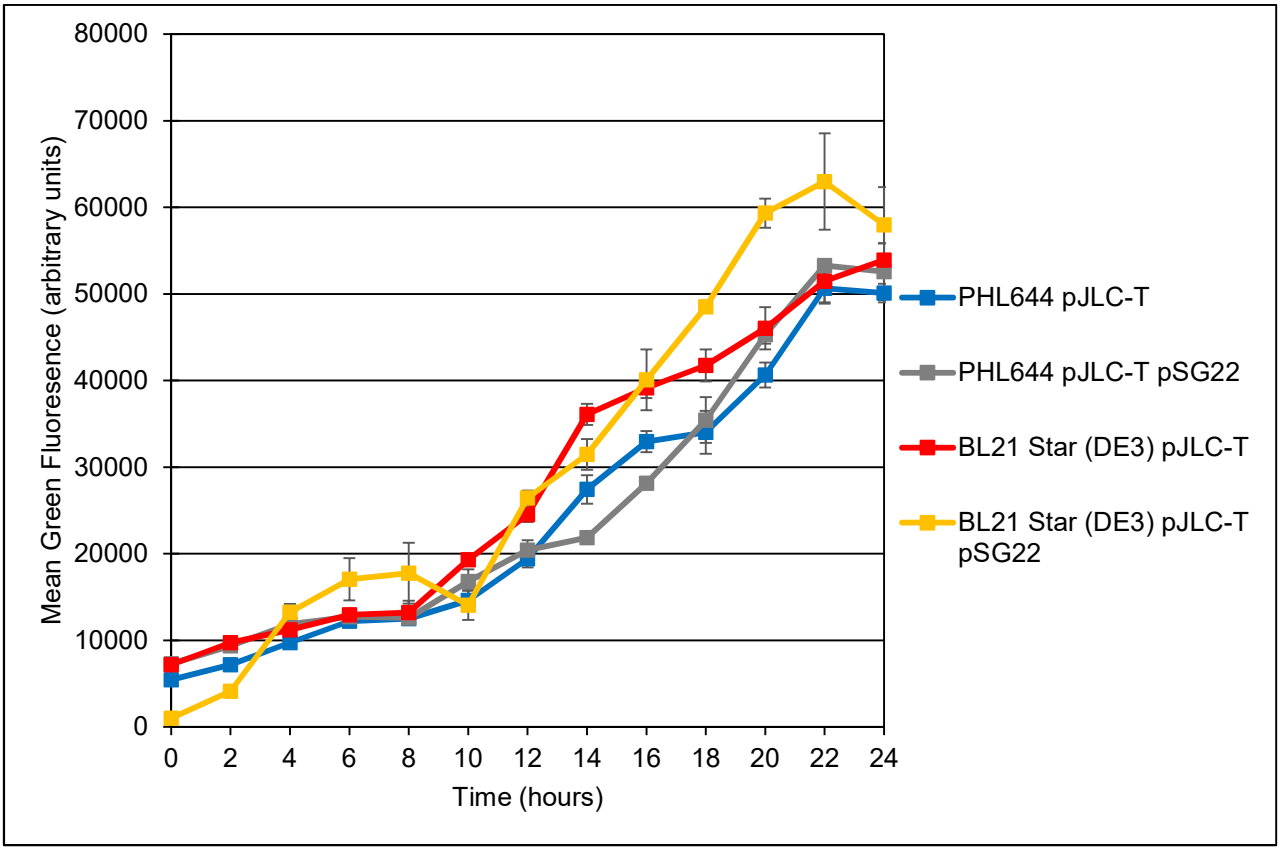

Figure 5.9: *Mean green fluorescence for PHL644 pJLC-T, BL21 Star (DE3) pJLC-T and their pSG22-transformed variants. Error bars represent 1 standard deviation from the mean of three independent cultures.*

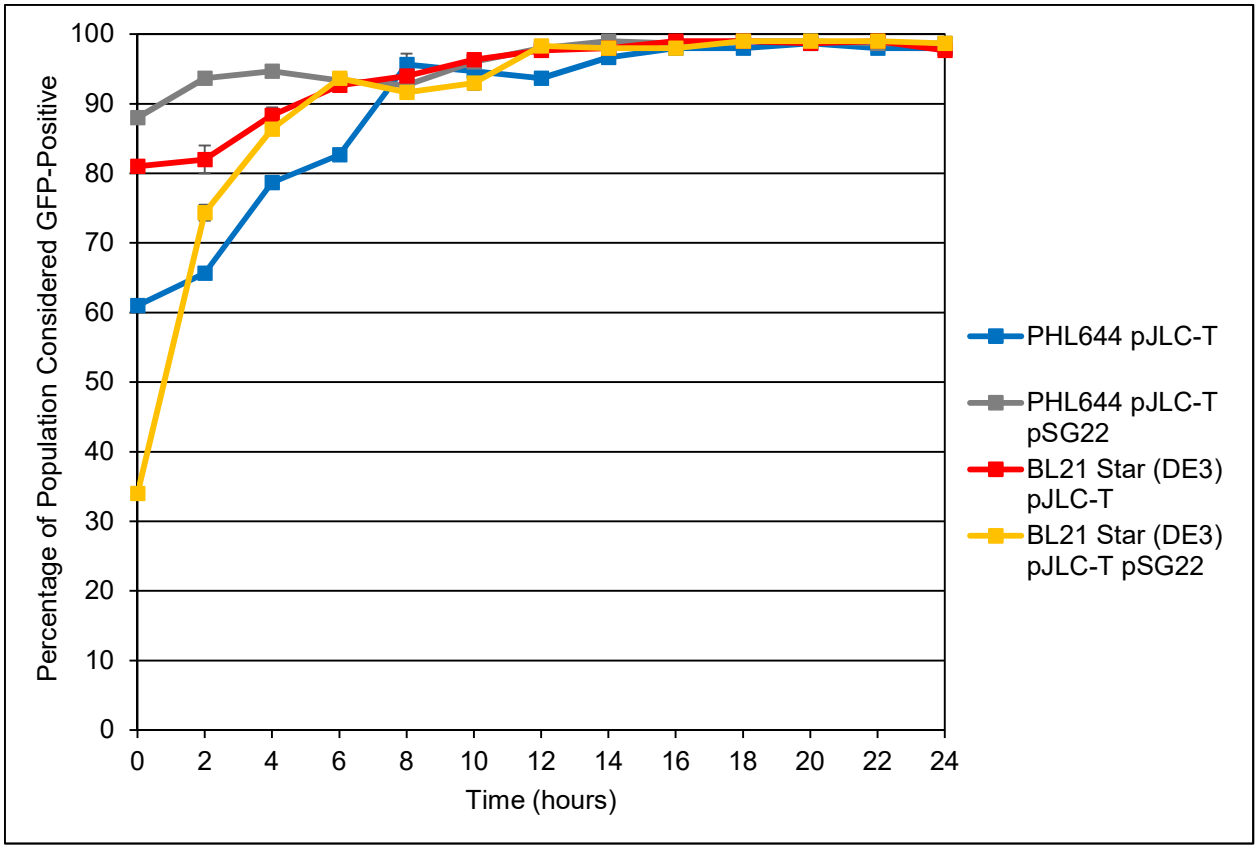

Figure 5.10: *Percentage of cells considered GFP-positive for PHL644 pJLC-T, BL21 Star (DE3) pJLC-T and their pSG22-transformed variants. Error bars represent 1 standard deviation from the mean of three independent cultures.*

5.2.3 Effect of pSG22 on Biofilm Formation

E. coli PHL644 pSG22 and BL21 Star (DE3) pSG22 were analysed for biofilm formation ability and compared to their untransformed variants. Biofilms were grown under standard conditions (with 100 µM IPTG) for 3 days on PTFE-wrapped slides and analysed using CV staining and CLSM.

As shown by Figure 5.11, PHL644 pSG22 and PHL644 biofilms exhibited an extremely similar CV retention (within 1 standard deviation) with an A_{580} of approximately 0.142, indicating that pSG22 had no significant effect on biofilm formation in PHL644. BL21 Star

(DE3) pSG22 biofilm formation was slightly reduced compared to BL21 Star (DE3), although not to the extent of pSTB7. Again, this was likely due to the metabolic burden of PrnA overexpression. Unlike pSTB7, pSG22 did not have exceptionally detrimental effects on either PHL644 or BL21 Star (DE3), and was thus considered suitable for testing in a biocatalytic biofilm.

As shown by CLSM images (Figure 5.12), pSG22 did not affect the structure of PHL644 and BL21 Star (DE3) biofilms to any great extent, displaying defined thick 3D structures which showed little difference to untransformed variants. Interestingly, BL21 Star (DE3) pSG22 developed more mushroom-shaped structures than the untransformed strain suggesting a possible direct effect. However, this did not appear to be detrimental to biofilm formation. This further indicates that pSG22 has little effect on *E. coli* biofilm formation.

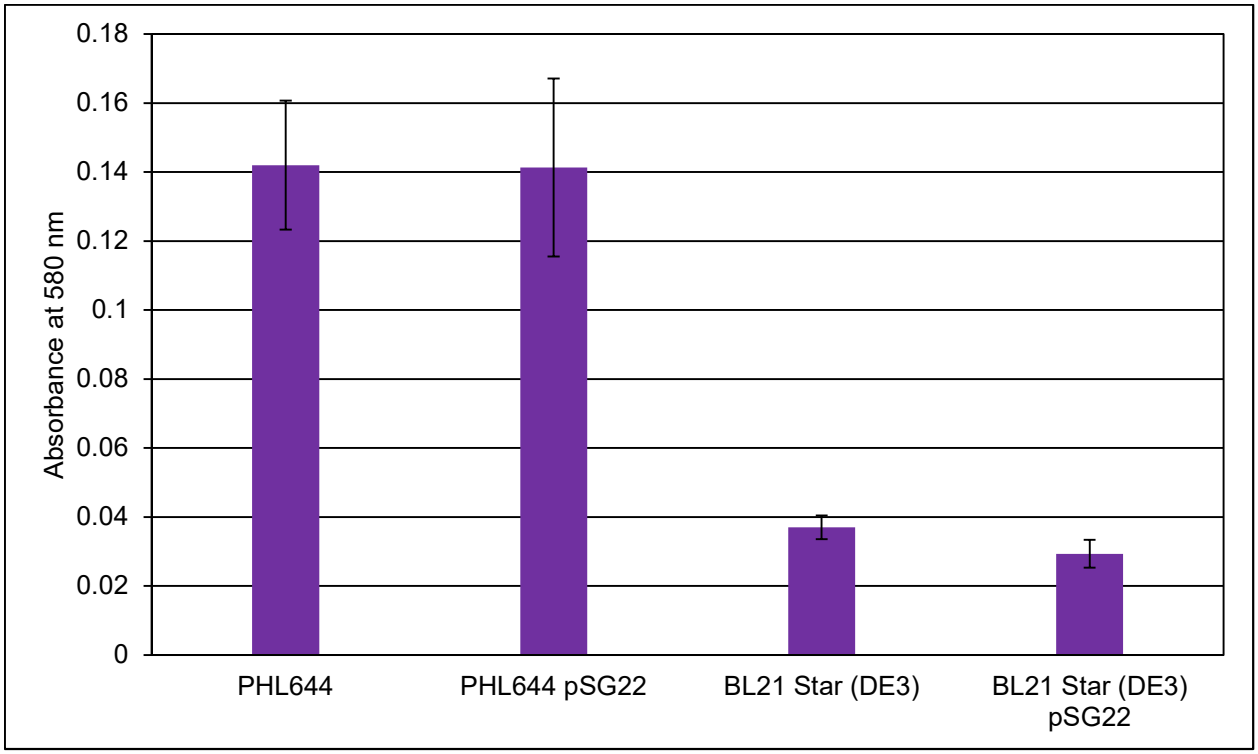

Figure 5.11: *Graph of crystal violet retention for PHL644, BL21 Star (DE3) and their pSG22-transformed variants. Error bars represent 1 standard deviation from the mean of three independent cultures.*

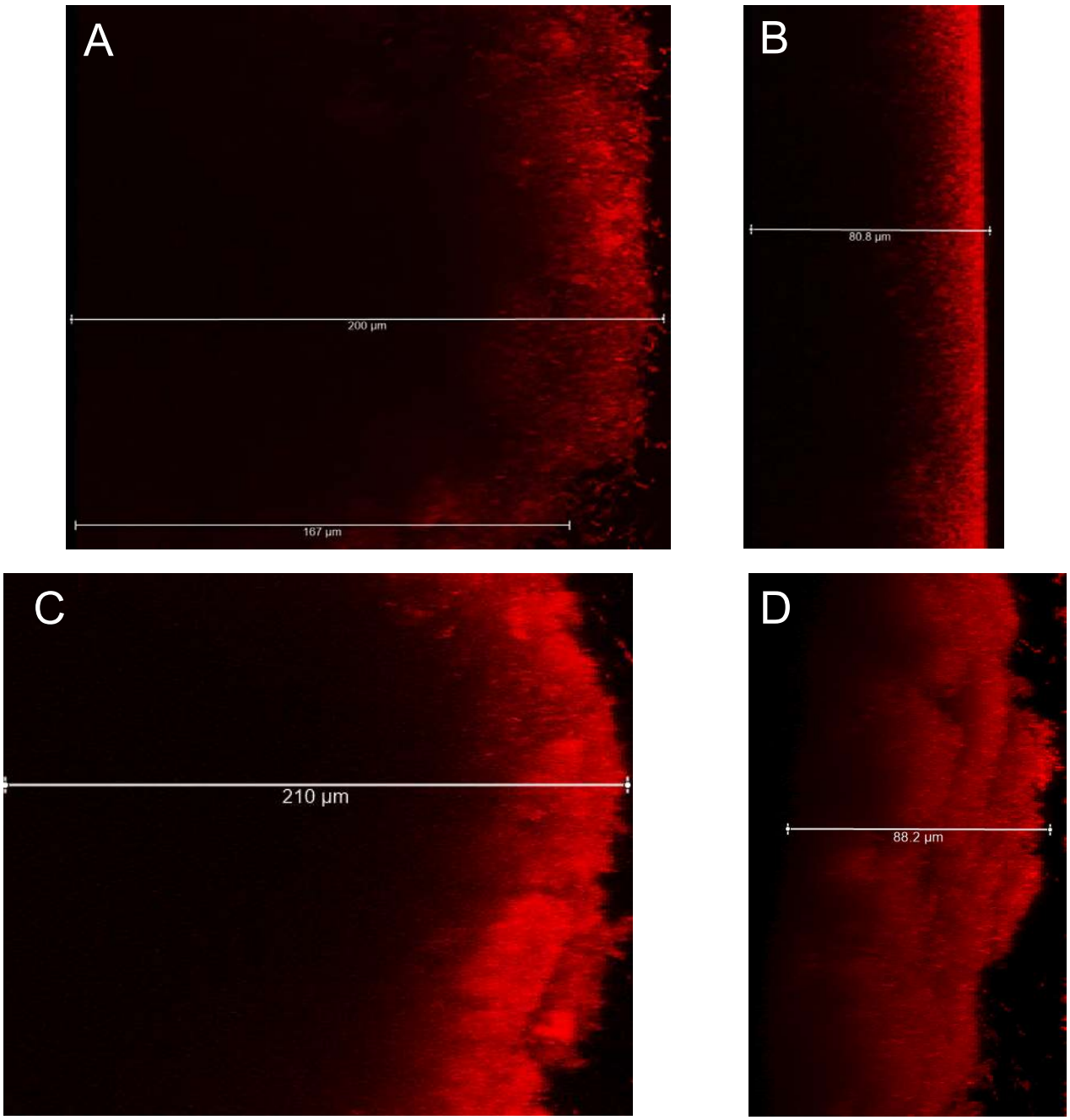

Figure 5.12a: *Representative side-view CLSM images of PHL644 pSG22 and BL21 Star (DE3) pSG22 biofilms and their untransformed counterparts. Biofilms were grown using the Duran Bottle method. A – PHL644 biofilm. B – BL21 Star (DE3) biofilm. C – PHL644 pSG22 biofilm. D – BL21 Star (DE3) pSG22. In all images, the base of the biofilm is on the left.*

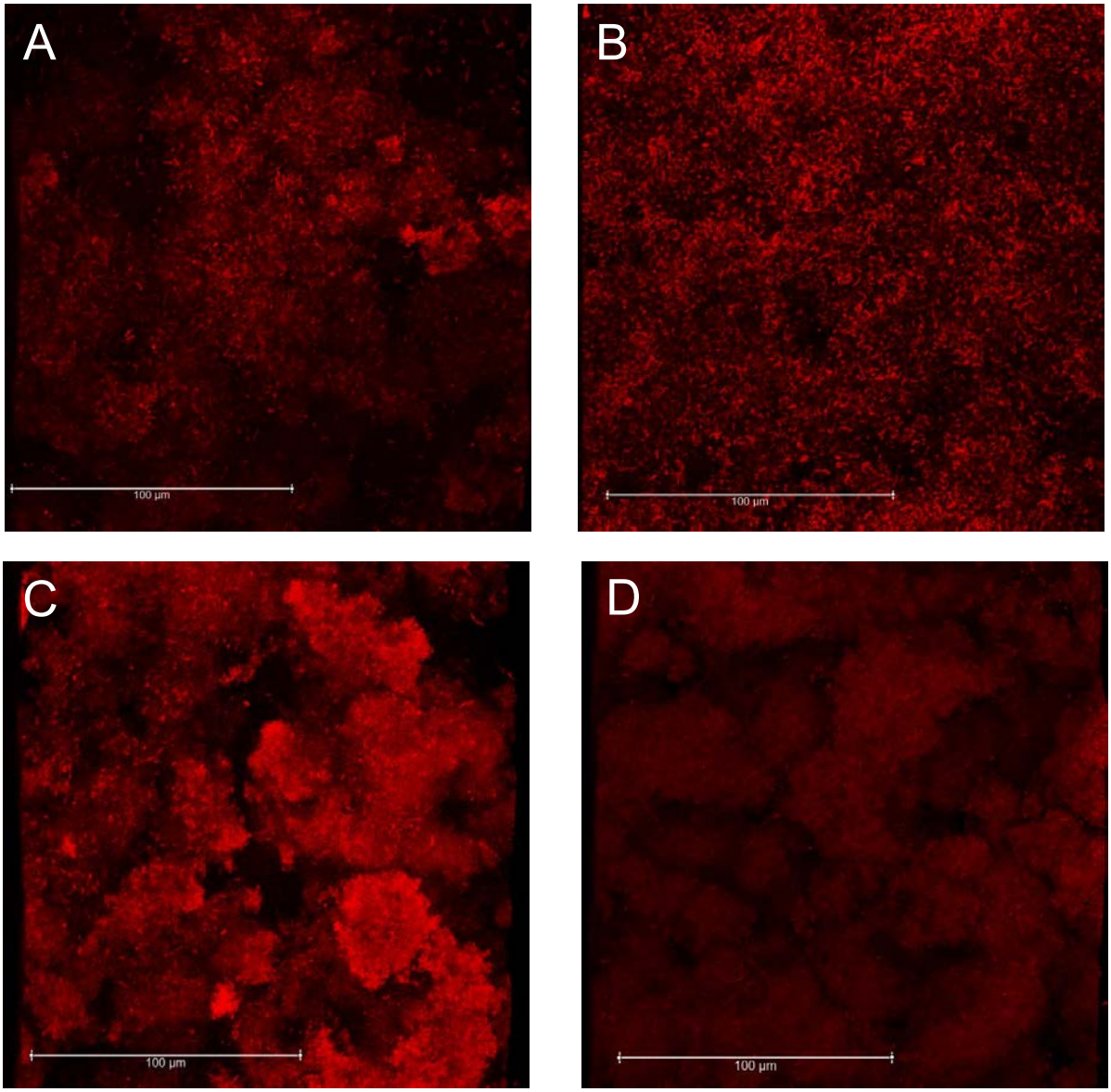

Figure 5.12b: *Representative top-down-view CLSM images of PHL644 pSG22 and BL21 Star (DE3) pSG22 biofilms and their untransformed counterparts. Biofilms were grown using the Duran Bottle method. A – PHL644 biofilm. B – BL21 Star (DE3) biofilm. C – PHL644 pSG22 biofilm. D – BL21 Star (DE3) pSG22.*

5.2.4 Formation of 7-chloro-L-tryptophan by pSG22 in Planktonic *E. coli* Cells

Biocatalysis experiments were initially performed in planktonic cells to allow comparisons to be made to biofilm cells. *E. coli* PHL644 pSG22 and BL21 Star (DE3) pSG22 were grown in 100 mL Duran bottles in M63+ at 30°C and 70 RPM for 3 days (with 100 µM IPTG). Cultures were then centrifuged, washed with PBS, centrifuged again, then resuspended in reaction buffer and adjusted to an OD_{600} of 1. The reaction buffer for this experiment contained 100 mM KH_2PO_4, 20 mM NaCl, 2 mM L-tryptophan and was adjusted to pH7. The resuspensions were inserted into clean, sterile 100 mL Duran bottles. Reactions were performed at 30°C and 70 RPM for 24 hours. 500 µL samples were taken every 2 hours for 0-8hrs and then at 24hrs. Samples were filtered (0.22 µm) before transfer to glass HPLC tubes and stored at 4°C until analysed.

HPLC was performed as noted in Section 2.4.1.2. The concentration of L-tryptophan and 7-chloro-L-tryptophan present in the samples was measured, as these were the reactant and desired product respectively. However, it was deemed prudent to also note the levels of indole and 7-chloroindole in the samples, due to the preference of *E. coli* to degrade L-tryptophan, and potentially 7-chloro-L-tryptophan, into indole or 7-chloroindole (Li G & Young KD, 2013). Calibration charts were made for L-tryptophan, indole and 7-chloroindole (Section 2.4.1.3). The three chemicals produced three distinct peaks on the chromatographs. 7-chloro-L-tryptophan could not be obtained for calibration due to its cost, but it was theorised that the product would produce a unique peak on the chromatograph that would be distinct from the other chemicals.

Although 2 mM tryptophan was added to the reaction buffer, only approximately 1.67 mM could be detected in the final buffer after filtration. This was assumed to be due to loss during

filtration. All initial concentrations of tryptophan in samples were therefore adjusted to be 1.67 mM.

In all samples (pSG22-containing and untransformed), no peaks could be determined for 7-chloroindole and no additional peaks appeared which could not be attributed to compounds in the reaction buffer. It was concluded that halogenation did not occur during the experiments. Peaks were quantified for L-tryptophan and indole (Figure 5.13). In all cultures, over the 24 hour course of the experiment, all measurable L-tryptophan was consumed. After 8 hours, more than 50% of the added L-tryptophan was consumed by the cells. Of the four cultures, BL21 Star (DE3) pSG22 consumed L-tryptophan most quickly, followed by untransformed BL21 Star (DE3). After 24 hours, in all cultures most of the L-tryptophan was converted into indole (62%). As initial indole concentrations were 0 mM in all samples, it can be inferred that all indole production was a direct result of L-tryptophan degradation, as no other carbon source was present in the buffer for *de novo* synthesis of either compound. It is likely that any L-tryptophan unaccounted for (38%) was consumed by the cells for other cellular processes such as protein synthesis. In all cultures, the level of indole produced by the cells was extremely similar, between 1.03 and 1.06 mM. The similarity may indicate that these strains reached a 'maximum' concentration of extracellular indole which they could survive in and feedback mechanisms prevented this level from rising. Additional experiments to modulate the concentration of tryptophan would prove this, but these results complement previous studies performed under similar conditions (Li G & Young KD, 2013).

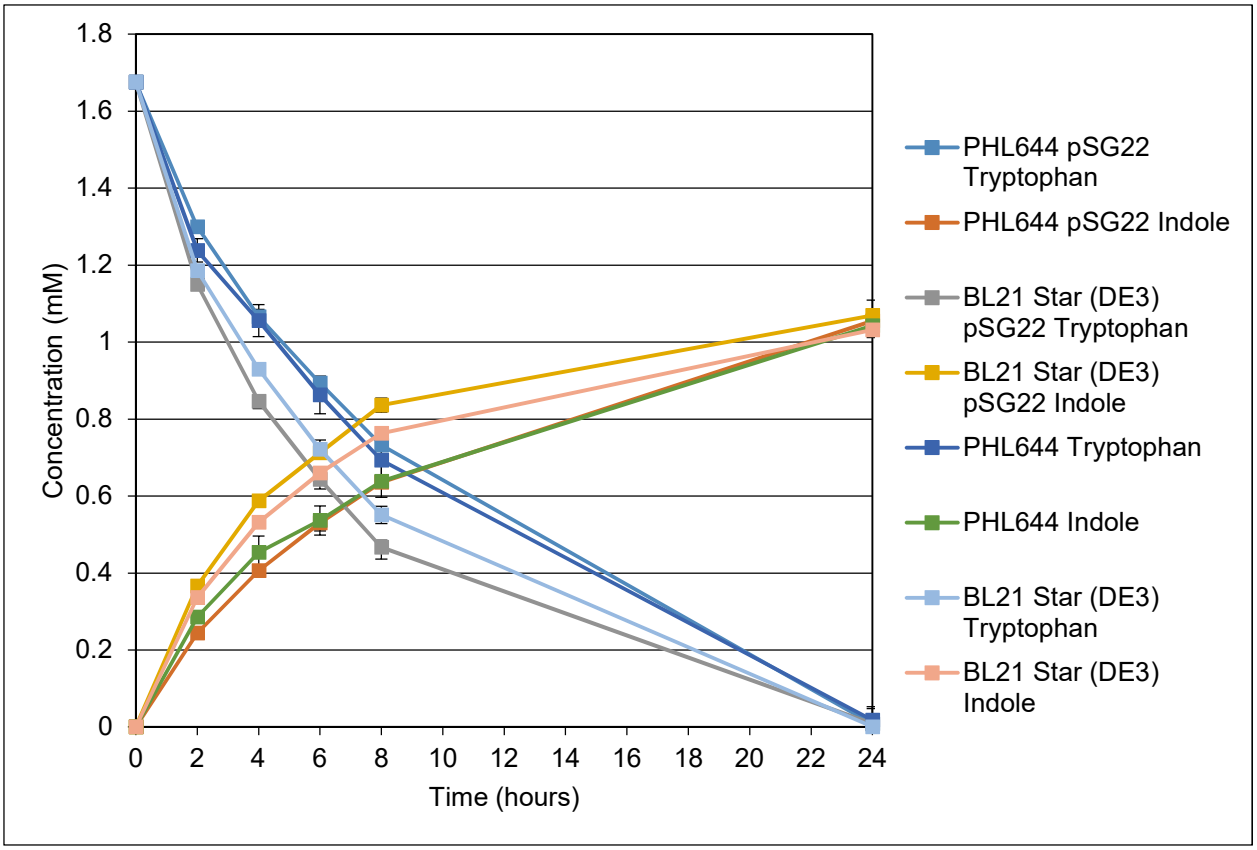

Figure 5.13: *Consumption of tryptophan and synthesis of indole by planktonic PHL644, BL21 Star (DE3) and their pSG22-transformed variants in halogenation buffer. Error bars represent 1 standard deviation from the mean of three independent cultures.*

While it was unsurprising that planktonic *E. coli* would rapidly consume L-tryptophan in the buffer, it was surprising that no halogenated products could be detected in the samples. The reasons for this will be theorised in Section 5.2.6. Despite these negative results, it was hoped that biofilm cells would provide a better outcome due to a reduced metabolic need and thus may not consume tryptophan so rapidly, permitting halogenation.

5.2.5 Formation of 7-chloro-L-tryptophan by pSG22 in *E. coli* Biofilm

Biofilm experiments were performed in much the same way as planktonic experiments to ensure fair testing. *E. coli* PHL644 pSG22 and BL21 Star (DE3) pSG22 were grown in 100 mL Duran bottles in M63+ at 30°C and 70 RPM for 3 days (with 100 µM IPTG). A PTFE-wrapped slide was inserted to provide a surface for biofilm formation. The PTFE-wrapped slide was then removed, washed twice by submersion in PBS, then inserted into a clean sterile 100 mL Duran bottle containing the previously described reaction buffer. Reactions were performed at 30°C and 70 RPM for 24 hours. 500 µL samples were taken every 2 hours for 0-8hrs and then at 24hrs. Samples were filtered (0.22 µm) before transfer to glass HPLC tubes. As before, loss of L-tryptophan was noted after filtration. Initial L-tryptophan concentration in these experiments was therefore quantified as 1.78 mM.

As with the planktonic cultures, no halogenated products could be determined in the samples, indicating that no 7-chloro-L-tryptophan was produced (Figure 5.14). Strikingly, although L-tryptophan and indole could be quantified in the samples, their concentrations changed very little over the course of the experiment, suggesting that very little of either chemical was consumed or produced. After 24 hours, the concentration of L-tryptophan had decreased from 1.78 mM to 1.66 mM in all cases, while the concentration of indole had increased from 0 mM to 0.055 mM. This indicates that 0.12 mM L-tryptophan was consumed during the experiments, and 46% of this was converted into indole, far less than was converted by planktonic cells. Untransformed BL21 Star (DE3) biofilms were omitted from the graphs due to an issue with the HPLC analysis which could not be rectified due to time constraints. Despite this, it is most likely that BL21 Star (DE3) samples would have followed the patterns of the other experiments.

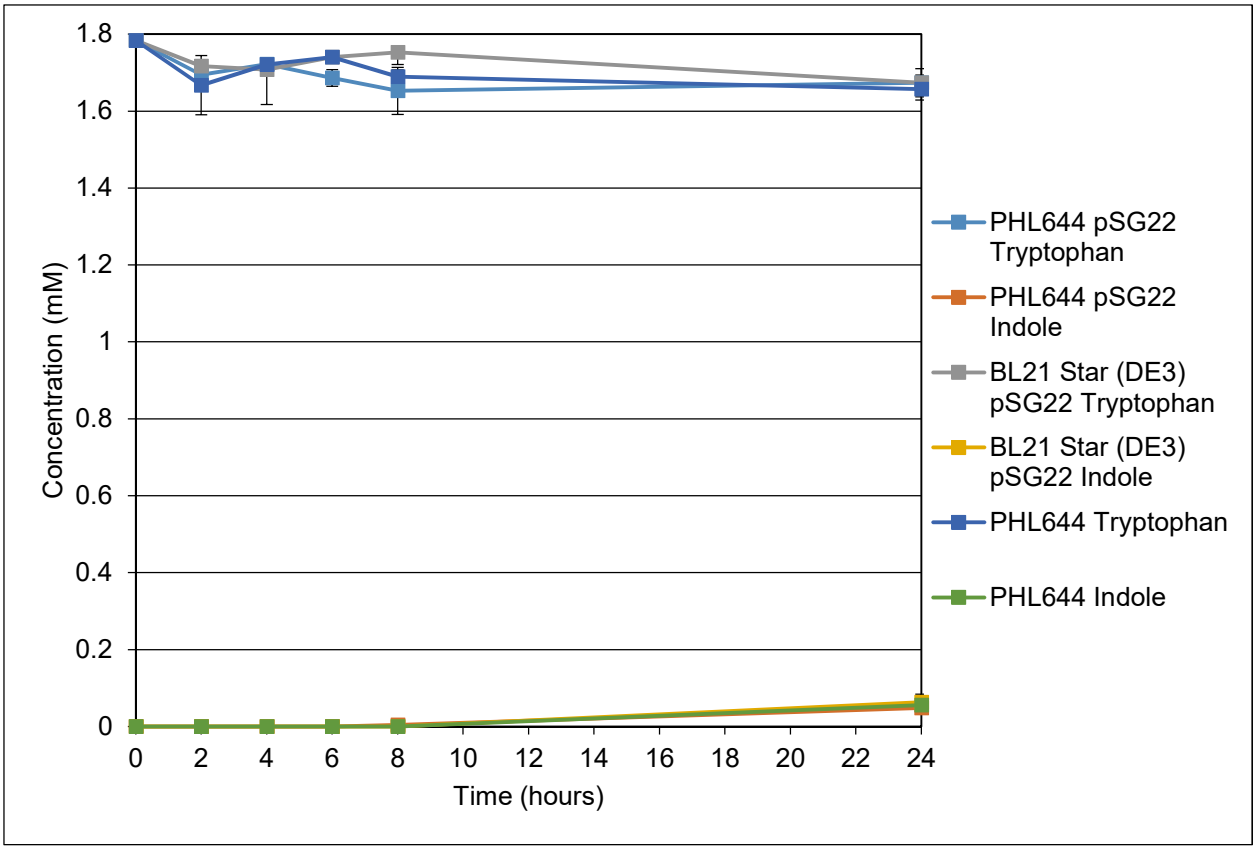

***Figure 5.14**: Consumption of tryptophan and synthesis of indole by PHL644, PHL644 pSG22 and BL21 Star (DE3) pSG22. Untransformed BL21 Star (DE3) was omitted due to a HPLC analysis issue, but was unlikely to differ from the data obtained for untransformed PHL644. Error bars represent 1 standard deviation from the mean of three independent cultures.*

The determination that 7-chloro-L-tryptophan could not be produced by either biofilm-phase or planktonic pSG22-containing *E. coli* cells was surprising and will be reflected upon in the discussion. However, due to time and funding issues, no further experiments could be performed to improve the processes applied in this work.

5.2.6 Discussion

It was concluded that 7-chloro-L-tryptophan could not be produced in either planktonic or biofilm-phase cells. The reasons for this require examination.

As no halogenated products could be detected in any experiments, it may be theorised that the PrnA produced from the pSG22 plasmid may have been non-functional. While the encoded PrnA has been reported by collaborators to produce 7-chloro-L-tryptophan (unpublished data), a random loss-of function mutation occurring since acquisition cannot be ruled out. The plasmid would require sequencing or replacement from the source to confirm this.

PrnA is dependent on $FADH_2$ and oxygen to perform halogenation reactions (Dong C *et al*., 2005). $FADH_2$ is an essential cofactor in many enzymatic processes in *E. coli*, and thus would be assumed to be present and abundant in *E. coli* cells, as well as constantly regenerated from FAD, even in a slowly-metabolising biofilm. Typically, *E. coli* cultures are kept aerated by high speed agitation. In this project, it was noted to be beneficial to keep agitation low to aid biofilm growth (Section 3.3.13). This may have limited oxygen flow into the planktonic and biofilm cells. However, *E. coli* biofilm processes are negatively regulated by low oxygen conditions and thus biofilm would not be expected to form if the cells did not have a suitable supply of oxygen (Colón-González M *et al*., 2004). As biofilms grew well under these experimental conditions, oxygen limitation is unlikely to have been a factor.

L-tryptophan requires active transport for uptake by *E. coli*, and thus its transporter proteins must be active for this to occur (Cosgriff AJ & Pittard AJ, 1997). The consumption of L-tryptophan and conversion to indole by planktonic and biofilm-phase cells indicates that tryptophan was able to enter the cells to some extent. However, the reduced L-tryptophan-indole conversion by biofilm-phase *E. coli* cells may indicate that L-tryptophan was restricted

from entering these cells. This may be due to limited active transport of L-tryptophan, possibly a result of reduced metabolic demand. Additionally, this may be due to the biofilm matrix restricting access to the cells. The polysaccharide colanic acid is produced by both PHL644 and BL21 Star (DE3) as an architectural biofilm element and has been shown to provide hydrophilicity to the biofilm matrix (Yoshida K *et al*., 2015). L-tryptophan is a relatively hydrophobic amino acid and thus may be repelled by colanic acid-containing biofilm, preventing *E. coli* cells from taking up L-tryptophan for halogenation or conversion into indole. Colanic acid is an essential architectural element in *E. coli* biofilms and unfortunately cannot be removed from this particular biofilm model to test this theory (Danese PN *et al*., 2000). The use of a cosolvent may decrease the restriction of L-tryptophan and allow the reactant to pass through the biofilm matrix. If this is the case, further experiments would need to be performed to determine whether the cosolvent affected the biofilm matrix itself. As stated before, these theories could not be tested due to a lack of time and funds.

5.3 Formation of Acetophenone using CV2025 ω-transaminase

ω-transaminases (ωTAs) are used in biocatalysis for the synthesis of amine molecules which require chiral specificity (Malik MS *et al*., 2012). An ωTA reaction requires a chiral amine donor and a non-chiral amine acceptor as reactants, whereby the amine group is transferred from the donor to the acceptor, creating a novel chiral aminated molecule. In typical biocatalysis reactions, this transfer occurs as a replacement of a non-chiral keto-group with a chiral amine group. Such reactions can be used to synthesise L-form amino acids with a high degree of specificity. ωTAs require pyridoxal-5'-phosphate (PLP) as a cofactor, which is produced and regenerated by *E. coli* (Simon RC *et al*., 2014).

The *Chromobacterium violaceum* transaminase CV2025 was used in these experiments as it has been noted as having a wide substrate spectrum and being an efficient transaminase at conditions similar to those used for biofilm growth (30°C, pH 7) (Kaulmann U *et al*., 2007, Villegas-Torres MF *et al*., 2015). Additionally, a simple method for analysis has been designed for testing this enzyme. CV2025 can efficiently convert (S)-(-)-α-methylbenzylamine ((S)-(-)-α-MBA) and pyruvate into acetophenone and L-alanine (Figure 5.15). In this reaction, (S)-(-)-α-MBA acts as the amine donor while pyruvate acts as the amine acceptor. The non-chiral pyruvate molecule is thus converted into the chiral amino acid L-alanine. Increases in acetophenone concentration, the keto-group-containing side-product of this reaction, can be detected using a UV-spectrophotometer at 245 nm. It has been shown that changes in absorbance at 245 nm can be used to rapidly determine the efficiency of a CV2025 biocatalysis reaction without the necessity of HPLC (Schätzle S *et al*., 2009). Due to time constraints, this analysis method was employed for this reaction.

In these experiments, CV2025 was expressed from the plasmid pQR801 (Villegas-Torres MF *et al*., 2015). pQR801 encodes CV2025 under the control of a pT7 promoter. The plasmid features a kanamycin resistance cassette and so could only be used in BL21 Star (DE3) as PHL644 features this resistance marker in its genome.

Due to a lack of time, only experiments relating to biofilm formation and planktonic and biofilm-phase biocatalysis could be performed for this plasmid.

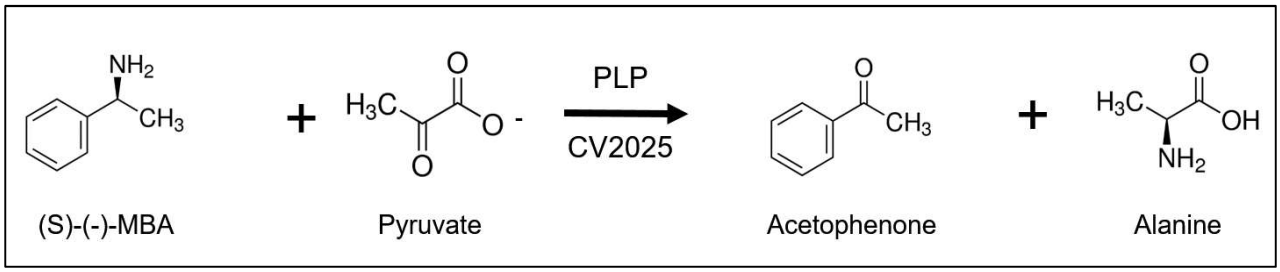

Figure 5.15: *Conversion of (S)-(-)-α-MBA and pyruvate into acetophenone and alanine by CV2025.*

5.3.1 Effect of pQR801 on Biofilm Formation

pQR801 was transformed into *E. coli* BL21 Star (DE3) using project-standard conditions. No colony-formation defects on agar were noted during growth at 30°C. BL21 Star (DE3) pQR801 and BL21 Star (DE3) were grown in 100 mL Duran bottles in M63+ at 30°C and 70 RPM for 3 days (with 100 µM IPTG to induce CV2025 expression). A PTFE-wrapped slide was inserted to provide a surface for biofilm formation. Biofilms were analysed using CV staining and CLSM.

Figure 5.16 indicates that BL21 Star (DE3) pQR801 slightly exceeded BL21 Star (DE3) in terms of CV retention, but not to a statistically significant degree (result was within 1 standard deviation). CLSM images (Figure 5.17) further indicate that BL21 Star (DE3) pQR801 biofilms were very similar to their untransformed variants. These data suggest that pQR801 had no detrimental effect on biofilm formation when induced with IPTG, and thus the plasmid was suitable for use in a biofilm biocatalyst.

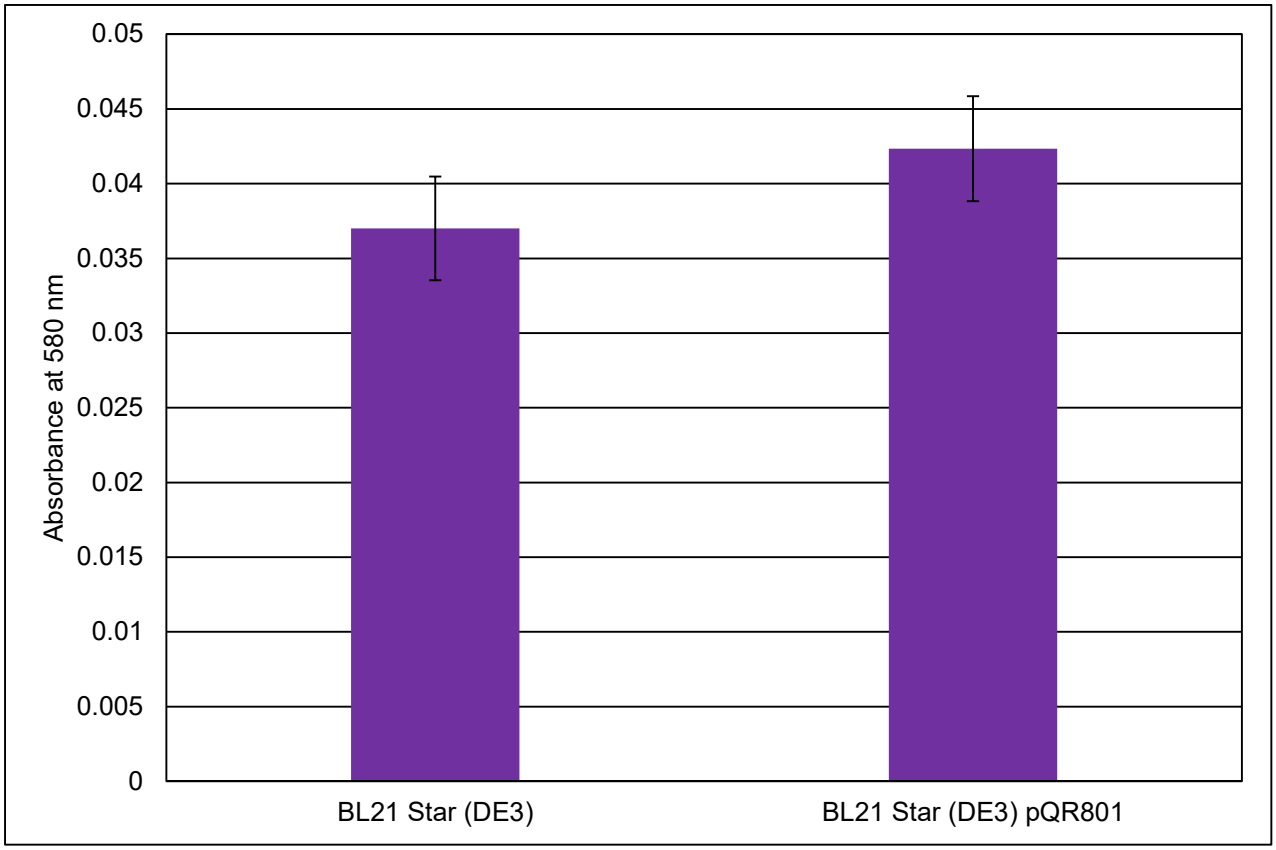

Figure 5.16: *Graph of crystal violet retention for BL21 Star (DE3) and BL21 Star (DE3) pQR801. Error bars represent 1 standard deviation from the mean of three independent cultures.*

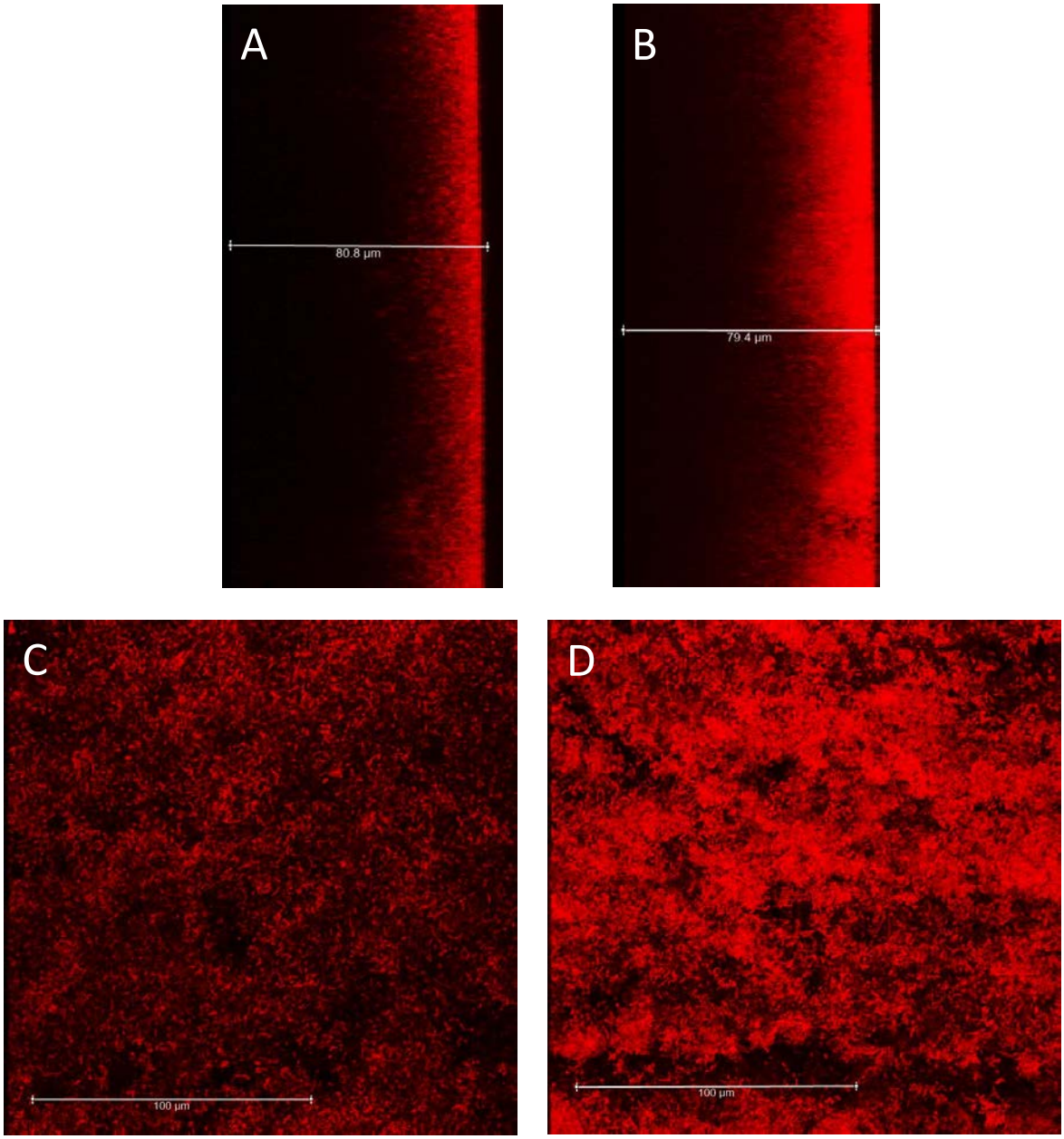

Figure 5.17: *Representative side-view and top-down CLSM images of BL21 Star (DE3) and BL21 Star (DE3) pQR801 biofilms. Biofilms were grown using the Duran Bottle method. A – side-view BL21 Star (DE3) biofilm. B – side-view BL21 Star (DE3) pQR801 biofilm. C – top-down-view BL21 Star (DE3) biofilm. D – top-down-view BL21 Star (DE3) pQR801 biofilm. In all images, the base of the biofilm is on the left.*

5.3.2 Formation of Acetophenone by pQR801 in Planktonic *E. coli* Cells

BL21 Star (DE3) pQR801 and BL21 Star (DE3) were grown in 100 mL Duran bottles in M63+ (without antibiotic) at 30°C and 70 RPM for 3 days (with 100 µM IPTG to induce CV2025 expression). Cultures were then centrifuged at 3200 RPM for 15 mins, washed with PBS, centrifuged again, then resuspended in reaction buffer and adjusted to an OD_{600} of 1. The reaction buffer for this experiment contained 100 mM KH_2PO_4, 2 mM (S)-(-)-α-MBA, 2 mM sodium pyruvate and was adjusted to pH7. Resuspended cultures were inserted into clean, sterile 100 mL Duran bottles. Reactions were performed at 30°C and 70 RPM. 500 µL samples were taken every 2 hours for 0-8hrs and then at 24hrs. These samples were diluted as necessary, then filtered (0.22 µm) and immediately analysed with a spectrophotometer at 245 nm. As negative controls, cultures in reaction buffer lacking (S)-(-)-α-MBA were also analysed to determine the level of absorbance produced by non-acetophenone elements in the buffer.

Calibration graphs for determination of acetophenone concentration can be found in Section 2.4.2.

As shown by Figure 5.18, the level of absorbance in all samples changed little over the course of the experiment. Additionally, the samples containing (S)-(-)-α-MBA did not deviate significantly from those lacking (S)-(-)-α-MBA, indicating that acetophenone was not produced during the experiment. Absorbance values were not converted to concentration values as there were no significant changes.

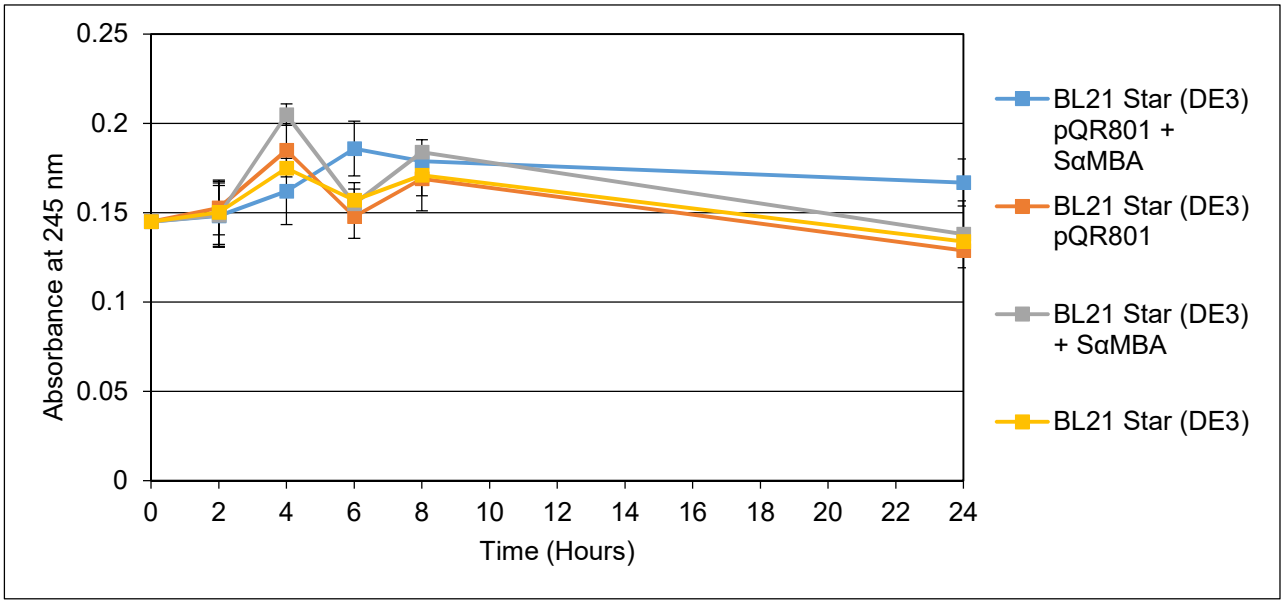

Figure 5.18: *Change in absorbance at 245 nm in planktonic BL21 Star (DE3) and BL21 Star (DE3) pQR801 in transaminase buffer containing or lacking (S)-(-)-α-MBA (abbreviated as SαMBA). Error bars represent 1 standard deviation from the mean of three independent cultures.*

5.3.3 Formation of Acetophenone by pQR801 in *E. coli* Biofilm

BL21 Star (DE3) pQR801 and BL21 Star (DE3) were grown in 100 mL Duran bottles in M63+ at 30°C and 70 RPM for 3 days (with 100 µM IPTG to induce CV2025 expression). A PTFE-wrapped slide was inserted to provide a surface for biofilm formation. The PTFE-wrapped slide was then removed, washed twice by submersion in PBS, then inserted into a clean sterile 100 mL Duran bottle containing the previously described reaction buffer. Reactions were performed at 30°C and 70 RPM. 500 µL samples were taken every 2 hours for 0-8hrs and then at 24hrs. These samples were diluted as necessary, then filtered (0.22 µm) and immediately analysed with a spectrophotometer at 245 nm. As negative controls, cultures

without (S)-(-)-α-MBA were also analysed to determine the level of absorbance produced by non-acetophenone elements in the buffer.

As with planktonic cells, no significant changes were noted in terms of absorbance at 245 nm that deviated from samples which did not contain the necessary biocatalysis elements (Figure 5.19), indicating that acetophenone was not being produced in this experiment.

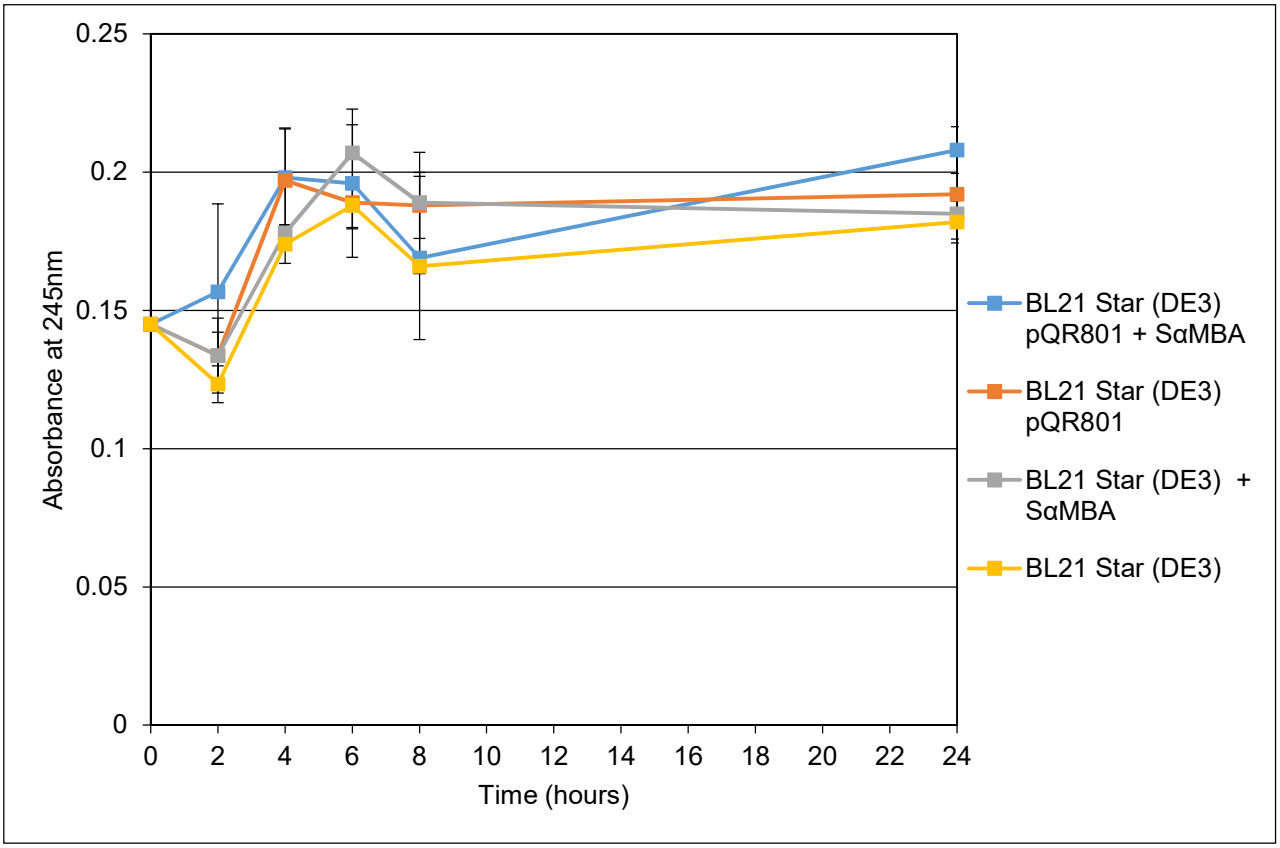

Figure 5.19: *Change in absorbance at 245 nm in BL21 Star (DE3) and BL21 Star (DE3) pQR801 biofilms in transaminase buffer containing or lacking (S)-(-)-α-MBA (abbreviated as SαMBA). Error bars represent 1 standard deviation from the mean of three independent cultures.*

5.3.4 Discussion

As with pSG22, a lack of time and funds meant that further optimisation of these processes was not possible, and neither was discerning why the experiment did not proceed as intended.

As before, random mutation of the pQR801 plasmid or the CV2025 ORF may have prevented enzymatic function. Additionally, transport of reactants and products into or out of the cells or biofilm may have presented too large a barrier for efficient biocatalysis and retrieval of product from the buffer. PLP cofactor deficiency is unlikely to have played a major role in the result of the experiment as PLP is present and regenerated in normal *E. coli* metabolism (Simon RC *et al*., 2014).

Chapter 6
Final Conclusions and Further Work

6.1 Chapter 3 Development of a Biocatalytic Biofilm Platform

The work presented in Chapter 3 led to the development of a robust, replicable and inexpensive platform for the generation of *E. coli* biofilms. The use of PTFE as a surface for biofilm formation was found to significantly improve attachment and 3D biofilm development over any other material tested (in PHL644 and BL21 Star (DE3)), likely due to interactions with hydrophobic curli fimbriae. PHL644 exhibited the greatest biofilm formation in terms of CV stain retention and thickness. Surprisingly, this was not due to increased expression of curli genes, as the reporter data indicated that PHL644 did not display higher expression of curli genes than BL21 Star (DE3). This suggests that the *ompR234* mutation has other positive effects on biofilm formation than the ones proven for curli gene expression (Pringent-Combaret C *et al*., 2001). CsgD has already been proven to activate expression of the DGC DgcC (Brombacher E *et al*., 2006). An *ompR234* mutation may increase the level of CsgD and DgcC in the cell, leading to increased intracellular c-di-GMP concentrations and greater activation of biofilm-related pathways such as exopolysaccharide production. Thus the *ompR234* mutation may increase the production of components essential to the structure of the biofilm, not just curli, and allow it to grow thicker structures than other strains.

Both PHL644 and BL21 Star (DE3) are derived from commensal bacteria isolated from the gut of human patients (Section 1.6.1). Nissle 1917 also colonises the human gut and has beneficial competitive properties against pathogenic *E. coli* strains (Section 1.6.1). The fact that Nissle 1917 grew thin biofilms on all materials tested compared to PHL644 and BL21 Star (DE3) was surprising, and suggests that Nissle 1917 is more highly adapted to the gut than environmental conditions. Alternatively, these specific conditions may simply be unsuitable for biofilm growth in this strain, and may lack gut-specific stimuli.

The use of reporter technology and flow cytometry in this work allowed rapid determination of both *csgBAC* gene activation and expression level. More precise measurements of expression than gene reporter methods, such as those afforded by quantitative PCR techniques, are preferable in many transcription studies. However, these methods assume homogeneous expression in all cells in a culture. The data presented here indicate that planktonic and biofilm cells exhibit heterogeneous gene expression and so these techniques may be misleading. Flow cytometry allows the analysis of a large set of individuals, and was therefore invaluable in analysing gene expression variations within biofilms, as shown by the data presented here.

Reporter technology revealed that not all cells attached to the PTFE surface were expressing curli genes, suggesting that attached cells downregulate their expression to prevent redundant production of curli proteins. While it was not possible to provide visual evidence of *csgBAC*-inactivated cells on the PTFE surface due to equipment and resource limitations, the success of the flow cytometry data indicates that this technique may have wider applications in determining gene expression within a biofilm, perhaps in metabolic processes as well as other biofilm gene expression.

To conclude, the work presented in Chapter 3 led to insights on how various stimuli led to increased or decreased biofilm formation in the strains tested herein, as well as how curli gene expression was affected by the growth of the biofilm. Additionally, a novel method for growing *E. coli* biofilm was developed which allowed quantification, imaging and analysis of gene expression.

6.2 Chapter 4 Modulation of the Biocatalytic Biofilm via Molecular Biology Practices

The biofilm-modulating plasmids used in Chapter 4 were shown to have several interesting, if not necessarily beneficial, effects on the biofilm-forming strains.

Overexpression of CsgD via pT7-CgsD led to a greater abundance of biofilm on PTFE for PHL644 but not for BL21 Star (DE3). In both cases, the biofilms exhibited loose cells leading to the conclusion that the plasmid did not improve biofilm cohesion. As shown by data in Chapter 3, CsgD expression is negatively-regulated on attachment to the PTFE surface, which suggests that further CsgD expression after attachment has been established is detrimental to the cells and the growth of the biofilm. PHL644 pT7-CsgD biofilms may have been thicker, but they lacked the architecture and cohesion of PHL644 biofilms, likely afforded by the downregulation of curli fimbriae and the upregulation and production of polysaccharides such as colanic acid. BL21 Star (DE3) pT7-CsgD biofilms exhibited a similar phenotype, but were thinner and appeared to be less cohered. To theorise, the overproduction of curli genes may have led to increased intracellular amyloid toxicity for which BL21 Star (DE3) is unable to control due to the deletions of the Lon and OmpT proteases. However, no data exists on which proteases degrade curli proteins other than that they are degraded in the absence of the curli secretion channel CsgG (Loferer H *et al*., 1997). Increased toxicity may have reduced the ability of the cells to produce a biofilm. The level of intracellular curli proteins could be measured using SDS-PAGE as gene reporter technology would not reflect the abundance and accumulation of intracellular proteins.

DgcM overexpression led to reductions in biofilm abundance in both PHL644 and BL21 Star (DE3). CLSM images reveal that the architecture of the PHL644 pYdaM biofilm, while reduced in thickness, was similar to that of the untransformed strains with characteristic 3D outgrowth. This was not reflected by BL21 Star (DE3) which appeared less cohered and

much thinner than the untransformed strain. As shown by Section 4.2, strains transformed with pYdaM grew more slowly, suggesting that the reduction in abundance is due to fewer cells present in the culture and therefore the biofilm. DgcM is normally bound by PdeR when c-di-GMP levels are low, repressing its activity. DgcM overexpression leads to a higher concentration of unbound DgcM, which binds to MlrA and activates curli gene expression at the incorrect time. Production of curli proteins may lead to increased intracellular amyloid toxicity as evidenced by slower growth. As shown by fluorescence experiments, *csgBAC* expression was slightly increased in PHL644 pYdaM between 10 and 12 hours, and between 4 and 8 hours for BL21 Star (DE3) pYdaM before being reduced for the rest of the 24 hours. This suggests that the *csgBAC* level in the cell is responded to by the cell, perhaps by amyloid stress mechanisms, which keeps the level of curli gene expression under control. These data indicate that DgcM overexpression is detrimental to both cell growth and biofilm formation, perhaps through increased amyloid toxicity. However, this theory will be reflected on when analysing the data obtained for pYaiC.

DgcO overexpression led to reductions in biofilm abundance in both PHL644 and BL21 Star (DE3). Although DgcO overexpression has been linked to cell division interference, which was noted in CLSM images of PHL644 pYddV biofilms, planktonic growth of PHL644 and BL21 Star (DE3) appeared unaffected by the presence of DgcO. This suggests that the elongation effects seen in the images are dependent on adhesion. This would require regular CLSM imaging during the 24 hour period to test, and was unfeasible in this study. Strains transformed with pYddV exhibited the lowest mean fluorescence of any strain throughout the experiment, suggesting a negative effect on curli production. This likely explains the reduction in biofilm abundance seen for both strains. However, it is unclear why DgcO overexpression would lead to reduced curli production, as the two pathways appear

unlinked, except by c-di-GMP production. As DgcO controls the activity of polynucleotide phosphorylase (PNPase), overexpression of DgcO may lead to increased PNPase activity, leading to the degradation of mRNA fragments linked to curli gene expression. However, no direct evidence exists of this link. These data indicate that DgcO overexpression is detrimental to biofilm abundance and physiology, and curli gene expression, but not to planktonic cell growth.

DgcC overexpression led to statistically significant increases in biofilm abundance in BL21 Star (DE3) but not in PHL644. CLSM images indicate that PHL644 pYaiC biofilms were slightly thinner than their untransformed counterparts but were largely unchanged in terms of architecture. This leads to the conclusion that pYaiC is not beneficial to PHL644 biofilm formation, but is not substantially detrimental either. BL21 Star (DE3) pYaiC biofilms, in contrast, exceeded BL21 Star (DE3) in both thickness and the development of 3D architecture. BL21 Star (DE3) most likely benefitted from the increase in cellulose production that DgcC has been shown to provide. Increased cellulose would permit a stronger, thicker biofilm architecture. PHL644 may not benefit from DgcC overexpression simply because it does not produce cellulose. As such, pYaiC was determined to be beneficial to the growth of BL21 Star (DE3) biofilm, but not PHL644. Further to this, pYaiC exhibited no detrimental effects on the planktonic growth of either strain, and led to substantial increases in *csgBAC* expression. Increased curli protein expression during planktonic phase likely somewhat explains the increased biofilm abundance in BL21 Star (DE3), as this would allow increased successful attachment events. As pYaiC-transformed strains produced more *csgBAC* than any other strain, and this did not lead to slow growth or reduced biofilm formation as seen for pYdaM, this suggests that the previous theory of increased amyloid toxicity is incorrect. The explanation for these results is therefore still unclear.

To conclude, pYdaM and pYddV were both determined to negatively affect the formation of *E. coli* PHL644 and BL21 Star (DE3) biofilms, although the reasons for this are unclear. Extensive analysis would be required to understand the role these plasmids play in biofilm formation, which was unfeasible in this project, but nevertheless these data offer initial insights into a complex regulatory network. pYaiC was shown to have positive effects on the growth of BL21 Star (DE3) biofilm but not on PHL644. Further work may include mutating the genomic promoter of *dgcC* in BL21 Star (DE3) or another cellulose-producing strain into an inducible overexpressing promoter. This would allow control over the level of DgcC present in the cell and modulate biofilm formation. DgcC is therefore revealed as a potential target for synthetic biology in developing controllable biofilm formation.

Further work in this area may involve the testing of PDE overexpression in this model to determine specific effects on biofilm formation and how biofilm formation may be controlled.

6.3 Chapter 5 Use of the Biocatalytic Biofilm in Biocatalysis

While none of the three biocatalysis processes applied in the *E. coli* biofilm biocatalyst were capable of synthesising their desired product, it should be noted that optimisation of the three processes could not be performed due to time and funding issues. It may transpire that pSG22 and pQR801 were simply non-functional plasmids and obtaining new plasmids may rectify this problem. However, several other elements cannot be ignored in determining whether this model can be used as a 'plug-and-play' biofilm biocatalyst.

The conversion of L-tryptophan into indole is central to the regulation of biofilm formation in *E. coli*, especially in the conditions employed in these experiments (30°C) (Gaimster H & Summers D, 2015). Reactions involving L-tryptophan-derived compounds or reactions disrupting the L-tryptophan-indole balance are clearly a poor choice for use in an *E. coli* biofilm biocatalyst. It is therefore reasonable to state that an informed decision based on previous data in both biocatalysis research and microbiology is crucial when choosing a biocatalysis process. It may also be more feasible to use a biofilm-forming organism which does not produce indole, such as certain *Pseudomonas* species (Chu W *et al*., 2012), when dealing with L-tryptophan-based reactants or products.

The variant composition of any bacterial biofilm is also a major factor is deciding whether certain reactants and products are suitable for use in a biofilm biocatalyst. Biofilm matrix components can vary in charge and hydrophobicity and are employed by bacteria to prevent certain compounds passing through and harming the cells. In turn, the matrix must also permit essential nutrients and molecules to reach the cells and allow them to survive. A thorough understanding of the relationship between a candidate reactant or product and the biofilm matrix is also therefore crucial. Moreover, an understanding of if and/or how these

molecules are transported into or out of the bacterial cell is necessary for efficient recovery of the product. This was not possible in this project due to time and funding constraints.

It should be noted that these experiments were performed using a novel biofilm testing technique and as such a method more suitable for a biofilm biocatalyst may be developed. Furthermore, screening of more plasmids may lead to the discovery of biocatalytic processes which are more suitable for use in the biofilm biocatalyst. Negative results from three experiments is not proof that the biofilm biocatalyst is unfeasible, but it does suggest that not every biocatalysis application will be successful.

The concept of a 'plug-and-play' platform; one in which any biocatalysis plasmid can be transformed into biofilm-forming cells and perform efficient biocatalysis, requires further development. Extensive synthetic biology modifications would need to be applied to *E. coli* to ensure that the biofilm platform could work under industrially determined conditions, as has been applied to *P. putida* and *P. taiwanensis* (Benedetti I *et al*., 2016, Volmer J *et al*., 2014). Nevertheless, it may be more beneficial to perform further engineering on *Pseudomonas spp.* and develop those species as multipurpose biocatalysts as they have already been shown to perform efficient biocatalysis in multiple selected applications (Nikel PI *et al*., 2016). Every bacterial species has diverse properties, metabolic requirements and resistances and thus developing a single species to be able to perform any recombinant biocatalysis task in a biofilm phase may not be practical, and it may be more prudent to develop species for industrial biocatalytic processes on a case-by-case basis.

6.4 Summary of Aims

1. Develop a reliable means of generating *E. coli* biofilm which can be analysed using quantitative and imaging techniques.

This aim was met in Chapter 3 by developing a novel, simple and inexpensive biofilm generation technique, termed the “Duran Bottle Method”. The biofilms produced using this method were replicable and were able to be analysed and compared using quantitative CV staining techniques as well as by CLSM imaging.

2. Optimise biofilm generation by modulating surface, growth conditions or *E. coli* strain.

This aim was met in Chapter 3 by using varied materials, media composition, incubation conditions and *E. coli* strains to determine which conditions were optimal for producing significant *E. coli* biofilm. This was analysed using CV staining and CLSM imaging.

3. Characterise the expression of curli fimbriae during biofilm formation using reporter gene technology.

This aim was met in Chapter 3 by using the novel pJLC-T reporter plasmid to provide data on the expression of the *csgBAC* operon through planktonic and biofilm growth. Flow cytometry allowed the quantification of *csgBAC* expression in single cells within populations, giving information on expression variation between populations.

4. Utilise DGC-overexpressing plasmids to modulate biofilm formation and determine effects on biofilm architecture and curli fimbriae expression.

This aim was met in Chapter 4 by transforming various biofilm-modulating plasmids into the biofilm-forming *E. coli* strains. Their effects on biofilm formation, analysed by CV staining and CLSM imaging, suggested how these plasmids affected the various pathways involved in biofilm formation. These plasmids were used in conjunction with pJLC-T to further provide insights on how the overexpression of proteins involved in biofilm formation directly affect a major biofilm component, namely curli fimbriae.

5. Utilise recombinant biocatalysis enzymes to determine whether the developed biofilms are capable of performing biocatalysis processes.

This aim was met in Chapter 5 by testing three separate biocatalysis reactions in the biofilm biocatalyst. While the reactions were unsuccessful, and significant optimisation may be required to allow them to function, these data gave insights into how the biofilm biocatalyst may be improved and how some reactions may be detrimental to biofilm formation.

6.5 Future Work

6.4.1 Further Development of the Biofilm Biocatalyst and Study of Curli Gene Expression

- Dilution of LB medium to determine whether diluted rich medium may improve biofilm growth.
- Modulation of sodium and succinate concentrations in M63+ to determine their direct effects on biofilm formation.
- Perform more frequent CLSM observations to develop a clearer picture of how these biofilms mature in terms of architecture.

- Link varied growth conditions such as glucose concentration and temperature to their effects on curli gene expression.
- Collect data on MC4100 (base strain of PHL644) to determine if or how this strain produces curli genes.
- Collect curli gene data on BL21 Star (DE3) biofilm-phase cells and compare to PHL644.

6.4.2 Further Study of the Effects of the DGC-Overexpression Plasmids

- Collect curli gene data on biofilm-phase cells carrying the DGC-overexpression plasmids.
- Study biofilm growth over several days to determine how these modulated biofilms develop over time

6.4.3 Characterisation and Optimisation of Reactions in the Biofilm Biocatalyst

- Further characterise the effects of pSTB7 or TrpBA expression on *E. coli* growth and biofilm formation. An interesting aspect would be whether the detrimental effects seen at 30°C in minimal medium are also noted at 37°C or in rich medium.
- Optimisation of the pSG22 and pQR801-mediated reactions, including modulation of biofilm thickness to determine whether this is a limiting factor.
- Test cosolvents to ameliorate entry of reactants into, and products out of, the biofilm.

6.6 Final Remarks

The primary aim of this work was to develop a platform for generating an *E. coli* biofilm suitable for use in biocatalysis. While the development and optimisation of the platform was

successful in terms of creating a cheap and reliable biofilm platform, the application of biocatalysis processes in this model were not found to be viable based on preliminary data. Nevertheless, the biofilm generation model was proven to provide insight into biofilm morphology, formation and the regulation of the complex c-di-GMP network. Additionally, the model was able to determine heterogeneity in the expression of an important biofilm element, curli fimbriae. These results suggest that the Duran Bottle biofilm generation model may be of significant use to researchers who lack the funding for more expensive devices such as the CDC reactor.

With regards to industrial outputs, the work presented in this thesis proves that the generation of significant *E. coli* biofilm on a solid 2D surface is feasible with relatively inexpensive conditions. However, as indicated by differences in biofilm growth between the 6-Well Plate and Duran Bottle biofilm generators, upscaling of these models may require extensive research. As has been proven for whole-cell biocatalysis in other species, biofilms represent a potentially more efficient and reusable platform for the production of fine chemicals than standard planktonic processes. While the concept of a multipurpose *E. coli* biofilm biocatalyst is a lucrative idea, more development is clearly essential to realise the potential of this platform.

Chapter 7

Bibliography

Abdel-Nour M *et al*. Biofilms: The Stronghold of *Legionella pneumophila*. *International Journal of Molecular Sciences*. 2013; 14(11), 21660-21675

Adediran J *et al*. An *Escherichia coli* Nissle 1917 missense mutant colonizes the streptomycin-treated mouse intestine better than the wild type but is not a better probiotic. *Infection and Immunity.* 2014; 82(2):670-82

Adnan M *et al*., Contribution of rpoS and bolA genes in biofilm formation in *Escherichia coli* K-12 MG1655. *Molecular and Cell Biochemistry*. 2010;342(1-2):207-13

Adrio JL & Demain AL. Genetic improvement of processes yielding microbial products. *FEMS Microbiology Reviews.* 2005; 30(2):187-214

Ahimou F *et al.,* Effect of protein, polysaccharide, and oxygen concentration profiles on biofilm cohesiveness. *Applied and Environmental Microbiology*. 2007;73(9):2905-10

Ali L *et al*., Investigating the suitability of the Calgary Biofilm Device for assessing the antimicrobial efficacy of new agents. *Bioresource Technology*. 2006; 97(15):1887-93

Amadio J *et al*., Filamentous fungal biofilm for production of human drug metabolites. *Applied Microbiology and Biotechnology*. 2013;97(13):5955-5963

Ambriz-Aviña V *et al*., Applications of flow cytometry to characterize bacterial physiological responses. *Biomed Research International*. 2014; 2014:461941

Arciola CR *et al*., Polysaccharide intercellular adhesin in biofilm: structural and regulatory aspects. *Frontiers in Cellular and Infection Microbiology*. 2015; 5:7

Azevado AS *et al*., Impact of polymicrobial biofilms in catheter-associated urinary tract infections. *Critical Reviews in Microbiology*. 2016;1-17

Bak G *et al*., Identification of novel sRNAs involved in biofilm formation, motility, and fimbriae formation in *Escherichia coli*. *Scientific Reports*. 2015;5:15287

Bancroft JD & Gamble M, *Theory and Practice of Histological Techniques.* Elsevier Health Sciences. 2008

Barnhart MM & Chapman MR, Curli biogenesis and function. *Annual Review of Microbiology*. 2006;60:131-47

Batchelor E *et al*., The *Escherichia coli* CpxA-CpxR envelope stress response system regulates expression of the porins ompF and ompC. *Journal of Bacteriology*. 2005;187(16):5723-31

Beloin C *et al*., *Escherichia coli* biofilms. *Current Topics in Microbiology and Immunology*. 2008;322:249-89

Benedetti I *et al*., Genetic programming of catalytic *Pseudomonas putida* biofilms for boosting biodegradation of haloalkanes. *Metabolic Engineering*. 2016;33:109-18

Bernardes PC *et al*., Assessment of hydrophobicity and roughness of stainless steel adhered by an isolate of *Bacillus cereus* from a dairy plant. *Brazilian Journal of Microbiology*. 2010;41(4):984-92

Berne C *et al*., Adhesins Involved in Attachment to Abiotic Surfaces by Gram-Negative Bacteria. *Microbiology Spectrum*. 2015;3(4)

Besharova O *et al*., Diversification of Gene Expression during Formation of Static Submerged Biofilms by *Escherichia coli*. *Frontiers in Microbiology*. 2016;7:1568

Billings N *et al*., Material properties of biofilms-a review of methods for understanding permeability and mechanics. *Reports on Progress in Physics*. 2015;78(3)

Biosurface Technologies Corporation website. http://biofilms.biz/products/biofilm-reactors. Accessed 27/04/2017.

Biswal NR & Paria S, Wetting of PTFE and Glass Surfaces by Aqueous Solutions of Cationic and Anionic Double-Chain Surfactants. *Industrial and Engineering Chemistry Research*. 2012;51(30);10172–10178

Bjarnscholt T, The role of bacterial biofilms in chronic infections. *APMIS Supplementum*. 2013;(136):1-51

Blattner FR *et al*., The complete genome sequence of *Escherichia coli* K-12. *Science*. 1997;277(5331):1453-62

Bordi C *et al*., Genes regulated by TorR, the trimethylamine oxide response regulator of *Shewanella oneidensis*. *Journal of Bacteriology*. 2004;186(14):4502-9

Brombacher E *et al*., Gene expression regulation by the Curli activator CsgD protein: modulation of cellulose biosynthesis and control of negative determinants for microbial adhesion. *Journal of Bacteriology*. 2006;188(6):2027-37

Brombacher E *et al*., The curli biosynthesis regulator CsgD co-ordinates the expression of both positive and negative determinants for biofilm formation in *Escherichia coli*. *Microbiology*. 2003;149(Pt 10):2847-57

BSSA website, FAQs section, http://www.bssa.org.uk/faq.php. Accessed 12/07/2017
Burkovski A, Corynebacterium glutamicum: From Systems Biology to Biotechnological Applications 1st Edition. Caister Academic Press. 2015

Carbone EAD *et al*., How to increase the hydrophobicity of PTFE surfaces using an r.f. atmospheric-pressure plasma torch. *Surface and Interface Analysis*. 2009;42(6-7):1014-8

Castonguay MH *et al*., Biofilm formation by *Escherichia coli* is stimulated by synergistic interactions and co-adhesion mechanisms with adherence-proficient bacteria. *Research in Microbiology*. 2006;157(5):471-8
Castro J *et al*., *Escherichia coli* and *Enterococcus faecalis* are able to incorporate and enhance a pre-formed *Gardnerella vaginalis* biofilm. *Pathogens and Disease*. 2016;74(3)

Cerca N *et al*., Confocal laser scanning microscopy analysis of *S. epidermidis* biofilms exposed to farnesol, vancomycin and rifampicin. *BMC Research Notes*. 2012;5:244

Ceri H *et al*., The Calgary Biofilm Device: new technology for rapid determination of antibiotic susceptibilities of bacterial biofilms. *Journal of Clinical Microbiology*. 1999;37(6):1771-6

Cha JO *et al*., Investigation of Biofilm Formation and its Association with the Molecular and Clinical Characteristics of Methicillin-resistant *Staphylococcus aureus*. *Osong Public Health and Research Perspectives*. 2013;4(5):225-32

Chambers JR & Sauer K, Small RNAs and their role in biofilm formation. *Trends in Microbiology.* 2013;21(1):39-49

Chant EL & Summers DK, Indole signalling contributes to the stable maintenance of *Escherichia coli* multicopy plasmids. *Molecular Microbiology*. 2007;63(1):35-43

Chauhan A *et al*., Did I pick the right colony? Pitfalls in the study of regulation of the phase variable antigen 43 adhesin. *PLoS One*. 2013;8(9):e73568

Chen CH *et al*., A facile approach to tryptophan derivatives for the total synthesis of argyrin analogues. *Organic and Biomolecular Chemistry.* 2014;12:9764-8

Chimerel C *et al*., Indole prevents *Escherichia coli* cell division by modulating membrane potential. *Biochimica et Biophysica Acta*. 2012;1818(7):1590-4

Cho SH *et al*., Detecting envelope stress by monitoring β-barrel assembly. *Cell.* 2014;159(7):1652-64

Choi JM *et al*., Industrial applications of enzyme biocatalysis: Current status and future aspects. *Biotechnology Advances*. 2015;33(7):1443-54

Choo EJ & Chamber HF, Treatment of Methicillin-Resistant *Staphylococcus aureus* Bacteremia. *Infection and Chemotherapy*. 2016;48(4):267-273

Chu W *et al*., Indole production promotes *Escherichia coli* mixed-culture growth with *Pseudomonas aeruginosa* by inhibiting quorum signalling. *Applied and Environmental Microbiology*. 2012;78(2):411-9

Cinelli RA *et al*., The enhanced green fluorescent protein as a tool for the analysis of protein dynamics and localization: local fluorescence study at the single-molecule level. *Photochemistry and Photobiology*. 2000;71(6):771-6

Coffey BM & Anderson GG, Biofilm formation in the 96-well microtiter plate. *Methods in Molecular Biology*. 2014;1149:631-41

Colón-González M *et al*., Anaerobic growth does not support biofilm formation in *Escherichia coli* K-12. Research in Microbiology. 2004;155(7):514-21

Conway T & Cohen PS, Commensal and Pathogenic *Escherichia coli* Metabolism in the Gut. *Microbiology Spectrum*. 2015;3(3)

Cooper GM & Hausman RE, *The Cell: A Molecular Approach*. ASM Press. 2007

Cosgriff AJ & Pittard AJ, A topological model for the general aromatic amino acid permease, AroP, of *Escherichia coli*. *Journal of Bacteriology*. 1997;179(10):3317-23

Culotti A & Packman AI, *Pseudomonas aeruginosa* promotes *Escherichia coli* biofilm formation in nutrient-limited medium. *PLoS One*. 2014;9(9):e107186

Danese PN *et al*., Exopolysaccharide production is required for development of *Escherichia coli* K-12 biofilm architecture. *Journal of Bacteriology*. 2000;182(12):3593-6

Datta S *et al*., Enzyme immobilization: an overview on techniques and support materials. *3 Biotech*. 2013;3(1): 1–9

de Carvalho CCCR, Whole cell biocatalysts: essential workers from Nature to the industry. *Microbial Biotechnology*. 2016;10(2);250-263

de Luna Md *et al*., The *Escherichia coli* biofilm-promoting protein Antigen 43 does not contribute to intestinal colonization. *FEMS Microbiology Letters*. 2008;284(2):237-46

de Regil R & Sandoval G, Biocatalysis for biobased chemicals. *Biomolecules*. 2013;3(4):812-47

Dequin S, The potential of genetic engineering for improving brewing, wine-making and baking yeasts. *Applied Microbiology and Biotechnology*. 2001;56(5-6):577-88

Desai AA, Sitagliptin manufacture: a compelling tale of green chemistry, process intensification, and industrial asymmetric catalysis. *Angewandte Chemie*. 2011;50(9):1974-6

DiCosimo R *et al*., Industrial use of immobilized enzymes. *Chemical Society Reviews*. 2013;42(15):6437-74

Dong C *et al*., Tryptophan 7-halogenase (PrnA) structure suggests a mechanism for regioselective chlorination. *Science*. 2005;309(5744):2216-9

Donlan RM, Biofilms: microbial life on surfaces. *Emerging Infectious Diseases*. 2002;8(9):881-90

Dove SL *et al*., Control of *Escherichia coli* type 1 fimbrial gene expression in stationary phase: a negative role for RpoS. *Molecular and General Genetics*. 1997;18;254(1):13-20

Eisenmesser EZ *et al*., Enzyme dynamics during catalysis. *Science*. 2002;295(5559):1520-3

Elias S & Banin E, Multi-species biofilms: living with friendly neighbors. *FEMS Microbiology Reviews*. 2012

Enterina JR *et al*., Emerging fluorescent protein technologies. *Current Opinion in Chemical Biology*. 2015; 27:10-7

Evans ML *et al*., The bacterial curli system possesses a potent and selective inhibitor of amyloid formation. *Molecular Cell*. 2015;57(3):445-55

Ferrières L *et al*., The yjbEFGH locus in *Escherichia coli* K-12 is an operon encoding proteins involved in exopolysaccharide production. *Microbiology*. 2007;153(Pt 4):1070-80

Field CM & Summers DK, Indole inhibition of ColE1 replication contributes to stable plasmid maintenance. *Plasmid*. 2012;67(2):88-94

Filoche SK *et al*., Biofilm growth of *Lactobacillus* species is promoted by *Actinomyces* species and *Streptococcus mutans*. *Oral Microbiology and Immunology*. 2004;19(5):322-6

Flemming H-C & Wingender J, The biofilm matrix. *Nature Reviews Microbiology*. 2010;8(9):623-33

Flemming H-C *et al*., Biofilms: an emergent form of bacterial life. *Nature Reviews Microbiology*. 2016;14(9):563-75

Flores-Mireles AL *et al*., Urinary tract infections: epidemiology, mechanisms of infection and treatment options. *Nature Reviews Microbiology.* 2015;13(5):269-84

Francez-Charlot A *et al*., Osmotic regulation of the *Escherichia coli* bdm (biofilm-dependent modulation) gene by the RcsCDB His-Asp phosphorelay. *Journal of Bacteriology*. 2005;187(11):3873-7

Fredericks CE *et al*., Acetyl phosphate-sensitive regulation of flagellar biogenesis and capsular biosynthesis depends on the Rcs phosphorelay. *Molecular Microbiology*. 2006;61(3):734-47

Gaimster H & Summers DK, Regulation of Indole Signalling during the Transition of *E. coli* from Exponential to Stationary Phase. *PLoS One*. 2015;10(9):e0136691

Gaimster H *et al*., The indole pulse: a new perspective on indole signalling in *Escherichia coli*. *PLoS One*. 2014;9(4):e93168

Gallone B *et al*., Domestication and Divergence of *Saccharomyces cerevisiae* Beer Yeasts. *Cell*. 2016;166(6):1397-1410.e16

Gally DL *et al*., Interaction of FimB and FimE with the fim switch that controls the phase variation of type 1 fimbriae in *Escherichia coli* K-12. *Molecular Microbiology*. 2006;21(4):725-38

Garcia S *et al*., Impact of the surface roughness of AISI 316L stainless steel on biofilm adhesion in a seawater-cooled tubular heat exchanger-condenser. *Biofouling*. 2016;32(10):1185-1193

Garrett TR *et al*., Characterisation of bacterial adhesion and removal in a flow chamber by micromanipulation measurements. *Biotechnology Letters*. 2008;30(3):427-33

Geornaras I *et al*., Antimicrobial activity of epsilon-polylysine against *Escherichia coli* O157:H7, *Salmonella Typhimurium*, and *Listeria monocytogenes* in various food extracts. *Journal of Food Science*. 2007;72(8):M330-4

Gerdes HH & Kaether C, Green fluorescent protein: applications in cell biology. *FEBS Letters*. 1996;389(1):44-7

Gilmore BF *et al*., Validation of the CDC biofilm reactor as a dynamic model for assessment of encrustation formation on urological device materials. *Journal of Biomedical Materials Research*. 2010;93(1):128-40

Goeres DM *et al*., Statistical assessment of a laboratory method for growing biofilms. *Microbiology*. 2005;151(Pt 3):757-62

Goller C *et al*., The cation-responsive protein NhaR of *Escherichia coli* activates pgaABCD transcription, required for production of the biofilm adhesin poly-beta-1,6-N-acetyl-D-glucosamine. *Journal of Bacteriology*. 2006;188(23):8022-32

Griffith KL & Wolf RE Jr, Measuring beta-galactosidase activity in bacteria: cell growth, permeabilization, and enzyme assays in 96-well arrays. *Biochemical and Biophysical Research Communications*. 2002;290(1):397-402

Gronbach K *et al*., Safety of probiotic *Escherichia coli* strain Nissle 1917 depends on intestinal microbiota and adaptive immunity of the host. *Infection and Immunity*. 2010;78(7):3036-46

Gross R *et al*., Engineered catalytic biofilms for continuous large scale production of n-octanol and (S)-styrene oxide. *Biotechnology and Bioengineering*. 2012;110(2):424-36

Gualdi L *et al*., Cellulose modulates biofilm formation by counteracting curli-mediated colonization of solid surfaces in *Escherichia coli*. *Microbiology*. 2008;154(Pt 7):2017-24

Gupta S *et al*., In vitro production of biofilm in a flow cell system in a strain of *Pseudomonas aeruginosa* and *Staphylococcus aureus* and determination of efficiency of ciprofloxacin against them. *Indian Journal of Pathology and Microbiology*. 2011;54(3):569-71

Guttenplan SB & Kearns DB, Regulation of flagellar motility during biofilm formation. *FEMS Microbiology Reviews*. 2013;37(6):849-71

Guzik U *et al*., Immobilization as a strategy for improving enzyme properties-application to oxidoreductases. *Molecules*. 2014;19(7):8995-9018

Hammer ND *et al*., The curli nucleator protein, CsgB, contains an amyloidogenic domain that directs CsgA polymerization. *Proceedings of the National Academy of Sciences of the United States of America.* 2007;104(30):12494-9

Hancock V *et al*., Functional genomics of probiotic *Escherichia coli* Nissle 1917 and 83972, and UPEC strain CFT073: comparison of transcriptomes, growth and biofilm formation. *Molecular Genetics and Genomics*. 2010;284(6):437-54

Harrison JJ *et al*., The use of microscopy and three-dimensional visualization to evaluate the structure of microbial biofilms cultivated in the Calgary Biofilm Device. *Biological Procedures Online.* 2006;8:194-215

Hegde M *et al*., Chemotaxis to the quorum-sensing signal AI-2 requires the Tsr chemoreceptor and the periplasmic LsrB AI-2-binding protein. *Journal of Bacteriology*. 2011;193(3):768-73

Hengge R, Principles of c-di-GMP signalling in bacteria. *Nature Reviews Microbiology*. 2009;7(4):263-73

Hengge R, Trigger phosphodiesterases as a novel class of c-di-GMP effector proteins. *Philosophical Transactions of the Royal Society of London*. 2016;371(1707)

Heyland J et al., Simple enzymatic procedure for L-carnosine synthesis: whole-cell biocatalysis and efficient biocatalyst recycling. Microbial Biotechnology. 2010;3(1):74-83

Hirano Y *et al*., Structural studies of the Cpx pathway activator NlpE on the outer membrane of *Escherichia coli*. *Structure*. 2007;15(8):963-76

Høiby N *et al*., *Pseudomonas aeruginosa* biofilms in cystic fibrosis. *Future Microbiology*. 2010;5(11):1663-74

Hook AL *et al*., Combinatorial discovery of polymers resistant to bacterial attachment. *Nature Biotechnology*. 2012;30:868-875

Horber C *et al*., Improved Dechlorinating Performance of Upflow Anaerobic Sludge Blanket Reactors by Incorporation of *Dehalospirillum multivorans* into Granular Sludge. *Applied and Environmental Microbiology*. 1998;64(5):1860-3

Hu M *et al*., Indole affects biofilm formation in bacteria. *Indian Journal of Microbiology*. 2010;50(4):362-8

Huang CJ *et al*., Industrial production of recombinant therapeutics in *Escherichia coli* and its recent advancements. *Journal of Industrial Microbiology and Biotechnology*. 2012;39(3):383-99

Hufnagel DA *et al*., The Catabolite Repressor Protein-Cyclic AMP Complex Regulates *csgD* and Biofilm Formation in Uropathogenic *Escherichia coli*. *Journal of Bacteriology*. 2016;198(24):3329-3334

Jackson DW et al., Catabolite repression of *Escherichia coli* biofilm formation. *Journal of Bacteriology*. 2002;184(12):3406-10

Jacobsen SM *et al*., Complicated catheter-associated urinary tract infections due to *Escherichia coli* and *Proteus mirabilis*. *Clinical Microbiology Reviews*. 2008;21(1):26-59

Jesis JS & Owen RW, Biological fluid-bed treatment for BOD and nitrogen removal. *Journal of Water Pollution Control*. 1977;49:816

Johnson MD *et al*., RcsB is required for inducible acid resistance in *Escherichia coli* and acts at gadE-dependent and -independent promoters. *Journal of Bacteriology*. 2011;193(14):3653-6

Jubelin G *et al*., CpxR/OmpR interplay regulates curli gene expression in response to osmolarity in *Escherichia coli*. *Journal of Bacteriology*. 2005;187(6):2038-49

Kaulmann U *et al*., Substrate spectrum of ω-transaminase from *Chromobacterium violaceum* DSM30191 and its potential for biocatalysis. *Enzyme and Microbial Technology*. 2007;41:628-637

Kaur P *et al*., Enteroaggregative *Escherichia coli*: An Emerging Enteric Food Borne Pathogen. *Interdisciplinary Perspectives on Infectious Diseases*. 2010;2010:254159

Kawasaki H *et al*., Site-specific mutagenesis of the alpha subunit of tryptophan synthase from *Salmonella typhimurium*. Changing arginine 179 to leucine alters the reciprocal transmission of substrate-induced conformational changes between the alpha and beta 2 subunits. *Journal of Biological Chemistry*. 1987;262(22):10678-83

Keller S *et al*., Purification and Partial Characterization of Tryptophan 7-Halogenase (PrnA) from *Pseudomonas fluorescens*. *Angewandte Chemie*. 2000;39(13):2300-2

Kim J and Park W, Indole: a signalling molecule or a mere metabolic byproduct that alters bacterial physiology at a high concentration? *Journal of Microbiology*. 2015;53(7):421-8

Klapper I *et al*., Viscoelastic fluid description of bacterial biofilm material properties. *Biotechnology and Bioengineering*. 2002;80(3):289-96

Klumpp S *et al*., Growth rate-dependent global effects on gene expression in bacteria. *Cell*. 2009;139(7):1366-75

Koe LCC & Yang F, Evaluation of a Pilot-Scale Bioscrubber for the Removal of Hydrogen Sulphide. *Water and Environment Journal*. 2000;14(6):432-5

Koeller KM & Wong CH, Enzymes for chemical synthesis. *Nature*. 2001;409(6817):232-40

Koeth RA *et al*., Intestinal microbiota metabolism of L-carnitine, a nutrient in red meat, promotes atherosclerosis. *Nature Medicine*. 2013;19(5):576-85

Kunduru MR & Pometto AL 3rd, Continuous ethanol production by *Zymomonas mobilis* and *Saccharomyces cerevisiae* in biofilm reactors. *Journal of Industrial Microbiology*. 1996;16(4):249-56

Lacanna E *et al*., Evidence for *Escherichia coli* Diguanylate Cyclase DgcZ Interlinking Surface Sensing and Adhesion via Multiple Regulatory Routes. *Journal of Bacteriology*. 2016;198(18):2524-35

Lacour S & Landini P, SigmaS-dependent gene expression at the onset of stationary phase in *Escherichia coli*: function of sigmaS-dependent genes and identification of their promoter sequences. *Journal of Bacteriology*. 2004;186(21):7186-95

Laganenka L *et al*., Chemotaxis towards autoinducer 2 mediates autoaggregation in *Escherichia coli*. *Nature Communications*. 2016;7:12984

Lam TB *et al*., Types of indwelling urethral catheters for short-term catheterisation in hospitalised adults. *The Cochrane Database of Systematic Reviews*. 2014;(9):CD004013

Landick R *et al*., Replacement of the *Escherichia coli trp* operon attenuation control codons alters operon expression. *Journal of Molecular Biology*. 1990;216(1):25-37

Lane AN & Kirschner K, Mechanism of the physiological reaction catalyzed by tryptophan synthase from *Escherichia coli*. *Biochemistry*. 1991;30(2):479-84

Laopornpichayanuwat W *et al*., 3-D Surface roughness profile of 316-stainless steel using vertical scanning interferometry with a superluminescent diode. *Measurement*. 2012;45(10):2400-6

Latham J *et al*., Development of Halogenase Enzymes for Use in Synthesis. *Chemistry Reviews*. 2017

Lawrence EL & Turner IG, Materials for urinary catheters: a review of their history and development in the UK. *Medical Engineering and Physics*. 2005;27(6):443-53

Le HH *et al*., Bisphenol A is released from polycarbonate drinking bottles and mimics the neurotoxic actions of estrogen in developing cerebellar neurons. *Toxicology Letters*. 2008;30;176(2):149-56

Lee J *et al*., Indole cell signalling occurs primarily at low temperatures in *Escherichia coli*. *The ISME Journal*. 2008;2(10):1007-23

Lee J *et al*., Indole is an inter-species biofilm signal mediated by SdiA. *BMC Microbiology*. 2007;7:42.

Lelong C *et al*., The Crl-RpoS regulon of *Escherichia coli*. *Molecular and Cell Proteomics*. 2007;6(4):648-59

Le-Tien C *et al*., Modified alginate and chitosan for lactic acid bacteria immobilization. *Biotechnology and Applied Biochemistry*. 2004;39(Pt 3):347-54

Li G & Young KD, A cAMP-independent carbohydrate-driven mechanism inhibits tnaA expression and TnaA enzyme activity in *Escherichia coli*. *Microbiology*. 2014;160(Pt 9):2079-88

Li G & Young KD, A new suite of tnaA mutants suggests that *Escherichia coli* tryptophanase is regulated by intracellular sequestration and by occlusion of its active site. *BMC Microbiology*. 2015;15:14

Li G & Young KD, Indole production by the tryptophanase TnaA in *Escherichia coli* is determined by the amount of exogenous tryptophan. *Microbiology*. 2013;159(Pt 2):402-10

Limoli DH *et al*., Bacterial Extracellular Polysaccharides in Biofilm Formation and Function. *Microbiology Spectrum*. 2015;3(3)

Lindenberg S *et al*., The EAL domain protein YciR acts as a trigger enzyme in a c-di-GMP signalling cascade in *E. coli* biofilm control. *The EMBO Journal*. 2013;32(14):2001-14

Little DJ *et al*., Structural basis for the De-N-acetylation of Poly-β-1,6-N-acetyl-D-glucosamine in Gram-positive bacteria. *Journal of Biological Chemistry*. 2014;289(52):35907-17

Liu X *et al*., Elimination of the formation of biofilm in industrial pipes using enzyme cleaning technique. *MethodsX*. 2014;1:130-6

Liu Y & Tay JH, The essential role of hydrodynamic shear force in the formation of biofilm and granular sludge. *Water Research*. 2002;36(7):1653-65

Liu Z *et al*., CsgD regulatory network in a bacterial trait-altering biofilm formation. *Emerging Microbes and Infections*. 2014;3(1)

M2 Scientifics website, Lab Plastics Guide. https://www.m2scientifics.com/blog/lab-plastics-guide. Accessed 28/04/2017.

Macia MD *et al*., Antimicrobial susceptibility testing in biofilm-growing bacteria. *Clinical Microbiology and Infection*. 2014;20(10):981-90

Majdalani N & Gottesman S, The Rcs phosphorelay: a complex signal transduction system. *Annual Review of Microbiology*. 2005;59:379-405

Malik MS *et al*., Features and technical applications of ω-transaminases. *Applied Microbiology and Biotechnology*. 2012

Mamat U *et al*., Detoxifying *Escherichia coli* for endotoxin-free production of recombinant proteins. *Microbial Cell Factories*. 2015;14:57.

Marisch K *et al*., A comparative analysis of industrial *Escherichia coli* K-12 and B strains in high-glucose batch cultivations on process-, transcriptome- and proteome level. *PLoS One*. 2013;8(8):e70516

Mauro JC *et al*., Grand challenges in glass science. *Frontiers in Materials*. 2014

May T & Okabe S, *Escherichia coli* harboring a natural IncF conjugative F plasmid develops complex mature biofilms by stimulating synthesis of colanic acid and Curli. *Journal of Bacteriology*. 2008;190(22):7479-90

Mazia D *et al*., Adhesion of cells to surfaces coated with polylysine. Applications to electron microscopy. *Journal of Cell Biology*. 1975;66(1):198-200

McAdow M *et al*., Preventing *Staphylococcus aureus* sepsis through the inhibition of its agglutination in blood. *PLoS Pathogens*. 2011;7(10):e1002307

McCarthy H *et al*., Methicillin resistance and the biofilm phenotype in *Staphylococcus aureus*. *Frontiers in Cellular and Infection Microbiology*. 2015;5:1

Méndez-Ortiz MM *et al*., Genome-wide Transcriptional Profile of *Escherichia coli* in Response to High Levels of the Second Messenger 3′,5′-Cyclic Diguanylic Acid. *Journal of Biological Chemistry*. 2006;281:8090-99

Mika F *et al*., Targeting of *csgD* by the small regulatory RNA RprA links stationary phase, biofilm formation and cell envelope stress in *Escherichia coli*. *Molecular Microbiology*. 2012;84(1):51-65

Miller WG *et al*., Improved gfp and inaZ broad-host-range promoter-probe vectors. *Molecular Plant-Microbe Interactions*. 2000;13(11):1243-50

Mitra A *et al*., Integration of AI-2 Based Cell-Cell Signalling with Metabolic Cues in *Escherichia coli*. *PLoS One*. 2016;11(6):e0157532

Mohsin M *et al*., Probiotic *Escherichia coli* Nissle 1917 reduces growth, Shiga toxin expression, release and thus cytotoxicity of enterohemorrhagic *Escherichia coli*. *International Journal of Medical Microbiology*. 2015;305(1):20-6

Monteiro C *et al*., Characterization of cellulose production in *Escherichia coli* Nissle 1917 and its biological consequences. *Environmental Microbiology*. 2009;11(5):1105-16

Murphy TF *et al*., *Pseudomonas aeruginosa* in chronic obstructive pulmonary disease. *American Journal of Respiratory and Critical Care Medicine*. 2008;177(8):853-60

Nan L *et al*., Anti-biofilm formation of a novel stainless steel against *Staphylococcus aureus*. *Materials Science and Engineering*. 2015;51:356-61

Nassif X *et al*., Positive control of colanic acid synthesis in *Escherichia coli* by rmpA and rmpB, two virulence-plasmid genes of *Klebsiella pneumoniae*. 1989;3(10):1349-59

Naves P *et al*., Measurement of biofilm formation by clinical isolates of *Escherichia coli* is method-dependent. *Journal of Applied Microbiology*. 2008;105(2):585-90

Neidhardt FC *et al*., *Escherichia Coli and Salmonella: Cellular and Molecular Biology*. American Society for Microbiology. 1996

Nenninger AA *et al*., Localized and efficient curli nucleation requires the chaperone-like amyloid assembly protein CsgF. *Proceedings of the National Academy of Sciences of the United States of America.* 2009;106(3):900-5

Nguyen PQ *et al*., Programmable biofilm-based materials from engineered curli nanofibres. *Nature Communications*. 2014;5:4945

Nguyen Y *et al*., Structural and mechanistic roles of novel chemical ligands on the SdiA quorum-sensing transcription regulator. *mBio*. 2015; 6(2)

Nikel PI *et al*., From dirt to industrial applications: *Pseudomonas putida* as a Synthetic Biology chassis for hosting harsh biochemical reactions. *Current Opinion in Chemical Biology.* 2016;34:20-29

O'Neill GP *et al*., Overproduction from a Cellulase Gene with a High Guanosine-Plus-Cytosine Content in *Escherichia coli*. *Applied and Environmental Microbiology*. 1986;52(4):737-743

O'Toole GA, Microtiter dish biofilm formation assay. *Journal of Visualised Experiments.* 2011;(47)

Olsén A *et al*., Environmental regulation of curli production in *Escherichia coli*. *Infectious Agents and Disease*. 1993;2(4):272-4

Ophir T & Gutnick DL, A role for exopolysaccharides in the protection of microorganisms from desiccation. *Applied and Environmental Microbiology.* 1994;60(2):740-5

Otto K & Silhavy TJ, Surface sensing and adhesion of *Escherichia coli* controlled by the Cpx-signaling pathway. *Proceedings of the National Academy of Sciences of the United States of America.* 2002;99(4):2287-92

Overton TW, Recombinant protein production in bacterial hosts. *Drug Discovery Today*. 2014;19(5):590-601

Park A *et al*., Effect of shear stress on the formation of bacterial biofilm in a microfluidic channel. *BioChip Journal*. 2011;5(236)

Patel J *et al*., Effect of curli expression and hydrophobicity of *Escherichia coli* O157:H7 on attachment to fresh produce surfaces. *Journal of Applied Microbiology*. 2011;110(3):737-45

Pawar DM *et al*., Role of curli fimbriae in mediating the cells of enterohaemorrhagic *Escherichia coli* to attach to abiotic surfaces. *Journal of Applied Microbiology.* 2005;99(2):418-25

Pawley J, *Handbook of Biological Confocal Microscopy*. Springer. 2006

Perni S *et al*., Optimisation of engineered *Escherichia coli* biofilms for enzymatic biosynthesis of l-halotryptophans. *AMB Express*. 2013;3(1):66

Peters JE *et al*., Definition of the *Escherichia coli* MC4100 genome by use of a DNA array. *Journal of Bacteriology*. 2003;185(6):2017-21

Pons L *et al*., Effect of surface roughness, biofilm coverage and biofilm structure on the electrochemical efficiency of microbial cathodes. *Bioresource Technology*. 2011;102(3):2678-83

Pratt LA & Kolter R, Genetic analysis of *Escherichia coli* biofilm formation: roles of flagella, motility, chemotaxis and type I pili. *Molecular Microbiology.* 1998;30(2):285-93

Pringent-Combaret C *et al*., Complex regulatory network controls initial adhesion and biofilm formation in *Escherichia coli* via regulation of the *csgD* gene. *Journal of Bacteriology*. 2001;183(24):7213-23

Purcell O *et al*., Temperature dependence of ssrA-tag mediated protein degradation. *Journal of Biological Engineering*. 2012;6(10)

Qin X *et al*., Hydrophobicity of mucosal surface and its relationship to gut barrier function. *Shock.* 2008;29(3):372-6

Qureshi N *et al*., Biofilm reactors for industrial bioconversion processes: employing potential of enhanced reaction rates. *Microbial Cell Factories.* 2005;4:24

Randez-Gil F *et al*., Genetic and phenotypic characteristics of baker's yeast: relevance to baking. *Annual Review of Food Science and Technology.* 2013;4:191-214

Rasamiravaka T *et al*., The formation of biofilms by *Pseudomonas aeruginosa*: a review of the natural and synthetic compounds interfering with control mechanisms. *BioMed Research International*. 2015;2015:759348

Reetz MT, Biocatalysis in organic chemistry and biotechnology: past, present, and future. *Journal of the American Chemical Society*. 2013;135(34):12480-96
Reisner A *et al*., Development and maturation of *Escherichia coli* K-12 biofilms. *Molecular Microbiology*. 2003;48(4):933-946

Reisner A *et al*., In vitro biofilm formation of commensal and pathogenic *Escherichia coli* strains: impact of environmental and genetic factors. *Journal of Bacteriology*. 2006;188(10):3572-81

Ren D *et al*., Stationary-phase quorum-sensing signals affect autoinducer-2 and gene expression in *Escherichia coli*. *Applied and Environmental Microbiology*. 2004;70(4):2038-43

Richter M, Functional diversity of organic molecule enzyme cofactors. *Natural Product Reports.* 2013;30(10):1324-45

Rodriguez A *et al*., Effect of surface roughness and stainless steel finish on *Listeria monocytogenes* attachment and biofilm formation. *Journal of Food Protection*. 2008;71(1):170-5

Rodriguez A *et al*., Engineering *Escherichia coli* to overproduce aromatic amino acids and derived compounds. *Microbial Cell Factories*. 2014;13(126)

Römling U & Galperin MY, Bacterial cellulose biosynthesis: diversity of operons, subunits, products, and functions. *Trends in Microbiology.* 2015;23(9):545-57

Römling U *et al*., Cyclic di-GMP: the first 25 years of a universal bacterial second messenger. *Microbiology and Molecular Biology Reviews.* 2013;77(1):1-52

Rosa MF *et al*., Biofilm development and ammonia removal in the nitrification of a saline wastewater. *Bioresource Technologies*. 1998;65 135-8

Rosano GL & Ceccarelli EA, Recombinant protein expression in *Escherichia coli*: advances and challenges. *Frontiers in Microbiology.* 2014;5:172

Rother C & Nidetzky B, Enzyme Immobilization by Microencapsulation: Methods, Materials, and Technological Applications. *Encyclopedia of Industrial Biotechnology*. 2014;1-21

Rudkin JK *et al*., Methicillin resistance reduces the virulence of healthcare-associated methicillin-resistant *Staphylococcus aureus* by interfering with the agr quorum sensing system. *Journal of Infectious Diseases.* 2012;205(5):798-806

Rühs PA *et al*., In-Situ Quantification of the Interfacial Rheological Response of Bacterial Biofilms to Environmental Stimuli. *PLOS One*. 2013

Ryu J-H & Beuchat LR, Biofilm formation by *Escherichia coli* O157:H7 on stainless steel: effect of exopolysaccharide and Curli production on its resistance to chlorine. *Applied and Environmental Microbiology*. 2005;71(1):247-54

Sabag-Daigle A *et al*., The acyl homoserine lactone receptor, SdiA, of *Escherichia coli* and *Salmonella enterica* serovar Typhimurium does not respond to indole. *Applied and Environmental Microbiology.* 2012;78(15):5424-31

Saldaña Z *et al*., Synergistic role of curli and cellulose in cell adherence and biofilm formation of attaching and effacing *Escherichia coli* and identification of Fis as a negative regulator of curli. *Environmental Microbiology*. 2009;11(4):992-1006

Salo J *et al*., Biofilm formation by *Escherichia coli* isolated from patients with urinary tract infections. *Clinical Nephrology*. 2009;71(5):501-7

Santacoloma PA *et al*., Multi-catalyzed processes: next generation biocatalysis. *Organic Process Research and Development.* 2011;15:113-8

Schätzle S *et al*., Rapid and sensitive kinetic assay for characterization of omega-transaminases. *Analytical Chemistry*. 2009;81(19):8244-8

Schenborn E & Groskreutz D, Reporter gene vectors and assays. *Molecular Biotechnology*. 1999;13(1):29-44

Schilling JD *et al*., Structure and function of *Escherichia coli* type 1 pili: new insight into the pathogenesis of urinary tract infections. *The Journal of Infectious Diseases*. 2001;183 Suppl 1:S36-40

Schwering M *et al*., Multi-species biofilms defined from drinking water microorganisms provide increased protection against chlorine disinfection. *Biofouling*. 2013;29(8):917-28

Serra DO *et al*., Cellulose as an architectural element in spatially structured *Escherichia coli* biofilms. *Journal of Bacteriology*. 2013;195(24):5540-54

Shimada T *et al*., Roles of cell division control factor SdiA: recognition of quorum sensing signals and modulation of transcription regulation targets. *Genes to Cells*. 2014;19(5):405-18

Shu Q *et al*., Solution NMR structure of CsgE: Structural insights into a chaperone and regulator protein important for functional amyloid formation. *Proceedings of the National Academy of Sciences of the United States of America.* 2016;113(26):7130-5

Silhavy TJ *et al*., The bacterial cell envelope. *Cold Spring Harbor Perspectives in Biology.* 2010;2(5):a000414

Silverman PM & Clarke MB, New insights into F-pilus structure, dynamics, and function. *Integrative Biology.* 2009;2(1):25-31

Simm R *et al*., GGDEF and EAL domains inversely regulate cyclic di-GMP levels and transition from sessility to motility. *Molecular Microbiology*. 2004;53(4):1123-34

Simon RC *et al*., Recent Developments of Cascade Reactions Involving ω-Transaminases. *ACS Catalysis*. 2014;4(1):129-143

Smith SW, Chiral toxicology: it's the same thing...only different. *Toxicological Sciences.* 2009;110(1):4-30

Soto SM, Importance of Biofilms in Urinary Tract Infections: New Therapeutic Approaches. *Advances in Biology*. 2014;2014:543974

Spurbeck RR *et al*., Enzymatically active and inactive phosphodiesterases and diguanylate cyclases are involved in regulation of Motility or sessility in *Escherichia coli* CFT073. *mBio*. 2012;3(5)

Stefani M, Protein misfolding and aggregation: new examples in medicine and biology of the dark side of the protein world. *Biochimica et Biophysica Acta*. 2004;1739(1):5-25

Sternberg C & Tolker-Nielsen T, Growing and analyzing biofilms in flow cells. *Current Protocols in Microbiology*. 2006;Chapter 1:Unit 1B.2

Stevenson G *et al*., Organization of the *Escherichia coli* K-12 gene cluster responsible for production of the extracellular polysaccharide colanic acid. *Journal of Bacteriology.* 1996;178(16):4885-93

Stout V *et al*., RcsA, an unstable positive regulator of capsular polysaccharide synthesis. *Journal of Bacteriology.* 1991;173(5):1738-47

Studier FW & Moffatt BA, Use of bacteriophage T7 RNA polymerase to direct selective high-level expression of cloned genes. *Journal of Molecular Biology*. 1986;189(1):113-30

Suzuki K *et al*., Regulatory circuitry of the CsrA/CsrB and BarA/UvrY systems of *Escherichia coli*. *Journal of Bacteriology.* 2002;184(18):5130-40

Tagliabue L *et al*., The diguanylate cyclase YddV controls production of the exopolysaccharide poly-N-acetylglucosamine (PNAG) through regulation of the PNAG biosynthetic *pgaABCD* operon. *Microbiology*. 2010;156(10):2901-11

Taylor RG *et al*., *E. coli* host strains significantly affect the quality of small scale plasmid DNA preparations used for sequencing. *Nucleic Acid Research*. 1993;21(7):1677-8

ThermoFisher Scientific website, Catalogue No. C601003. https://www.thermofisher.com/order/catalog/product/C601003 Accessed 29/04/2017.

Thomason MK *et al*., A small RNA that regulates motility and biofilm formation in response to changes in nutrient availability in *Escherichia coli*. *Molecular Microbiology*. 2012;84(1):17-35

Thormann E *et al*., Interactions between a polystyrene particle and hydrophilic and hydrophobic surfaces in aqueous solutions. *Langmuir*. 2008;24(14):7278-84

Trautner BW & Darouiche RO, Role of biofilm in catheter-associated urinary tract infection. *American Journal of Infection Control*. 2004;32(3):177-83

Tschowri N *et al*., The BLUF-EAL protein YcgF acts as a direct anti-repressor in a blue-light response of *Escherichia coli*. *Genes and Development*. 2009;23(4):522-34

Tsoligkas AN *et al*., Characterisation of spin coated engineered *Escherichia coli* biofilms using atomic force microscopy. *Colloids and Surfaces. B, Biointerfaces*. 2012;89:152-60

Tsoligkas AN *et al*., Engineering biofilms for biocatalysis. *Chembiochem*. 2011;12(9):1391-5

Uhlich GA *et al*., Phage insertion in *mlrA* and variations in *rpoS* limit curli expression and biofilm formation in *Escherichia coli* serotype O157: H7. *Microbiology*. 2013;159(Pt 8):1586-96

Ulett GC *et al*., Antigen-43-mediated autoaggregation impairs motility in *Escherichia coli*. *Microbiology*. 2006;152(Pt 7):2101-10

Uppada V *et al*., Cofactor regeneration – an important aspect of biocatalysis. *Current Science*. 2014;106(7):946-957

van der Woude MW & Bäumler AJ, Phase and antigenic variation in bacteria. *Clinical Microbiology Reviews.* 2004;17(3):581-611

van der Woude MW & Henderson IR, Regulation and function of Ag43 (flu). *Annual Review of Microbiology*. 2008;62:153-69

Van Houdt R *et al*., N-acyl-L-homoserine lactone signal interception by *Escherichia coli*. *FEMS Microbiology Letters*. 2006;256(1):83-9

Vianney A *et al*., *Escherichia coli tol* and *rcs* genes participate in the complex network affecting curli synthesis. *Microbiology*. 2005;151(Pt 7):2487-97

Vidal O *et al*., Isolation of an *Escherichia coli* K-12 mutant strain able to form biofilms on inert surfaces: involvement of a new *ompR* allele that increases curli expression. *Journal of Bacteriology.* 1998;180(9):2442-9

Villegas-Torres MF *et al*., Multi-step biocatalytic strategies for chiral amino alcohol synthesis. *Enzyme and Microbial Technology*. 2015;81:23-30

Vistoli G *et al*., Exploring the space of histidine containing dipeptides in search of novel efficient RCS sequestering agents. *European Journal of Medical Chemistry*. 2013;66:153-60

Volmer J *et al*., Engineering of *Pseudomonas taiwanensis* VLB120 for constitutive solvent tolerance and increased specific styrene epoxidation activity. *Applied and Environmental Microbiology.* 2014;80(20):6539-48

Wachtmeister J & Rother D, Recent advances in whole cell biocatalysis techniques bridging from investigative to industrial scale. *Current Opinion in Biotechnology*. 2016;42:169-177

Weatherspoon-Griffin N *et al*., The CpxR/CpxA two-component regulatory system up-regulates the multidrug resistance cascade to facilitate *Escherichia coli* resistance to a model antimicrobial peptide. *The Journal of Biological Chemistry*. 2014;289(47):32571-82

Weber N *et al*., Engineered baker's yeast as whole-cell biocatalyst for one-pot stereo-selective conversion of amines to alcohols. *Microbial Cell Factories.* 2014;13:118

Wei ZY *et al*., Production of Bioactive Recombinant Bovine Chymosin in Tobacco Plants. *International Journal of Molecular Sciences*. 2016;17(5)

Weiser MC & Moucha CS, The Current State of Screening and Decolonization for the Prevention of *Staphylococcus aureus* Surgical Site Infection After Total Hip and Knee Arthroplasty. *The Journal of Bone and Joint Surgery*. 2015;97(17):1449-58

Westers L *et al*., *Bacillus subtilis* as cell factory for pharmaceutical proteins: a biotechnological approach to optimize the host organism. *Biochimica et Biophysica Acta.* 2004;1694(1-3):299-310

Wood WB, Host specificity of DNA produced by *Escherichia coli*: bacterial mutations affecting the restriction and modification of DNA. *Journal of Molecular Biology*. 1966;16(1):118-33

Wu H *et al*., Strategies for combating bacterial biofilm infections. *International Journal of Oral Science*. 2015;7(1):1-7

Wyre C & Overton TW, Flow cytometric analysis of *E. coli* on agar plates: implications for recombinant protein production. *Biotechnology Letters*. 2014;36(7):1485-94

Yang L *et al*., Current understanding of multi-species biofilms. *International Journal of Oral Science*. 2011b;3(2):74-81;13(7):1705-17

Yang L *et al*., Distinct roles of extracellular polymeric substances in *Pseudomonas aeruginosa* biofilm development. *Environmental Microbiology*. 2011a

Yang TT *et al*., Optimized codon usage and chromophore mutations provide enhanced sensitivity with the green fluorescent protein. *Nucleic Acids Research*. 1996;24(22):4592-3

Yeh E *et al*., Robust in vitro activity of RebF and RebH, a two-component reductase/halogenase, generating 7-chlorotryptophan during rebeccamycin biosynthesis.

Proceedings of the National Academy of Sciences of the United States of America. 2005;102(11):3960-5

Yeh JH & Chen J, Production of slime polysaccharide by EHEC and STEC as well as the influence of culture conditions on slime production in *Escherichia coli* O157:H7. *Letters in Applied Microbiology*. 2004;38(6):488-92

Yoshida K *et al*., Impacts of hydrophilic colanic acid on bacterial attachment to microfiltration membranes and subsequent membrane biofouling. *Water Research*. 2015;76:33-42

Yousif E & Haddad R, Photodegradation and photostabilization of polymers, especially polystyrene: review. *SpringerPlus*. 2013;2:398

Zhang G *et al*., An enhanced green fluorescent protein allows sensitive detection of gene transfer in mammalian cells. *Biochemical and Biophysical Research Communications*. 1996;(227(3):707-11

Zhang H *et al*., Engineering nanoscale roughness on hydrophobic surface – Preliminary assessment of fouling behaviour. *Science and Technology of Advanced Materials*. 2005;6:236-9

Zuverink M & Barbieri JT, From GFP to β-lactamase: advancing intact cell imaging for toxins and effectors. *Pathogens and Disease*. 2015;73(9):ftv097

Chapter 8

Appendix

8.1 Supplementary Data for Chapter 2 and 3: MUSCLE Sequence Alignment Output for *csgBAC* Promoter Sequences in *E. coli* MC4100, BL21(DE3) and Nissle 1917

```
CLUSTAL multiple sequence alignment by MUSCLE (3.8)


MC4100          GATGAAACCCCGCTTTTTTTATTGATCGCACACCTGACAGCTGCCTCTAAAATAGAAGCA
BL21(DE3)       GATGAAACCCCGCTTTTTTTATTGATCGCACACCTGACAGCTGCCTCTAAAATAGAAGCA
Nissle1917      GATGAAACCCCGCTTTTTTTATTGATCGCACACCTGACAGCTGCCTCTAAAATAGAAGCA
                ************************************************************

MC4100          CCAGAAGTACTGACAGATGTTGCACTGCTGTGTGTAGTAATAAATCAGCCCTAAATGGGT
BL21(DE3)       CCAGAAGTACTGACAGATGTTGCACTGCTGTGTGTAGTAATAAATCAGCCCTAAATGGGT
Nissle1917      CCAGAAGTACTGACAGATGTTGCACTGCTGTGTGTAGTAATAAATCAGCCCTAAATGGGT
                ************************************************************

MC4100          AAAATATAAAACTAATGGATTACATCTGATTTCAATCTAGCCATTACAAATCTTAAATCA
BL21(DE3)       AAAATATAAAACTAATGGATTACATCTGATTTCAATCTAGCCATTACAAATCTTAAATCA
Nissle1917      AAAATATAAAACTAATGGATTACATCTGATTTCAATCTAGCCATTACAAATCTTAAATCA
                ************************************************************

MC4100          AGTGTTAAACATGTAACTAAATGTAACTCGTTATATTAAAATGTTAACCTTAAGGTTTTA
BL21(DE3)       AGTGTTAAACATGTAACTAAATGTAACTCGTTATATTAAAATGTTAACCTTAAGGTTTTA
Nissle1917      AGTGTTAAACATGTAACTAAATGTAACTCGTTATATTAAAATGTTAACCTTAAGGTTTTA
                ************************************************************

MC4100          TTAAGTTTAGAAATGATAGAAAAGTTGTACATTTGGTTTTTATTGCACAATTTTAAAAAA
BL21(DE3)       TTAAGTTTAGAAATGATAGAAAAGTTGTACATTTGGTTTTTATTGCACAATTTTAAAAAA
Nissle1917      TTAAGTTTATAAATGATAGAAAAGTTGTACATTTGGTTTTTATTGCACAATTTTAAAAAA
                ********* **************************************************

MC4100          TCATACAAATGGTGATAACTTACTAATAATGCATATAAAAAATATTTCGGTGTAGTCCTT
BL21(DE3)       TCATACAAATGGTGATAACTTACTAATAATGCATATAAAAAATATTTCGGTGTAGTCCTT
Nissle1917      TCATACAAATGGTGCTAACTTACTAATAATGCATATAAAAAATATTTCGCTGTAGTCCTT
                ************** ********************************** ***********

MC4100          TCGTCATGTAAAACGTTCTTGTTTTTTCTCCACACCTCCGTGGACAATTTTTTACTGCAA
BL21(DE3)       TCGTCATGTAAAACGTTCTTGTTTTTTCTCCACACCTCCGTGGACAATTTTTTACTGCAA
Nissle1917      TCGTCATGAAAAACGTTCTTGTTTTTTCTCCATACCACCGTGGACAATTTTTTACTGCAA
                ******** ********************** *** ************************

MC4100          AAAGACGAGGTTTGTCACGGCTTGTGCGCAAGACATATCGCAGCAATCAGCGACGGGCAA
BL21(DE3)       AAAGACGAGGTTTGTCACGGCTTGTGCGCAAGACATATCGCAGCAATCAGCGACGGGCAA
Nissle1917      AAAGACGAGGTTTGTCACGGCTTGTGCGCAAGACATATCGCAGCAATCAGCGACGGGCAA
                ************************************************************

MC4100          GAAGAATGACTGTCTGGTGCTTTTTGATAGCGGAAAACGGAGATTTAAAAGAAAACAAAA
BL21(DE3)       GAAGAATGACTGTCTGGTGCTTTTTGATAGCGGAAAACGGAGATTTAAAAGAAAACAAAA
Nissle1917      GAAGAATGACTGTCTGGTGATTTTTGATAGCGGAAAACGGAGATTTAAAAGAAAACAAAA
                ****************** ****************************************

MC4100          TATTTTTTTGCGTAGATAACAGCGTATTTACGTGGGTTTTAATACTTTGGTATGAACTAA
BL21(DE3)       TATTTTTTTGCGTAGATAACAGCGTATTTACGTGGGTTTTAATACTTTGGTATGAACTAA
Nissle1917      TA--TTTTTGCGTAGATAACAGCGTATTTACGTGGGTTTTAATACTTTGGTATGAACAAA
                **  ************************************************** **

MC4100          AAAAGAAAAATACAACGCGCGGGTGAGTTATTAAAAATATTTCCGCAGACATACTTTCCA
BL21(DE3)       AAAAGAAAAATACAACGCGCGGGTGAGTTATTAAAAATATTTCCGCAGACATACTTTCCA
Nissle1917      AAAAGAAAAATACAACGTGCGGGTGAGTTATTAAAAATATTTCCGCAGACATACTTTCCA
                ***************** ****************************************

MC4100          TCGTAACGCAGCGTTAACAAAATACAGGTTGCGTTAACAACCAAGTTGAAATGATTTAAT
BL21(DE3)       TCGTAACGCAGCGTTAACAAAATACAGGTTGCGTTAACAACCAAGTTGAAATGATTTAAT
Nissle1917      TCGTAACGCAGCGTTAACAAAATACAGGTTGCGTTAACAACCAAGTTGAAATGATTTAAT
                ************************************************************

MC4100          TTCTTAAATGTACGACCAGGTCCAGGGTGACAAC
BL21(DE3)       TTCTTAAATGTACGACCAGGTCCAGGGTGACAAC
Nissle1917      TTCTTAAATGTACGACCAGGTCCAGGGTGACAAC
                  *********************************
```